Surface Modification and In-process Steam Cleaning of Ceramic Membranes Used in the Treatment of Wastewaters Containing Bituminous Fines

uOttawa

L'Université canadienne
Canada's university

Charbel Atallah

Thesis submitted

in partial fulfillment of the requirements for the

degree of Doctor of Philosophy in Chemical Engineering

Department of Chemical and Biological Engineering

Faculty of Engineering

University of Ottawa

Abstract

Synthetic membranes have a high separation efficiency, small footprint, low energy consumption and ease of operation, making them an attractive alternative to traditional separation operations. For this reason, membranes have been extensively studied for the treatment and recycling of bitumen-containing wastewaters. Such wastewaters include petroleum produced water, residual pipeline cleaning solutions and contaminated water from oil spills. Ceramic membranes are preferred in these applications over polymeric membranes because they are highly resistant to solvents and can be operated at high temperatures over a wide range of pH. Fine clays and silicates, coated with bitumen, are significant foulants for membrane filtration systems. These foulants possess acidic, basic and amphoteric groups, leading to the presence of both positive and negative surface charges. Ceramic membranes in aqueous media have a pH dependent surface charge. It was hypothesized that these surface charges are responsible for the high fouling of ceramic membranes that is observed when treating wastewaters containing bituminous fines.

The overall objective of this research was to reduce fouling and increase the lifetime of ceramic membranes in treating oil sands produced water; an example of a wastewater containing bituminous fines. This goal was achieved through the surface modification of the ceramic membrane's selective layer, as well as by the implementation of a novel in-place steam regeneration technique. All membrane filtration tests were performed with field samples of oil sands produced water that were supplied to CanmetMINING (NRCan) by three Canadian oil sands companies.

Organosilanes are silicon-based monomers that can possess a wide array of chemical functionality due to their organic moieties. They are capable of reacting with oxide surfaces, and have seen extensive use as surface modification agents for ceramic membranes in various applications. To maintain desirable hydrophilic properties without surface charges, highly hydrophilic and non-ionic polyethylene oxide (PEO) based organosilanes were identified. These PEO-silanes were then used to modify ceramic membranes of several different selective layer materials, and the thermal stability of the silane layer was studied using FTIR, SEM, zeta potential and contact angle measurements. The modification procedure with PEO-silanes was first applied to lab-scale membrane disks, and subsequently to commercial scale multilumen

membrane tubes that were tested in a pilot-scale system at CanmetMINING. Results obtained from both sets of experiments were promising and demonstrate that ceramic membranes can be surface modified in a way that successfully renders them fouling resistant to the bituminous fines present in these wastewaters. Upon surface modification, foulants were more readily released from the membrane surface, resulting in an enhanced flux and separation performance.

A novel steam regeneration technique was also applied as a means of bituminous fouling alleviation. This technique was tested in the CanmetMINING pilot-scale system and consisted of periodically injecting steam into the membrane lumen feed channels during operation. Direct steam injection rapidly heated foulant cake layers, and water droplets in the saturated steam caused surface abrasions that ultimately resulted in the scouring of bitumen away from the membrane surface. Membrane fluxes when steam regeneration was active were up to 4 times higher when compared to tests where only traditional permeate backflushing was used.

The fouling remediation techniques developed in this work have broad potential applicability in ceramic membrane filtration systems aimed at treating all wastewaters containing bituminous compounds, such as process waters in general and contaminated water from oil spills.

Résumé

Les membranes synthétiques ont une efficacité de séparation élevée, une faible consommation d'énergie et une facilité d'utilisation, ce qui en fait une alternative attrayante aux opérations de séparation traditionnelles. Pour cette raison, les membranes ont été largement étudiées pour le traitement et le recyclage des eaux usées contenant du bitume. Ces eaux usées comprennent l'eau de pétrole, les solutions de nettoyage des pipelines et l'eau contaminée provenant de marées noires. Les membranes céramiques sont préférées dans ces applications par rapport aux membranes polymères car elles sont très résistantes aux solvants et peuvent être utilisées à des températures élevées sur une large plage de pH. Les argiles fines et les silicates recouverts de bitume sont des impuretés importantes pour les systèmes de filtration à membrane. Ces espèces encrassantes possèdent des groupes acides, basiques et amphotères, ce qui entraîne la présence de charges superficielles positives et négatives. Les membranes céramiques en milieu aqueux ont une charge de surface dépendante du pH. On a émis l'hypothèse que ces charges de surface sont responsables de l'encrassement sévère des membranes céramiques observé lors du traitement des eaux usées contenant des fines bitumineuses.

L'objectif général de cette recherche était de réduire l'encrassement et d'augmenter la durée de vie des membranes céramiques lors du traitement de l'eau produite par les sables bitumineux; un exemple d'eaux usées contenant des fines bitumineuses. Cet objectif a été atteint grâce à la modification superficielle de la couche sélective de la membrane céramique ainsi qu'à la mise en œuvre d'une nouvelle technique de régénération de membrane utilisant de la vapeur sur place. Tous les tests de filtration à membrane ont été réalisés avec des échantillons de terrain d'eau produite par les sables bitumineux, fournie à CanmetMINES (RNCan) par trois compagnies opérant dans les sables bitumineux canadiens.

Les organosilanes sont des monomères à base de silicium ayant un large éventail de fonctionnalités chimiques possible en raison de leurs fractions organiques. Ils sont capables de réagir avec les surfaces d'oxydes et ont été largement utilisés comme agents de modification de surface pour les membranes céramiques dans diverses applications. Afin de maintenir les propriétés hydrophiles sans charges de surface, des organosilanes à base de poly (oxyde d'éthylène) (PEO) fortement hydrophiles et non ioniques ont été identifiés. Ces PEO-silanes ont ensuite été utilisés pour modifier des membranes céramiques de plusieurs matériaux de couche

sélective différents, et la stabilité thermique de la couche de silane a été étudiée à l'aide de mesures FTIR, SEM, de potentiel zêta et d'angle de contact. La procédure de modification avec des PEO-silanes a d'abord été appliquée à des disques membranaires à l'échelle du laboratoire, puis à des membranes tubulaires à l'échelle commerciale testés dans un système pilote à CanmetMINES. Les résultats obtenus dans les deux séries d'expériences sont prometteurs et démontrent que les membranes céramiques peuvent être modifiées d'une manière qui les rend résistantes à l'encrassement des fines bitumineuses présentes dans ces eaux usées. En résultat de la modification de la surface, les impuretés sont plus facilement libérées de la surface de la membrane, ce qui améliore les performances de flux et de séparation.

Une nouvelle technique de régénération de membrane à la vapeur a également été appliquée comme moyen d'atténuer l'encrassement bitumineux. Cette technique a été testée dans le système pilote à CanmetMINES et consistait à injecter périodiquement de la vapeur dans les canaux d'alimentation de la membrane. L'injection directe de vapeur chauffait rapidement les espèces encrassantes à la surface de la membrane, et les gouttelettes d'eau dans la vapeur saturée provoquaient des abrasions superficielles qui finissaient par écorcher le bitume de la surface de la membrane. Les flux membranaires lorsque la régénération à la vapeur était active étaient jusqu'à 4 fois plus élevés que ceux des tests utilisant uniquement le rétrolavage au perméat traditionnel.

Les techniques d'atténuation d'encrassements développées dans ce travail ont une large applicabilité potentielle dans les systèmes de filtration à membrane céramique destinés à traiter toutes les eaux usées contenant des composés bitumineux, telles que les eaux de pétrole en général et les eaux contaminées provenant de déversements d'hydrocarbures.

Statement of Contributions of Collaborators

I am the first author of all the paper-based chapters written in this thesis.

Chapters 1, 2 and 8 were written solely by me with editorial comments provided by Dr. André Y. Tremblay.

Chapter 3 is a manuscript published in a peer-reviewed academic journal. The initial membrane modifications, membrane filtration set-up and tests were all developed under the supervision of Dr. Tremblay. The filtration runs, FTIR measurements and particle size analyses were all performed by myself. ICP and TOC sample characterization were performed by the CanmetMINING Analytical Services Group (ASG). Data analysis was performed by myself with the assistance of Dr. Tremblay. The manuscript was written solely by myself with editorial comments provided by Dr. Tremblay and Dr. Mortazavi (NRCan). They are both co-authors on the manuscript.

Chapter 4 is a manuscript published in a peer-reviewed academic journal. I performed all membrane modifications and membrane filtration tests, as well as all FTIR, contact angle and zeta potential measurements and SEM images. The membrane EDS spectra were taken by Jianqun Wang of the Nano Imaging Facility at Carleton University. Data analysis was performed by myself with the assistance of Dr. Tremblay. The manuscript was written solely by myself with editorial comments provided by Dr. Tremblay and Dr. Mortazavi (NRCan). They are both co-authors on the manuscript.

Chapter 5 is a manuscript published in a peer-reviewed academic journal. The original equipment for membrane tube modification was designed by Dr. Tremblay and myself. Initial membrane modifications were performed by Dr. Tremblay and I, while all subsequent modifications were carried out by myself. Membrane filtration tests were performed at CanmetMINING by Alex Doiron (NRCan) and myself with the aid of Aartee Khandelwal (NRCan). Mrs. Khandelwal is acknowledged in the published manuscript. Mr. Doiron also assisted with the writing of the experimental section of the manuscript and is listed as a co-author. The rest of the manuscript was written solely by myself with editorial comments provided by Dr. Tremblay and Dr. Mortazavi (NRCan), who both also assisted with data

analysis. They are both co-authors on the manuscript. Feed and permeate sample characterizations were performed by the CanmetMINING Analytical Services Group (ASG).

Chapter 6 is a manuscript published in a peer-reviewed academic journal. Membrane filtration tests were performed at CanmetMINING by Alex Doiron (NRCan) and myself with the aid of Aartee Khandelwal (NRCan). Mrs. Khandelwal is acknowledged in the published manuscript. Mr. Doiron also assisted with the writing of the experimental section of the manuscript and is listed as a co-author. The rest of the manuscript was written solely by myself with editorial comments provided by Dr. Tremblay and Dr. Mortazavi (NRCan), who both also assisted with data analysis. They are both co-authors on the manuscript. Feed and permeate sample characterizations were performed by the CanmetMINING Analytical Services Group (ASG), except for particle size analyses which were performed by myself.

Chapter 7 is a manuscript prepared for submission to a peer-reviewed academic journal. The experimental data used in conjunction with the various filtration models was taken from experiments that were presented in our previous published works (Chapters 3 & 6). All of the calculations and computations were performed by myself. The manuscript was solely written by myself with editorial comments provided by Dr. Tremblay, who is listed as a co-author. Some of the experimental data used was obtained at CanmetMINING in collaboration with Dr. Mortazavi, who is listed as a co-author.

Acknowledgements

First and foremost, I wish to express my genuine gratitude to my supervisor, Professor André Tremblay. His guidance over the course of my stay at uOttawa, dating back to my undergraduate studies, has had a profound influence on my development, both academic and personal. He provided me with the freedom to pursue my own ideas while still offering valuable suggestions and encouragement, and I will greatly miss our weekly discussions. I consider myself fortunate to have had a supervisor who dedicates so much time and attention to his students and hope to one day be able to emulate his example.

I would also like to thank Dr. Saviz Mortazavi of Natural Resources Canada (NRCan) for the support and guidance he provided during my graduate studies. I am particularly grateful for having had the opportunity to work at the CanmetMINING facilities for a portion of my time as a doctoral student. The experience I gained there was invaluable, and many thanks go to the members of Dr. Mortazavi's group who were there during my tenure (Alex Doiron, Sanaz Mosadegh, Lucie Morin and Aartee Khandelwal).

Much of the experimental work I performed at uOttawa could not have been possible without the Chemical & Biological Engineering technical staff (Louis Tremblay, Franco Ziroldo, Gérard Nina and James Macdermid). Their indispensable assistance is gratefully acknowledged. A special thanks also goes to the department's administrative staff (Francine Pétrin and Sylvie Saindon) for their help with administrative matters over the years.

I am incredibly thankful for the many friends that I have made in the department over the last five years. I can only hope to one day work again in an environment with people as wonderful as my graduate school colleagues. Yasmine, Fahad, Dean, Katrina, Shaz, Tolu, Shidan, Emily, Géraldine, Farhad, Sean, David, Vida, Marie, Johnny, Alex, Milad, Ali, Amir, Niloofar, Mohamed, Chris, Curtis…and I could probably go on for another few lines. Each of you positively impacted my journey, and I wish you all nothing but the best in all future personal and professional endeavors.

Lastly, I wish to acknowledge funding support from NRCan through the Program for Energy Research and Development (PERD) and the eco-Energy Innovation Initiative (eco-EII). I am also grateful to have received scholarships through the Ontario Graduate Scholarship (OGS) and the NSERC Canada Graduate Scholarships – Master's (CGS M) and Postgraduate Scholarship – Doctoral (PGS D) programs.

Dedication

I wish to dedicate this thesis to my parents, Elias and Helene. They left behind their previous lives and the country they considered home when they moved from Lebanon to Canada. They did so with no assurances of prosperity, but simply with the hope of providing a better outlook for the future of their family. Their selflessness and unconditional love towards me will always be unparalleled. The opportunity to pursue my passion for knowledge and understanding is owed to them, and for that I will forever be infinitely grateful.

I love you, mama and baba.
Thank you, and I hope I have made you proud.

TABLE OF CONTENTS

List of Figures

List of Tables

Nomenclature

Acronyms

ATR	Attenuated total reflectance
BIS-PEO_{25-30}TES	Bis(3-triethoxysilylpropyl)polyethylene oxide (25–30 EO)
CFV	Crossflow velocity
DOM	Dissolved organic matter
EDS	Energy dispersive X-ray spectroscopy
FAS	Fluoroalkylsilane
FRR	Flux recovery ratio
FTIR	Fourier-transform infrared spectroscopy
HA	Humic acid
ICP-AES	Inductively coupled plasma atomic emission spectroscopy
IEP	Isoelectric point
IGF	Induced gas flotation
Lmh	Liters per meter squared per hour
LOD	Limit of detection
MD	Membrane distillation
MW	Molecular weight
MWCO	Molecular weight cutoff
NA	Naphthenic acid
NDIR	Non-dispersive infrared spectroscopy
NMR	Nuclear magnetic resonance
NRCan	Natural Resources Canada
OE	Osmotic evaporation
ORF	Oil removal filter
PDMS	Polydimethylsiloxane
PEG	Polyethylene glycol
PEO	Polyethylene oxide
PEOTMS	2-[methoxy(polyethyleneoxy)6–9propyl]trimethoxysilane
PEO_{6-9}TMS	See PEOTMS
PEO_{9-12}TMS	2-[methoxy(polyethyleneoxy)9–12propyl]trimethoxysilane
PV	Pervaporation
PVP	Polyvinylpyrrolidone
PVAc	Poly(vinyl acetate)
PWP	Pure water permeate
RMSE	Root-mean-square error
SAGD	Steam-assisted gravity drainage
SEM	Scanning electron microscopy
TMP	Transmembrane pressure
TOC	Total organic carbon
VTAS	Vinyltrialkoxysilane
WLF	Williams-Landel-Ferry

Symbols – Latin Letters

A	Membrane surface area (m^2)
A_o	Initial membrane surface area (m^2)
C_b	Bulk concentration (kg/m^3)
C_F	Concentration of total oil, TOC, sulphate or chloride in the feed (ppm)
C_P	Concentration of total oil, TOC, sulphate or chloride in the permeate (ppm)
C_1	WLF equation constant
C_2	WLF equation constant (K)
d_P	Particle diameter (m)
D_h	Pore hydraulic diameter (m)
D_B	Brownian diffusivity (m^2/s)
D_S	Shear-induced diffusivity (m^2/s)
$\widehat{D}_S$	Dimensionless shear-induced diffusivity
f	Friction factor
f'	Fraction of solutes that contribute to fouling deposit growth
g_z	Gravitational acceleration in the axial z-direction (m/s^2)
J	Permeate flux ($m^3/m^2/s$)
J_A	First recorded flux after a backflush ($L/m^2/h$)
J_B	Last recorded flux before a backflush ($L/m^2/h$)
J_{cr}	Critical flux ($m^3/m^2/s$)
J_N	Permeate flux normalized for temperature and pressure ($L/m^2/h$)
J_o	Initial flux though a clean membrane ($m^3/m^2/s$)
k	Geometric correction factor in the modified Hagen-Poiseuille equation
k_B	Boltzmann constant (J/K)
K	Constant in Hou et al. combined filtration model
K_b	Constant in Hou et al. combined filtration model (s^{-1})
K_c	Constant in Hou et al. combined filtration model (s/m^2)
K_{CB}	Constant in complete blocking model (s^{-1})
K_{CF}	Constant in cake filtration model (s^{-1})
K_{IB}	Constant in intermediate blocking model (s^{-1})
K_{PC}	Constant in pore constriction model (s^{-1})
K_1	Constant in Ho & Zydney combined filtration model (s^{-1})
K_2	Constant in Ho & Zydney combined filtration model (s^{-1})
K_3	Constant in Ho & Zydney combined filtration model (s^{-1})
L	Membrane module length (m)
L_o	Pore length (m)
$\dot{m}$	Mass flow rate (kg/s)
N	Number of pores
N_o	Initial pore density (kg/m^3)
P	Pressure (Pa)
P_N	Normalization pressure (Pa)
Q	Pure water flow rate through a membrane (m^3/s)

Q_{cr} Double integral related to the critical excess particle flux towards membrane surface (m^4/s^2)
r Radial position in a cylinder (m)
r_o Cylindrical membrane channel radius (m)
r_p Particle radius (m)
R_c Cake resistance (m^{-1})
R_c' Specific cake resistance (m^{-2})
R_{IB} Filter resistance in intermediate blocking model (m^{-1})
R_m Hydraulic resistance of the membrane (m^{-1})
R_{c0} Resistance of a single solute aggregate (m^{-1})
Re Reynolds number
t Time (s)
T Temperature (K)
T_r Reference temperature (K)
V Accumulated permeate volume per membrane surface area (m^3/m^2)
V_F Initial volume of feed solution in the feed tank (m^3)
V_P Accumulated permeate volume at a given time (m^3)
v Velocity (m/s)
v_z Velocity in the axial z-direction (m/s)
X_{cr} Critical length (m)
z Axial position in a cylinder (m)

Symbols – Greek Letters

α Pore blockage parameter (m^2/kg)
α_{CB} Pore blockage efficiency
α_{PC} Pore constriction efficiency
$\dot{\gamma}$ Shear rate (s^{-1})
$\dot{\gamma}_w$ Shear rate related to the shear stress at the membrane wall (s^{-1})
δ_c Cake thickness (m)
ε Membrane surface roughness (m)
η Dimensionless relative viscosity
μ Viscosity (Pa·s)
μ_N Viscosity of the permeate at the normalization temperature (Pa·s)
μ_o Viscosity of the feed solution (Pa·s)
ρ Density (kg/m^3)
σ_{IB} Blocked area per unit permeate volume (m^2/m^3)
τ_{rz} Shear stress in the radial direction due to fluid motion in the axial direction (Pa)
Φ Particle volume fraction
Φ_{max} Particle volume fraction in a maximally packed cake
Φ_o Particle volume fraction in the feed solution

1 General Introduction

1.1 Background and motivation

The treatment of oily process waters containing bitumen is a demanding application for any technology. Such contaminated waters are differentiated from simple oil-in-water emulsions by the fact that they contain bituminous fine clays and colloids that can act as severe scalants. This causes many problems in treatment processes as scaling negatively affects equipment like tubing, valves and pumps [1]. Oily process waters are produced in large volumes on a daily basis mostly as a consequence of oil and gas extraction processes, but also by oil spills. In all cases, it is desirable to treat the contaminated waters for purposes of recycling or disposal.

Oil spills entail the accidental release of petroleum products into the environment. These events can release significant amounts of oil into marine ecosystems, as was seen with the Deepwater Horizon tanker in 2010 where 4.9 million barrels of oil were spilled into the Gulf of Mexico [2]. Treatment of these spills includes physical, chemical and biological methods. Common physical techniques involve the skimming of oil from the water surface or the use of high-temperature booms to burn surface oil in-situ [2]. These techniques however lack the efficient capability of removing emulsified oils. The most predominant chemical method is the use of sorbents that have a high affinity for crude oil uptake. Much research has been focused on developing highly efficient sorbent materials. These include polymeric foams [3–6], fibers [7,8], sponges [9] and waste products [10], as well as mineral powders [11]. Natural bio-based materials have also been investigated as environmentally friendly alternative sorbents [12–17]. Such sorbent materials are however limited to small-scale oil spills [2]. All current oil spill cleanup techniques possess limitations pertaining to inefficiency, high cost and environmental harmfulness, offering the possibility of new methods to be used in this application [18].

In the oil and gas industry, water that is produced as a by-product during extraction processes is termed produced water. Worldwide, upwards of 70 billion barrels of produced water are produced annually [19]. Produced water can result from natural gas, oilfield, coal bed methane, shale gas or oil sands operations among many others. Depending on the source and the utilized extraction technology, the chemical composition and physical characteristics of produced water can vary significantly, although bitumen is a common constituent. A significant amount of the

generated produced water is discharged into the environment [20], which raises critical environmental concerns. It has been well documented that this release of produced water can lead to adverse effects such as air pollution and contamination of soil and water resources [21,22]. Regulations for discharge vary from region to region, with allowable oil concentrations ranging from 10–50 ppm [23]. Discharge regulations have become stricter over the years, with some organizations adopting "zero discharge" policies as environmental effects become more evident. Produced water can also be recycled for reuse in many applications including livestock watering, wildlife habitat watering, irrigation and algae production, with each application having its own purification requirements [19]. In the case of the Canadian oil sands, where only 18% of oil sands deposits are recoverable by surface mining, steam-based in-situ extraction technologies are applied and the treated produced water is recycled for steam production [24]. However, the boilers used to produce steam cannot tolerate solids contents in excess of 8000 ppm [25]. Many conventional treatment technologies have been developed to address the requirements of produced water purification for recycle or discharge. These include physical, chemical, thermal and biological processes [19,20,23,26–29]. Physical treatment techniques consist mostly of filtration, flotation, hydrocyclones, electrodialysis and adsorption technologies. Chemical treatment is achieved using precipitation, oxidation, electrochemical, coagulation, ion exchange and demulsifcation processes among many others. Biological methods entail the usage of activated sludge, aerated filters, microalgae and microbial fuel cells. Thermal technologies for produced water treatment include evaporation, multistage flash, multi-effect distillation, vapour compression distillation and freeze thaw/evaporation. Alternative technologies are currently under development that are capable of generating steam directly from the source produced water while requiring low separation of particulates. An example of such a process is high-pressure oxy-firing direct contact steam generation [30].

Many of the aforementioned treatment options are marred by high costs and a lack of efficiency. This is especially true in the case of thermal technologies, where high energy costs are a result of low energy efficiency. Inefficient separation processes that result in oil-contaminated produced water can lead to downstream process upsets, such as scaling and failure in steam boilers, which require costly cleaning and maintenance downtime. This is the case in the Canadian oil sands, where the conventional oil separation process cannot reliably and consistently provide clean produced water for steam production [25]. The result of this contamination is an overall increase

in the greenhouse gas emissions of the steam injection extraction processes that are used [31]. A developing technology to remedy this problem is the use of membrane filtration to treat produced water. Membranes are considered the most promising technology in this application due to high separation and energy efficiency, easy operation and low maintenance cost [32–34]. Their use in produced water filtration is a highly topical issue, as evidenced by the many review papers recently published [35–40]. Membrane fouling, however, remains a significant obstacle to the widespread acceptance of membrane filtration as a produced water treatment technology.

When identifying foulants in the filtration of produced water or oil spill wastewater, bitumen associated solids must be taken into consideration. These solids include aggregates of quartz, clays and heavy minerals that are bound together by carbonates, iron oxide and humic matter [41]. The most problematic of the bitumen associated solids have been determined as being ultrafine clays [41–44]. These ultrafines are very thin aluminosilicate clay crystallites onto which organic bitumen molecules and humic matter are adsorbed. A conceptual visualization of these bituminous fines is shown in Figure 1.1 below.

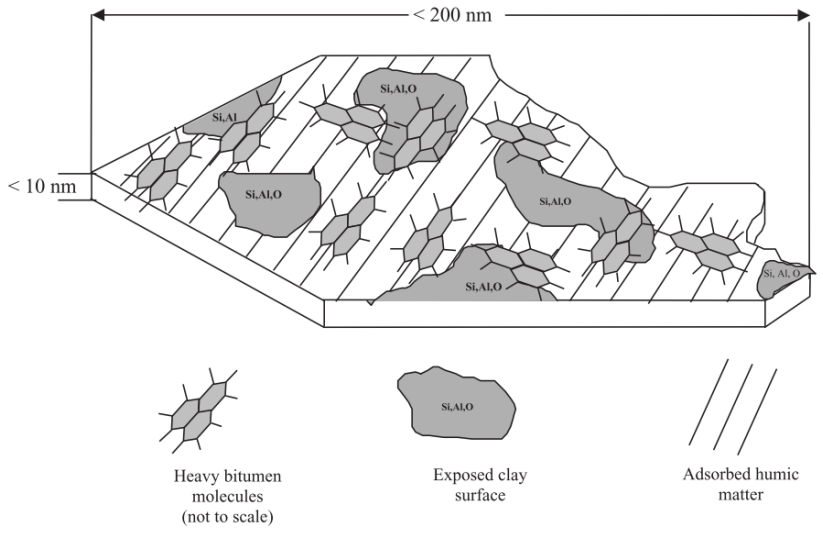

Figure 1.1: Conceptual visualization of bituminous ultrafine clay crystallites [41].

Therefore, major potential foulants in this application are silicates and adsorbed carbon-rich solids. The surfaces of heavy bitumen molecules, such as asphaltenes, have been shown to possess acidic, basic and amphoteric functional groups [45–47]. This indicates that bituminous fines can exhibit both negative and positive surface charges. An example of a possible molecular structure for bituminous asphaltenes is shown in Figure 1.2.

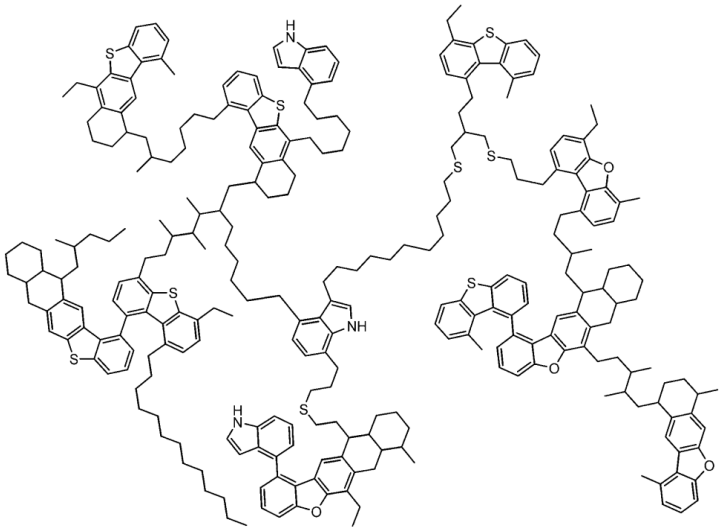

Figure 1.2: Possible molecular structure for asphaltenes [48].

Asphaltenes are among the three main constituents of bitumen, along with maltenes and resins. Maltenes are considered as the continuous oily bitumen phase, in which asphaltenes exist as colloidal suspensions [49]. The colloids are stabilized by the resins, as asphaltenes would aggregate and flocculate in their absence. These compounds can be quantified through fractionation, during which solvents such as benzene and toluene are used to solubilize and extract asphaltenes. Membrane surfaces are often also charged, much like the discussed bituminous foulants. It is possible that this mutual surface charging is a major contributor to the severe fouling observed in treating bitumen-laden waters with membranes. Two methods of fouling mitigation that can be explored in this challenging application are the use of surface modifications to yield antifouling membranes [50] and the employment of two-phase flow regimes to clear surface deposits [51].

1.2 Project objectives and hypothesis

The overall goal of this project was to increase the lifetime of ceramic membranes in applications for the treatment of wastewater containing highly charged organic and/or particulate bituminous matter. This was attempted using two methods; firstly through surface modification of the membranes to render them fouling-resistant, and secondly by using direct periodic steam injection to generate two-phase flow regimes that remove foulants from the membrane surface.

Based on these objectives, the hypotheses of this thesis are as follows:

1. *Charge neutral and hydrophilic ceramic membrane surfaces will reduce membrane fouling in treating produced waters containing bituminous fines.*
2. *Use of steam fed directly in the membrane lumen will enhance flux and separation performance.*

1.3 Thesis structure

This thesis consists of 8 chapters. The current chapter is the General Introduction. Chapter 2 presents a review of the literature on ceramic membrane filtration of produced water and the surface modification of ceramic membranes. Chapters 3 to 7 each represent an independent article published in or prepared for submission to a peer-reviewed academic journal. Due to this structure, some repetition of ideas and elements (i.e. experimental methodology) was inevitable. Chapter 8 provides a general discussion, conclusions, and recommendations for future work that pertains to the entire thesis. Literature cited is included in the form of separate bibliographies at the end of each individual chapter.

CHAPTER 3 – Silane Surface Modified Ceramic Membranes for the Treatment and Recycling of SAGD Produced Water; published in the Journal of Petroleum Science and Engineering 157 (2017): 349–358.

A lab-scale study on the use of polyethylene oxide (PEO)-based organosilanes for surface modification of ceramic membranes in the treatment of steam-assisted gravity drainage (SAGD) produced water was carried out in this work. A straight chain PEO-silane with 6–9 PEO repeat units was used to modify the surfaces of flat ceramic membrane disks with pore sizes of 0.14 µm, 300 kDa and 150 kDa. These membranes were then used to treat real oil sands produced water obtained from SAGD facilities in Alberta. The results successfully demonstrated that it was possible to modify ceramic membranes to exhibit fouling-resistant properties to bituminous solids and consequently enhance their performance in treating SAGD produced waters. In all cases, surface modification increased permeate flux relative to unmodified membranes. The filtered water obtained from the modified membranes was also of superior quality, to that of the untreated membrane, as evidenced by total organic carbon analysis.

CHAPTER 4 – Thermal Stability of Hydrophilic PEO-silane Modified Ceramic Membranes; published in Colloids and Surfaces A: Physicochemical and Engineering Aspects 561 (2019): 254–266.

In this work, a detailed study on the treatment conditions during the surface modification of ceramic membranes with PEO-based organosilanes was performed. The effects of silane concentration, water concentration and silylation reaction time on the extent of surface modification with various ceramic membrane materials were studied. The thermal stability of PEO-silane layers was also investigated. Membrane surfaces were characterized using FTIR, SEM and contact angle and zeta potential measurements. The most reactive and thermally stable material was determined to be TiO_2, which retained more surface silane upon exposure to elevated temperatures relative to ZrO_2 and ZrO_2-TiO_2 membranes. It was also found that increasing the number of repeat PEO units in the silane from 6–9 to 9–12 increased the silane layer's thermal stability. The results suggest that in enhancing the suitability of ceramic membranes in challenging applications, TiO_2 membranes over ZrO_2 and ZrO_2-TiO_2 should be used and modified with PEO-silanes containing 9–12 repeat units to ensure maximal surface coverage and enhanced thermal stability.

CHAPTER 5 – Surface Modified Multi-lumen Tubular Membranes for SAGD Produced Water Treatment; published in Energy & Fuels 33 (2019): 5766–5776.

A pilot-scale study that extends the lab-scale study presented in Chapter 3 was carried out in this work. Commercially available multilumen tubular ceramic membranes with selective layers of TiO_2 or γ-Al_2O_3 were surface modified with various straight-chain and dipodal PEO-based organosilanes. The membrane tubes were tested in a pilot-scale crossflow ultrafiltration system at CanmetMINING with field samples of SAGD produced water from the oil sands in Alberta. Results indicated that the modification led to an improvement in permeate flux by factors as high as 2.9 relative to unmodified membranes. The modifications also improved membrane flux recovery factors upon backflushing. Furthermore, modified membranes were able to maintain high fluxes and showed less flux decline upon exposure to more recalcitrant produced water feeds with higher pH and TOC. The success observed with the PEO-silane modified lab-scale membrane disks was thus extended to pilot-scale commercial membrane tubes.

CHAPTER 6 – In-process Steam Cleaning of Ceramic Membranes Used in the Treatment of Oil Sands Produced Water; published in Industrial & Engineering Chemistry Research 58 (2019): 15232–15243.

In this work, a pilot-scale study to evaluate the potential of an in-process steam cleaning technique for ceramic membranes in the treatment of oil sands produced water was performed. This regeneration technique consisted of periodically injecting pressurized saturated steam at 120 °C directly into the membrane feed channels. Commercially available multilumen tubular ceramic membranes were tested in the same pilot-scale setup used in Chapter 5 at CanmetMINING. Permeate flux improvements by factors as high as 4 were observed when the steam regeneration method was activated. Application of steam cleaning also improved separation performance, increasing membrane retention of various foulants by 10–20%. The continuous in-process steam cleaning method offers many possibilities for waste minimization since chemical cleaning fluids are entirely avoided.

CHAPTER 7 – Modeling of Membrane Filtration and Fouling in the Treatment of Bitumen-containing Wastewater; to be submitted to a peer-reviewed academic journal.

This study consisted of a theoretical investigation of membrane filtration and fouling in the treatment of oil sands produced water. Various filtration models accounting for both single and combined fouling mechanisms were fitted to some of the experimental data presented in Chapters 3 and 6. The results of the fitted models suggested that bituminous fouling occurs via a combined intermediate/standard blocking and cake filtration mechanism, and that the contribution of cake formation increases at smaller membrane pore sizes. The cake thickness and particle size values that were calculated from these fitted models were in good agreement with previously published empirical data. The effect of temperature on foulant layer mobility and formation was also theoretically investigated. It was shown that filtration would need to occur at temperatures in the vicinity of 120 °C to avoid the formation of a stagnant cake layer in treating oil sands produced water without backflushing. This suggests that traditional permeate backflushing should be coupled with a high temperature fouling mitigation technique, such as steam cleaning, when treating recalcitrant bituminous feed wastewaters.

References

[1] M. Crabtree, D. Eslinger, P. Fletcher, M. Miller, A. Johnson, G. King, Fighting Scale — Removal and Prevention, Oilfield Review. (1999) 30–45.

[2] B. Doshi, M. Sillanpää, S. Kalliola, A review of bio-based materials for oil spill treatment, Water Research. 135 (2018) 262–277.

[3] J. Pinto, A. Athanassiou, D. Fragouli, Surface modification of polymeric foams for oil spills remediation, Journal of Environmental Management. 206 (2018) 872–889.

[4] O. Oribayo, X. Feng, G.L. Rempel, Q. Pan, Synthesis of lignin-based polyurethane/graphene oxide foam and its application as an absorbent for oil spill clean-ups and recovery, Chemical Engineering Journal. 323 (2017) 191–202.

[5] O. Oribayo, X. Feng, G.L. Rempel, Q. Pan, Modification of formaldehyde-melamine-sodium bisulfite copolymer foam and its application as effective sorbents for clean up of oil spills, Chemical Engineering Science. 160 (2017) 384–395.

[6] H. Li, L. Liu, F. Yang, Oleophilic Polyurethane Foams for Oil Spill Cleanup, Procedia Environmental Sciences. 18 (2013) 528–533.

[7] I.A.H. Al Zubaidi, A.K. Al Tamimi, H. Ahmed, Remediation of water from crude oil spill using a fibrous sorbent, Environmental Technology and Innovation. 6 (2016) 105–114.

[8] J. Lin, Y. Shang, B. Ding, J. Yang, J. Yu, S.S. Al-Deyab, Nanoporous polystyrene fibers for oil spill cleanup, Marine Pollution Bulletin. 64 (2012) 347–352.

[9] D. Wu, L. Fang, Y. Qin, W. Wu, C. Mao, H. Zhu, Oil sorbents with high sorption capacity, oil/water selectivity and reusability for oil spill cleanup, Marine Pollution Bulletin. 84 (2014) 263–267.

[10] J. Saleem, C. Ning, J. Barford, G. McKay, Combating oil spill problem using plastic waste, Waste Management. 44 (2015) 34–38.

[11] M. Patowary, R. Ananthakrishnan, K. Pathak, Superhydrophobic and oleophilic barium sulfate material for oil spill clean-ups: Fabrication of surface modified sorbent by a one-step interaction approach, Journal of Environmental Chemical Engineering. 2 (2014) 2078–2084.

[12] G. Alaa El-Din, A.A. Amer, G. Malsh, M. Hussein, Study on the use of banana peels for oil spill removal, Alexandria Engineering Journal. 57 (2018) 2061–2068.

[13] O.A. Galblaub, I.G. Shaykhiev, S. V. Stepanova, G.R. Timirbaeva, Oil spill cleanup of water surface by plant-based sorbents: Russian practices, Process Safety and Environmental Protection. 101 (2016) 88–92.

[14] M.M. Tijani, A. Aqsha, N. Mahinpey, Development of oil-spill sorbent from straw biomass waste: Experiments and modeling studies, Journal of Environmental Management. 171 (2016) 166–176.

[15] T. Dong, G. Xu, F. Wang, Oil spill cleanup by structured natural sorbents made from cattail fibers, Industrial Crops and Products. 76 (2015) 25–33.

[16] O. Abdelwahab, Assessment of raw luffa as a natural hollow oleophilic fibrous sorbent for oil spill cleanup, Alexandria Engineering Journal. 53 (2014) 213–218.

[17] V.R. Olga, V.I. Darina, A.I. Alexandr, A.O. Alexandra, Cleanup of Water Surface from Oil Spills Using Natural Sorbent Materials, Procedia Chemistry. 10 (2014) 145–150.

[18] A.A. Al-Majed, A.R. Adebayo, M.E. Hossain, A sustainable approach to controlling oil spills, Journal of Environmental Management. 113 (2012) 213–227.

[19] M.A. Al-Ghouti, M.A. Al-Kaabi, M.Y. Ashfaq, D.A. Da'na, Produced water characteristics, treatment and reuse: A review, Journal of Water Process Engineering. 28 (2019) 222–239.

[20] E.T. Igunnu, G.Z. Chen, Produced water treatment technologies, International Journal of Low-Carbon Technologies. 9 (2014) 157–177.

[21] S. Jamaly, A. Giwa, S.W. Hasan, Recent improvements in oily wastewater treatment: Progress, challenges, and future opportunities, Journal of Environmental Sciences. 37 (2015) 15–30.

[22] J. Pitchel, Oil and Gas Production Wastewater: Soil Contamination and Pollution Prevention, Applied and Environmental Soil Science. 2016 (2016).

[23] S. Jiménez, M.M. Micó, M. Arnaldos, F. Medina, S. Contreras, State of the art of produced water treatment, Chemosphere. 192 (2018) 186–208.

[24] E.W. Allen, Process water treatment in Canada's oil sands industry: I. Target pollutants and treatment objectives, Journal of Environmental Engineering and Science. 7 (2008) 123–138.

[25] V. Lightbown, New SAGD Technologies Show Promise in Reducing Environmental Impact of Oil Sand Production, Oil, Gas, and Mining. 1 (2012) 1–12.

[26] M. Nasiri, I. Jafari, B. Parniankhoy, Oil and Gas Produced Water Management: A Review of Treatment Technologies, Challenges, and Opportunities, Chemical Engineering Communications. 204 (2017) 990–1005.

[27] R.T. Duraisamy, A.H. Beni, A. Henni, State of the Art Treatment of Produced Water, in: W. Elshorbagy, R.K. Chowdhury (Eds.), Water Treatment, IntechOpen, 2013: pp. 199–222.

[28] A. Fakhru'l-Razi, A. Pendashteh, L.C. Abdullah, D.R.A. Biak, S.S. Madaeni, Z.Z. Abidin, Review of technologies for oil and gas produced water treatment, Journal of Hazardous Materials. 170 (2009) 530–551.

[29] E.W. Allen, Process water treatment in Canada's oil sands industry: II. A review of emerging technologies, Journal of Environmental Engineering and Science. 7 (2008) 499–524.

[30] P.E.C. Cairns, B.R. Clements, R. Hughes, T. Herage, L. Zheng, A. Macchi, E.J. Anthony, High-Pressure Oxy-Firing (HiPrOx) of Fuels with Water for the Purpose of Direct Contact Steam Generation, Energy and Fuels. 29 (2015) 4522–4533.

[31] Y. Wang, S. Ren, L. Zhang, C. Hu, Energy efficiency and greenhouse gas emissions of current steam injection process and promising steam based techniques for heavy oil reservoirs, Journal of Petroleum Science and Engineering. 166 (2018) 842–849.

[32] M. Padaki, R. Surya Murali, M.S. Abdullah, N. Misdan, A. Moslehyani, M.A. Kassim, N. Hilal, A.F. Ismail, Membrane technology enhancement in oil-water separation. A review, Desalination. 357 (2015) 197–207.

[33] S. Huang, R.H.A. Ras, X. Tian, Antifouling membranes for oily wastewater treatment: Interplay between wetting and membrane fouling, Current Opinion in Colloid and Interface Science. 36 (2018) 90–109.

[34] Y. Zhu, D. Wang, L. Jiang, J. Jin, Recent progress in developing advanced membranes for emulsified oil/water separation, NPG Asia Materials. 6 (2014) e101.

[35] S. Adham, A. Hussain, J. Minier-Matar, A. Janson, R. Sharma, Membrane applications and opportunities for water management in the oil & gas industry, Desalination. 440 (2018) 2–17.

[36] K.L. Jepsen, M.V. Bram, S. Pedersen, Z. Yang, Membrane fouling for produced water treatment: A review study from a process control perspective, Water. 10 (2018) 847.

[37] J.M. Dickhout, J. Moreno, P.M. Biesheuvel, L. Boels, R.G.H. Lammertink, W.M. De Vos, Produced water treatment by membranes : A review from a colloidal perspective, Journal of Colloid and Interface Science. 487 (2017) 523–534.

[38] S. Munirasu, M.A. Haija, F. Banat, Use of membrane technology for oil field and refinery produced water treatment–A review, Process Safety and Environmental Protection. 100 (2016) 183–202.

[39] S. Alzahrani, A.W. Mohammad, Challenges and trends in membrane technology implementation for produced water treatment: A review, Journal of Water Process Engineering. 4 (2014) 107–133.

[40] K.S. Ashaghi, M. Ebrahimi, P. Czermak, Ceramic Ultra- and Nanofiltration Membranes for Oilfield Produced Water Treatment: A Mini Review, Open Environmental Sciences. 1 (2008) 1–8.

[41] B.D. Sparks, L.S. Kotlyar, J.B. O'Carroll, K.H. Chung, Athabasca oil sands: effect of organic coated solids on bitumen recovery and quality, Journal of Petroleum Science and Engineering. 39 (2003) 417–430.

[42] L.S. Kotlyar, B.D. Sparks, J.R. Woods, K.H. Chung, Solids associated with the asphaltene fraction of oil sands bitumen, Energy & Fuels. 13 (1999) 346–350.

[43] F. Bensebaa, L. Kotlyar, B. Sparks, Organic coated solids in Athabasca bitumen: characterization and process implications, The Canadian Journal of Chemical Engineering. 78 (2000) 610–616.

[44] J. Liu, Z. Xu, J. Masliyah, Role of fine clays in bitumen extraction from oil sands, AIChE Journal. 50 (2004) 1917–1927.

[45] A. Jada, M. Salou, Effects of the asphaltene and resin contents of the bitumens on the water-bitumen interface properties, Journal of Petroleum Science and Engineering. 33 (2002) 185–193.

[46] M.A. Rodríguez-Valverde, M.A. Cabrerizo-Vílchez, A. Páez-Dueñas, R. Hidalgo-Álvarez, Stability of highly charged particles: bitumen-in-water dispersions, Colloids and Surfaces A: Physicochemical and Engineering Aspects. 222 (2003) 233–251.

[47] O. V. Abramov, V.O. Abramov, S.K. Myasnikov, M.S. Mullakaev, Extraction of bitumen, crude oil and its products from tar sand and contaminated sandy soil under effect of ultrasound, Ultrasonics Sonochemistry. 16 (2009) 408–416.

[48] J.M. Sheremata, M.R. Gray, H.D. Dettman, W.C. McCaffrey, Quantitative molecular representation and sequential optimization of Athabasca asphaltenes, Energy & Fuels. 18 (2004) 1377–1384.

[49] L.S. Kotlyar, B.D. Sparks, J.R. Woods, S. Raymond, Y. Le Page, W. Shelfantook, Distribution and Types of Solids Associated With Bitumen, Petroleum Science and Technology. 16 (1998) 1–19.

[50] D. Rana, T. Matsuura, Surface modifications for antifouling membranes, Chemical Reviews. 110 (2010) 2448–2471.

[51] Y. Wibisono, E.R. Cornelissen, A.J.B. Kemperman, W.G.J. Van Der Meer, K. Nijmeijer, Two-phase flow in membrane processes: A technology with a future, Journal of Membrane Science. 453 (2014) 566–602.

2 Literature Review

2.1 Membranes for produced water treatment

2.1.1 Introduction

Historically, polymeric membranes have been used in the treatment of oily wastewaters more frequently than ceramic membranes [1–5]. Recent years, however, have seen a transition towards the more common use of ceramic membranes. This is in part due to the fact that ceramic membranes possess higher thermal and chemical stability relative to polymeric counterparts while offering similar filtration performance [6]. This allows oily wastewaters to be treated at higher temperatures in order to reduce their viscosity and improve flux performance. It has also been demonstrated that ceramic membranes possess a lower fouling tendency towards natural organic matter and enhanced cleaning efficiency [7]. Another advantage is the fact that, unlike polymeric membranes, ceramic membranes are not susceptible to swelling in the presence of chemicals and solvents [8,9]. Previous work with polymeric membrane filtration of bituminous wastewaters has been negatively hindered by membrane swelling caused by ions and charged organic matter in the feed water [10]. For these reasons, ceramic membranes are being increasingly studied in this application and will be the focus of this literature review.

2.1.2 Filtration of synthetic oily water emulsions

Produced water is at its essence an unstable emulsion of oil and bitumen in water. Studies involving the application of ceramic membranes in the treatment of synthetic oil-in-water emulsions are abundant dating back several decades. In the literature, synthetic mixtures are prepared by emulsifying either pure hydrocarbons [11–17], crude oil [18–29], petroleum products [21,30–39], waste oils [40,41], edible oils [42–48] or commercial oils [6,49–54] with water. In these studies, both high fluxes (>500 $L/m^2/h$) and high oil rejection rates (>95%) are often reported. Furthermore, many of these works have also endeavoured to characterize the fouling mechanisms involved in synthetic oil/water emulsion separation and the fouling phenomenon is generally well-established in this application. Recent work in this area has mainly been focused on the synthesis and development of novel ceramic membranes made from inexpensive raw materials such as fly ash and various clay mixtures. However, the performance of ceramic membranes in treating synthetic oil/water emulsions is not representative of their performance in treating produced water. The utilized oily water mixtures do not accurately

represent the complex chemical composition of actual produced water, which contains a significant amount of dispersed and dissolved organic-coated solids and clays.

2.1.3 Filtration of synthetic produced water

A few studies have attempted to prepare synthetic oily water emulsions that better emulate the physicochemical characteristics of real produced water. This was accomplished by the addition of inorganic salts and other solids to the emulsions. Studies that made use of such synthetic feeds are summarized in Table 2.1. In all cases, membrane performance was found to decrease upon introduction of solids and particulates to the emulsion feeds. Tanudjaja et al. [55] determined that even the addition of NaCl salt without any other solids to hexadecane emulsions decreased the membrane critical flux, indicating a higher propensity for foulant layer formation at the membrane surface. Recently, Abdalla et al. [31] observed that the addition of bentonite clay to a diesel oil emulsion decreased membrane permeability by a factor of 16 when compared to the native emulsion.

Table 2.1: Previous studies on ceramic membrane filtration of synthetic produced water feeds.

Membrane material	**Organics**	**Inorganics**	**Surfactant**	**Base water**	**Ref.**
300 kDa ZrO_2	Iranian crude oil	Suspended solids from settler of activated sludge plant	N/A	Settler supernatant	[56]
0.1, 0.2 & 0.5 µm α-Al_2O_3	Crude oil (350 ppm)	Kaolin (50 ppm) Scaling/corrosion inhibitor (10 ppm)	SERDOX (200 ppm)	Salt water 3.5% salinity (NaCl)	[57]
0.1, 0.2 & 0.5 µm α-Al_2O_3	Crude oil (50, 150, 250, 350 ppm)	Kaolin (50 ppm) Scaling/corrosion inhibitor (10 ppm)	SERDOX (65, 450 ppm)	Salt water 1w/v% salinity (NaCl)	[58]
Natural zeolites	Toluene (20-100 mg/L)	Sea salts Na^+ (1159 mg/L) Ca^{2+} (93 mg/L) Mg^{2+} (169 mg/L) K^+ (289 mg/L)	N/A	Municipal water	[59]
0.1 µm ZrO_2	Crude oil (180 mg/L)	NaCl (25 000, 50 000, 75 000, 100 000 mg/L)	N/A	Distilled water	[60]
0.1 µm ZrO_2	Crude oil (100 mg/L)	NaCl (98 800 mg/L)	N/A	Distilled water	[61]
200 nm Al_2O_3	Hexadecane (50–50 ppm)	NaCl (5000–35 000 ppm)	Tween 20	Deionized water	[55]
0.45 µm ZrO_2-TiO_2	Engine diesel oil (86 300 mg/L)	Bentonite (1500 mg/L)	Ethylene tetrakis (2040 mg/L)	Deionized water	[31]

2.1.4 Filtration of field produced water

While the studies involving synthetic produced water prove more useful than their counterparts that use simple oil/water emulsions, it is still preferable to test ceramic membranes with field samples of actual produced water. Despite the fact that obtaining such feed samples may involve considerable logistics and cost, their use in studying industrially relevant problems is very important and provides unique insight into this separation problem. For this reason, ceramic membranes were first used in the early 1990s to treat industrial samples of produced water from U.S. petrochemical plants [62,63]. It was proven in these early works that ceramic membranes are promising candidates for the removal of oil and suspended solids from produced water, and they offered the opportunity of reducing operational costs relative to other membrane technologies. Since then, many studies have tested ceramic membranes in the treatment of produced water obtained from refineries located in Iran, China, Germany, Brazil and the Arabian Gulf, as well as from the Canadian oil sands. These studies are summarized in Table 2.2 with information regarding the source and characteristics of the utilized produced water feeds. Some studies have attempted to estimate the operating costs associated with ceramic membrane treatment of produced water with results ranging from US$ 0.27–2 per m^3 of treated water [61,64].

Despite these reduced costs, membrane fouling remains a significant problem in this application. Fouling propensity was also determined to increase as the field samples were aged [65]. This phenomenon was attributed to bituminous molecules reacting with oxygen from air, which led to the formation of highly compressible foulant layers at the membrane surfaces. Many researchers have found that economically viable fluxes can only be sustained when continuous fouling mitigation techniques are applied during operation. Such techniques include chemical cleaning-in-place [66,67], submerged filtration [68] or dynamic filtration [26]. In the treatment of oil sands produced water, Thibault et al. [69] found that saturation of the membrane selective layer by bitumen led to a significant irreversible effect on membrane integrity and performance. They further suggested that modifying the ceramic surface to limit interaction with bitumen should be effective in improving performance.

Table 2.2: Previous studies on ceramic membrane treatment of field samples of produced water.

Membrane material	**Pore size**	**Source of produced water**	**Produced water characteristics**	**Ref.**
MF (α-Al_2O_3)	0.2 & 0.8 µm	Two Louisiana onshore and two Gulf of Mexico offshore facilities	TDS = 152660–212100 mg/L TSS = 73–350 mg/L pH = 6–7 Oil & grease = 28–574 mg/L	[62]
Bentonite clay	Not given	Facility near Loco Hills, New Mexico	TDS = 196250 mg/L pH = 6.98	[70]
MF (ZrO_2)	0.2 µm	Refinery Plant of Yangtze Petrochemical Company (China)	Oil content = 6 g/L COD = 3 g/L Solid content = 5 wt%	[71]
MF (Al_2O_3) UF (TiO_2) NF (TiO_2)	0.1 & 0.2 µm 0.05 µm 750 & 1000 Da	Tank dewatering from German BP AG, Oil Refinery Emsland, Lingen	Oil content = 200-1000 mg/L pH = 6-8 Conductivity = 0.02-0.08 S/cm TOC = 200-2000 mg/L	[40,41]
MF (mullite/mullite-Al_2O_3)	0.25 µm	Desalter unit outlet of Seraje, Ghom gas wells	TOC = 1060 ppm Salinity = 230 g/L	[39]
MF (α-Al_2O_3)	0.2 µm	Outlet of API unit of Tehran refinery	TSS = 92 mg/L Oil content = 26 mg/L TOC = 141 mg/L Turbidity = 21 NTU	[72]
MF (γ-Al_2O_3)	0.2 µm	Olefin plant of the Marun petrochemical Co. (Iran, Mahshahr)	COD = 1600-2210 mg/L BOD = 150-225 mg/L TDS = 151-265 mg/L TSS = 23-27 mg/L Turbidity = 178-251 NTU	[73]
UF (Al_2O_3)	0.1 µm	Outlet of a skim tank at a SAGD plant operating in Northern Alberta, Canada	Conductivity = 0.9 mS/cm TOC = 440 mg/L pH = 7.1 DO = 2.8 mg/L	[65]
MF (Al_2O_3) UF (Al_2O_3/$MgAl_2O_4$)	0.2 µm 7 nm	Tank dewatering from German BP AG, Oil Refinery Emsland, Lingen	Oil content = 200-1000 mg/L pH = 6-8 Conductivity = 0.02-0.08 S/cm TOC = 200-2000 mg/L Iron = 66 mg/L Zinc = 0.55 mg/L	[26]

MF (mullite) MF (mullite-Al_2O_3)	0.476 μm 0.521, 0.634 & 0.728 μm	Desalter unit outlet of Seraje, Ghom gas wells	TSS = 82 mg/L TDS = 23 g/L COD = 596 mg/L TOC = 1060 mg/L Turbidity = 97 NTU	[74]
UF (TiO_2/ZrO_2)	1 kDa	OSPW recycling pond in Fort McMurray, Alberta, Canada	pH = 8.1 COD = 266.7 mg/L AEF = 48.7 mg/L TOC = 56.1 mg/L NAs =8.95 mg/L Conductivity = 4.3 mS/cm Turbidity = 6.3 NTU TSS = 5.3 mg/L TDS = 599.3 mg/L	[75]
MF (Al_2O_3) MF (SiO_2 modified Al_2O_3) MF (TiO_2 modified Al_2O_3)	100 nm 80 nm 80 nm	Oil sands tailings ponds in Northern Alberta	pH = 6.9 Conductivity = 3.6715 mS/cm Turbidity = 25.6 NTU TOC = 41.2 mg/L COD = 134.6 mg/L TSS = 21.2 mg/L TDS = 1906.2 mg/L	[68]
MF (α-Al_2O_3)	0.2 μm	Inlet & outlet of skimmers in desalination units operating in Iran	Oil content = 9-43 mg/L TDS = 59628-65473 mg/L COD = 450-500 mg/L TSS = 108-109 mg/L Turbidity = 95-150 NTU TOC = 110-165 mg/L pH = 8	[64]
UF (ZrO_2)	0.1 μm	Oil production unit	Conductivity = 100 mS/cm pH = 6.6 Oil content = 100 mg/L TOC = 113 mg/L DOC = 52 mg/L Salinity = 98800 mg/L TSS = 60 mg/L	[61]

UF (ZrO_2)	0.1 µm	Brazilian oil production unit	Conductivity = 100 mS/cm pH = 6.6 Oil content = 25 mg/L TSS = 60 mg/L Salinity = 98800 mg/L	[76]
MF (Al_2O_3) MF (Al_2O_3) UF (ZrO_2)	100 nm 50 nm 20 kDa	SAGD plant in Alberta, Canada	Oil content = 125 mg/L pH = 10	[77]
UF (TiO_2)	0.1 µm	Header of the main hydrocyclones of the cooling water recycle system from the Canadian Natural Resources Limited (CNRL) Horizon operation	pH = 8.1 TSS = 215 mg/L TDS = 1963 mg/L TOC = 43.6 mg/L Oil content =27 mg/L	[78,79]
MF (SiC) UF (SiC) MF (TiO_2) UF (TiO_2)	0.5 µm 0.04 µm 2 µm 50 kDa	Downstream of IGF stage of a classical hydrocyclone-IGF treatment train from an oil platform operating in the Arabian Gulf	pH = 6.7-7.5 Conductivity = 94.3-101 mS/cm TSS = 79-86 g/L TOC = 46-237 mg/L Iron = 0.9-3.1 mg/L	[66]
UF (TiO_2/γ-Al_2O_3)	3 to 30 nm	SAGD operations in the Canadian oil sands	TOC = 182 ppm Turbidity = 327 NTU Chloride = 185 ppm Sulphate = 3.2 ppm	[69]
Al_2O_3, TiO_2, ZrO_2, Mg/Al_2O_4, SiC	Tubular: 470 Da – 0.25µm Disk: 7, 30, 200 nm Hollow fiber: 40 nm	Tank dewatering from German BP AG, Oil Refinery Emsland, Lingen	Dispersed oil = 30-1000 ppm pH = 6.0-8.0 Conductivity = 20000-80000 µS/cm Viscosity = 0.6-0.7 mPa·s TOC = 200-2000 ppm	[29]
MF (SiC) UF (SiC)	2 µm 0.04 µm	Downstream of IGF stage of a classical hydrocyclone-IGF treatment train from an oil platform operating in the Arabian Gulf	Oil and grease = 24-52 mg/L Turbidity = 21-663 NTU	[67]
MF (Si_3N_4)	0.68 µm	Sinopec petroleum and chemical corporation in Beijing, China	Oil content = 21000 ppm pH = 6.5	[80]

2.1.5 Summary

The application of ceramic membranes in the treatment of oily wastewaters is abundant in the scientific literature. High performance is often reported when membranes are used with synthetic oil-in-water emulsions, but performance significantly declines upon the introduction of salts and suspended solids to the feed samples. When field samples of produced water are used, membrane fouling remains a significant obstacle that must be addressed. Membrane surface modification has the potential to generate ceramic membranes that are inherently fouling-resistant to bituminous compounds. This fouling mitigation approach has sparsely been explored in the literature for the treatment bitumen-containing wastewaters. Bituminous compounds such as asphaltenes and resins are known to possess amphoteric surface regions [81–87]. This indicates that at any given pH, the surfaces of bitumen-associated molecules can exhibit both positive and negative charges that could interact with charged membrane surfaces and cause severe membrane fouling. Therefore, membrane surfaces should be modified in a way that renders them non-ionic to mitigate this interaction. The surface modification of ceramic membranes will be discussed in detail in the following section.

2.2 Surface modification of ceramic membranes

2.2.1 Introduction

The surface modification of inorganic membranes has historically been accomplished using many different approaches. Perhaps the most common method is through the grafting of a polymer brush layer or coating onto inorganic substrates. This is often done by initially attaching a vinyltrialkoxysilane (VTAS) to the membrane via reactions with surface hydroxyl groups. The polymer of interest is then grafted onto the surface by reacting with the double bond of the terminal alkene group on the VTAS. Such approaches have been successfully applied in grafting ceramic membranes with polymers such as polyvinylpyrrolidone (PVP) [88–92], poly(vinyl acetate) (PVAc) [92–96] and polydimethylsiloxane (PDMS) [97–99] for various applications ranging from protein separation to pervaporation. Illustrative examples of surface modification with PVP, PVAc and PDMS are shown in Figure 2.1. Recent work in this area has led to the development of an even more sophisticated “mussel-inspired” grafting technique that yields polymer coatings incorporating metal nanoparticles [100], as depicted in Figure 2.2.

(a)

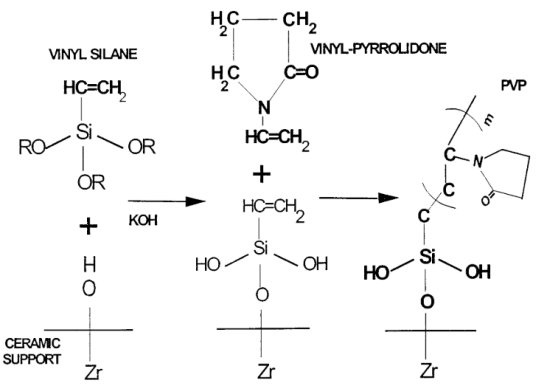

(b)

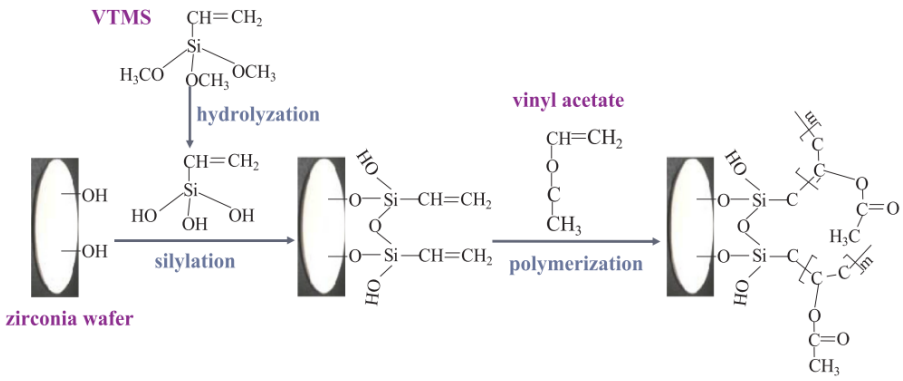

(c)

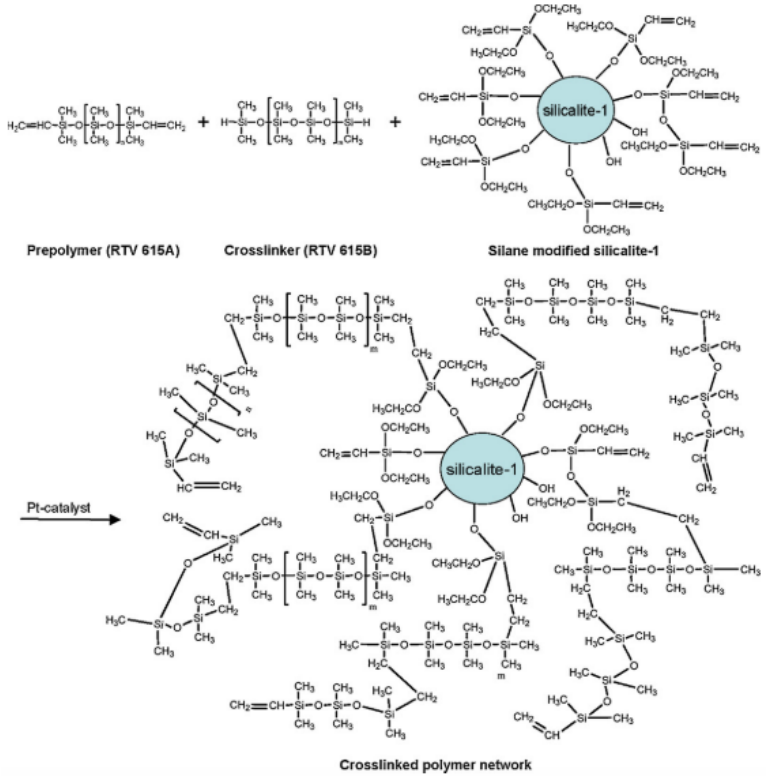

Figure 2.1: Reaction schemes for polymer grafting of ceramic surfaces by (a) PVP, (b) PVAc and (c) PDMS [14,93,97].

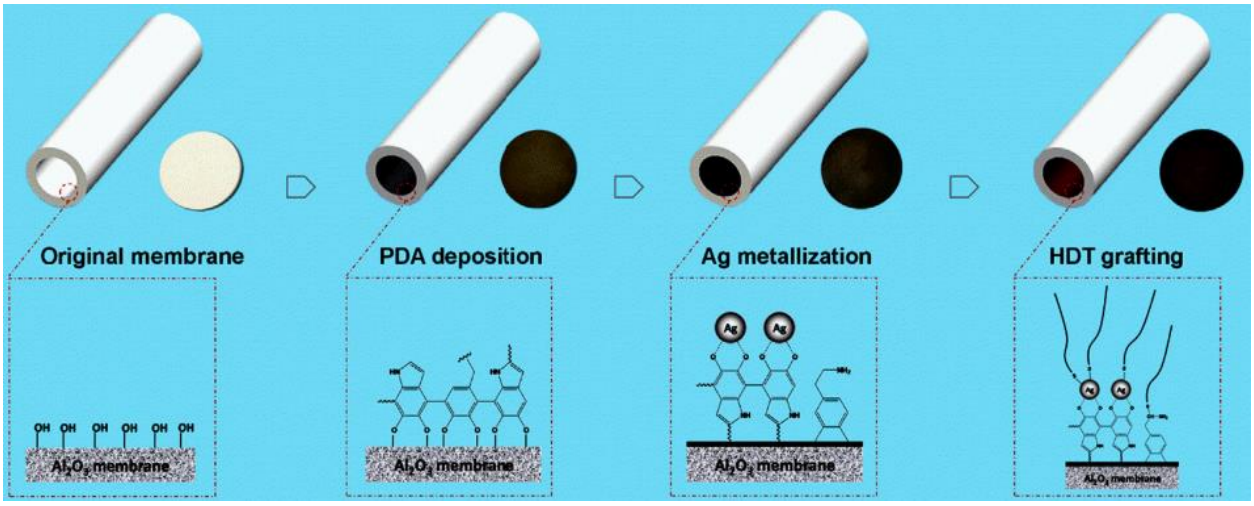

Figure 2.2: Mussel-inspired superhydrophobic nanostructured coating of ceramic surfaces [100].

When dealing with the treatment of simple oil-in-water emulsions, membrane researchers of past have sought to increase the surface hydrophilicity of ceramic membranes. This goal was achieved by modifying the surface with metal-oxide nanoparticles that are similar in material to the ceramic membrane itself. These include nanoparticles composed of Al_2O_3 [51], TiO_2 [53,101], ZrO_2 [52], Fe_2O_3 [102,103] and SiO_2 [104] among several others. Figure 2.3 illustrates an example of such modification with rod-shaped TiO_2 nanoparticles.

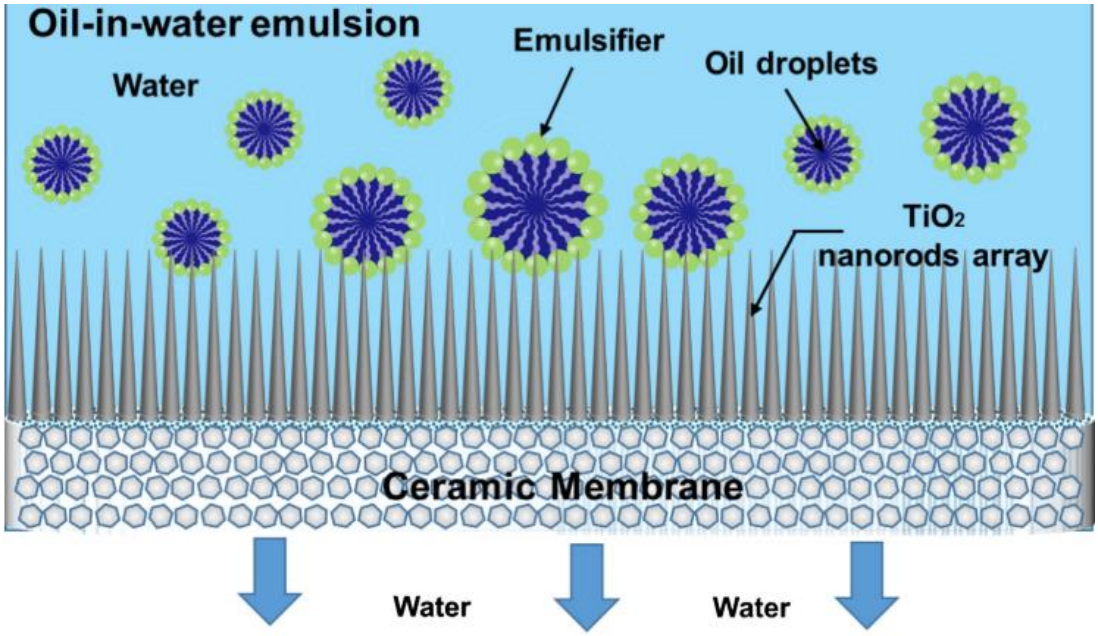

Figure 2.3: Modification of ceramic membrane with TiO_2 nanorods for oil-in-water emulsion treatment [101].

Zeolites have similarly been used to enhance hydrophilicity and increase water permeation [50]. Recent years have seen the development of "superhydrophilic" ceramic membranes that have been modified with graphene oxide [105,106] or cysteic acid [107] for improved oil/water separation and higher water fluxes.

It is desirable to be able to functionalize ceramic membrane surfaces via simple single-step processes to suit the needs of specific industrial separation applications of interest. The use of grafted polymers allows for the functionalization of ceramic surfaces, but involves complex reaction schemes that are unsuitable for sustained commercial development. Conversely, surface modification with metal-oxide nanoparticles is relatively facile but simply increases hydrophilicity without any further functionalization. As a solution to these shortcomings, surface modification techniques that involve reacting functional molecules directly with hydroxyl groups on the ceramic substrate have been studied extensively. Modification agents that are capable of reacting in this manner include alcohols [108] and phosphonic acids [109]. These chemicals, however, lack the ability to crosslink and form reinforced surface layers. The best-known method for this type of surface modification is the use of organosilanes, which are the most versatile type of modifying agents with a broad range of commercially available organic functionality [110].

2.2.2 Organosilane chemistry

Organosilanes are monomeric silicon molecules that contain at least one carbon-silicon bond within their chemical structure [111]. The basic structure of the organosilane molecule is shown in Figure 2.4.

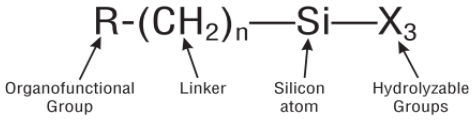

Figure 2.4: Basic structure of organosilanes [112].

Here, R is any non-hydrolyzable and organofunctional moiety. This organic chain can be reactive or non-reactive, depending on the needs of the application. A linker, or spacer, is placed between the organic group and the silicon atom. This spacer is often a short alkyl chain. The silicon atom is also bound to at least one hydrolyzable group (X), such as alkoxy or chlorine

groups. These groups are what allow the organosilane to react with hydroxyl groups that are present on inorganic or organic substrates. Before linkage with such substrate surfaces, organosilanes must undergo hydrolysis in order to form silanols with hydroxyl groups. The hydrolysis of organosilanes can be accomplished in either acidic of basic media. The kinetics of silane hydrolysis and condensation reactions have been extensively studied using NMR [113] and FTIR [114] based techniques. It has been established that conducting the reaction in an acidic environment enhances the hydrolysis reaction and produces stable silanols, while simultaneously slowing down the rate of self-condensation reactions [115–118]. Rapid hydrolysis rates while limiting the polymerization of the formed silanols is desirable when attempting to silylate solid surfaces [119]. The reaction mechanism for acid-catalyzed hydrolysis is shown in Figure 2.5.

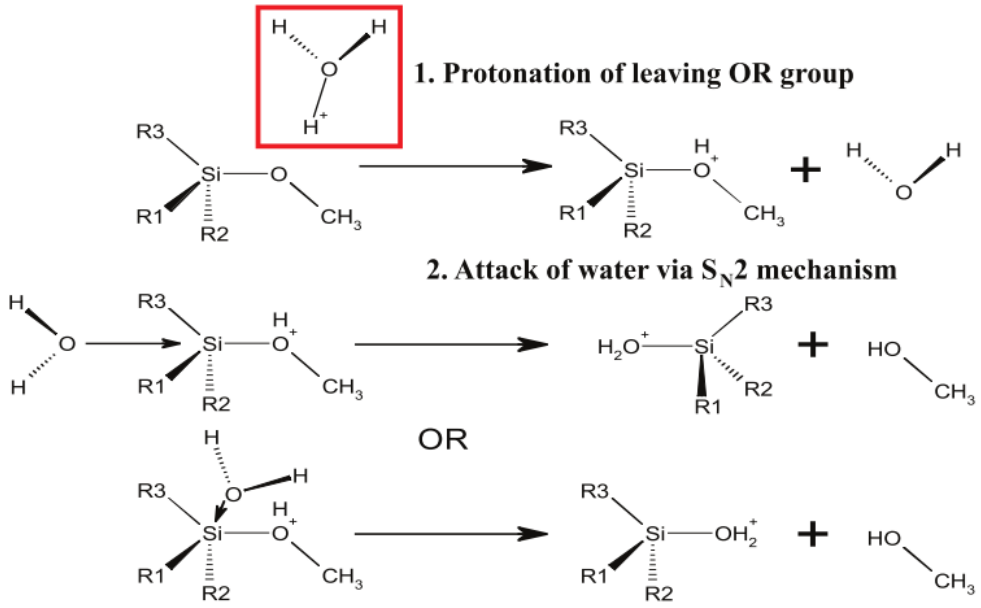

Figure 2.5: Mechanism for acid-catalyzed hydrolysis of organosilanes [111].

Once hydrolysis and silanol formation is achieved, individual silanol molecules can then form covalent bonds by reacting with hydroxyl groups on substrate surfaces. This mechanism is shown for a metal oxide surface in Figure 2.6.

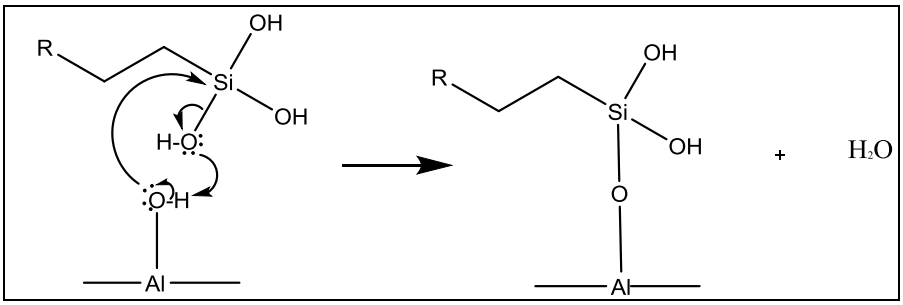

Figure 2.6: Covalent bonding of silanols with metal oxide surfaces.

The formed silanols can also react with other silanol molecules through condensation of their hydroxyl groups. This can occur both in solution to form polymerized silanols (Figure 2.7a) and on the substrate surface to form self-assembled monolayers (Figure 2.7b).

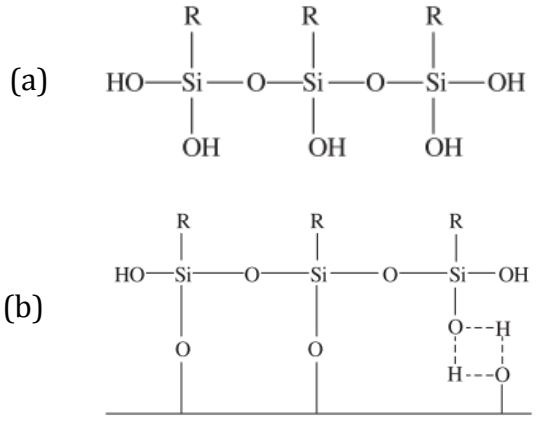

Figure 2.7: Condensation of silanols (a) in solution and (b) on substrate surfaces [112].

If reacted under the proper conditions, organosilanes can therefore be made to form tight siloxane polymeric networks on various inorganic substrates, thus changing the surface properties of the substrate. Evidently, the exact nature of the change in physicochemical properties will depend on the functionality of the silane's organic group.

2.2.3 Application of silylated ceramic membranes

The adhesion of organosilanes to the surface of inorganic materials is an application that dates back over half a century [120]. Successful methods for the self-assembly of silane monolayers were initially developed and applied to inorganic minerals with polar surfaces [121–123]. Eventually, surface modification using organosilanes was extended to individual oxide substrates, including SiO_2, TiO_2 and ZrO_2 [109,124–129]. The success of these studies in

forming mono- or multilayered silylated surfaces on oxide surfaces was foreseen to have great use in ceramic membrane technology. Researchers soon began more commonly investigating the application of various organosilanes as surface modifying agents for ceramic membranes. The ability of organosilanes to affect the wetting properties of ceramic surfaces, by changing their nature from hydrophilic to hydrophobic, had been of particular interest [130–138]. Moreover, there has been evidence that silylation of ceramic membranes not only affects wetting, but also electrical properties [139]. Thus, organosilanes can be tailored and selected in order to achieve certain desired surface properties for ceramic membranes. For this reason, they have been applied in various separation applications as surface modifying agents for ceramic membranes.

2.2.3.1 Gas separations

Gas separation was the first application that surface-silylated ceramic membranes were subjected to. Pioneering work was accomplished three decades ago by modifying porous glass membranes with tetraethoxysilane for enhanced He/O_2 separation [140]. It has since widely been demonstrated that the single gas permeances of many common gaseous species through alumina membranes can effectively be decreased by using chloro- or alkoxysilanes with fluorinated or simple hydrocarbon chain moieties to modify the metal oxide surface [141–144]. These gases include atmospheric inerts (e.g. He, Ar, N_2) and greenhouse gases (e.g. CO_2, CH_4, SF_6). Over the years, extensive research has been performed with such silanes on the separation of binary gas mixtures using modified ceramic membranes. These include mixtures of CO_2 with N_2 [145–154], H_2 [154–157], He [154,158], CO [159], SF_6 [154] and alkane gases [153–155]. The separation of light paraffin gases such as methane, propane and butane from mixtures containing N_2 [153,160–163], H_2 [153,155] and other paraffins or olefins [153,162–164] has also received much attention. In all of these studies, it was found that the silylation of the ceramic membrane surfaces was capable of increasing the permselectivity of a desired gas over another.

2.2.3.2 Membrane distillation

Membrane distillation (MD) is a separation process that has garnered much interest as an efficient means of desalting highly saline waters [165]. MD is a process in which the membrane acts as a barrier and liquid-vapour interface between the liquid feed and vapour permeate. Unlike traditional membrane technologies, which utilize pressure gradients as the driving force for separation, MD makes use of a thermally-driven vapour pressure difference across the

membrane. Vapour water is expected to permeate through the membrane, leaving behind an increasingly salt-concentrated solution on the feed side. To block the entrance of liquid water from the feed solution into the membrane pores, hydrophobic membranes must be utilized. For this reason, ceramic membranes require surface modification prior to use in such processes. Fluoroalkylsilanes (FAS), organosilanes with fluorinated hydrocarbon chains of varying lengths, have emerged as the most widespread means of hydrophobizing ceramic membranes. FAS-modified ceramic membrane have been extensively and successfully applied in MD processes aimed at treating synthetic seawater in the form of aqueous NaCl solutions [166–186]. They have also been utilized for the purification of real seawater [177,179,187] and oily wastewater [188], as well as the separation of volatile organic solvents [189,190] and arsenic [191] from water. FAS have also been used in osmotic evaporation (OE) processes for juice concentration [192,193]. OE is a process similar to MD in which the vapour pressure difference is induced by a water activity difference between the juice and an osmotic solution. Recent work has been aimed at exploring the application of non-fluorinated hydrophobic silanes to replace the widespread use of FAS as surface modifying agents in ceramic membrane MD processes [194–197].

2.2.3.3 Pervaporation

Much like in membrane distillation, pervaporation (PV) processes involve the usage of a membrane as a barrier between the liquid feed solution and the vapour permeate. The separation of liquid mixtures is dependent on the diffusion rates of the individual components in the feed through the membrane. The permeate side is kept under a vacuum to allow for the evaporation of permeated species. Ceramic membranes often require surface modification prior to use in PV in order to reduce their pore sizes so that larger molecules are retained while water or volatile organic molecules pass through to the permeate side. Furthermore, when the feed solution is a mixture of water and volatile organic solvents, the modification must render the ceramic membrane surface hydrophobic in order to limit the penetration of water into the pores. Initial work in this regard was accomplished using various hydrophobic alkylsilanes for the separation of binary organic mixtures as well as the extraction of volatile organics from water [143,198–200]. As was the case with MD processes, later years brought forth the emergence of FAS as the modifying agents of choice for obtaining hydrophobic ceramic membranes for PV applications [166,189,201–203].

2.2.3.4 Liquid separations

The investigation of silane surface modified ceramic membranes in the filtration of liquid solutions has not been explored to the same extent as gas separation, MD and PV processes. Aminofunctional silanes have been applied in the rejection of charged species like heavy metals [204,205] and proteins [206] from aqueous solutions, and in the deposition of catalytic nanoparticles for liquid phase reactions [207–209]. Alkylchlorosilanes and their fluorinated equivalents have been used to render ceramic membrane surfaces hydrophobic to reduce water permeability and increase the permeability of non-polar organic solvents such as hexane, cyclohexane, toluene, decane and tetradecane [147,210–213]. Silylated ceramic membrane are also abundantly used in many biomedical applications [214]. These include retention of both viruses and bacteria by membranes modified with aminofunctional [215,216] and hydrophobic alkylated silanes [217]. A recent study applied a hydrophobic alkylsilane-modified microfiltration ceramic membrane in the concentration of dairy products and determined that using MD was more efficient in this application [218].

Separation of oil/water mixtures has mostly been investigated in the context of water-in-oil emulsions. Membranes modified using alkylsilanes or FAS with varying hydrocarbon chain lengths were used to filter emulsions of water in kerosene, isooctane or hexane [219–223]. Despite the success of previous studies in the filtration of organic solvents and water-in-oil emulsions, their work cannot be extended and applied to produced water filtration. The available studies consisted of the hydrophobization of ceramic membranes for the removal of water as an oil contaminant. Evidently, this is not the ideal situation when dealing with bituminous wastewater treatment, in which it is preferred to recuperate the purified water as the permeate using membranes that are still highly hydrophilic. In recent years, Lee et al. have investigated the use of ceramic membranes modified with hydrophilic silanes having different surface charges in the filtration of negatively charged humic acid solutions [224,225]. It was determined that negatively charged silanes with sulfonic groups were the most efficient, emphasizing the importance of surface charges in reducing fouling and improving membrane performance.

2.2.4 Summary

Historically, organosilane-modified ceramic membranes have been predominantly used in gas separation, MD and PV processes. In most of these studies, hydrophobic membranes were

synthesized by modification with silanes having fluorinated or simple hydrocarbon organic moieties. These same hydrophobic silanes have been used in the modification of ceramic membranes for the separation of water-in-oil emulsions. Recent work has seen the use of hydrophilic silane-modified membranes for the treatment of humic acid aqueous solutions, where it was established that silane surface charge plays an important role in the separation process. In the case of bituminous wastewater treatment, where foulants are often amphoteric, a charge neutral hydrophilic silane is required. A commonly used non-ionic modification agent for ceramic membranes is polyethylene glycol (PEG). PEG-based modifications have been frequently applied in protein separation applications [226–229]. Recently, they have also been used in organic solvent nanofiltration [230]. In most of these studies, attachment of PEG to the ceramic surface involved an intermediate step, such as silylation with aminofunctional silanes. However, highly hydrophilic PEG-functional silanes that can react directly with membrane surfaces are available commercially and warrant extensive investigation as surface modifying agents for ceramic membranes used in the treatment of bituminous wastewaters.

References

[1] E. Gorouhi, M. Sadrzadeh, T. Mohammadi, Microfiltration of oily wastewater using PP hydrophobic membrane, Desalination. 200 (2006) 319–321.

[2] A. Salahi, A. Gheshlaghi, T. Mohammadi, S.S. Madaeni, Experimental performance evaluation of polymeric membranes for treatment of an industrial oily wastewater, Desalination. 262 (2010) 235–242.

[3] E.S. Kim, Y. Liu, M. Gamal El-Din, Evaluation of membrane fouling for in-line filtration of oil sands process-affected water: The effects of pretreatment conditions, Environmental Science & Technology. 46 (2012) 2877–2884.

[4] M. Sadrzadeh, J. Hajinasiri, S. Bhattacharjee, D. Pernitsky, Nanofiltration of oil sands boiler feed water: Effect of pH on water flux and organic and dissolved solid rejection, Separation and Purification Technology. 141 (2015) 339–353.

[5] B. Khorshidi, A. Bhinder, T. Thundat, D. Pernitsky, M. Sadrzadeh, Developing high throughput thin film composite polyamide membranes for forward osmosis treatment of SAGD produced water, Journal of Membrane Science. 511 (2016) 29–39.

[6] G.N. Vatai, D.M. Krstic, A.K. Koris, I.L. Gáspár, M.N. Tekic, Ultrafiltration of oil-in-water emulsion: Comparison of ceramic and polymeric membranes, Desalination and Water Treatment. 3 (2009) 162–168.

[7] S.-J. Lee, J.-H. Kim, Differential natural organic matter fouling of ceramic versus polymeric ultrafiltration membranes, Water Research. 48 (2014) 43–51.

[8] J. Wang, Y. Mo, S. Mahendra, E.M.V. Hoek, Effects of water chemistry on structure and performance of polyamide composite membranes, Journal of Membrane Science. 452 (2014) 415–425.

[9] J.M. Dickhout, J. Moreno, P.M. Biesheuvel, L. Boels, R.G.H. Lammertink, W.M. De Vos, Produced water treatment by membranes : A review from a colloidal perspective, Journal of Colloid and Interface Science. 487 (2017) 523–534.

[10] G. Hurwitz, D.J. Pernitsky, S. Bhattacharjee, E.M.V. Hoek, Targeted Removal of Dissolved Organic Matter in Boiler-Blowdown Wastewater: Integrated Membrane Filtration for Produced Water Reuse, Industrial & Engineering Chemistry Research. 54 (2015) 9431–9439.

[11] A.B. Koltuniewicz, R.W. Field, T.C. Arnot, Cross-flow and dead-end microfiltration of oily-water emulsion. Part I: Experimental study and analysis of flux decline, Journal of Membrane Science. 102 (1995) 193–207.

[12] A.B. Koltuniewicz, R.W. Field, Process factors during removal of oil-in-water emulsions with cross-flow microfiltration, Desalination. 105 (1996) 79–89.

[13] T.C. Arnot, R.W. Field, A.B. Koltuniewicz, Cross-flow and dead-end microfiltration of oily-water emulsions. Part II. Mechanisms and modelling of flux decline, Journal of Membrane Science. 169 (2000) 1–15.

[14] R.S. Faibish, Y. Cohen, Fouling and rejection behavior of ceramic and polymer-modified ceramic membranes for ultrafiltration of oil-in-water emulsions and microemulsions, Colloids and Surfaces A: Physicochemical and Engineering Aspects. 191 (2001) 27–40.

[15] R.S. Faibish, Y. Cohen, Fouling-resistant ceramic-supported polymer membranes for

ultrafiltration of oil-in-water microemulsions, Journal of Membrane Science. 185 (2001) 129–143.

[16] Y. Yang, R. Chen, W. Xing, Integration of ceramic membrane microfiltration with powdered activated carbon for advanced treatment of oil-in-water emulsion, Separation and Purification Technology. 76 (2011) 373–377.

[17] E.N. Tummons, V. V. Tarabara, J.W. Chew, A.G. Fane, Behavior of oil droplets at the membrane surface during crossflow microfiltration of oil-water emulsions, Journal of Membrane Science. 500 (2016) 211–224.

[18] J. Mueller, Y. Cen, R.H. Davis, Crossflow microfiltration of oily water, Journal of Membrane Science. 129 (1997) 221–235.

[19] B.K. Nandi, R. Uppaluri, M.K. Purkait, Treatment of Oily Waste Water Using Low-Cost Ceramic Membrane: Flux Decline Mechanism and Economic Feasibility, Separation Science and Technology. 44 (2009) 2840–2869.

[20] B. Das, B. Chakrabarty, P. Barkakati, Separation of oil from oily wastewater using low cost ceramic membrane, Korean Journal of Chemical Engineering. 34 (2017) 2559–2569.

[21] D. Lu, T. Zhang, J. Ma, Ceramic membrane fouling during ultrafiltration of oil/water emulsions: Roles played by stabilization surfactants of oil droplets, Environmental Science & Technology. 49 (2015) 4235–4244.

[22] B.K. Nandi, A. Moparthi, R. Uppaluri, M.K. Purkait, Treatment of oily wastewater using low cost ceramic membrane: Comparative assessment of pore blocking and artificial neural network models, Chemical Engineering Research and Design. 88 (2010) 881–892.

[23] P. Monash, G. Pugazhenthi, Effect of TiO2 addition on the fabrication of ceramic membrane supports: A study on the separation of oil droplets and bovine serum albumin (BSA) from its solution, Desalination. 279 (2011) 104–114.

[24] D. Vasanth, G. Pugazhenthi, R. Uppaluri, Fabrication and properties of low cost ceramic microfiltration membranes for separation of oil and bacteria from its solution, Journal of Membrane Science. 379 (2011) 154–163.

[25] D. Vasanth, G. Pugazhenthi, R. Uppaluri, Cross-flow microfiltration of oil-in-water emulsions using low cost ceramic membranes, Desalination. 320 (2013) 86–95.

[26] M. Ebrahimi, O. Schmitz, S. Kerker, F. Liebermann, P. Czermak, Dynamic cross-flow filtration of oilfield produced water by rotating ceramic filter discs, Desalination and Water Treatment. 51 (2013) 1762–1768.

[27] S. Emani, R. Uppaluri, M.K. Purkait, Cross flow microfiltration of oil–water emulsions using kaolin based low cost ceramic membranes, Desalination. 341 (2014) 61–71.

[28] R. Vinoth Kumar, A. Kumar Ghoshal, G. Pugazhenthi, Elaboration of novel tubular ceramic membrane from inexpensive raw materials by extrusion method and its performance in microfiltration of synthetic oily wastewater treatment, Journal of Membrane Science. 490 (2015) 92–102.

[29] M. Ebrahimi, S. Kerker, O. Schmitz, A.A. Schmidt, P. Czermak, Evaluation of the fouling potential of ceramic membrane configurations designed for the treatment of oilfield produced water, Separation Science and Technology. 53 (2018) 349–363.

[30] S.H. Hyun, G.T. Kim, Synthesis of Ceramic Microfiltration Membranes for Oil/Water Separation,

Separation Science and Technology. 32 (1997) 2927–2943.

[31] M. Abdalla, M. Nasser, A. Kayvani Fard, H. Qiblawey, A. Benamor, S. Judd, Impact of combined oil-in-water emulsions and particulate suspensions on ceramic membrane fouling and permeability recovery, Separation and Purification Technology. 212 (2019) 215–222.

[32] H. Ohya, J.J. Kim, A. Chinen, M. Aihara, S.I. Semenova, Y. Negishi, O. Mori, M. Yasuda, Effects of pore size on separation mechanisms of microfiltration of oily water, using porous glass tubular membrane, Journal of Membrane Science. 145 (1998) 1–14.

[33] P. Srijaroonrat, E. Julien, Y. Aurelle, Unstable secondary oil/water emulsion treatment using ultrafiltration: Fouling control by backflushing, Journal of Membrane Science. 159 (1999) 11–20.

[34] S.J. Lue, J. Chow, C. Chien, H. Chen, Cross-Flow Microfiltration of Oily Water using a Ceramic Membrane: Flux Decline and Oil Adsorption, Separation Science and Technology. 44 (2009) 3435–3454.

[35] Z. Sadeghian, F. Zamani, S.N. Ashrafizadeh, Removal of oily hydrocarbon contaminants from wastewater by γ-alumina nanofiltration membranes, Desalination and Water Treatment. 20 (2010) 80–85.

[36] L. Li, E.Z. Gao, H. Abadikhah, J.W. Wang, L.Y. Hao, X. Xu, S. Agathopoulos, Preparation of a porous, sintered and reaction-bonded Si3N4(SRBSN) planar membrane for filtration of an oil-in-water emulsion with high flux performance, Materials. 11 (2018) 990–1004.

[37] M. Abbasi, M. Reza Sebzari, T. Mohammadi, Enhancement of Oily Wastewater Treatment by Ceramic Microfiltration Membranes using Powder Activated Carbon, Chemical Engineering and Technology. 34 (2011) 1252–1258.

[38] M. Abbasi, M.R. Sebzari, A. Salahi, S. Abbasi, T. Mohammadi, Flux decline and membrane fouling in cross-flow microfiltration of oil-in-water emulsions, Desalination and Water Treatment. 28 (2011) 1–7.

[39] M. Abbasi, M. Mirfendereski, M. Nikbakht, M. Golshenas, T. Mohammadi, Performance study of mullite and mullite-alumina ceramic MF membranes for oily wastewaters treatment, Desalination. 259 (2010) 169–178.

[40] M. Ebrahimi, K.S. Ashaghi, L. Engel, D. Willershausen, P. Mund, P. Bolduan, P. Czermak, Characterization and application of different ceramic membranes for the oil-field produced water treatment, Desalination. 245 (2009) 533–540.

[41] M. Ebrahimi, K.S. Ashaghi, L. Engel, D. Willershausen, P. Mund, P. Bolduan, P. Czermak, Investigations on the use of different ceramic membranes for efficient oil-field produced water treatment, Desalination. 250 (2010) 991–996.

[42] A. Lobo, Á. Cambiella, J.M. Benito, C. Pazos, J. Coca, Ultrafiltration of oil-in-water emulsions with ceramic membranes: Influence of pH and crossflow velocity, Journal of Membrane Science. 278 (2006) 328–334.

[43] F.L. Hua, Y.F. Tsang, Y.J. Wang, S.Y. Chan, H. Chua, S.N. Sin, Performance study of ceramic microfiltration membrane for oily wastewater treatment, Chemical Engineering Journal. 128 (2007) 169–175.

[44] Q. Zhang, Y. Fan, N. Xu, Effect of the surface properties on filtration performance of Al2O3–TiO2 composite membrane, Separation and Purification Technology. 66 (2009) 306–312.

[45] H. Falahati, A.Y. Tremblay, Flux dependent oil permeation in the ultrafiltration of highly concentrated and unstable oil-in-water emulsions, Journal of Membrane Science. 371 (2011) 239–247.

[46] Z. Zhong, W. Xing, B. Zhang, Fabrication of ceramic membranes with controllable surface roughness and their applications in oil/water separation, Ceramics International. 39 (2013) 4355–4361.

[47] L. Zhu, M. Chen, Y. Dong, C.Y. Tang, A. Huang, L. Li, A low-cost mullite-titania composite ceramic hollow fiber microfiltration membrane for highly efficient separation of oil-in-water emulsion, Water Research. 90 (2016) 277–285.

[48] D. Zou, M. Qiu, X. Chen, E. Drioli, Y. Fan, One step co-sintering process for low-cost fly ash based ceramic microfiltration membrane in oil-in-water emulsion treatment, Separation and Purification Technology. 210 (2019) 511–520.

[49] M. Matos, A. Lobo, E. Fernández, J.M. Benito, C. Pazos, J. Coca, Recycling of oily ultrafiltration permeates to reformulate O/W emulsions, Colloids and Surfaces A: Physicochemical and Engineering Aspects. 331 (2008) 8–15.

[50] J. Cui, X. Zhang, H. Liu, S. Liu, K.L. Yeung, Preparation and application of zeolite/ceramic microfiltration membranes for treatment of oil contaminated water, Journal of Membrane Science. 325 (2008) 420–426.

[51] Q. Chang, J.E. Zhou, Y. Wang, J. Wang, G. Meng, Hydrophilic modification of Al2O3 microfiltration membrane with nano-sized γ-Al2O3 coating, Desalination. 262 (2010) 110–114.

[52] J.E. Zhou, Q. Chang, Y. Wang, J. Wang, G. Meng, Separation of stable oil-water emulsion by the hydrophilic nano-sized ZrO2 modified Al2O3 microfiltration membrane, Separation and Purification Technology. 75 (2010) 243–248.

[53] Q. Chang, J.E. Zhou, Y. Wang, J. Liang, X. Zhang, S. Cerneaux, X. Wang, Z. Zhu, Y. Dong, Application of ceramic microfiltration membrane modified by nano-TiO2 coating in separation of a stable oil-in-water emulsion, Journal of Membrane Science. 456 (2014) 128–133.

[54] J.K. Milić, I. Petrinić, A. Goršek, M. Simonič, Ultrafiltration of oil-in-water emulsion by using ceramic membrane: Taguchi experimental design approach, Central European Journal of Chemistry. 12 (2014) 242–249.

[55] H.J. Tanudjaja, V. V. Tarabara, A.G. Fane, J.W. Chew, Effect of cross-flow velocity, oil concentration and salinity on the critical flux of an oil-in-water emulsion in microfiltration, Journal of Membrane Science. 530 (2017) 11–19.

[56] S. Elmaleh, N. Ghaffor, Upgrading oil refinery effluents by cross-flow ultrafiltration, Water Science and Technology. 34 (1996) 231–238.

[57] S.H.D. Silalahi, T. Leiknes, Cleaning strategies in ceramic microfiltration membranes fouled by oil and particulate matter in produced water, Desalination. 236 (2009) 160–169.

[58] S.H.D. Silalahi, T. Leiknes, High frequency back-pulsing for fouling development control in ceramic microfiltration for treatment of produced water, Desalination and Water Treatment. 28 (2011) 137–152.

[59] P. Swenson, B. Tanchuk, E. Bastida, W. An, S.M. Kuznicki, Water desalination and de-oiling with natural zeolite membranes - Potential application for purification of SAGD process water, Desalination. 286 (2012) 442–446.

[60] S.E. Weschenfelder, A.C.C. Mello, C.P. Borges, J.C. Campos, Oilfield produced water treatment by ceramic membranes: Preliminary process cost estimation, Desalination. 360 (2015) 81–86.

[61] S.E. Weschenfelder, C.P. Borges, J.C. Campos, Oilfield produced water treatment by ceramic membranes: Bench and pilot scale evaluation, Journal of Membrane Science. 495 (2015) 242–251.

[62] A.S.C. Chen, J.T. Flynn, R.G. Cook, A.L. Casaday, Removal of Oil, Grease, and Suspended Solids From Produced Water With Ceramic Crossflow Microfiltration, SPE Production Engineering. 6 (1991) 131–136.

[63] R.J. Lahiere, K.P. Goodboy, Ceramic membrane treatment of petrochemical wastewater, Environmental Progress. 12 (1993) 86–96.

[64] A. Reyhani, H. Mashhadi Meighani, Optimal operating conditions of micro- and ultra-filtration systems for produced-water purification: Taguchi method and economic investigation, Desalination and Water Treatment. (2015) 1–13.

[65] A.Y. Ku, C.S. Henderson, M.A. Petersen, D.J. Pernitsky, A.Q. Sun, Aging of Water from Steam-Assisted Gravity Drainage (SAGD) Operations Due to Air Exposure and Effects on Ceramic Membrane Filtration, Industrial & Engineering Chemistry Research. 51 (2012) 7170–7176.

[66] T. Zsirai, A.K. Al-Jaml, H. Qiblawey, M. Al-Marri, A. Ahmed, S. Bach, S. Watson, S. Judd, Ceramic membrane filtration of produced water: Impact of membrane module, Separation and Purification Technology. 165 (2016) 214–221.

[67] T. Zsirai, H. Qiblawey, P. Buzatu, M. Al-Marri, S.J. Judd, Cleaning of ceramic membranes for produced water filtration, Journal of Petroleum Science and Engineering. 166 (2018) 283–289.

[68] S. Dong, E. Kim, A. Alpatova, H. Noguchi, Y. Liu, M.G. El-Din, Treatment of oil sands process-affected water by submerged ceramic membrane microfiltration system, Separation and Purification Technology. 138 (2014) 198–209.

[69] Y. Thibault, J. Gamage McEvoy, S. Mortazavi, D. Smith, A. Doiron, Characterization of fouling processes in ceramic membranes used for the recovery and recycle of oil sands produced water, Journal of Membrane Science. 540 (2017) 307–320.

[70] L. Liangxiong, T.M. Whitworth, R. Lee, Separation of inorganic solutes from oil-field produced water using a compacted bentonite membrane, Journal of Membrane Science. 217 (2003) 215–225.

[71] J. Zhong, X. Sun, C. Wang, Treatment of oily wastewater produced from refinery processes using flocculation and ceramic membrane filtration, Separation and Purification Technology. 32 (2003) 93–98.

[72] S.R.H. Abadi, M.R. Sebzari, M. Hemati, F. Rekabdar, T. Mohammadi, Ceramic membrane performance in microfiltration of oily wastewater, Desalination. 265 (2011) 222–228.

[73] S.S. Madaeni, H. Ahmadi Monfared, V. Vatanpour, A. Arabi Shamsabadi, E. Salehi, P. Daraei, S. Laki, S.M. Khatami, Coke removal from petrochemical oily wastewater using γ-Al2O3 based ceramic microfiltration membrane, Desalination. 293 (2012) 87–93.

[74] M. Abbasi, D. Mowla, Analysis of membrane pore-blocking models applied to the MF of real oily wastewaters treatment using mullite and mullite–alumina ceramic membranes, Desalination and Water Treatment. 52 (2014) 2481–2493.

[75] A. Alpatova, E.S. Kim, S. Dong, N. Sun, P. Chelme-Ayala, M. Gamal El-Din, Treatment of oil

sands process-affected water with ceramic ultrafiltration membrane: Effects of operating conditions on membrane performance, Separation and Purification Technology. 122 (2014) 170–182.

[76] S.E. Weschenfelder, A.M.T. Louvisse, C.P. Borges, E. Meabe, J. Izquierdo, J.C. Campos, Evaluation of ceramic membranes for oilfield produced water treatment aiming reinjection in offshore units, Journal of Petroleum Science and Engineering. 131 (2015) 51–57.

[77] A. Guirgis, R. Gay-de-Montella, R. Faiz, Treatment of produced water streams in SAGD processes using tubular ceramic membranes, Desalination. 358 (2015) 27–32.

[78] K. Loganathan, P. Chelme-Ayala, M. Gamal El-Din, Pilot-scale study on the reverse osmosis treatment of oil sands tailings pond water: Impact of pretreatment on process performance, Desalination. 360 (2015) 52–60.

[79] K. Loganathan, P. Chelme-Ayala, M.G. El-Din, Effects of different pretreatments on the performance of ceramic ultrafiltration membrane during the treatment of oil sands tailings pond recycle water : A pilot-scale study, Journal of Environmental Management. 151 (2015) 540–549.

[80] H. Abadikhah, J.W. Wang, S.A. Khan, X. Xu, S. Agathopoulos, Morphological engineering of silicon nitride hollow fiber membrane for oil-field-produced-water treatment, Ceramics International. 45 (2019) 10541–10549.

[81] A. Jada, M. Salou, Effects of the asphaltene and resin contents of the bitumens on the water-bitumen interface properties, Journal of Petroleum Science and Engineering. 33 (2002) 185–193.

[82] D. Lesueur, The colloidal structure of bitumen: Consequences on the rheology and on the mechanisms of bitumen modification, Advances in Colloid and Interface Science. 145 (2009) 42–82.

[83] M.A. Rodríguez-Valverde, M.A. Cabrerizo-Vílchez, A. Páez-Dueñas, R. Hidalgo-Álvarez, Stability of highly charged particles: bitumen-in-water dispersions, Colloids and Surfaces A: Physicochemical and Engineering Aspects. 222 (2003) 233–251.

[84] O. V. Abramov, V.O. Abramov, S.K. Myasnikov, M.S. Mullakaev, Extraction of bitumen, crude oil and its products from tar sand and contaminated sandy soil under effect of ultrasound, Ultrasonics Sonochemistry. 16 (2009) 408–416.

[85] J.G. Speight, Chemical and physical studies of petroleum asphaltenes, in: T.F. Yen, G.V. Chilinggarian (Eds.), Asphaltenes and Asphalt, Elsevier Science B.V., Amsterdam, 1994: pp. 7–65.

[86] G. Gu, Z. Xu, K. Nandakumar, J.H. Masliyah, Influence of water-soluble and water-insoluble natural surface active components on the stability of water-in-toluene-diluted bitumen emulsion, Fuel. 81 (2002) 1859–1869.

[87] J. Liu, Z. Xu, J. Masliyah, Role of fine clays in bitumen extraction from oil sands, AIChE Journal. 50 (2004) 1917–1927.

[88] R.P. Castro, Y. Cohen, H.G. Monbouquette, The permeability behavior of polyvinylpyrrolidone-modified porous silica membranes, Journal of Membrane Science. 84 (1993) 151–160.

[89] R.P. Castro, Y. Cohen, H.G. Monbouquette, Silica-supported polyvinylpyrrolidone filtration membranes, Journal of Membrane Science. 115 (1996) 179–190.

[90] M. Rovira-Bru, F. Giralt, Y. Cohen, Protein Adsorption onto Zirconia Modified with Terminally

Grafted Polyvinylpyrrolidone., Journal of Colloid and Interface Science. 235 (2001) 70–79.

[91] R.P. Castro, H.G. Monbouquette, Y. Cohen, Shear-induced permeability changes in a polymer grafted silica membrane, Journal of Membrane Science. 179 (2000) 207–220.

[92] W. Yoshida, Y. Cohen, Ceramic-supported polymer membranes for pervaporation of binary organic/organic mixtures, Journal of Membrane Science. 213 (2003) 145–157.

[93] D. Li, J. Yao, B. Liu, H. Sun, S. van Agtmaal, C. Feng, Preparation and characterization of surface grafting polymer of ZrO2 membrane and ZrO2 powder, Applied Surface Science. 471 (2019) 394–402.

[94] W. Yoshida, Y. Cohen, Removal of methyl tert-butyl ether from water by pervaporation using ceramic-supported polymer membranes, Journal of Membrane Science. 229 (2004) 27–32.

[95] W. Yoshida, Y. Cohen, Topological AFM characterization of graft polymerized silica membranes, Journal of Membrane Science. 215 (2003) 249–264.

[96] J.-D. Jou, W. Yoshida, Y. Cohen, A novel ceramic-supported polymer membrane for pervaporation of dilute volatile organic compounds, Journal of Membrane Science. 162 (1999) 269–284.

[97] S. Yi, Y. Su, Y. Wan, Preparation and characterization of vinyltriethoxysilane (VTES) modified silicalite-1/PDMS hybrid pervaporation membrane and its application in ethanol separation from dilute aqueous solution, Journal of Membrane Science. 360 (2010) 341–351.

[98] E. Jannatduost, A.A. Babaluo, F. Abbasi, M.A. Ardestani, M. Peyravi, Surface modification of nanocomposite ceramic membranes by PDMS for condensable hydrocarbons separation, Desalination. 250 (2010) 1136–1139.

[99] G. Liu, F. Xiangli, W. Wei, S. Liu, W. Jin, Improved performance of PDMS/ceramic composite pervaporation membranes by ZSM-5 homogeneously dispersed in PDMS via a surface graft/coating approach, Chemical Engineering Journal. 174 (2011) 495–503.

[100] N. Gao, Z.-K. Xu, Ceramic membranes with mussel-inspired and nanostructured coatings for water-in-oil emulsions separation, Separation and Purification Technology. 212 (2019) 737–746.

[101] D. Zhang, G. Wang, S. Zhi, K. Xu, L. Zhu, W. Li, Z. Zeng, Q. Xue, Superhydrophilicity and underwater superoleophobicity TiO2/Al2O3 composite membrane with ultra low oil adhesion for highly efficient oil-in-water emulsions separation, Applied Surface Science. 458 (2018) 157–165.

[102] D. Lu, W. Cheng, T. Zhang, X. Lu, Q. Liu, J. Jiang, J. Ma, Hydrophilic Fe2O3 dynamic membrane mitigating fouling of support ceramic membrane in ultrafiltration of oil/water emulsion, Separation and Purification Technology. 165 (2016) 1–9.

[103] D. Lu, T. Zhang, L. Gutierrez, J. Ma, J.P. Croué, Influence of Surface Properties of Filtration-Layer Metal Oxide on Ceramic Membrane Fouling during Ultrafiltration of Oil/Water Emulsion, Environmental Science & Technology. 50 (2016) 4668–4674.

[104] R. Liu, A.K.Y. Raman, I. Shaik, C. Aichele, S.J. Kim, Inorganic microfiltration membranes incorporated with hydrophilic silica nanoparticles for oil-in-water emulsion separation, Journal of Water Process Engineering. 26 (2018) 124–130.

[105] P. Gao, Z. Liu, D.D. Sun, W.J. Ng, The efficient separation of surfactant-stabilized oil–water emulsions with a flexible and superhydrophilic graphene–TiO2 composite membrane, Journal of Materials Chemistry A. 2 (2014) 14082–14088.

[106] X. Hu, Y. Yu, J. Zhou, Y. Wang, J. Liang, X. Zhang, Q. Chang, L. Song, The improved oil/water separation performance of graphene oxide modified Al2O3 microfiltration membrane, Journal of Membrane Science. 476 (2015) 200–204.

[107] S.J. Maguire-Boyle, J.E. Huseman, T.J. Ainscough, D.L. Oatley-Radcliffe, A.A. Alabdulkarem, S.F. Al-Mojil, A.R. Barron, Superhydrophilic Functionalization of Microfiltration Ceramic Membranes Enables Separation of Hydrocarbons from Frac and Produced Water, Scientific Reports. 7 (2017) 1–9.

[108] A. Dafinov, R. Garcia-Valls, J. Font, Modification of ceramic membranes by alcohol adsorption, Journal of Membrane Science. 196 (2002) 69–77.

[109] P.H. Mutin, V. Lafond, A.F. Popa, M. Granier, L. Markey, A. Dereux, Selective surface modification of SiO2-TiO2 supports with phosphonic acids, Chemistry of Materials. 16 (2004) 5670–5675.

[110] V. Meynen, H. Castricum, A. Buekenhoudt, Class II Hybrid Organic-inorganic Membranes Creating New Versatility in Separations, Current Organic Chemistry. 18 (2014) 2334–2350.

[111] T. Materne, F. de Buyl, G.L. Witucki, Organosilane Technology in Coating Applications: Review and Perspectives, Dow Corning. (2012) 16.

[112] B. Arkles, Silane Coupling Agents: Connceting Across Boundaries, Gelest, Inc. (2014) 72.

[113] B. Díaz-Benito, F. Velasco, F.J. Martínez, N. Encinas, Hydrolysis study of bis-1,2-(triethoxysilyl)ethane silane by NMR, Colloids and Surfaces A: Physicochemical and Engineering Aspects. 369 (2010) 53–56.

[114] J. Rubio, M.A. Mazo, A. Martín-Ilana, A. Tamayo, FT-IR study of the hydrolysis and condensation of 3-(2-amino-ethylamino)propyl-trimethoxy silane, Boletin de La Sociedad Espanola de Ceramica y Vidrio. 57 (2018) 160–168.

[115] M.C. Brochier Salon, M.N. Belgacem, Competition between hydrolysis and condensation reactions of trialkoxysilanes, as a function of the amount of water and the nature of the organic group, Colloids and Surfaces A: Physicochemical and Engineering Aspects. 366 (2010) 147–154.

[116] M.C. Brochier Salon, M.N. Belgacem, Hydrolysis-condensation kinetics of different silane coupling agents, Phosphorus, Sulfur and Silicon and the Related Elements. 186 (2011) 240–254.

[117] M.C. Brochier Salon, P.A. Bayle, M. Abdelmouleh, S. Boufi, M.N. Belgacem, Kinetics of hydrolysis and self condensation reactions of silanes by NMR spectroscopy, Colloids and Surfaces A: Physicochemical and Engineering Aspects. 312 (2008) 83–91.

[118] O. Paquet, M.C.B. Salon, E. Zeno, M.N. Belgacem, Hydrolysis-condensation kinetics of 3-(2-amino-ethylamino)propyl- trimethoxysilane, Materials Science and Engineering C. 32 (2012) 487–493.

[119] F.D. Osterholtz, E.R. Pohl, Kinetics of the hydrolysis and condensation of organofunctional alkoxysilanes: a review, Journal of Adhesion Science and Technology. 6 (1992) 127–149.

[120] S. Sterman, J.G. Marsden, Silane Coupling Agents, Industrial & Engineering Chemistry. 58 (1966) 33–37.

[121] E.P. Plueddemann, Adhesion Through Silane Coupling Agents, The Journal of Adhesion. 2 (1970) 184–201.

[122] P.G. Pape, E.P. Plueddemann, Methods for improving the performance of silane coupling agents,

Journal of Adhesion Science and Technology. 5 (1991) 831–842.

[123] C.R. Kessel, S. Granick, Formation and characterization of a highly ordered and well- anchored alkylsilane monolayer on mica by self-assembly, Langmuir. 7 (1991) 532–538.

[124] A.Y. Fadeev, T.J. McCarthy, Trialkylsilane monolayers covalently attached to silicon surfaces: Wettability studies indicating that molecular topography contributes to contact angle hysteresis, Langmuir. 15 (1999) 3759–3766.

[125] A.Y. Fadeev, T.J. McCarthy, Self-assembly is not the only reaction possible between alkyltrichlorosilanes and surfaces: monomolecular and oligomeric covalently attached layers of dichloro- and trichloroalkylsilanes on silicon, Langmuir. 16 (2000) 7268–7274.

[126] W. Yoshida, R.P. Castro, J.D. Jou, Y. Cohen, Multilayer alkoxysilane silylation of oxide surfaces, Langmuir. 17 (2001) 5882–5888.

[127] H. Sugimura, A. Hozumi, T. Kameyama, O. Takai, Organosilane self-assembled monolayers formed at the vapour/solid interface, Surface and Interface Analysis. 34 (2002) 550–554.

[128] R. Helmy, A.Y. Fadeev, Self-assembled monolayers supported on TiO2: Comparison of C18H37SiX3 (X = H, Cl, OCH3), C18H37Si(CH3)2Cl, and C18H37PO(OH)2, Langmuir. 18 (2002) 8924–8928.

[129] S. Marcinko, A.Y. Fadeev, Hydrolytic stability of organic monolayers supported on TiO2 and ZrO2., Langmuir. 20 (2004) 2270–2273.

[130] C. Picard, A. Larbot, F. Guida-Pietrasanta, B. Boutevin, A. Ratsimihety, Grafting of ceramic membranes by flourinated silanes: Hydrophobic features, Separation and Purification Technology. 25 (2001) 65–69.

[131] S.R. Krajewski, W. Kujawski, F. Dijoux, C. Picard, A. Larbot, Grafting of ZrO2 powder and ZrO2 membrane by fluoroalkylsilanes, Colloids and Surfaces A: Physicochemical and Engineering Aspects. 243 (2004) 43–47.

[132] C. Picard, A. Larbot, E. Tronel-Peyroz, R. Berjoan, Characterisation of hydrophilic ceramic membranes modified by fluoroalkylsilanes into hydrophobic membranes, Solid State Sciences. 6 (2004) 605–612.

[133] H.L. Castricum, A. Sah, M.C. Mittelmeijer-Hazeleger, J.E. Ten Elshof, Hydrophobisation of mesoporous γ-Al2O3 with organochlorosilanes-efficiency and structure, Microporous and Mesoporous Materials. 83 (2005) 1–9.

[134] C.C. Wei, K. Li, Preparation and characterization of a robust and hydrophobic ceramic membrane via an improved surface grafting technique, Industrial & Engineering Chemistry Research. 48 (2009) 3446–3452.

[135] J.L. Hardin, N.A. Oyler, E.D. Steinle, G.A. Meints, Spectroscopic analysis of interactions between alkylated silanes and alumina nanoporous membranes, Journal of Colloid and Interface Science. 342 (2010) 614–619.

[136] N.A. Ahmad, C.P. Leo, A.L. Ahmad, Synthesis of superhydrophobic alumina membrane: Effects of sol-gel coating, steam impingement and water treatment, Applied Surface Science. 284 (2013) 556–564.

[137] M. Khemakhem, S. Khemakhem, R. Ben Amar, Surface modification of microfiltration ceramic membrane by fluoroalkylsilane, Desalination and Water Treatment. 52 (2014) 1786–1791.

[138] J. Kujawa, W. Kujawski, Functionalization of Ceramic Metal Oxide Powders and Ceramic Membranes by Perfluroalkylsilanes and Alkylsilanes Possessing Different Reactive Groups – Physicochemical and Tribological Properties, ACS Applied Materials & Interfaces. 8 (2016) 7509–7521.

[139] A.Y. Ku, J.A. Ruud, T.A. Early, R.R. Corderman, Evidence of ion transport through surface conduction in alkylsilane-functionalized nanoporous ceramic membranes, Langmuir. 22 (2006) 8277–8280.

[140] T. Okubo, H. Inoue, Introduction of specific gas selectivity to porous glass membranes by treatment with tetraethoxysilane, Journal of Membrane Science. 42 (1989) 109–117.

[141] J.R. Miller, W.J. Koros, The formation of chemically modified γ-alumina microporous membranes, Separation Science and Technology. 25 (1990) 1257–1280.

[142] C. Leger, H.L. De Lira, R. Paterson, Preparation and properties of surface modified ceramic membranes. Part III. Gas permeation of 5 nm alumina membranes modified by trichloro-octadecylsilane, Journal of Membrane Science. 120 (1996) 187–195.

[143] J. Caro, M. Noack, P. Kölsch, Chemically modified ceramic membranes, Microporous and Mesoporous Materials. 22 (1998) 321–332.

[144] S. Koonaphapdeelert, K. Li, Preparation and characterization of hydrophobic ceramic hollow fibre membrane, Journal of Membrane Science. 291 (2007) 70–76.

[145] S.H. Hyun, S.Y. Jo, B.S. Kang, Surface modification of γ-alumina membranes by silane coupling for CO2 separation, Journal of Membrane Science. 120 (1996) 197–206.

[146] N. Abidi, A. Sivade, D. Bourret, A. Larbot, B. Boutevin, F. Guida-Pietrasanta, A. Ratsimihety, Surface modification of mesoporous membranes by fluoro-silane coupling reagent for CO2 separation, Journal of Membrane Science. 270 (2006) 101–107.

[147] G.D. Bothun, K. Peay, S. Ilias, Role of tail chemistry on liquid and gas transport through organosilane-modified mesoporous ceramic membranes, Journal of Membrane Science. 301 (2007) 162–170.

[148] Y. Sakamoto, K. Nagata, K. Yogo, K. Yamada, Preparation and CO2 separation properties of amine-modified mesoporous silica membranes, Microporous and Mesoporous Materials. 101 (2007) 303–311.

[149] M. Ostwal, R.P. Singh, S.F. Dec, M.T. Lusk, J.D. Way, 3-Aminopropyltriethoxysilane functionalized inorganic membranes for high temperature CO2/N2 separation, Journal of Membrane Science. 369 (2011) 139–147.

[150] T. Takahashi, R. Tanimoto, T. Isobe, S. Matsushita, A. Nakajima, Surface modification of porous alumina filters for CO2 separation using silane coupling agents, Journal of Membrane Science. 497 (2016) 216–220.

[151] E. Magnone, H.J. Lee, J.W. Che, J.H. Park, High-performance of modified Al2O3 hollow fiber membranes for CO2 absorption at room temperature, Journal of Industrial and Engineering Chemistry. 42 (2016) 19–22.

[152] M.A. Abdulhameed, M.H.D. Othman, A.F. Ismail, T. Matsuura, Z. Harun, M.A. Rahman, M.H. Puteh, J. Jaafar, M. Rezaei, S.K. Hubadillah, Carbon dioxide capture using a superhydrophobic ceramic hollow fibre membrane for gas-liquid contacting process, Journal of Cleaner Production. 140 (2017) 1731–1738.

[153] K.C. McCarley, J.D. Way, Development of a model surface flow membrane by modification of porous γ-alumina with octadecyltrichlorosilane, Separation and Purification Technology. 25 (2001) 195–210.

[154] R.P. Singh, J.D. Way, K.C. McCarley, Development of a Model Surface Flow Membrane by Modification of Porous Vycor Glass with a Fluorosilane, Industrial & Engineering Chemistry Research. 43 (2004) 3033–3040.

[155] R.M. De Vos, W.F. Maier, H. Verweij, Hydrophobic silica membranes for gas separation, Journal of Membrane Science. 158 (1999) 277–288.

[156] X. Gu, Z. Tang, J. Dong, On-stream modification of MFI zeolite membranes for enhancing hydrogen separation at high temperature, Microporous and Mesoporous Materials. 111 (2008) 441–448.

[157] Q. Wei, F. Wang, Z.R. Nie, C.L. Song, Y.L. Wang, Q.Y. Li, Highly hydrothermally stable microporous silica membranes for hydrogen separation, Journal of Physical Chemistry B. 112 (2008) 9354–9359.

[158] D. Luebke, C. Myers, H. Pennline, Hybrid membranes for selective carbon dioxide separation from fuel gas, Energy & Fuels. 20 (2006) 1906–1913.

[159] O.C. Vangeli, G.E. Romanos, K.G. Beltsios, D. Fokas, C.P. Athanasekou, N.K. Kanellopoulos, Development and characterization of chemically stabilized ionic liquid membranes-Part I: Nanoporous ceramic supports, Journal of Membrane Science. 365 (2010) 366–377.

[160] A. Javaid, D.A. Krapchetov, D.M. Ford, Solubility-based gas separation with oligomer-modified inorganic membranes: Part III. Effects of synthesis conditions, Journal of Membrane Science. 246 (2005) 181–191.

[161] R.P. Singh, J.D. Way, S.F. Dec, Silane modified inorganic membranes: Effects of silane surface structure, Journal of Membrane Science. 259 (2005) 34–46.

[162] A. Javaid, M.P. Hughey, V. Varutbangkul, D.M. Ford, Solubility-based gas separation with oligomer-modified inorganic membranes, Journal of Membrane Science. 187 (2001) 141–150.

[163] A. Javaid, D.M. Ford, Solubility-based gas separation with oligomer-modified inorganic membranes: Part II. Mixed gas permeation of 5 nm alumina membranes modified with octadecyltrichlorosilane, Journal of Membrane Science. 215 (2003) 157–168.

[164] R. Faiz, M. Fallanza, I. Ortiz, K. Li, Separation of olefin paraffin gas mixtures using ceramic hollow fiber membrane contactors, Industrial & Engineering Chemistry Research. 52 (2013) 7918–7929.

[165] A. Alkhudhiri, N. Darwish, N. Hilal, Membrane distillation: A comprehensive review, Desalination. 287 (2012) 2–18.

[166] J. Kujawa, S. Cerneaux, W. Kujawski, Investigation of the stability of metal oxide powders and ceramic membranes grafted by perfluoroalkylsilanes, Colloids and Surfaces A: Physicochemical and Engineering Aspects. 443 (2014) 109–117.

[167] A. Larbot, L. Gazagnes, S.R. Krajewski, M. Bukowska, W. Kujawski, Water desalination using ceramic membrane distillation, Desalination. 168 (2004) 367–372.

[168] Y. Fan, S. Chen, H. Zhao, Y. Liu, Distillation membrane constructed by TiO2 nanofiber followed by fluorination for excellent water desalination performance, Desalination. 405 (2017) 51–58.

[169] C.-C. Ko, C.-H. Chen, Y.-R. Chen, Y.-H. Wu, S.-C. Lu, F.-C. Hu, C.-L. Li, K.-L. Tung, Increasing the Performance of Vacuum Membrane Distillation Using Micro-Structured Hydrophobic Aluminum Hollow Fiber Membranes, Applied Sciences. 7 (2017) 357–366.

[170] C.-Y. Huang, C.-C. Ko, L.-H. Chen, C.-T. Huang, Y.-C. Liao, A simple coating method to prepare superhydrophobic layers on ceramic alumina for vacuum membrane distillation, Separation and Purification Technology. 198 (2018) 79–86.

[171] C.-C. Ko, A. Ali, E. Drioli, K.-L. Tung, C.-H. Chen, Y.-R. Chen, F. Macedonio, Performance of ceramic membrane in vacuum membrane distillation and in vacuum membrane crystallization, Desalination. 440 (2018) 48–58.

[172] S.K. Hubadillah, M.H.D. Othman, T. Matsuura, M.A. Rahman, J. Jaafar, A.F. Ismail, S.Z.M. Amin, Green silica-based ceramic hollow fiber membrane for seawater desalination via direct contact membrane distillation, Separation and Purification Technology. 205 (2018) 22–31.

[173] J.W. Wang, L. Li, J.W. Zhang, X. Xu, C.S. Chen, β-Sialon ceramic hollow fiber membranes with high strength and low thermal conductivity for membrane distillation, Journal of the European Ceramic Society. 36 (2016) 59–65.

[174] Y. Yang, Q. Liu, H. Wang, F. Ding, G. Jin, C. Li, H. Meng, Superhydrophobic modification of ceramic membranes for vacuum membrane distillation, Chinese Journal of Chemical Engineering. 25 (2017) 1395–1401.

[175] L. García-Fernández, B. Wang, M.C. García-Payo, K. Li, M. Khayet, Morphological design of alumina hollow fiber membranes for desalination by air gap membrane distillation, Desalination. 420 (2017) 226–240.

[176] R. Das, K. Sondhi, S. Majumdar, S. Sarkar, Development of hydrophobic clay–alumina based capillary membrane for desalination of brine by membrane distillation, Journal of Asian Ceramic Societies. 4 (2016) 243–251.

[177] L. Gazagnes, S. Cerneaux, M. Persin, E. Prouzet, A. Larbot, Desalination of sodium chloride solutions and seawater with hydrophobic ceramic membranes, Desalination. 217 (2007) 260–266.

[178] S.R. Krajewski, W. Kujawski, M. Bukowska, C. Picard, A. Larbot, Application of fluoroalkylsilanes (FAS) grafted ceramic membranes in membrane distillation process of NaCl solutions, Journal of Membrane Science. 281 (2006) 253–259.

[179] S. Khemakhem, R. Ben Amar, Modification of Tunisian clay membrane surface by silane grafting: Application for desalination with Air Gap Membrane Distillation process, Colloids and Surfaces A: Physicochemical and Engineering Aspects. 387 (2011) 79–85.

[180] S. Cerneaux, I. Struzynska, W.M. Kujawski, M. Persin, A. Larbot, Comparison of various membrane distillation methods for desalination using hydrophobic ceramic membranes, Journal of Membrane Science. 337 (2009) 55–60.

[181] Z.D. Hendren, J. Brant, M.R. Wiesner, Surface modification of nanostructured ceramic membranes for direct contact membrane distillation, Journal of Membrane Science. 331 (2009) 1–10.

[182] H. Fang, J.F. Gao, H.T. Wang, C.S. Chen, Hydrophobic porous alumina hollow fiber for water desalination via membrane distillation process, Journal of Membrane Science. 403–404 (2012) 41–46.

[183] J. Kujawa, W. Kujawski, S. Koter, K. Jarzynka, A. Rozicka, K. Bajda, S. Cerneaux, M. Persin, A.

Larbot, Membrane distillation properties of TiO2 ceramic membranes modified by perfluoroalkylsilanes, Desalination and Water Treatment. 51 (2013) 1352–1361.

[184] J. Kujawa, S. Cerneaux, S. Koter, W. Kujawski, Highly Efficient Hydrophobic Titania Ceramic Membranes for Water Desalination, ACS Applied Materials & Interfaces. 6 (2014) 14223–30.

[185] C. Ren, H. Fang, J. Gu, L. Winnubst, C. Chen, Preparation and characterization of hydrophobic alumina planar membranes for water desalination, Journal of the European Ceramic Society. 35 (2015) 723–730.

[186] J. Kujawa, S. Cerneaux, W. Kujawski, M. Bryjak, J.K. Kujawski, How To Functionalize Ceramics by Perfluoroalkylsilanes for Membrane Separation Process? - Properties and Application of Hydrophobized Ceramic Membranes, ACS Applied Materials & Interfaces. 8 (2016) 7564–7577.

[187] S. Khemakhem, R. Ben Amar, Grafting of fluoroalkylsilanes on microfiltration Tunisian clay membrane, Ceramics International. 37 (2011) 3323–3328.

[188] M. Khemakhem, S. Khemakhem, R. Ben Amar, Emulsion separation using hydrophobic grafted ceramic membranes by, Colloids and Surfaces A: Physicochemical and Engineering Aspects. 436 (2013) 402–407.

[189] W. Kujawski, J. Kujawa, E. Wierzbowska, S. Cerneaux, M. Bryjak, J. Kujawski, Influence of hydrophobization conditions and ceramic membranes pore size on their properties in vacuum membrane distillation of water-organic solvent mixtures, Journal of Membrane Science. 499 (2016) 442–451.

[190] J. Kujawa, S. Al-Gharabli, W. Kujawski, K. Knozowska, Molecular Grafting of Fluorinated and Nonfluorinated Alkylsiloxanes on Various Ceramic Membrane Surfaces for the Removal of Volatile Organic Compounds Applying Vacuum Membrane Distillation, ACS Applied Materials & Interfaces. 9 (2017) 6571–6590.

[191] S.K. Hubadillah, M.H.D. Othman, A.F. Ismail, M.A. Rahman, J. Jaafar, A low cost hydrophobic kaolin hollow fiber membrane (h-KHFM) for arsenic removal from aqueous solution via direct contact membrane distillation, Separation and Purification Technology. 214 (2019) 31–39.

[192] F. Gabino, M.P. Belleville, L. Preziosi-Belloy, M. Dornier, J. Sanchez, Evaluation of the cleaning of a new hydrophobic membrane for osmotic evaporation, Separation and Purification Technology. 55 (2007) 191–197.

[193] A. Vargas-Garcia, B. Torrestiana-Sanchez, A. Garcia-Borquez, G. Aguilar-Uscanga, Effect of grafting on microstructure, composition and surface and transport properties of ceramic membranes for osmotic evaporation, Separation and Purification Technology. 80 (2011) 473–481.

[194] J. Kujawa, S. Cerneaux, W. Kujawski, K. Knozowska, Hydrophobic Ceramic Membranes for Water Desalination, Applied Sciences. 7 (2017) 402–412.

[195] X. Chen, X. Gao, K. Fu, M. Qiu, F. Xiong, D. Ding, Z. Cui, Z. Wang, Y. Fan, E. Drioli, Tubular hydrophobic ceramic membrane with asymmetric structure for water desalination via vacuum membrane distillation process, Desalination. 443 (2018) 212–220.

[196] S. Tao, Y.D. Xu, J.Q. Gu, H. Abadikhah, J.W. Wang, X. Xu, Preparation of high-efficiency ceramic planar membrane and its application for water desalination, Journal of Advanced Ceramics. 7 (2018) 117–123.

[197] J. Kujawa, W. Kujawski, A. Cyganiuk, L.F. Dumée, S. Al-Gharabli, Upgrading of zirconia membrane performance in removal of hazardous VOCs from water by surface functionalization,

Chemical Engineering Journal. 374 (2019) 155–169.

[198] S. Alami-Younssi, C. Kiefer, A. Larbot, M. Persin, J. Sarrazin, Grafting γ-alumina microporous membranes by organosilanes: Characterisation by pervaporation, Journal of Membrane Science. 143 (1998) 27–36.

[199] S. Alami Younssi, A. Iraqi, M. Rafiq, M. Persin, A. Larbot, J. Sarrazin, γ Alumina membranes grafting by organosilanes and its application to the separation of solvent mixtures by pervaporation, Separation and Purification Technology. 32 (2003) 175–179.

[200] D.H. Park, N. Nishiyama, Y. Egashira, K. Ueyama, Separation of organic/water mixtures with silylated MCM-48 silica membranes, Microporous and Mesoporous Materials. 66 (2003) 69–76.

[201] W. Kujawski, S. Krajewska, M. Kujawski, L. Gazagnes, A. Larbot, M. Persin, Pervaporation properties of fluoroalkylsilane (FAS) grafted ceramic membranes, Desalination. 205 (2007) 75–86.

[202] J. Kujawa, S. Cerneaux, W. Kujawski, Removal of hazardous volatile organic compounds from water by vacuum pervaporation with hydrophobic ceramic membranes, Journal of Membrane Science. 474 (2015) 11–19.

[203] J. Kujawa, S. Cerneaux, W. Kujawski, Highly hydrophobic ceramic membranes applied to the removal of volatile organic compounds in pervaporation, Chemical Engineering Journal. 260 (2015) 43–54.

[204] S. Oh, T. Kang, H. Kim, J. Moon, S. Hong, J. Yi, Preparation of novel ceramic membranes modified by mesoporous silica with 3-aminopropyltriethoxysilane (APTES) and its application to Cu2+ separation in the aqueous phase, Journal of Membrane Science. 301 (2007) 118–125.

[205] J.R. Stephens, J.S. Beveridge, M.E. Williams, Diffusive flux of nanoparticles through chemically modified alumina membranes, Analyst. 136 (2011) 3797–3802.

[206] X. Ke, Y. Huang, T.R. Dargaville, Y. Fan, Z. Cui, H. Zhu, Modified alumina nanofiber membranes for protein separation, Separation and Purification Technology. 120 (2013) 239–244.

[207] M. Williams, C.A. Pineda-Vargas, E. V. Khataibe, B.J. Bladergroen, A.N. Nechaev, V.M. Linkov, Surface functionalization of porous ZrO2-TiO2 membranes using γ-aminopropyltriethoxysilane in palladium electroless deposition, Applied Surface Science. 254 (2008) 3211–3219.

[208] R. Chen, Y. Jiang, W. Xing, W. Jin, Fabrication and catalytic properties of palladium nanoparticles deposited on a silanized asymmetric ceramic support, Industrial & Engineering Chemistry Research. 50 (2011) 4405–4411.

[209] H. Li, H. Jiang, R. Chen, Y. Wang, W. Xing, Enhanced catalytic properties of palladium nanoparticles deposited on a silanized ceramic membrane support with a flow-through method, Industrial & Engineering Chemistry Research. 52 (2013) 14099–14106.

[210] T. Van Gestel, B. Van Der Bruggen, A. Buekenhoudt, C. Dotremont, J. Luyten, C. Vandecasteele, G. Maes, Surface modification of γ-Al2O3/TiO2 multilayer membranes for applications in non-polar organic solvents, Journal of Membrane Science. 224 (2003) 3–10.

[211] T. Tsuru, M. Miyawaki, H. Kondo, T. Yoshioka, M. Asaeda, Inorganic porous membranes for nanofiltration of nonaqueous solutions, Separation and Purification Technology. 32 (2003) 105–109.

[212] A. Sah, H.L. Castricum, A. Bliek, D.H.A. Blank, J.E. Ten Elshof, Hydrophobic modification of γ-

alumina membranes with organochlorosilanes, Journal of Membrane Science. 243 (2004) 125–132.

[213] B. Verrecht, R. Leysen, A. Buekenhoudt, C. Vandecasteele, B. Van der Bruggen, Chemical surface modification of γ-Al2O3 and TiO2 toplayer membranes for increased hydrophobicity, Desalination. 200 (2006) 385–386.

[214] L. Treccani, T. Yvonne Klein, F. Meder, K. Pardun, K. Rezwan, Functionalized ceramics for biomedical, biotechnological and environmental applications, Acta Biomaterialia. 9 (2013) 7115–7150.

[215] J. Bartels, M.N. Souza, A. Schaper, P. Árki, S. Kroll, K. Rezwan, Amino-Functionalized Ceramic Capillary Membranes for Controlled Virus Retention, Environmental Science & Technology. 50 (2016) 1973–1981.

[216] S. Kroll, L. Treccani, K. Rezwan, G. Grathwohl, Development and characterisation of functionalised ceramic microtubes for bacteria filtration, Journal of Membrane Science. 365 (2010) 447–455.

[217] J. Bartels, A.G. Batista, S. Kroll, M. Maas, K. Rezwan, Hydrophobic ceramic capillary membranes for versatile virus filtration, Journal of Membrane Science. 570–571 (2019) 85–92.

[218] J. Kujawa, E. Chrzanowska, W. Kujawski, Transport properties and fouling issues of membranes utilized for the concentration of dairy products by air-gap membrane distillation and microfiltration, Chemical Papers. (2018) 1–18.

[219] N. Gao, M. Li, W. Jing, Y. Fan, N. Xu, Improving the filtration performance of ZrO2 membrane in non-polar organic solvents by surface hydrophobic modification, Journal of Membrane Science. 375 (2011) 276–283.

[220] N. Gao, W. Ke, Y. Fan, N. Xu, Evaluation of the oleophilicity of different alkoxysilane modified ceramic membranes through wetting dynamic measurements, Applied Surface Science. 283 (2013) 863–870.

[221] N.A. Ahmad, C.P. Leo, A.L. Ahmad, Superhydrophobic alumina membrane by steam impingement: Minimum resistance in microfiltration, Separation and Purification Technology. 107 (2013) 187–194.

[222] N. Gao, Y. Fan, X. Quan, Y. Cai, D. Zhou, Modified ceramic membranes for low fouling separation of water-in-oil emulsions, Journal of Materials Science. 51 (2016) 6379–6388.

[223] D. Ding, H. Mao, X. Chen, M. Qiu, Y. Fan, Underwater superoleophobic-underoil superhydrophobic Janus ceramic membrane with its switchable separation in oil/water emulsions, Journal of Membrane Science. 565 (2018) 303–310.

[224] J. Lee, J.-H. Ha, I.-H. Song, Improving the antifouling properties of ceramic membranes via chemical grafting of organosilanes, Separation Science and Technology. 51 (2016) 2420–2428.

[225] J. Lee, J.-H. Ha, I.-H. Song, D.W. Shin, Enhanced fouling resistance of organosilane-grafted ceramic microfiltration membranes for water treatment, Journal of the Ceramic Society of Japan. 125 (2017) 899–905.

[226] S. Yeu, J.D. Lunn, H.M. Rangel, D.F. Shantz, The effect of surface modifications on protein microfiltration properties of Anopore membranes, Journal of Membrane Science. 327 (2009) 108–117.

[227] K.C. Popat, G. Mor, C.A. Grimes, T.A. Desai, Surface modification of nanoporous alumina surfaces with poly(ethylene glycol), Langmuir. 20 (2004) 8035–8041.

[228] K.C. Popat, G. Mor, C. Grimes, T.A. Desai, Poly (ethylene glycol) grafted nanoporous alumina membranes, Journal of Membrane Science. 243 (2004) 97–106.

[229] S.W. Lee, H. Shang, R.T. Haasch, V. Petrova, G.U. Lee, Transport and functional behaviour of poly(ethylene glycol)-modified nanoporous alumina membranes, Nanotechnology. 16 (2005) 1335–1340.

[230] C.R. Tanardi, R. Catana, M. Barboiu, A. Ayral, I.F.J. Vankelecom, A. Nijmeijer, L. Winnubst, Polyethyleneglycol grafting of γ-alumina membranes for solvent resistant nanofiltration, Microporous and Mesoporous Materials. 229 (2016) 106–116.

3 Silane Surface Modified Ceramic Membranes for the Treatment and Recycling of SAGD Produced Water

C. Atallah, A.Y. Tremblay, S. Mortazavi.

Manuscript published in the Journal of Petroleum Science and Engineering 157 (2017): 349–358.

DOI: 10.1016/j.petrol.2017.07.007

Abstract

The extraction of bitumen using oil extraction and recovery processes such as SAGD (steam assisted gravity drainage) produces oily process waters that must be treated and recycled when possible. Ceramic membranes are well suited for this task. However, ceramic membranes in aqueous media have a pH dependent surface charge. It was hypothesized that these surface charges are responsible for the high fouling of ceramic membranes in treating wastewaters containing bituminous fines. To maintain desirable hydrophilic properties without surface charges, a highly hydrophilic and neutral organosilane was used to modify the surface of ceramic membrane disks. Membranes having pore sizes of 150 kDa, 300 kDa and 0.14 μm were modified using this organosilane. The ceramic membranes were then used in the filtration of SAGD produced water. Results indicate that the modification was successful in mitigating the irreversible fouling caused by bituminous ultrafines. The permeate flux of the 150 and 300 kDa membranes more than doubled after modification in a 20% silane solution. Furthermore, the filtered water obtained from the modified membranes was of superior quality, to that of the untreated membrane, as evidenced by total organic carbon analysis. All of the ceramic membranes tested were shown to reduce the particle sizes in the produced water from >200 nm in the feed to <40 nm in the permeate.

3.1 Introduction

Ever since the early 20th century, petroleum has been the primary exploited resource globally utilized for energy generation. A prominent issue in oil and gas exploration and production processes is the production of large volumes of waste in the form of produced water. These waters are produced in large quantity and must be treated before recycling or disposal.

Canada's oil sands, located in Alberta, represent the third largest oil reserves found on our planet. In fact, an average of roughly 2.3 million barrels of crude oil per day was produced from the oil sands in 2014 alone [1]. The leading technology used for bitumen extraction from the oil sands is a process known as Steam Assisted Gravity Drainage (SAGD). In 2014, in-situ extraction techniques like the SAGD method accounted for 55% of the total crude bitumen production rate [1]. This extraction technique consists of drilling a pair of horizontal wells 4 to 6 meters apart. Steam is injected into the top well, known as the injection well. The steam heats the surrounding heavy oil, thus reducing its viscosity and allowing it to flow by gravity into the bottom well (producing well). This results in an emulsion of oil and condensed water that is then pumped to the surface for separation and treatment. Presently, about 2-3 barrels of water, injected as steam, are necessary to produce one barrel of oil [2]. Furthermore, river water is often used with the SAGD process, which could potentially lead to water shortages during future winters [3]. Hence, the treatment and recycling of this process water is an issue that requires increasing attention in order to maintain the sustainability of the oil sands industry, as well as to ensure the preservation of natural freshwater resources.

For many years, membrane separation technologies have been studied by the oil and gas industry in order to remove oil and other contaminants from produced water [4]. Currently, it is widely accepted that membrane technology is the most promising candidate for the treatment of oily wastewater. This is attributed to the high separation efficiency and the relatively simple operational process associated with membrane modules [5]. In this application, ceramic membranes are preferred for their chemical and thermal stability. They are less vulnerable to the surrounding media than polymeric membranes, and are suitable for use over a wide range of temperatures and pH [6]. However, universal acceptance of membranes for produced water treatment is presently hindered by the fouling observed in treating these feed streams.

Membrane fouling results from the adhesion of non-permeating species onto the membrane surface, or from the deposition of these particles into the pores of the membrane. Membrane

fouling obstructs the flow of the permeating species, thus resulting in a significant decline of the permeate flux. Moreover, the flux decline leads to an increase in transmembrane concentration and pressure gradients [4]. These problems have led to researchers developing various fouling remediation techniques. These include the application of ultrasonic fields to break up surface deposits, backflushing with permeate and the use of many different chemical cleaning agents [7–9]. However, these methods necessitate longer periods of process shutdown and inactivity in order to be implemented. Naturally, this leads to an unwanted increase of the associated operational costs of the process.

An indirect method that can also be used to reduce membrane fouling when treating produced water is through surface chemistry modifications of the membranes themselves. This is done through the addition of chemical compounds that adhere to the membrane surface, thus changing the physicochemical properties of the selective layer [4]. The chosen modification would ideally result in a reduction of the attractive forces to the components that have been identified as foulants. In the case of SAGD produced water, prominent foulants likely include a multitude of both organic and inorganic substances that possess high scale forming potential. Ceramic membranes have been modified using many different agents. These include metal oxide nanoparticles such as alumina, titania and zirconia [10–12], grafted polymers [13–15] and zeolites [16]. All of these common surface modifications have been proven successful in forming hydrophilic layers on the membrane surface. Consequently, the application of these modifying agents for the filtration of oil and water emulsions improved membrane flux and mitigated any irreversible fouling. Another group of low surface energy modifying agents are organosilanes. Organosilanes are capable of rendering active membrane layers that possess either hydrophilic or hydrophobic properties. They have been used to modify various hydroxyl group-bearing surfaces, having initially been used on inorganic minerals [17]. They have since been applied to ceramic membranes with selective layers composed of alumina, zirconia and titania [18–20]. However, the use of these silane-modified ceramic membranes has been heavily focused on gas separation [21–25], pervaporation [26–28] and membrane distillation [28–32]. Silane modifying agents have been sparsely explored as an application for the treatment of oil and water emulsions. Moreover, in the few studies that have been performed, alkyl or fluorosilanes were used in order to render the ceramic membranes hydrophobic and thus remove water as an oil contaminant [33–36]. Evidently, this is likely not the ideal situation when dealing with produced

water from processes such as SAGD, in which it is preferred to recuperate the purified water as the permeate.

The surfaces of unmodified ceramic membranes are hydrophilic due to the charged hydroxyl groups that populate the top layer. For metal oxide ceramics, the predominant surface charge is dependent on the pH. If the pH is above the isoelectric point (IEP) of the ceramic material, then the predominant surface charge is negative, while at a pH that is below the IEP, the predominant surface charge is positive. The pH is thus an important feed parameter, since it determines the surface charge of the membrane selective layer. The IEPs of common ceramic membrane materials in water are given in Table 3.1 below [37].

Table 3.1: Isoelectric points of various ceramic materials.

Ceramic material	SiO_2	ZrO_2	TiO_2	γ-Al_2O_3	α-Al_2O_3
Isoelectric point at 25°C	1.7-3.5	4-11	3.9-8.2	7-8	8-9

When identifying possible foulants in the filtration of SAGD produced water, bitumen associated solids must be taken into consideration. These solids include aggregates of quartz, clays and heavy minerals that are bound together by carbonates, iron oxide and humic matter [38]. However, the most problematic of the bitumen associated solids have been determined as being ultrafine clays [38,39]. These ultrafines are very thin aluminosilicate clay crystallites onto which organic bitumen molecules and humic matter are adsorbed. Therefore, major potential foulants in this application are silicates and adsorbed carbon-rich solids. The surfaces of heavy bitumen molecules, such as asphaltenes, have been shown to possess acidic, basic and amphoteric functional groups [40]. This indicates that bituminous fines can exhibit both negative and positive surface charges. Combining this with the fact that the IEPs of the ceramic materials discussed above can vary significantly, it becomes evident that maintaining the electrostatic repulsion of the identified foulants is a difficult task. Hence, the attraction of these foulants to the ceramic membrane surface is a significant hindrance that needs to be addressed.

The aim of this work was to verify the hypothesis that charge neutral hydrophilic ceramic membrane surfaces would enhance the performance of ceramic membranes in treating produced waters containing bituminous fines. In order to test the hypothesis, an organosilane modifying agent was selected that would both maintain the hydrophilicity of the metal oxide selective layer and reduce the number of hydroxyl groups on the oxide surface. Ceramic membrane disks were modified using this organosilane and subsequently challenged with SAGD produced waters.

3.2 Experimental section

3.2.1 Materials

The ceramic membrane disks studied in this work were purchased from Sterlitech Corporation (Kent, WA, USA). The membranes had a diameter of 47 mm, a thickness of 2.5 mm, and offered an overall mass transfer surface area of 13.1 cm^2. The support layer of these membranes was composed of titania. The selective layer of the 0.14 μm microfiltration membrane was made from alumina, while the selective layer of the 150 kDa and 300 kDa Molecular Weight Cut-off (MWCO) membranes contained a mix of ZrO_2 and TiO_2. The membrane specifications provided by the manufacturer were determined by mercury porosimetry for the 0.14 μm microfiltration membrane and the MWCO of the ultrafiltration membranes were determined according to the NFX45-103 standard.

Anhydrous ethanol (Fisherbrand) and acetic acid (ACS plus, Fisherbrand) were used in the silane surface grafting process. All silane solutions were supplied by Gelest, Inc. (Morrisville, PA, USA). A hydrophilic silane containing polyethylene oxide (PEO) (PEOTMS), was selected as the prime candidate because it offered an extremely low water contact angle of 15-16°, one of the lowest among commercially available organosilanes [41].

The feed used to conduct the filtration tests was a sample of SAGD produced water obtained from CanmetMINING (NRCan). It was originally supplied to NRCan from SAGD operations located in Canada's oil sands in Alberta. To prevent clogging the gear pump used to circulate feed in the test system, the SAGD process water was coarsely filtered using a 50 micron paper filter prior to use.

3.2.2 Surface modification procedure

The ceramic disk membranes obtained from Sterlitech were used, as received, in the silanation procedure. The silanating method chosen was the deposition from aqueous alcohol solutions. Firstly, a solution of 95% ethanol / 5% water by weight is prepared. The ethanol solution is then adjusted to a pH of 4.5–5.5 using acetic acid. The silanating agent is then added with stirring to yield a desired final concentration. When treating large objects, a silane concentration of 2 wt% typically results in the deposition of trialkoxysilanes as 3 to 8 molecular layers. In this work, the silane concentration was varied from 0.5 to 30 wt%. Following the addition of the silane, 5 minutes were allowed for hydrolysis and silanol formation. The membranes were then immersed

into the solution for 2 minutes while being gently agitated. Once removed from the silane solution, the membranes were briefly rinsed in ethanol in order to remove any excess materials and unreacted silane. Finally, the modified membranes were then placed in an oven, under nitrogen and at 110˚C, for 10 minutes in order to cure the silane layer.

3.2.3 Characterization of membranes, feed and permeate

In order to confirm the success of the surface silylation procedure, FTIR analyses of the ceramic membrane surfaces were conducted using a Cary 630 FTIR with an Attenuated Total Reflectance (ATR) diamond accessory (Agilent Technologies, Canada). Small amounts of material were scraped off of the surface of both unmodified and modified membranes, resulting in a powder that was then used to completely and evenly cover the diamond accessory.

The elemental composition of inorganics in the SAGD produced water samples was determined by inductively coupled plasma atomic emission spectroscopy (ICP-AES) and is provided in Table 3.2 below. Samples were taken at four different locations ranging from the top to the bottom of the barrel. The standard deviations in Table 3.2 were determined based on these four measurements.

Table 3.2: Average inorganic composition of SAGD produced water feed.

Component	Na	Si	B	K	S	Ca	Mg	Sr	Ba
Composition (ppm) with standard deviations	476 ±14.9	94.1 ±4.41	27.7 ±0.778	15.2 ±0.928	14.2 ±1.86	2.30 ±0.192	0.491 ±0.042	0.159 ±0.00592	0.0284 ±0.00332

Both the SAGD wastewater feed and the permeate samples were subjected to a particle size analysis. This allowed for the verification of the molecular weight cut-off of the ceramic membranes. The samples were all analyzed in a Zetasizer Nano S90 (Malvern Instruments Ltd, MA, USA). Samples of 3 mL were placed in the particle size analyzer, and the refractive index of diluted bitumen was taken as 1.58 [42]. The total organic carbon (TOC) of all feed and permeate samples was determined using a Total Organic Carbon analyzer.

For the experiments conducted in this study, five samples of wastewater feed were extracted from the same drum on different dates. SAGD wastewater, like most produced water, undergoes certain transformations upon aging during long term storage, which can affect filtration

performance [43]. It is important to track feed sample usage during testing to be able to feasibly compare results. In Table 3.3, these samples are assigned a label and their pH and TOC is given.

Table 3.3: Label, pH and TOC of SAGD wastewater feed samples, extracted from the same drum, used for filtration tests.

Feed Sample	F1	F2	F3	F4	F5
pH	7.93	8.84	7.58	7.75	7.99
TOC (ppm)	445	495	316	376	506

3.2.4 Filtration of SAGD produced water

The filtration experiments were conducted using a cross-flow filtration system. A schematic diagram of the test system can be found in Figure 3.1 below. The entire setup was placed in a walk-in fume hood in order to reduce emissions from the SAGD produced water recirculated in the system. All of the filtration tests were conducted at temperatures ranging from 84 to 88 °C. The experiments using the 0.14 μm membranes were carried out at a transmembrane pressure (TMP) of 68.95 kPa (10 psi), while all other membranes were subjected to a TMP of 172.6 kPa (25 psi). The TMP of each run was maintained constant through the use of a pressure relief valve. In order to remediate fouling, the system was backflushed with permeate for 5 seconds every 295 seconds at 103.4 kPa (15 psi) when using the 0.14 μm membrane, and at 206.8 kPa (30 psi) for all other membranes. Initially, 3.7 L of SAGD produced water was loaded into the feed tank and fed to the membrane with a cross-flow velocity of 1.2 m/s. The system was operated with total retentate recycling, while the permeate was collected in a separate container and periodically recycled back to the feed tank. The flowrate of the permeate stream was monitored using a Coriolis flow meter. The duration of each run ranged from approximately 3.5 to 4 hours, as this amount of time was considered to be sufficient in order to establish any differences between the modifications.

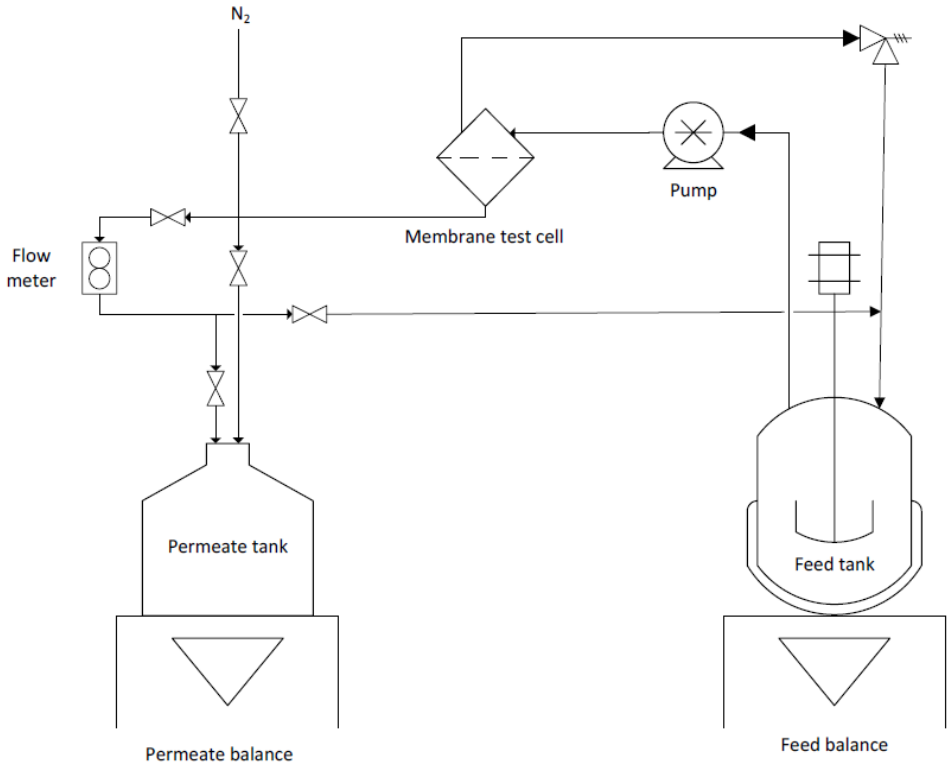

Figure 3.1: Schematic of filtration system.

3.3 Results and discussion

3.3.1 Surface silylation of ceramic membranes

An FTIR spectrum of a 300 kDa membrane surface before and after the surface modification procedure is shown in Figure 3.2. The modified membrane was modified using a 20 wt% silane solution. Analysis of this spectrum indicates that the ceramic surface was successfully silylated. The strong peak at 1090 cm^{-1} is characteristic of the Si-O-Si bonds in siloxanes [44], as well as the C-O-C bonds in the PEO chains of the silane, indicating the presence of silane PEOTMS on the ceramic surface. Moreover, the peak at 950 cm^{-1} is indicative of Si-O-Metal bonding, which is further evidence of the reaction between the silane and the metal oxide surface of the ceramic membrane. The peaks seen between 1350 and 1450 cm^{-1} represent the -C-H bending found in the silane's organic components, while the peak at 2850 cm^{-1} represents C-H stretching.

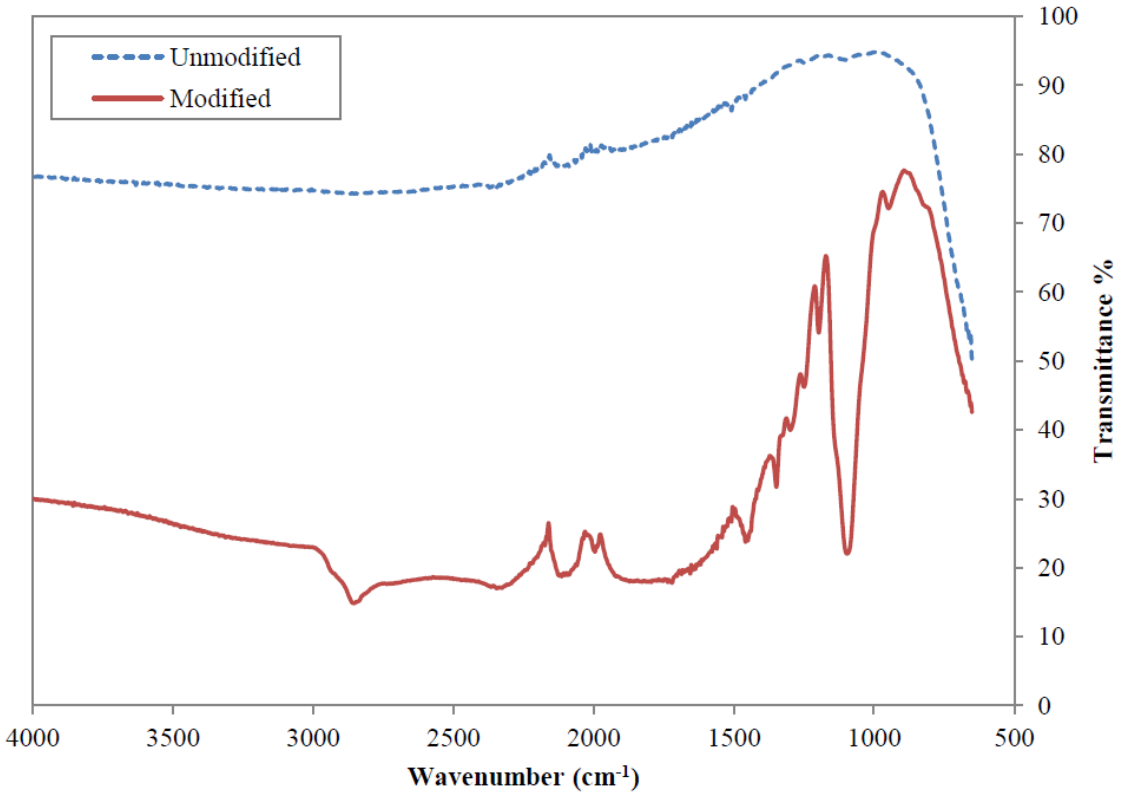

Figure 3.2: FTIR spectra of the surface of an unmodified 300 kDa membrane and a 20% PEOTMS modified 300 kDa membrane.

3.3.2 Membrane flux and lot number

After a number of tests to compare the flux of modified and unmodified membranes, it was observed that the flux of the unmodified membranes varied from one manufactured lot to another. While the pore size of the membrane was a manufacturer's criterion defining the membrane disks, membrane flux was not. The variations in flux could easily be due to different sol concentrations or coating dynamics during the deposition of the successive selective layers on top of the membrane substrate. In order to remove variations between lots, membrane flux was reported along with the lot number.

3.3.3 Membrane integrity on backflushing

The membranes tested in this work were cast on flat ceramic supports. Initially, membranes with a MWCO of 50 kDa were to be included. However, the supports for the 50 kDa membranes were different than those of the 150 kDa, 300 kDa and 0.14 µm membranes. The 50 kDa supports did not withstand the backflushing pressure of 206.8 kPa (30 psi). All of the 50 kDa membranes cracked during filtration and could not be adequately tested. All other membranes could be

backflushed with the exception of the unmodified 150 kDa membrane, which showed signs of failure in its selective layer after approximately 42 minutes. All other membranes were operated without showing signs of failure.

3.3.4 Membrane flux and silane concentration

The run conditions of the modified membranes using agent PEOTMS and the unmodified membranes are summarized in Tables 3.4 to 3.6 below. The tables are sectioned according to the manufacturer's membrane lot numbers. As previously mentioned, the increase or reduction in membrane flux as a result of treatment was compared within a lot and for the same feed. The average flux over the entire filtration period for the 150 kDa, 300 kDa and 0.14 µm membranes can be found in Figure 3.3 at different modifying agent concentrations. The permeate flux is given by the following equation, where J is flux in m/s, $\dot{m}$ is mass flowrate of permeate in kg/s, ρ is permeate density in kg/m^3 and A is active membrane surface area in m^2. The flux given in equation (3.1) was multiplied by 3.6 x 10^6 to give units of L/(m^{2}h) (Lmh).

$$J(m/s) = \frac{\dot{m}}{\rho \cdot A} \tag{3.1}$$

The dashed lines in the plot demonstrate the correlation between flux and silane concentration for filtration tests that were run using the same feed sample, as well as membranes originating from the same batch.

Table 3.4: Test conditions for the unmodified and modified 150 kDa membrane using agent PEOTMS. Operating pressure 172.6 kPa (25 psi) Trans Membrane Pressure, backflushing with permeate for 5s every 295s at 206.8 kPa (30 psi).

Surface Modification	Membrane Lot #	SAGD wastewater feed sample	Feed Temperature (°C)
Unmodified	131113U150	F4	85-87
5%	131113U150	F4	85-88
10%	131113U150	F4	85-88
20%	131113U150	F4	85-88
30%	131113U150	F5	85-88

Table 3.5: Test conditions for the unmodified and modified 300 kDa membrane using agent PEOTMS. Operating pressure 172.6 kPa (25 psi) Trans Membrane Pressure, backflushing with permeate for 5s every 295s at 206.8 kPa (30 psi).

Surface Modification	Membrane Lot #	Membrane Lot Label	SAGD wastewater feed sample	Feed Temperature (°C)
Unmodified	191110U300	B1	F2	87
0.5%	191110U300	B1	F2	84-87
1%	191110U300	B1	F2	85-87
Unmodified	140312U300	B2	F3	86-88
2%	140312U300	B2	F3	86-87
3%	140312U300	B2	F2	85-88
15%	140312U300	B2	F3	86-87
20%	140312U300	B2	F3	85-87

Table 3.6: Test conditions for the unmodified and modified 0.14 µm membrane using agent PEOTMS. Operating pressure 68.95 kPa (10 psi) Trans Membrane Pressure, backflushing with permeate for 5s every 295s at 103.4 kPa (15 psi).

Surface Modification	Membrane Lot #	SAGD wastewater feed sample	Feed Temperature (°C)
Unmodified	190310M014	F1	84-87
2%	190310M014	F1	87
10%	190310M014	F2	84-86

All membranes modified in a bath containing 20% of PEOTMS or less showed an increase in flux performance compared to the unmodified membranes. The greatest increase in performance was observed for the 150 kDa and 300 kDa membranes at a concentration of 20%, where the flux of the modified membrane was 2.5 and 2.2 times that of the unmodified membrane, respectively. The flux of the 0.14 µm membrane also showed an increase in flux along the trend of the 150 and 300 kDa membranes. The 30% PEOTMS 150 kDa membrane was run with a different feed sample and was not retained for comparison. Similar cases are seen with the 3% PEOTMS 300 kDa and 10% PEOTMS 0.14 µm membranes. All membranes were tested with SAGD produced water originating from a single drum. However, the feeds had slightly different pHs and TOC content. When membranes of the same batch were run using a feed having a higher pH and TOC, lower fluxes were observed. There are three experiments that illustrate this: the 30% modified 150 kDa membrane tested with feed F5 in Table 3.4, the 3% modified 300 kDa membrane tested

with feed F2 in Table 3.5, and the 10% modified 0.14 µm membrane tested with feed F2 in Table 3.6.

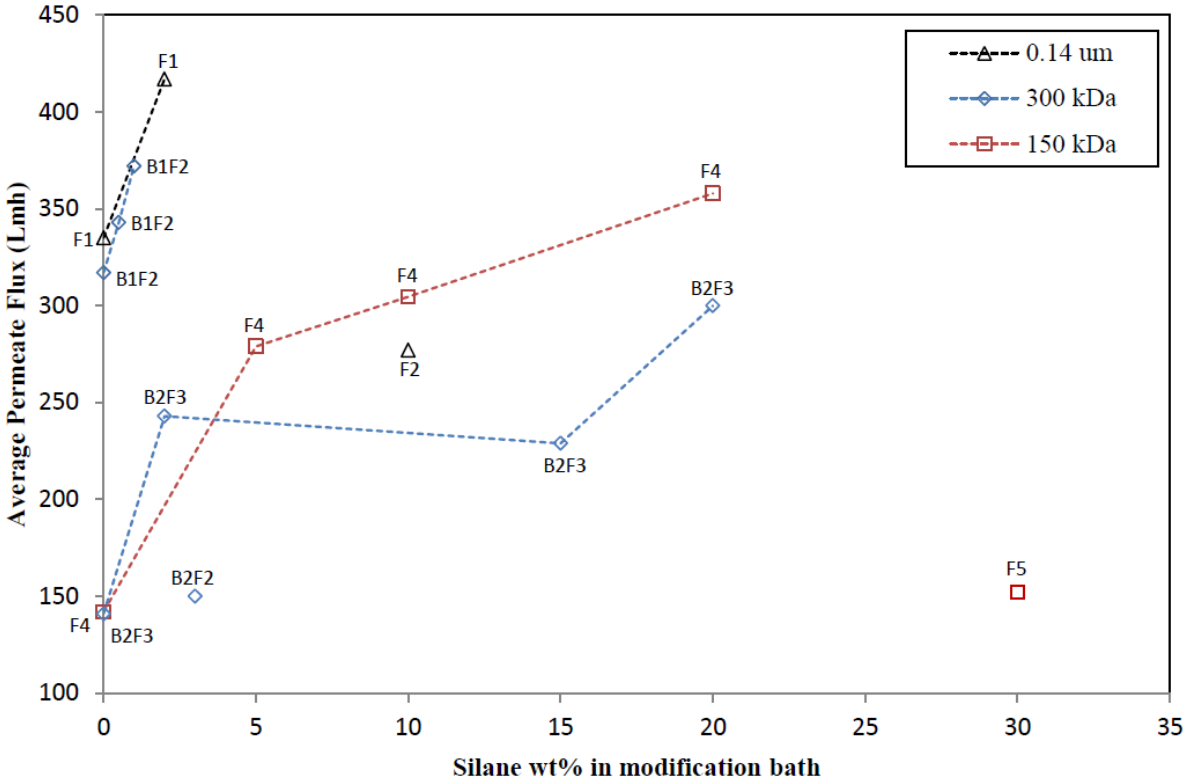

Figure 3.3: Permeate flux as a function of the concentration of silane PEOTMS in the modification bath for the 150 kDa, 300 kDa and 0.14 µm membrane disks. Labels indicate which runs were conducted using the same membrane batch and wastewater feed.

As seen in Table 3.3, feed sample F5 has a higher pH and TOC than feed sample F4, while feed sample F2 has a higher pH and TOC than both feed sample F3 and F1. The higher TOC values indicate a greater concentration of organics in the feeds that led to lower fluxes.

It has been shown that the dissociation of soluble silica, in the form of silicic acid, grows more prominent as the pH surpasses neutral [45]. Silicic acid dissociates into silicate anions, which can then react with the calcium or magnesium found in the wastewater feed to produce insoluble silicates. These have high scale forming potential, and could account for the observed decline in permeate flux at higher pH values.

Nonetheless, the flux of all membranes from the same batch and run with the same feed increased as a result of a treatment with agent PEOTMS. This trend was even observed for silane concentrations as low as 0.5%, as evidenced by the 300 kDa membranes. This indicates that the

modification is effective in releasing bitumen fines from the surface of the modified membrane and thus reducing the severity of the fouling phenomenon.

3.3.5 Flux as a function of time and concentration factor

The accumulation of colloids and fines on the surface of the membrane is a natural consequence of the filtration process which results in a decline of permeate flux over time. The accumulation of particles is mitigated by the presence of tangential flow over the surface of the membrane and backflushing. Particles on the surface of the membrane are partly swept away by feed circulating across the surface of the membrane and released from the surface by backflushing. Over time, the flux will stabilize, where an equal amount of particles are deposited on and released from the surface of the membrane. The number of particles arriving on the surface of the membrane will be related to the volume of process water filtered and the concentration of particulates and colloids in the process water.

During a run, permeate from the membrane was collected in a container placed on the permeate balance shown in Figure 3.1. It was recycled periodically back to the feed tank. Initially, the feed tank contained 3.7 L of SAGD produced water. As permeate was collected, the concentration of particulates in the feed increased. It is important to determine the effect of this increase in concentration on membrane flux. Hence, membrane flux was plotted as a function of the concentration factor in Figure 3.4 for the 150 kDa and Figure 3.5 for the 300 kDa pore sized membranes. The concentration factor is defined as follows, where V_F is the initial volume of produced water in the feed tank and V_P is the volume of permeate collected at a given time during a filtration test.

$$Concentration\ Factor = \frac{V_F}{V_F - V_P} \tag{3.2}$$

From Figure 3.4, it can be seen that the modified 150 kDa membranes maintained a high flux even when the feed water increased in concentration. The flux was also steady in the case of the 15% 300 kDa membrane shown in Figure 3.5. After an initial decline, the flux of the 15% 300 kDa membrane was stable for the second collection of permeate following its recycling. The flux of the 20% 300 kDa modified membrane was much higher than those of the 15% 300 kDa and the untreated membrane. However, at the 20% level, the 300 kDa membranes showed some decline without an indication of stability.

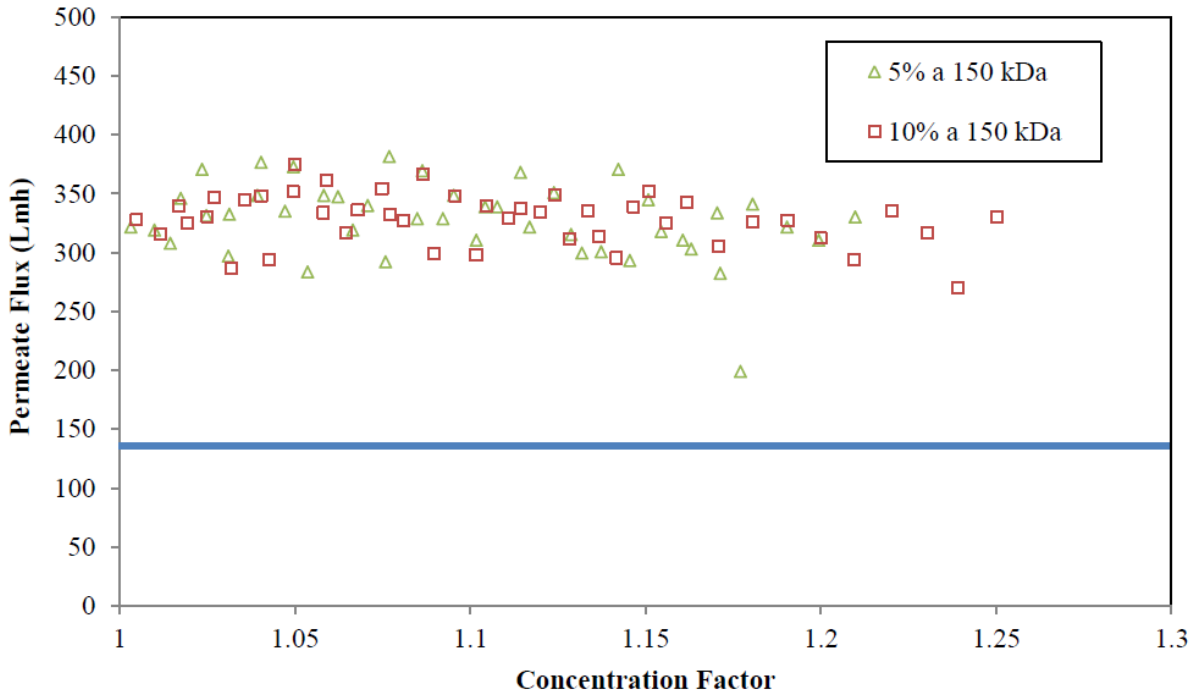

Figure 3.4: Permeate flux vs concentration factor for the 150 kDa membranes modified with agent PEOTMS. The solid line at a flux of 142 Lmh represents the flux of the unmodified membrane in the initial 42 minutes of its run.

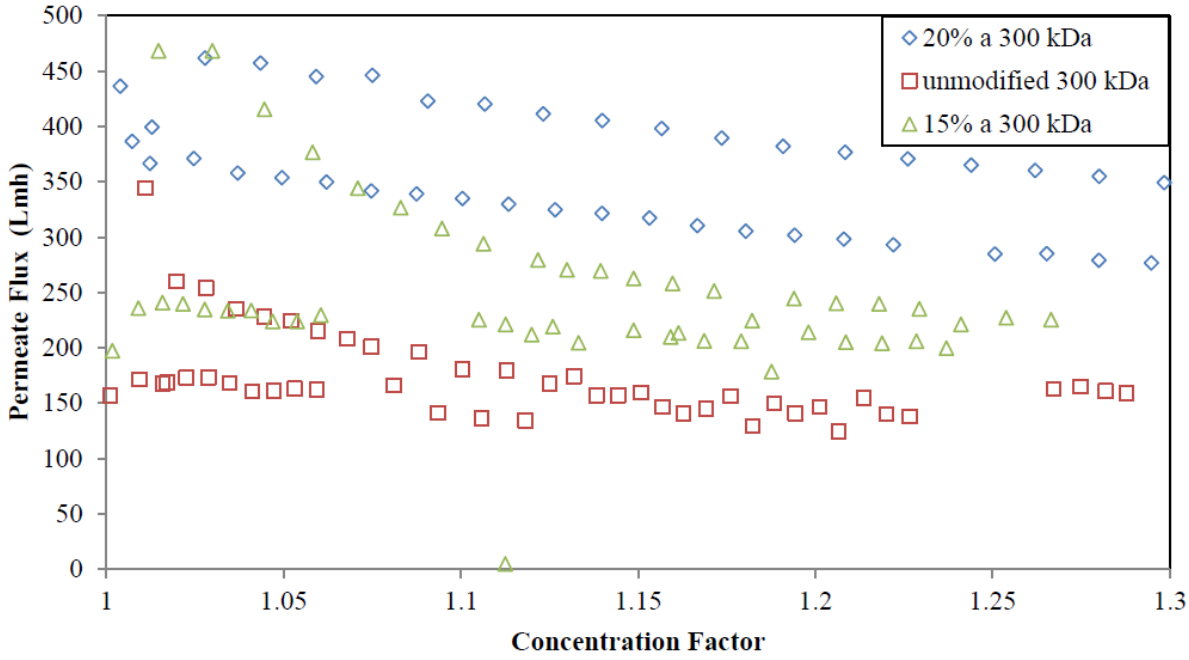

Figure 3.5: Permeate flux vs concentration factor for the 300 kDa membranes modified with agent PEOTMS.

3.3.6 Analysis of water quality

3.3.6.1 Total organic carbon analysis

The total organic carbon content of the feed SAGD produced water, as well as the permeate of each run, was measured for use as an indicator of water cleanliness. The results of this analysis can be found below. The fraction of the TOC removed in the permeate relative to the feed SAGD wastewater was plotted against both the silane modification concentration (Figure 3.6) and the permeate flux (Figure 3.7). This was done for the 150 kDa, 300 kDa and 0.14 µm membranes.

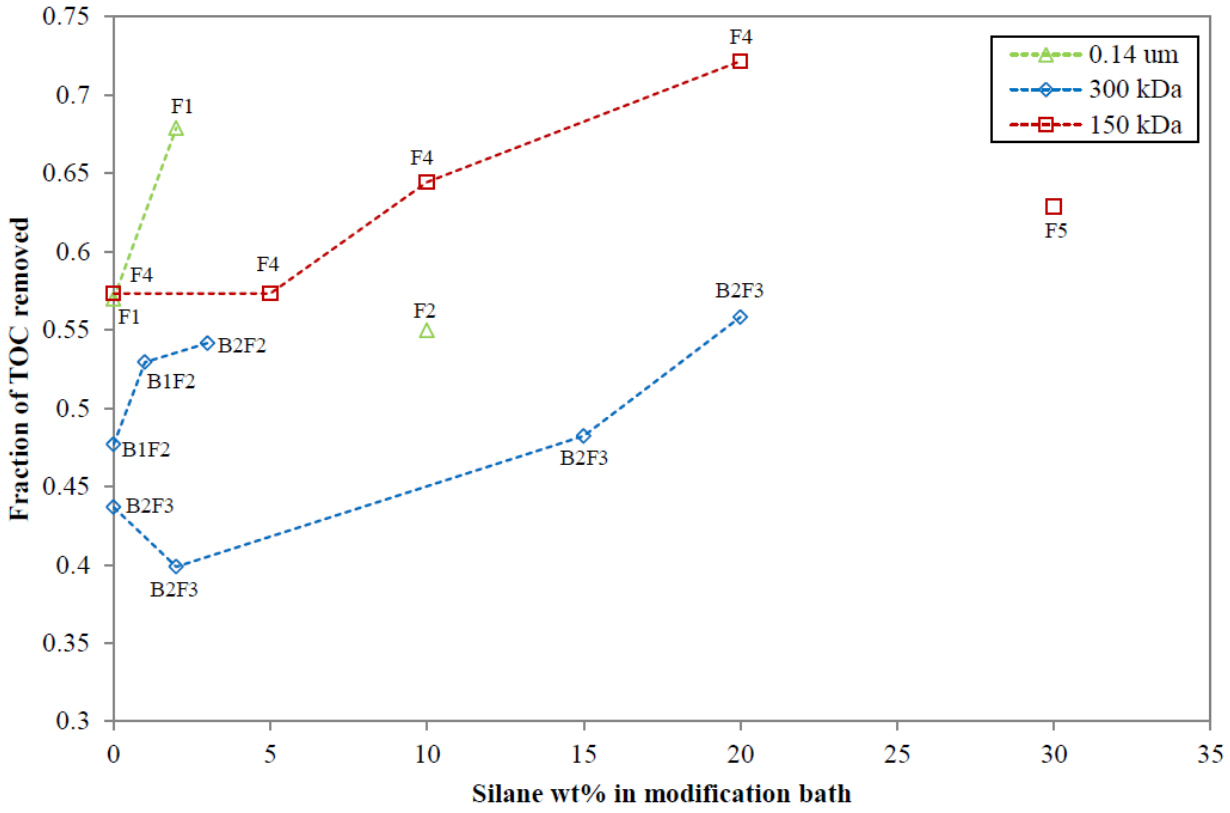

Figure 3.6: Total organic carbon separation as a function of the concentration of silane PEOTMS. Labels indicate which runs were done using the same batch of membranes and the same feed.

In Figure 3.6, the dashed lines indicate the correlation observed for membrane filtration tests using the same feed sample. Here, membranes originating from different manufactured batches could be compared as long as they used the same feed because TOC separation depends on the membrane pore size, and not the flux. It was observed that, in all cases, the silane surface modification lead to an increase in TOC separation when compared to the respective unmodified membranes. While the 10% PEOTMS 0.14 µm membrane showed a poorer TOC separation

relative to the unmodified 0.14 µm membrane, this can be attributed to the fact that the filtration test of this particular membrane was conducted using a different feed. This feed sample possessed a higher concentration of bituminous organic compounds. The higher concentration of foulants in the feed would have thus led to a reduction in TOC removal in comparison to the unmodified membrane that used a different feed. The same explanation can be offered for the 30% 150 kDa membrane, which showed a decrease TOC separation.

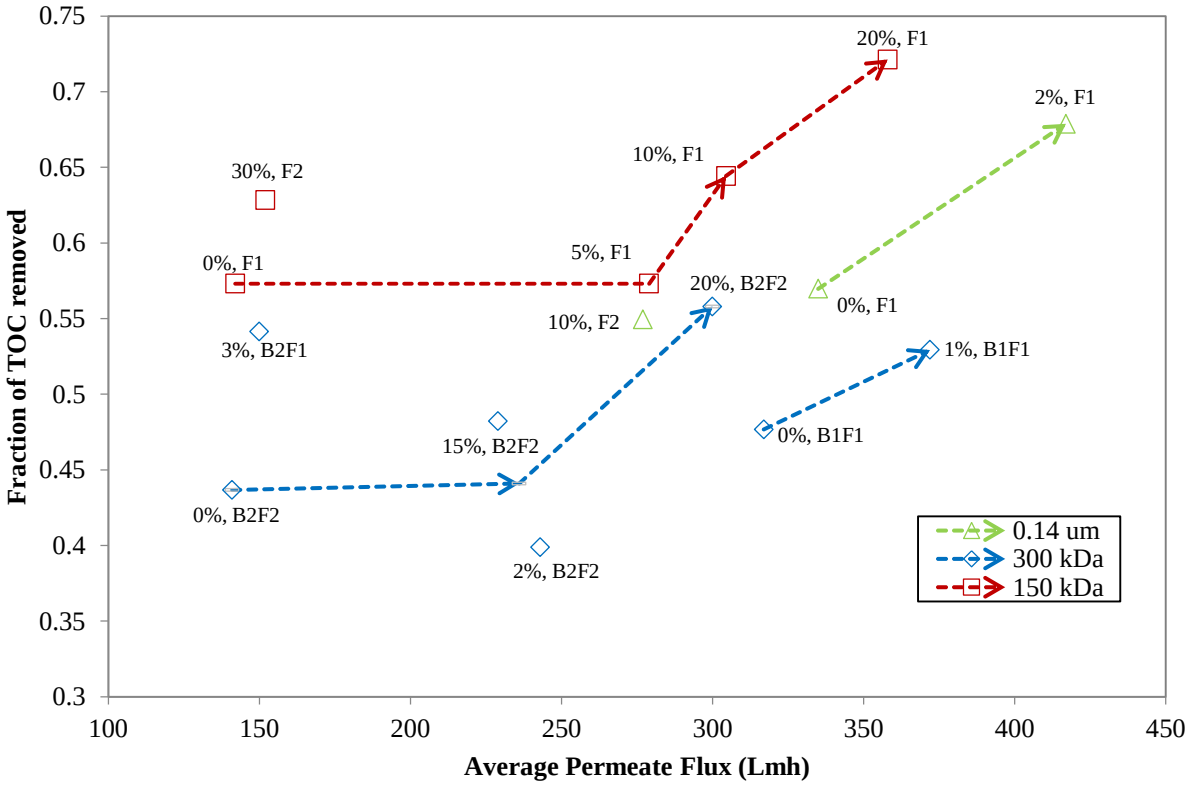

Figure 3.7: Total organic carbon separation as a function of permeate flux for the 150 kDa, 300 kDa and 0.14 um membranes. Labels indicate the silane modification concentration, the membrane batch and the feed sample of each run.

In Figure 3.7, the dashed lines and arrows indicate the general trend observed for filtration tests using the same feed sample and membrane batch. Each data point represents the average permeate flux from one filtration experiment. Since permeate flux was a parameter of interest in this comparison, both the membrane batch and the feed sample had to be taken into consideration. It can be observed that surface modification with silane PEOTMS leads to an increase in both permeate flux and TOC removal for all three sets of the tested ceramic membranes. Moreover, increasing the concentration of the silane in the modifying solution

resulted in further improvement in separation and permeate flux. Consequently, for the 150 and 300 kDa membranes, the highest silane concentration tested of 20% was found to be optimal in terms of maximizing flux and separation performance. The results of the TOC analysis indicate that the modification is successful in improving the rejection of bituminous organics during filtration of SAGD produced water.

3.3.6.2 Particle size analysis

As a method of characterizing the performance of the ceramic membranes tested in this study, the particle size distributions of both the feed and permeate samples were determined. The particle distribution of all feeds was measured. They did not vary significantly, containing particles ranging from 220 to 710 nm in diameter. The distributions of all five feed samples were plotted in Figure 3.8 below. Since the bituminous ultrafines in the tar sands are known to possess dimensions that are inferior to 300 nm [38], the larger particles seen in the produced water feed are likely aggregates of ultrafines. The high salt content in the wastewater could be causing the compaction of flat clay platelets to form larger clusters of three-dimension structures. The particle size distribution of the permeates obtained from the 150 kDa, 300 kDa and 0.14 µm membranes are given in Figures 3.9, 3.10 and 3.11, respectively. These distributions are reported along with the corresponding concentration of the silanating agent. All of the distributions show that the particle diameters in the permeates do not exceed 40 nm. The corresponding pore diameters of the 150 kDa and 300 kDa MWCO membranes are approximately 21.5 nm and 30 nm, respectively, based on models developed using dextran and pullulan molecules [46]. The distributions observed for permeate samples from these membranes are, therefore, in accordance with their pore sizes. The fact that filtration with the 0.14 µm membranes resulted in permeates with similar distributions to those obtained from the 150 and 300 kDa membranes is due to the characterization method as previously mentioned in the materials section.

In the case of the 300 kDa membranes, it can be seen in Figure 3.10 that the silane surface modified membranes all produced permeate particle size distributions that were lower compared to the unmodified membrane. However, this was not a general trend as seen in Figures 3.9 and 3.11 for the 150 kDa and 0.14 µm membranes respectively. The discrepancy can be attributed to the fact that the SAGD feed contained particles that could aggregate after they had permeated through the membrane. Altogether, the particle size analysis of the permeates demonstrates that

all of the ceramic membranes tested were effective in terms of rejecting particles of diameter larger than 40 nm in the five SAGD produced water samples.

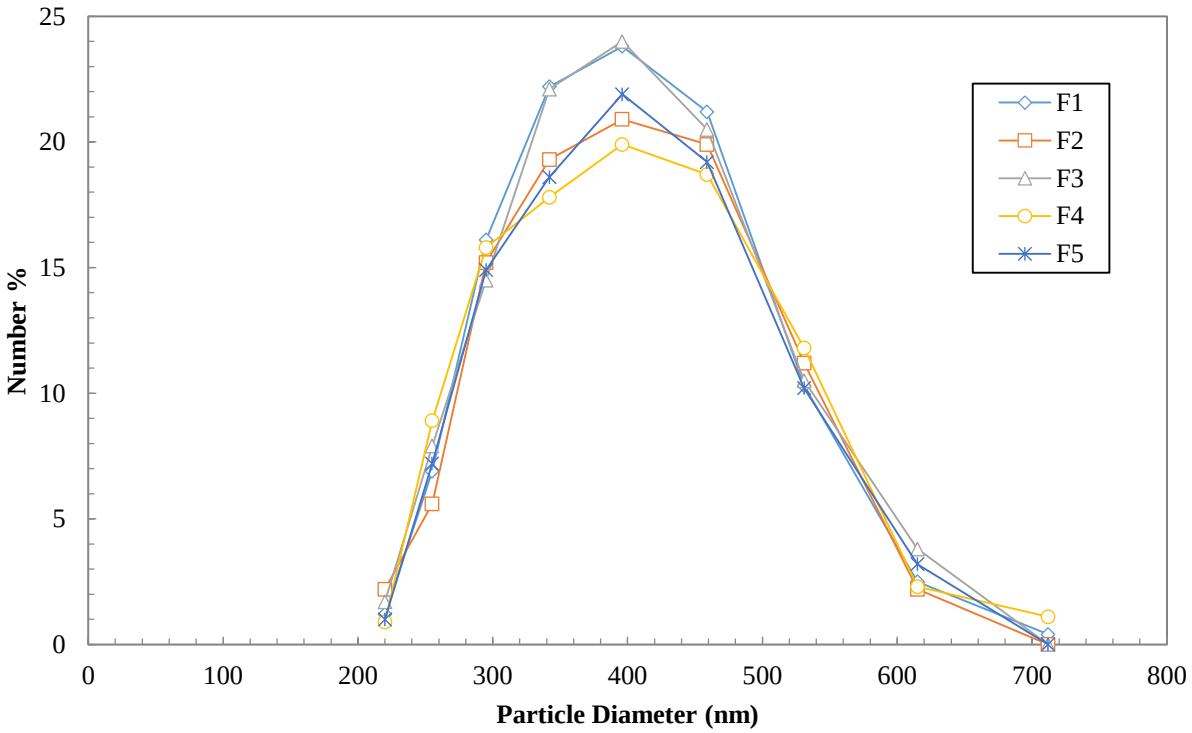

Figure 3.8: Particle size distributions of the SAGD produced water feeds.

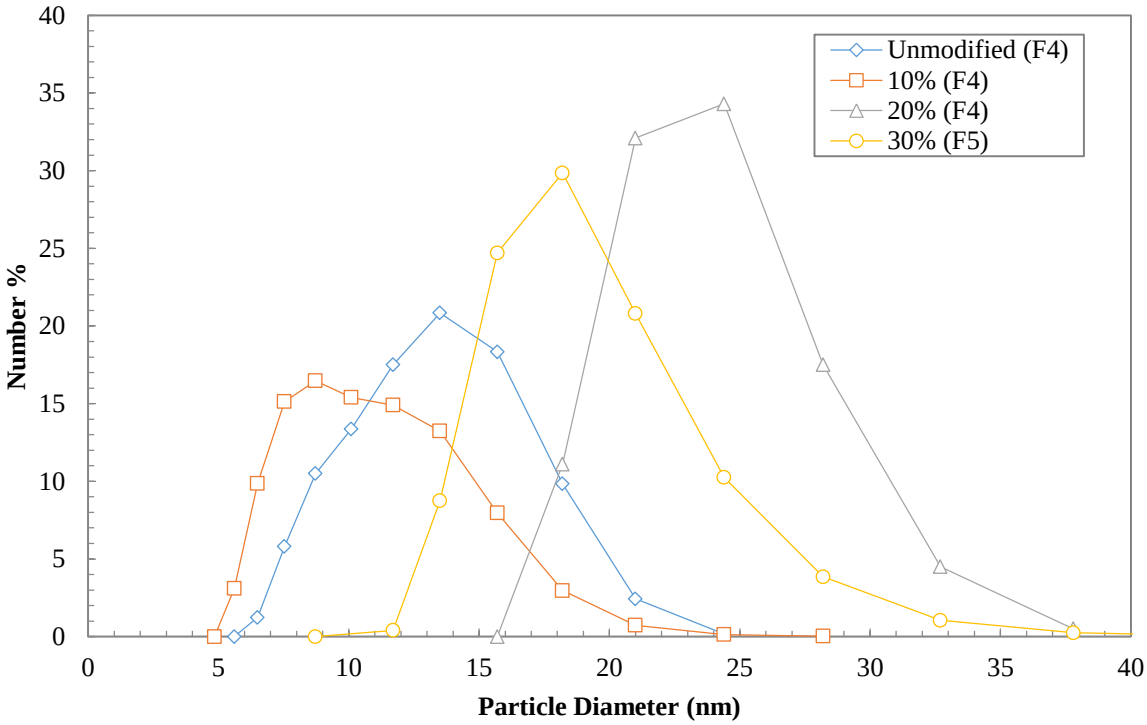

Figure 3.9: Particle size distributions of permeate samples from the 150 kDa membranes.

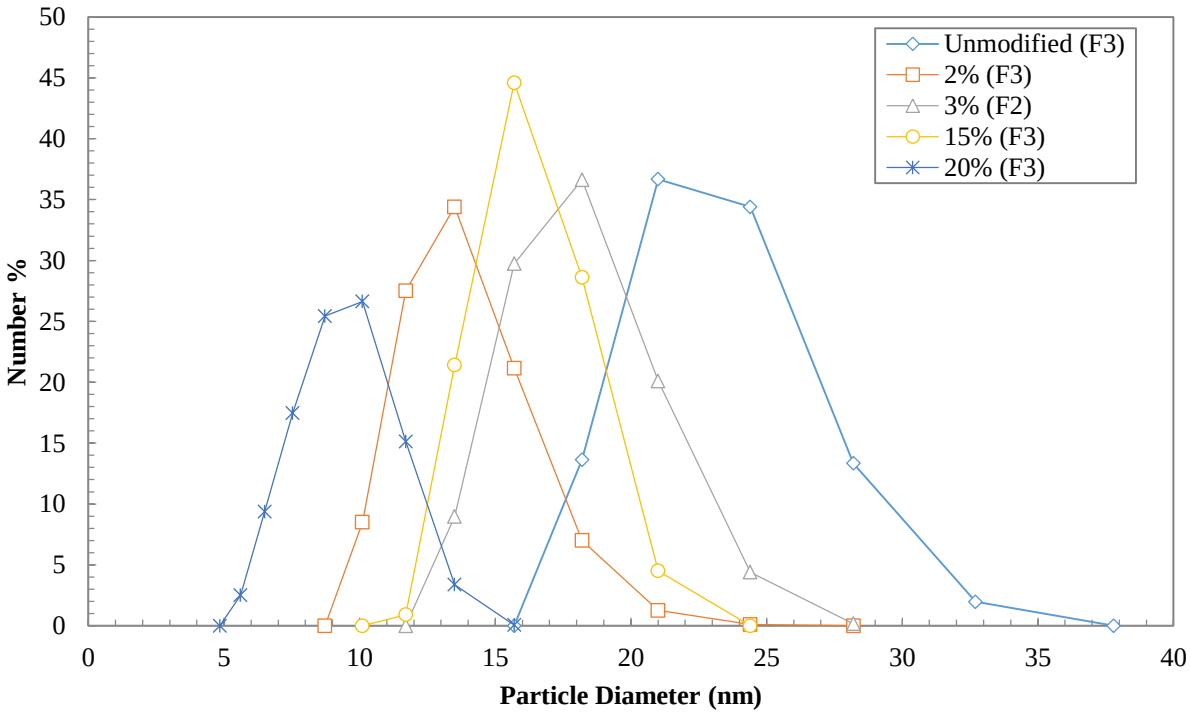

Figure 3.10: Particle size distributions of permeate samples from the 300 kDa membranes.

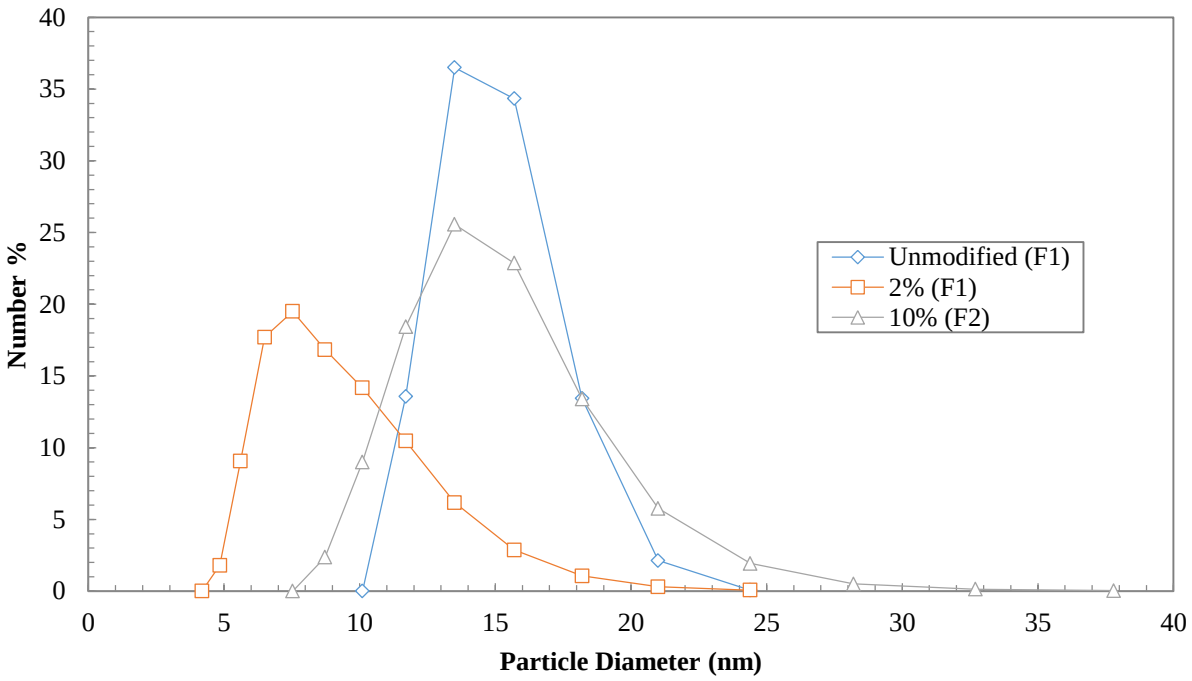

Figure 3.11: Particle size distributions of permeate samples from the 0.14 µm membranes.

3.4 Conclusions

Ceramic flat ultra- and micro-filtration membrane disks with pore sizes of 150 kDa, 300 kDa and 0.14 µm were modified using an organosilane surface modifying agent. The results successfully demonstrated that it was possible to modify ceramic membranes to exhibit fouling-resistant properties to bituminous solids and consequently enhance their performance in treating SAGD produced waters. Modification agent PEOTMS more than doubled the flux of the 150 kDa and 300 kDa ceramic membranes in treating these process waters relative to the unmodified membranes. The modified ceramic membranes were also found to successfully remove up to 72% of the total organic carbon found in SAGD produced water ensuring water cleanliness for recycling. Furthermore, all of the ceramic membranes tested were shown to reduce the particle sizes in the produced water from >200 nm in the feed to <40 nm in the permeate. The observed trends indicated that higher concentrations in the modification bath lead to both higher permeate flux and water quality. The results and protocols developed in this work can be used to modify commercial membranes. They will also permit us to better identify other surface modifying agents in order to improve membrane performance in treating SAGD produced waters.

References

[1] Alberta Official Statistics: Total Bitumen Production, Alberta, (2015) 1–3.

[2] P. Swenson, B. Tanchuk, E. Bastida, W. An, S.M. Kuznicki, Water desalination and de-oiling with natural zeolite membranes - Potential application for purification of SAGD process water, Desalination. 286 (2012) 442–446.

[3] S.M. Jordaan, Land and water impacts of oil sands production in Alberta, Environmental Science & Technology. 46 (2012) 3611–3617.

[4] E.W. Allen, Process water treatment in Canada's oil sands industry: II. A review of emerging technologies, Journal of Environmental Engineering and Science. 7 (2008) 499–524.

[5] M. Padaki, R. Surya Murali, M.S. Abdullah, N. Misdan, A. Moslehyani, M.A. Kassim, N. Hilal, A.F. Ismail, Membrane technology enhancement in oil-water separation. A review, Desalination. 357 (2015) 197–207.

[6] R. Sondhi, R. Bhave, G. Jung, Applications and benefits of ceramic membranes, Membrane Technology. 2003 (2003) 5–8.

[7] D. Chen, L.K. Weavers, H.W. Walker, Ultrasonic control of ceramic membrane fouling by particles: Effect of ultrasonic factors, Ultrasonics Sonochemistry. 13 (2006) 379–387.

[8] Y. Zhao, J. Zhong, H. Li, N. Xu, J. Shi, Fouling and regeneration of ceramic microfiltration membranes in processing acid wastewater containing fine TiO2 particles, Journal of Membrane Science. 208 (2002) 331–341.

[9] S.H.D. Silalahi, T. Leiknes, Cleaning strategies in ceramic microfiltration membranes fouled by oil and particulate matter in produced water, Desalination. 236 (2009) 160–169.

[10] J.E. Zhou, Q. Chang, Y. Wang, J. Wang, G. Meng, Separation of stable oil-water emulsion by the hydrophilic nano-sized ZrO2 modified Al2O3 microfiltration membrane, Separation and Purification Technology. 75 (2010) 243–248.

[11] Q. Chang, J.E. Zhou, Y. Wang, J. Wang, G. Meng, Hydrophilic modification of Al2O3 microfiltration membrane with nano-sized γ-Al2O3 coating, Desalination. 262 (2010) 110–114.

[12] Q. Chang, J.E. Zhou, Y. Wang, J. Liang, X. Zhang, S. Cerneaux, X. Wang, Z. Zhu, Y. Dong, Application of ceramic microfiltration membrane modified by nano-TiO2 coating in separation of a stable oil-in-water emulsion, Journal of Membrane Science. 456 (2014) 128–133.

[13] R.P. Castro, Y. Cohen, H.G. Monbouquette, Silica-supported polyvinylpyrrolidone filtration membranes, Journal of Membrane Science. 115 (1996) 179–190.

[14] R.S. Faibish, Y. Cohen, Fouling and rejection behavior of ceramic and polymer-modified ceramic membranes for ultrafiltration of oil-in-water emulsions and microemulsions, Colloids and Surfaces A: Physicochemical and Engineering Aspects. 191 (2001) 27–40.

[15] R.S. Faibish, Y. Cohen, Fouling-resistant ceramic-supported polymer membranes for ultrafiltration of oil-in-water microemulsions, Journal of Membrane Science. 185 (2001) 129–143.

[16] J. Cui, X. Zhang, H. Liu, S. Liu, K.L. Yeung, Preparation and application of zeolite/ceramic microfiltration membranes for treatment of oil contaminated water, Journal of Membrane Science. 325 (2008) 420–426.

[17] C.R. Kessel, S. Granick, Formation and characterization of a highly ordered and well- anchored

alkylsilane monolayer on mica by self-assembly, Langmuir. 7 (1991) 532–538.

[18] S.R. Krajewski, W. Kujawski, F. Dijoux, C. Picard, A. Larbot, Grafting of ZrO2 powder and ZrO2 membrane by fluoroalkylsilanes, Colloids and Surfaces A: Physicochemical and Engineering Aspects. 243 (2004) 43–47.

[19] J.L. Hardin, N.A. Oyler, E.D. Steinle, G.A. Meints, Spectroscopic analysis of interactions between alkylated silanes and alumina nanoporous membranes, Journal of Colloid and Interface Science. 342 (2010) 614–619.

[20] J. Kujawa, W. Kujawski, Functionalization of Ceramic Metal Oxide Powders and Ceramic Membranes by Perfluroalkylsilanes and Alkylsilanes Possessing Different Reactive Groups – Physicochemical and Tribological Properties, ACS Applied Materials & Interfaces. 8 (2016) 7509–7521.

[21] A. Javaid, D.A. Krapchetov, D.M. Ford, Solubility-based gas separation with oligomer-modified inorganic membranes: Part III. Effects of synthesis conditions, Journal of Membrane Science. 246 (2005) 181–191.

[22] N. Abidi, A. Sivade, D. Bourret, A. Larbot, B. Boutevin, F. Guida-Pietrasanta, A. Ratsimihety, Surface modification of mesoporous membranes by fluoro-silane coupling reagent for CO2 separation, Journal of Membrane Science. 270 (2006) 101–107.

[23] G.D. Bothun, K. Peay, S. Ilias, Role of tail chemistry on liquid and gas transport through organosilane-modified mesoporous ceramic membranes, Journal of Membrane Science. 301 (2007) 162–170.

[24] M. Ostwal, R.P. Singh, S.F. Dec, M.T. Lusk, J.D. Way, 3-Aminopropyltriethoxysilane functionalized inorganic membranes for high temperature CO2/N2 separation, Journal of Membrane Science. 369 (2011) 139–147.

[25] R. Faiz, M. Fallanza, I. Ortiz, K. Li, Separation of olefin paraffin gas mixtures using ceramic hollow fiber membrane contactors, Industrial & Engineering Chemistry Research. 52 (2013) 7918–7929.

[26] S. Alami Younssi, A. Iraqi, M. Rafiq, M. Persin, A. Larbot, J. Sarrazin, γ Alumina membranes grafting by organosilanes and its application to the separation of solvent mixtures by pervaporation, Separation and Purification Technology. 32 (2003) 175–179.

[27] W. Kujawski, S. Krajewska, M. Kujawski, L. Gazagnes, A. Larbot, M. Persin, Pervaporation properties of fluoroalkylsilane (FAS) grafted ceramic membranes, Desalination. 205 (2007) 75–86.

[28] J. Kujawa, S. Cerneaux, W. Kujawski, Investigation of the stability of metal oxide powders and ceramic membranes grafted by perfluoroalkylsilanes, Colloids and Surfaces A: Physicochemical and Engineering Aspects. 443 (2014) 109–117.

[29] A. Larbot, L. Gazagnes, S.R. Krajewski, M. Bukowska, W. Kujawski, Water desalination using ceramic membrane distillation, Desalination. 168 (2004) 367–372.

[30] S. Khemakhem, R. Ben Amar, Modification of Tunisian clay membrane surface by silane grafting: Application for desalination with Air Gap Membrane Distillation process, Colloids and Surfaces A: Physicochemical and Engineering Aspects. 387 (2011) 79–85.

[31] W. Kujawski, J. Kujawa, E. Wierzbowska, S. Cerneaux, M. Bryjak, J. Kujawski, Influence of hydrophobization conditions and ceramic membranes pore size on their properties in vacuum membrane distillation of water-organic solvent mixtures, Journal of Membrane Science. 499 (2016)

442–451.

[32] J. Kujawa, S. Cerneaux, W. Kujawski, M. Bryjak, J.K. Kujawski, How To Functionalize Ceramics by Perfluoroalkylsilanes for Membrane Separation Process? - Properties and Application of Hydrophobized Ceramic Membranes, ACS Applied Materials & Interfaces. 8 (2016) 7564–7577.

[33] N. Gao, M. Li, W. Jing, Y. Fan, N. Xu, Improving the filtration performance of ZrO2 membrane in non-polar organic solvents by surface hydrophobic modification, Journal of Membrane Science. 375 (2011) 276–283.

[34] N. Gao, W. Ke, Y. Fan, N. Xu, Evaluation of the oleophilicity of different alkoxysilane modified ceramic membranes through wetting dynamic measurements, Applied Surface Science. 283 (2013) 863–870.

[35] N.A. Ahmad, C.P. Leo, A.L. Ahmad, Superhydrophobic alumina membrane by steam impingement: Minimum resistance in microfiltration, Separation and Purification Technology. 107 (2013) 187–194.

[36] N. Gao, Y. Fan, X. Quan, Y. Cai, D. Zhou, Modified ceramic membranes for low fouling separation of water-in-oil emulsions, Journal of Materials Science. 51 (2016) 6379–6388.

[37] M. Kosmulski, The pH-dependent surface charging and points of zero charge, Journal of Colloid and Interface Science. 353 (2011) 1–15.

[38] B.D. Sparks, L.S. Kotlyar, J.B. O'Carroll, K.H. Chung, Athabasca oil sands: effect of organic coated solids on bitumen recovery and quality, Journal of Petroleum Science and Engineering. 39 (2003) 417–430.

[39] L.S. Kotlyar, B.D. Sparks, J.R. Woods, K.H. Chung, Solids associated with the asphaltene fraction of oil sands bitumen, Energy & Fuels. 13 (1999) 346–350.

[40] A. Jada, M. Salou, Effects of the asphaltene and resin contents of the bitumens on the water-bitumen interface properties, Journal of Petroleum Science and Engineering. 33 (2002) 185–193.

[41] B. Arkles, Y. Pan, Y.M. Kim, The Role of Polarity in the Structure of Silanes Employed in Surface Modification, Silanes and Other Coupling Agents. 5 (2009) 51–64.

[42] S.D. Taylor, J. Czarnecki, J. Masliyah, Refractive index measurements of diluted bitumen solutions, Fuel. 80 (2001) 2013–2018.

[43] A.Y. Ku, C.S. Henderson, M.A. Petersen, D.J. Pernitsky, A.Q. Sun, Aging of Water from Steam-Assisted Gravity Drainage (SAGD) Operations Due to Air Exposure and Effects on Ceramic Membrane Filtration, Industrial & Engineering Chemistry Research. 51 (2012) 7170–7176.

[44] P.J. Launer, Infrared Analysis of Organosilicon Compounds: Spectra-Structure Correlations, in: Silicone Compounds: Register and Review, Petrarch Sytsems, Bristol, PA, 1987: pp. 100–103.

[45] P. Sanciolo, N. Milne, K. Taylor, M. Mullet, S. Gray, Silica scale mitigation for high recovery reverse osmosis of groundwater for a mining process, Desalination. 340 (2014) 49–58.

[46] A. Rolland-Sabaté, S. Guilois, B. Jaillais, P. Colonna, A. Rolland-Sabate, Molecular size and mass distributions of native starches using complementary separation methods: Asymmetrical Flow Field Flow Fractionation (A4F) and Hydrodynamic and Size Exclusion Chromatography (HDC-SEC), Analytical and Bioanalytical Chemistry. 399 (2011) 1493–1505.

4 Thermal Stability of Hydrophilic PEO-silane Modified Ceramic Membranes

C. Atallah, S. Mortazavi, A.Y. Tremblay.

Manuscript published in Colloids and Surfaces A: Physicochemical and Engineering Aspects 561 (2019): 254–266.

DOI: 10.1016/j.colsurfa.2018.10.058

Abstract

Industrial oily wastewaters often contain many recalcitrant species, such as dissolved metal ions, salts, bitumen, clays and humics. These species possess surface charges due to acidic, basic and amphoteric groups, thus leading to severe ceramic membrane fouling. To address this problem, ceramic membrane surfaces were chemically modified with highly hydrophilic PEO-based organosilanes. Three different membrane surface layers (ZrO_2-TiO_2, ZrO_2 and TiO_2) were modified at varying silane concentrations and reaction times to test their reactivity and stability. All modified membranes maintained hydrophilic behavior, as shown by water contact angles of <25° and pure water fluxes of 500–600 Lmh. Modified TiO_2 membranes exhibited superhydrophilicity with contact angles <10°. It was found that TiO_2 membranes were the most reactive, achieving maximal silane surface coverage at lower concentrations and reaction times, followed by ZrO_2 and ZrO_2-TiO_2 membranes. The silylated TiO_2 membrane was also the most thermally stable surface at 130°C and 160°C. Increasing the length of the PEO chain in the silane was also found to increase the thermal stability of the silane surface. TiO_2 membranes modified with the higher molecular weight silane maintained 97% of the silane at the membrane surface when exposed to heat at 130°C. In enhancing the suitability of ceramic membranes in challenging applications; titania membranes over zirconia and zirconia-titania should be used and modified with PEO-silanes containing 9–12 repeat units to ensure maximal surface coverage and enhanced thermal stability.

4.1 Introduction

In the oil and gas industry, among many others, large amounts of oily wastewaters are produced on a daily basis. These waste streams need to be treated prior to their re-use or disposal for purposes of economic and environmental sustainability. Oil-contaminated water can cause downstream process upsets that require costly cleaning and maintenance downtime. Conventional processes cannot reliably and consistently provide clean produced water for re-use, such as for steam production. Therefore, a more efficient separation option is needed within the produced water deoiling process.

Both polymeric and inorganic membrane separation technologies have been studied by the oil and gas industry in order to remove oil and other contaminants from produced water [1]. This is attributed to the high separation efficiency and the relatively simple operational process associated with membrane modules [2]. Ceramic membranes are well suited for this oily water separation and are preferred over polymeric membranes for their superior chemical and thermal stability. They are less vulnerable to the surrounding media than polymeric membranes, and are suitable for use over a wide range of temperatures and pH [3]. Ceramic membranes also possess a lower fouling tendency towards natural organic matter [4] and have consequently seen extensive use in treating synthetic oil-in-water emulsions. In the literature, synthetic mixtures are prepared by emulsifying either pure hydrocarbons [5], crude oil/petroleum products [6,7], waste oils [8], edible oils [9] or commercial oils [10] with water. These oily water mixtures, however, do not accurately represent the chemical composition of real produced water, which contains a myriad of various inorganics, clays and alkali metals that accompany the organic composition of the oil. Many studies have attempted to rectify this, either by adding inorganic salts to the emulsions [11,12] or by using actual field produced water as the feed [13,14]. The difficulty of treating these wastewaters is evidenced by the low fluxes and short lifetimes offered by the membranes used in such studies. Therefore, universal acceptance of membranes for oily wastewater treatment is presently hindered by the fouling observed in treating these feed streams.

Industrial oily wastewater often includes the presence of many ionic species such as calcium, magnesium, silicon and iron, as well as various clays, silicates and carbonates [15]. All of these potential foulants possess surface charges, owing to their acidic, basic and amphoteric groups. Surface charge is among the surface layer properties that greatly influence membrane fouling

and performance, alongside surface roughness and hydrophilicity [16]. The surfaces of ceramic membranes are hydrophilic due to the charged hydroxyl (OH) groups that populate the top layer [17]. These surface charges increase the interaction between the membrane surface and fouling species, and are thus responsible for the high fouling observed when treating oily wastewaters using ceramic membranes. In order to mitigate the effect of this charge attraction, the selective layer of a membrane can be chemically modified to render it non-ionic.

Surface modification of ceramic membranes may be achieved through the use of organosilanes. These are silicon based monomers that are capable of reacting with and modifying oxide surfaces. Selection of a silane with the appropriate organic moiety can lead to changes in both the wetting [18] and electrical properties [19] of the membrane selective layer. The ability to render ceramic membrane surfaces hydrophobic using silanes has seen extensive use in many applications, including gas separation [20], membrane distillation [21], osmotic evaporation [22], pervaporation [23] and protein separation [24]. To date, the use of silylated ceramic membranes in liquid separations has often involved hydrophobization to remove water as an oil contaminant in water-in-oil emulsions [25–27]. However, the inherent hydrophilicity of ceramic surfaces is desirable in treating oily wastewaters, where the objective is to recover the purified water as the permeate. In a recent study, ceramic membranes were modified with hydrophilic silanes possessing different surface charges to treat a model solution of negatively charged humic acid [28]. A negatively charged silane with sulfonic groups was shown to be the most efficient in reducing humic acid fouling. However, foulants in oily wastewater often possess both positive and negative surface charges. Therefore, an organosilane whose organic moiety is both hydrophilic and non-ionic is ideal for treating industrial oily wastewaters.

A group of modifying agents that satisfy these criteria is that of polyethylene oxide (PEO) based silanes. They are known to offer extremely low water contact angles of 15–16°, which is among the lowest values reported with commercially available silanes [29]. PEO-based surface modifications of ceramic membranes have been utilized in various biomedical applications pertaining to protein adsorption, where the non-ionic PEGylated surface is used to achieve electrostatic repulsion of proteins in solution [30,31]. They have also recently been applied in organic solvent recovery via nanofiltration [32]. The use of PEO functionalized surface

modifying agents to mitigate inorganic membrane fouling is a current and active area of research, as evidenced by recent intellectual property publications [33,34].

In our previous work, ceramic membranes with zirconia (molecular weight cut-off MWCO, 150 kDa and 300 kDa) and alumina (pore size 0.14 μm) selective layers were modified using a PEO based silane and then used in the filtration of steam assisted gravity drainage (SAGD) produced water [35]. The modification successfully mitigated the irreversible fouling caused by bituminous ultrafines in the feed. The permeate flux of the 150 and 300 kDa membranes doubled after modification. The filtered water obtained from the modified membranes was of superior quality, to that of the untreated membrane, as evidenced by total organic carbon analysis. The membranes were shown to reduce the particle sizes in the produced water from >200 nm in the feed to <40 nm in the permeate.

The successful mitigation of fouling in treating these wastewaters does not increase membrane lifetime indefinitely and ceramic membranes will eventually require cleaning to maintain adequate performance. During the clean-in-place procedure, the membranes can be exposed to temperatures above 120°C [3]. Hence, the silane layer must be able to withstand these temperatures for the sustained practical use of the modified ceramic membrane. Thermal degradation of aminofunctional and fluorinated silane layers on ceramic substrates has been shown to begin in the vicinity of 250–350°C [36–38]. However, no such information is available for the PEO based silanes that are of current interest.

The aim of this work was to chemically modify the surfaces of ceramic membranes using PEO based organosilanes under varying modification parameters to determine optimal silylation conditions. Specifically, the effect of silane concentration in the modification bath and the immersion time of the membranes in the silane solution on silane surface coverage were studied. Furthermore, the thermal stability of the silylated metal oxide layers was investigated. Three different membrane surface layers (ZrO_2-TiO_2, ZrO_2 and TiO_2) were utilized and compared in order to establish any differences in their stability and reactivity with the silanes. Unmodified and modified membrane surfaces were analyzed using FTIR, SEM, and contact angle and zeta potential measurements.

4.2 Experimental

4.2.1 Materials

The ceramic membrane disks studied in this work varied in terms of their pore size and membrane material. Membrane disks with a pore size of 0.14 µm and a MWCO of 300 kDa were purchased from Sterlitech Corporation (Kent, WA, USA). The support layer of these membranes was composed of titania (TiO_2). Electron-dispersive X-ray spectroscopy (EDS) was performed on a 90 µm by 110 µm area of the selective layer to confirm its composition. The EDS spectra were obtained using a tungsten Tescan Vega II SEM equipped with Oxford X-ray detection systems (INCA EDS). The EDS scans are presented in Figure 4.1a and Figure 4.1b for the 0.14 µm and 300 kDa membrane, respectively. It was determined that the selective layer of the 0.14 µm membrane was made from a mixture of approximately 90% zirconia (ZrO_2) and 10% TiO_2, while the selective layer of the 300 kDa membrane was made from ZrO_2. These membranes had a diameter of 47 mm and a thickness of 2.5 mm. Membranes with pore sizes of 10 nm were provided by Inopor (Veilsdorf, Germany). The ceramic supports of these membranes were composed of α-Al_2O_3, while their selective layers were made from TiO_2.

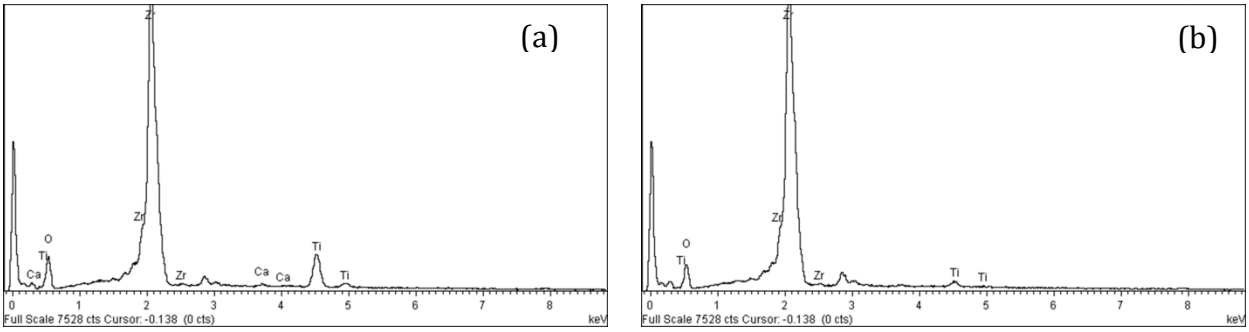

Figure 4.1: EDS spectra for the selective layer of (a) 0.14 µm and (b) 300 kDa membranes.

Poly(ethylene glycol) with an average molecular weight (MW) of 6000 was obtained from Sigma-Aldrich. Anhydrous ethanol (Fisherbrand) and acetic acid (ACS plus, Fisherbrand) were used in the silane surface grafting process. The organosilanes used for the silylation of the membrane surfaces are listed in Table 4.1 and their chemical structures are shown in Figure 4.2. All silane solutions were supplied by Gelest, Inc. (Morrisville, PA, USA). Hydrophilic silanes containing polyethylene oxide (PEO) chains were selected because they offered an extremely low water contact angle.

Table 4.1: Description of organosilanes used.

Name	Formula	Notation
2-[METHOXY(POLYETHYLENEOXY)6-9 PROPYL]TRIMETHOXYSILANE	$CH_3O(C_2H_4O)_{6\text{-}9}(CH_2)_3Si(OCH_3)_3$	$PEO_{6\text{-}9}TMS$
2-[METHOXY(POLYETHYLENEOXY)9-12PROPYL]TRIMETHOXYSILANE	$CH_3O(C_2H_4O)_{9\text{-}12}(CH_2)_3Si(OCH_3)_3$	$PEO_{9\text{-}12}TMS$

(a)

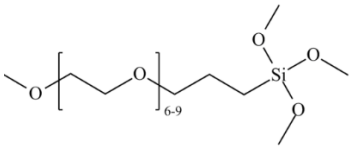

(b)

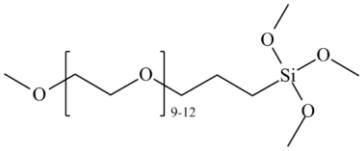

Figure 4.2: Chemical structures of silanes (a) $PEO_{6\text{-}9}TMS$ and (b) $PEO_{9\text{-}12}TMS$.

4.2.2 Surface modification procedure

Before linkage with oxide substrate surfaces, organosilanes must undergo hydrolysis in order to form silanols having hydroxyl groups. The hydrolysis of organosilanes can be accomplished in either acidic or basic media. Once hydrolysis and silanol formation is achieved, individual silanol molecules can then form covalent bonds by condensation reactions with hydroxyl groups on the oxide surface. Silanols can also undergo condensation reactions with each other to form mono- or multilayers at the membrane surface as shown in Figure 4.3 for $PEO_{6\text{-}9}TMS$.

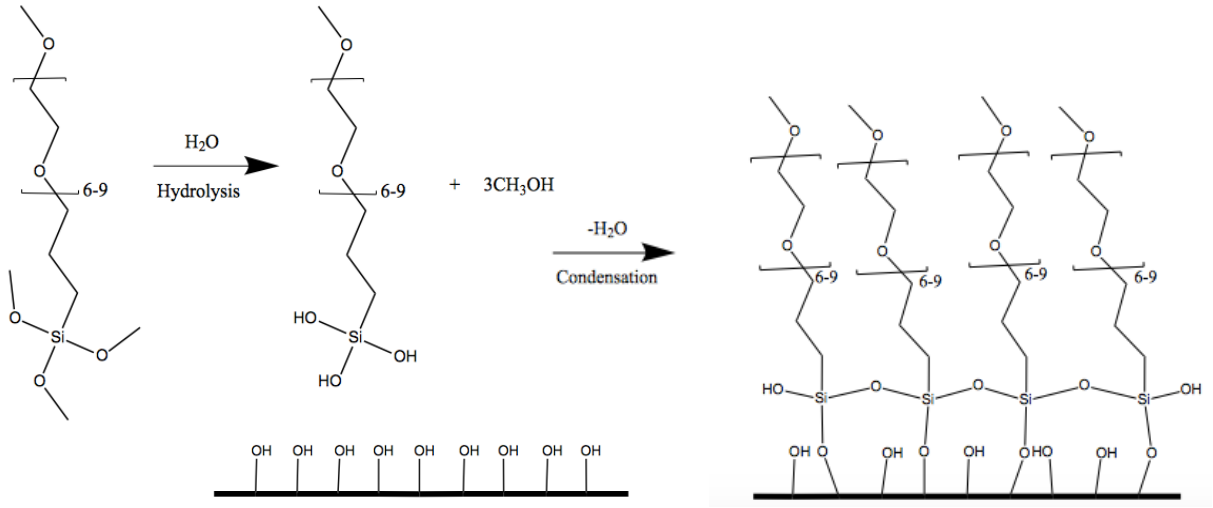

Figure 4.3: Reaction scheme of $PEO_{6-9}TMS$ with ceramic membrane surface.

Since hydrolyzed silanes must undergo a condensation reaction with hydroxyl groups, the number of these OH groups on the membrane surface has a significant impact on the surface modification process [39]. In order to ensure the presence of an adequate amount of hydroxyl groups on the membrane surface, the ceramic disks were subjected to a pre-treatment procedure prior to surface modification. Firstly, the ceramic membranes were soaked in deionized water for a period of 4 hours. Then, the membranes were removed from the water and placed in an oven that was maintained at 120°C for 24 hours. Finally, the membranes were removed from the oven and allowed to cool for at least 1 hour at room temperature inside a desiccator before surface modification. The desiccator was used in order to limit the adsorption of any additional moisture from the atmosphere onto the membranes, as excess surface water has been shown to negatively impact silane coverage of ceramic surfaces [40,41]. Drierite from W.A. Hammond Drierite Company (Xenia, OH, USA) was used as anhydrous desiccant in the desiccator.

Surface modification was achieved by the deposition of silanes from aqueous alcohol solutions. Firstly, a solution of 95% ethanol / 5% water by weight is prepared. The ethanol solution is then adjusted to a pH of 4.5 by adding acetic acid. The silylating agent is then added with stirring until the desired silane concentration is reached. In this work, silane concentrations of 0.1, 0.5, 5, 10 and 20 wt% were used. Following the addition of the silane, 5 minutes were allowed for hydrolysis and silanol formation. The membranes were then immersed into the silane solution for a desired reaction time while being gently agitated. In this work, reaction times of 2 and 30 minutes, and 6, 24 and 72 hours were tested. Once removed from the silane solution, the

membranes were rinsed by briefly dipping in ethanol in order to remove any excess materials from its surface and unreacted silane. Finally, the modified membranes were then placed in an oven, under nitrogen and at 110 °C, for 10 minutes in order to cure the silane layer.

4.2.3 Membrane surface characterization

In order to confirm the success of the surface silylation procedure, FTIR analyses of the ceramic membrane surfaces were conducted using a Cary 630 FTIR with an Attenuated Total Reflectance (ATR) diamond accessory (Agilent Technologies, Canada). Small amounts of material were scraped off the surface of the membrane, resulting in a powder that was then used to completely and evenly cover the diamond accessory.

SEM imaging was performed using a JEOL 6610LV SEM at accelerating voltages of 10 and 20 kV (Japan Electron Optics Laboratory, MA, USA) and a Phenom Pro Desktop SEM (Nanoscience Instruments, VA, USA) at accelerating voltages of 5 and 10 kV. Membrane samples were broken into smaller samples and fixed onto a metal holder using a conductive tape. Images were then taken at randomly chosen locations on the membrane surface at suitable magnifications.

The hydrophilicity of the ceramic membrane surface was analyzed by measuring static water contact angle using a VCA Optima Surface Analysis system (AST Products Inc., MA, USA). A 1 µL droplet of water was dropped onto a random location on the membrane surface using a micro syringe (Hamilton Company, NV, USA) and the contact angle was measured at varying time intervals.

A Zetasizer NanoZS (Malvern Instruments Ltd., UK) was used to calculate the zeta potential of unmodified and modified membranes. Small amounts of material were scraped off the surface of the membrane, resulting in a powder that was then subjected to the silane modification procedure described in Section 4.2.2. Unmodified and modified powders were then dispersed in microfiltered deionized water (pH 7). Zeta potential measurements of these aqueous solutions were then taken using a folded capillary cell and by applying the Smoluchowski model.

4.2.4 Membrane water filtration tests

Some of the unmodified and modified membranes were subjected to a filtration test with 10 L of microfiltered deionized water for 2 hours. The transmembrane pressure (TMP) was maintained at 10 psig (68.95 kPa) for the 0.14 µm membranes and 25 psig (172.4 kPa) for the 300 kDa

membranes, by means of a valve. The permeate was collected in a separate container while the retentate was recycled back to the feed tank. The permeate mass was recorded every 3 seconds and the pure water permeate (PWP) flux of the membranes was computed using the following equation:

$$J = \frac{m}{\rho \cdot A \cdot \Delta t} \tag{4.1}$$

where J is flux in L/(m^2·h), m is the mass of the permeate collected (g), ρ is the density of water (g/L), A is active membrane surface area (m^2) and Δt is the filtration time (h).

4.3 Results and discussion

4.3.1 Effect of silane concentration and silylation reaction time

When analyzing the surfaces of modified membranes, characteristic peaks pertaining to both organosilicon compounds and PEO chains were targeted during FTIR analysis in order to assess the extent of surface silylation with the PEO-based silanes. Descriptions of these characteristic peaks are summarized in Table 4.2 for organosilicon bonds [42] and Table 4.3 for PEO bonds [43].

Table 4.2: Characteristic FTIR peaks of organosilane compounds.

Wavenumber (cm^{-1})	Intensity	Assignment
1000-1130	Very strong	Si-O-Si
1000-1110	Strong, sharp	Si-O-CH_3
900-1000	Strong	Si-O-Metal
810-950	Broad	Si-OH

Table 4.3: Characteristic FTIR peaks of polyethylene oxide.

Wavenumber (cm^{-1})	Intensity	Assignment
2960	Strong	CH_2 asymmetrical stretching
2890	Strong	CH_2 symmetrical stretching
1470	Variable	CH_2 scissoring
1362	Variable	CH_2 wagging
1254-1289	Weak	CH_2 twisting
1070-1153	Strong	C-O stretching
845-964	Weak	CH_2 rocking

Ceramic membrane disks were surface modified using varying concentrations of silane $PEO_{6-9}TMS$ in the modification bath. The silane concentrations tested were 0.1, 0.5, 5, 10 and 20 wt%.

For each concentration, the membranes were immersed in the silane solution for durations of 2 minutes, 30 minutes, 6, 24 and 72 hours. These modification experiments were done with the goal of assessing the combined effect of silane concentration and reaction time between the silane and ceramic surface. FTIR spectra of the modified membrane surfaces were generated, and the spectra for several reaction times at a single silane concentration were plotted on the same figure. An example is shown in Figure 4.4, where the spectra for the 300 kDa ZrO_2 membranes modified in a 10 wt% silane solution are presented at different reaction times.

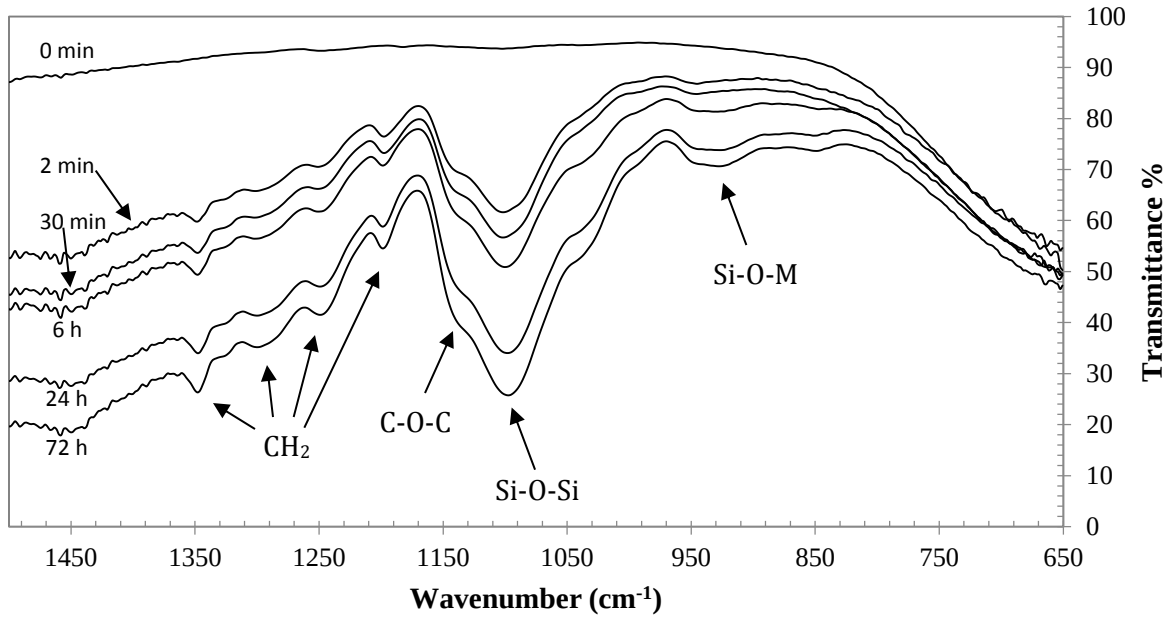

Figure 4.4: FTIR spectra for the 300 kDa ZrO_2 membranes modified with 10 wt% $PEO_{6\text{-}9}TMS$ at different silylation times. Baseline correction operated for all spectra.

The strongest expected peaks at 1140 cm^{-1} (C-O-C) and 1090 cm^{-1} (Si-O-Si) are clearly visible. They may be distinguished from one another due to a subtle inflection point at approximately 1130 cm^{-1}. These peaks dominate each spectrum and correspond to the ether bonds in the silane PEO chains and to the siloxane bonds between silane molecules at the surface. Membranes modified at other concentrations showed the same trends. Peaks pertaining to CH_2 vibrations become visible starting at silane concentrations of 5 wt%. Weak peaks characteristic of CH_2 scissoring (1450 cm^{-1}), wagging (1345 cm^{-1}), twisting (1240 & 1290 cm^{-1}) and rocking (840 cm^{-1}) are seen, while the broad peak in the vicinity of 2900 cm^{-1} represents CH_2 stretching. Moreover, the peaks observed in the range of 920–940 cm^{-1} are indicative of Si-O-Metal bonding, which is

further evidence of the reaction between the silane and the metal oxide surface of the ceramic membranes.

As a measure of the extent of surface silylation, the intensity of the Si-O-Si peak was evaluated by taking the difference in transmittance between the top and bottom of the Si-O-Si peak. This siloxane peak intensity was plotted as a function of silane concentration at each silylation time for the zirconia-titania (Figure 4.5a), zirconia (Figure 4.5b) and titania (Figure 4.5c) membranes. It is evident that there is very little surface modification taking place at silane concentrations of 0.1 and 0.5 wt%. Siloxane bonds only start significantly being detected after 72 hours of reaction time with all three membranes at such low concentrations. As the silane concentration is increased to 5, 10 and 20 wt%, a notable increase in peak intensity is observed.

From the spectra of the zirconia-titania and zirconia membranes, it is seen that the intensity of the observed peaks increases as the reaction time increases. Of particular interest is that the intensity of the Si-O-Si peaks is larger for the zirconia membrane than for the zirconia-titania membranes, at the same silane concentration and reaction time. For example, it can be seen that at concentrations of 5, 10 and 20 wt%, a reaction of time of 72 hours with the zirconia-titania surface is required to reach similar peak intensity achieved by the zirconia surface after only 30 minutes of reaction. This indicates that the ZrO_2 selective layer of the 300 kDa membranes is more reactive than the ZrO_2-TiO_2 selective layer of the 0.14 μm membranes with the silane. Furthermore, the peak intensities in the spectra of the titania membranes are even larger than those of the zirconia membranes. The higher reactivity of the TiO_2 selective layer is such that the observable effects of the tested reaction times are not nearly as significant as they are for the other two membranes. This indicates that with the titania membranes, a reaction time of 2 to 30 minutes may be sufficient for effective surface silylation.

It is seen with the zirconia and titania membranes that peak intensity seems to reach a plateau, as there is not much increase observed between silane concentrations of 10 and 20 wt%. This plateau is more evident with the titania membrane, further demonstrating its higher reactivity. Contrarily, the zirconia-titania surface shows an ongoing increase in peak intensity at conditions as high as 20 wt% silane for 72 hours, indicating the need for longer reaction times or higher silane concentrations to achieve maximum silylation. Higher reactivity of titania when grafting with organosilanes has been reported elsewhere, in terms of the percentage of available surface

OH groups used during silylation [44]. The increased reactivity of one membrane material over another could be due to differences in charge density of the metal ions in the different metal oxides. The van der Waals radii for zirconium and titanium are 0.23 nm and 0.215 nm, respectively [45]. Considering the respective valence electrons and charges of Zr^{4+} and Ti^{4+} in their crystalline metal oxide structures, and assuming spherical atoms, the volumetric charge density in TiO_2 is over 22% larger than in ZrO_2. This order of reactivity also indicates the effect of pore size, where the highest reactivity was observed with the membrane having the smallest pore size.

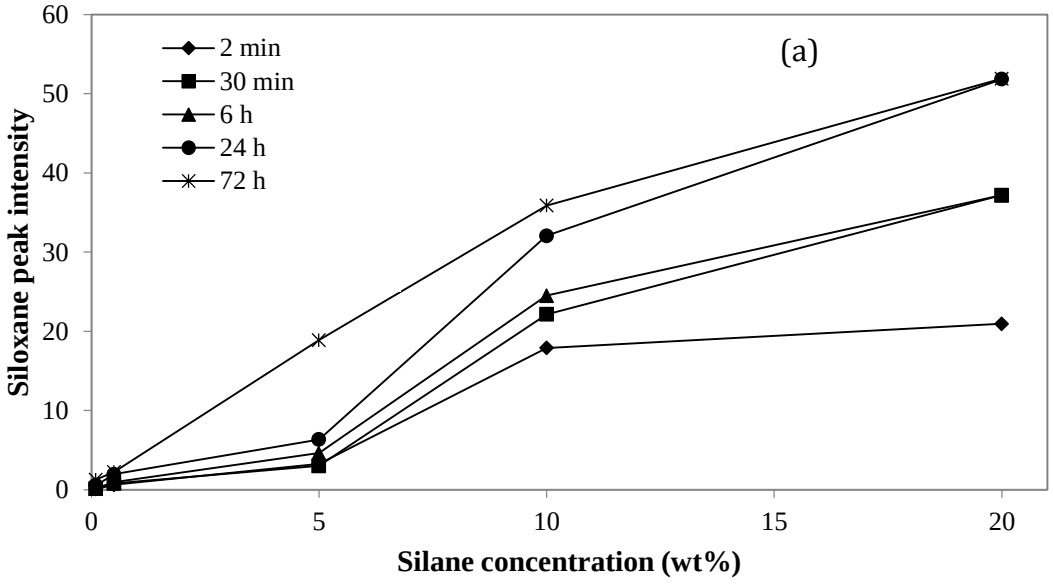

Figure 4.5 (continued next page)

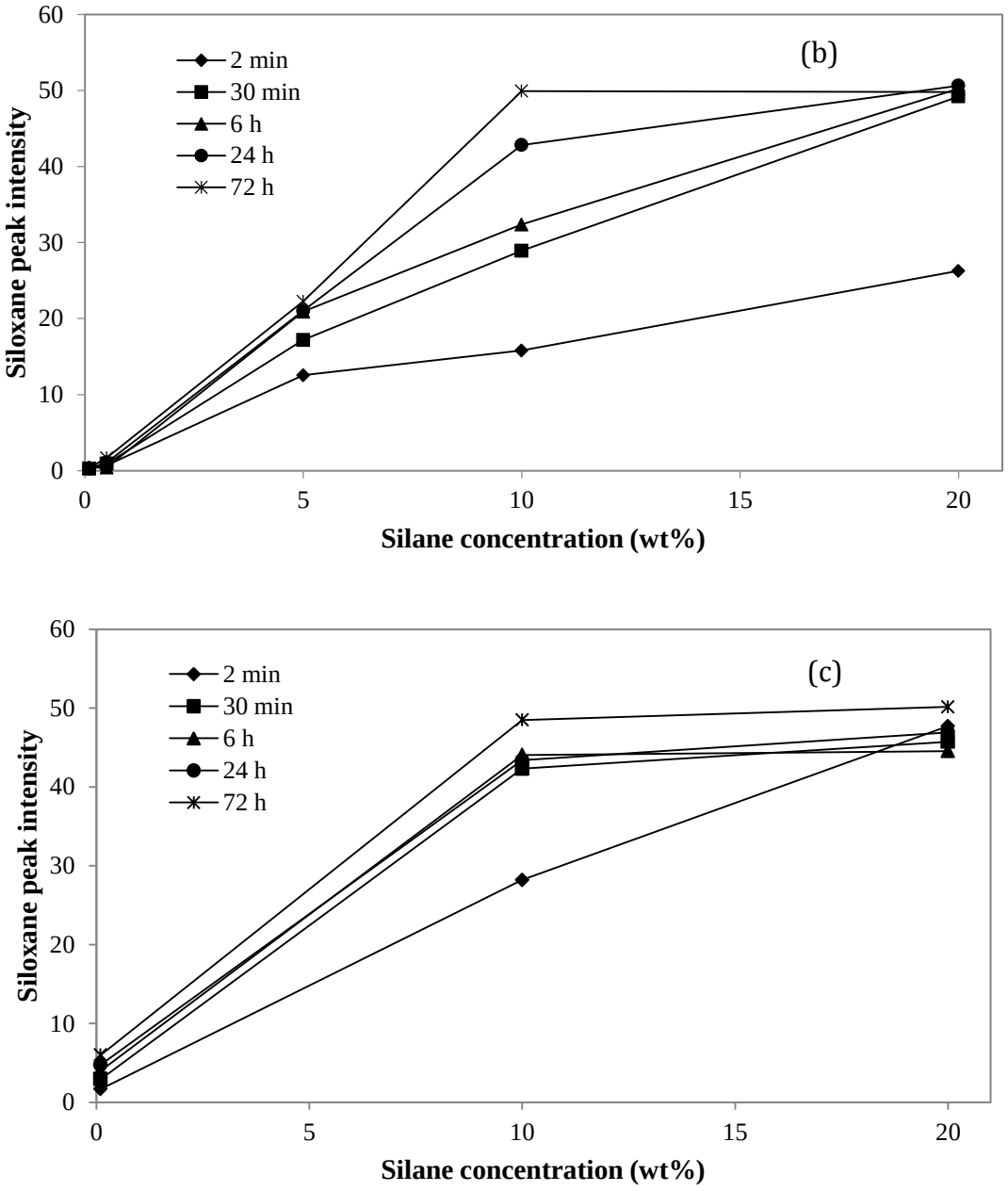

Figure 4.5: Si-O-Si FTIR peak intensity vs silylation time and concentration for (a) 0.14 µm ZrO_2-TiO_2, (b) 300 kDa ZrO_2 and (c) 10 nm TiO_2 membranes.

4.3.2 Effect of water content on silylation

The presence of an adequate amount of water in the silane hydrolysis solution plays a crucial role in the silylation process, as it enables the hydrolysis of the silane's methoxy groups [39]. As more of these groups are hydrolyzed, more hydroxyl groups are available to react with the membrane surface, thus increasing the stability of the formed silane surface layer. It was found

that immersing the membranes for 72 hours in solutions containing 20 wt% silane offered the best silane surface coverage, based on FTIR analysis. Zirconia-titania and zirconia membranes were thus subsequently modified under such conditions, but at varying H_2O concentrations in the modification bath. The water contents tested were 0.2, 0.5, 1, 2 and 5 wt%, the latter having been the standard used in all experiments thus far. The FTIR spectra at varying water concentrations are seen in Figure 4.6a for the zirconia-titania membranes and Figure 4.6b for the zirconia membranes. The intensities of the siloxane peaks in the spectra do not vary significantly within the tested range of water concentrations. There are however observable differences seen in the form of a slight broadening of the Si-O-Metal (940 cm^{-1}) peaks as the water concentration increases, indicating that the additional water results in a moderate increase in the number of hydrolyzed silane molecules which then react with the metal oxide surface. Overall, the results suggest that the standard water content in the modification bath of 5 wt% is preferable to allow for adequate silylation of both the zirconia-titania and zirconia ceramic membranes.

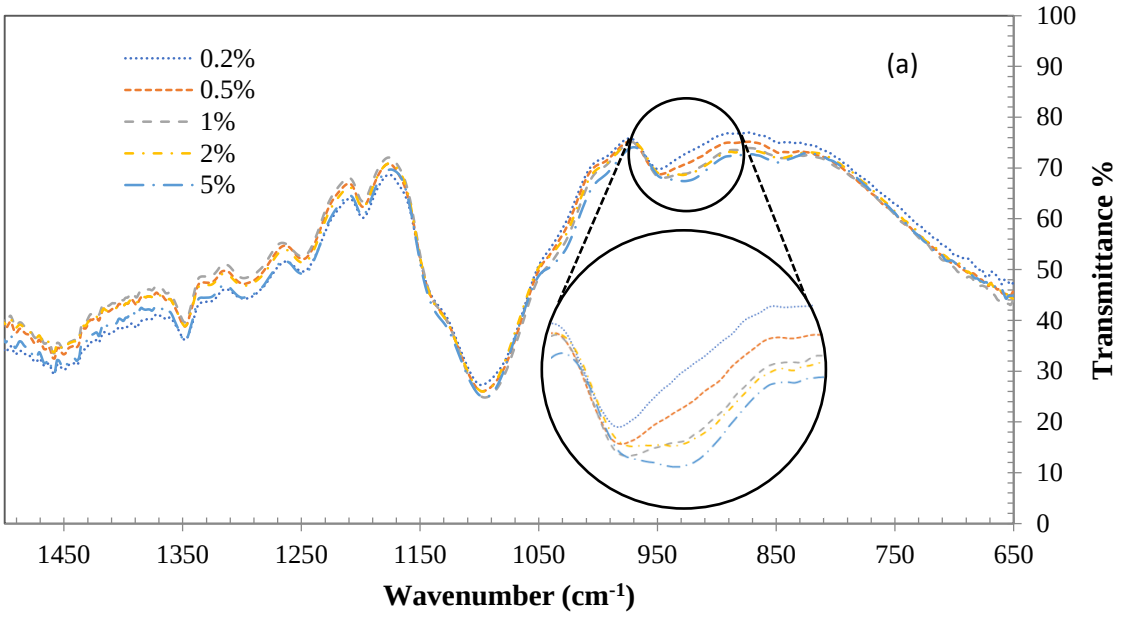

Figure 4.6 (continued next page)

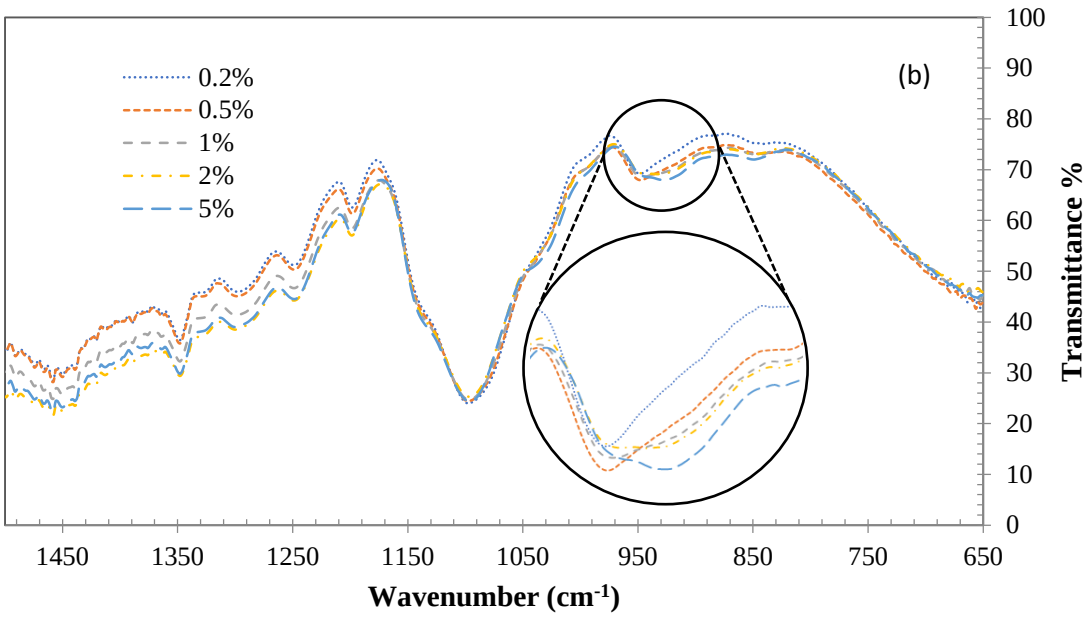

Figure 4.6: FTIR spectra of (a) 0.14 µm zirconia-titania and (b) 300 kDa zirconia membranes modified with 20 wt% $PEO_{6-9}TMS$ for 72h at varying H_2O concentrations. Baseline correction operated for all spectra.

4.3.3 Thermal stability of silane surface layer

To establish the thermal stability of silanes $PEO_{6-9}TMS$ and $PEO_{9-12}TMS$ at higher temperatures, ceramic membrane disks modified in 20 wt% solutions of these silanes for 72 hours were subsequently placed in an oven at temperatures of 130°C and 160°C for a duration of 2 hours. To determine the effect of this heat treatment on the silane layer, PWP fluxes, FTIR spectra, SEM images, contact angle and zeta potential measurements of the membrane surfaces were analyzed before and after the treatment.

4.3.3.1 Effect of modification on surface zeta potential

The zeta potential measurements of the unmodified, modified and 160°C heat treated ceramic powders are presented in Figure 4.7 for the zirconia-titania, zirconia and titania membranes. The zeta potentials of the unmodified powders were -37.90, -40.73 and -39.00 mV for the zirconia-titania, zirconia and titania selective layers, respectively. After surface modification in a 20 wt% solution of $PEO_{9-12}TMS$ for 72 hours, the zeta potentials increased to -26.17, -20.80 and -14.9 mV for zirconia-titania, zirconia and titania, respectively. The reduction in the absolute values of the zeta potential measurements indicates that modification with the PEO silane reduces charging at the membrane surface. The largest reduction in surface charging was observed with the titania

membrane, further highlighting its increased reactivity with the silane. This order indicates the influence of pore size where the highest reactivity was observed at the smallest pore size. After heat treatment at 160°C for 2 hours, the zeta potential measurements of the modified powders were repeated and the resulting values were -34.70, -36.90 and -32.27 mV for the zirconia-titania, zirconia and titania membranes, respectively. This indicates that the heat treatment removed the majority of the PEO-silane from the surface and partially restored the initial surface charge of the original ceramic membranes.

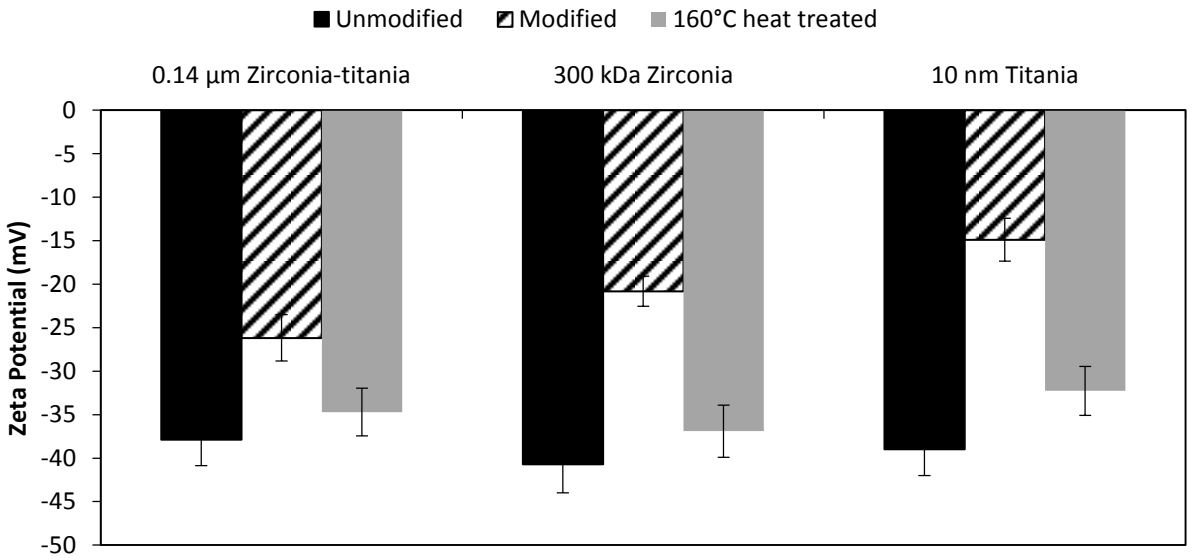

Figure 4.7: Zeta potential of ceramic membranes before and after surface modification with $PEO_{9\text{-}12}TMS$ (20% for 72 hours), and after heat treatment at 160°C for 2 hours.

4.3.3.2 Pure water permeability

The pure water fluxes through the zirconia-titania and zirconia membranes modified with $PEO_{6\text{-}9}TMS$ and $PEO_{9\text{-}12}TMS$ were measured before and after heat treatment. These results are presented in Figure 4.8a for the zirconia-titania membranes and in Figure 4.8b for the zirconia membranes. Pure water permeation could not be conducted on the titania membranes due to their limited supply. It was observed that the PWP flux decreased for all membranes upon modification with either silane, indicating that surface silylation reduced membrane wetting properties. Nonetheless, modified surfaces remained quite hydrophilic with PWP fluxes of 500-600 Lmh. Reduction in PWP flux was slightly higher for membranes modified with the longer chain silane, $PEO_{9\text{-}12}TMS$. After heat treatment at 130°C, PWP fluxes increased but did not reach the original fluxes of the unmodified membranes. This suggests that exposure to this

temperature leads to a volatilization of some of the silane at the surface, which in turn partially reinstates the inherent hydrophilicity of the metal oxide surface. The observed recuperation in PWP flux was more moderate for the zirconia membranes, indicating less release of silane from the modified surface and suggesting that the silane layer is more stable on the zirconia surface compared to the zirconia-titania surface. After heat treatment at 160°C, however, PWP flux of all membranes decreased to practically zero. This indicates that the loss of surface silane at 160°C is not only accompanied by volatilization of organic compounds, but also by degradation reactions, whose products reduce pore size and eventually plug membrane pores. In fact, decomposition of adsorbed silane molecules at inorganic membrane surfaces has previously been utilized to generate a silica-containing coke layer that effectively reduces pore dimensions [46].

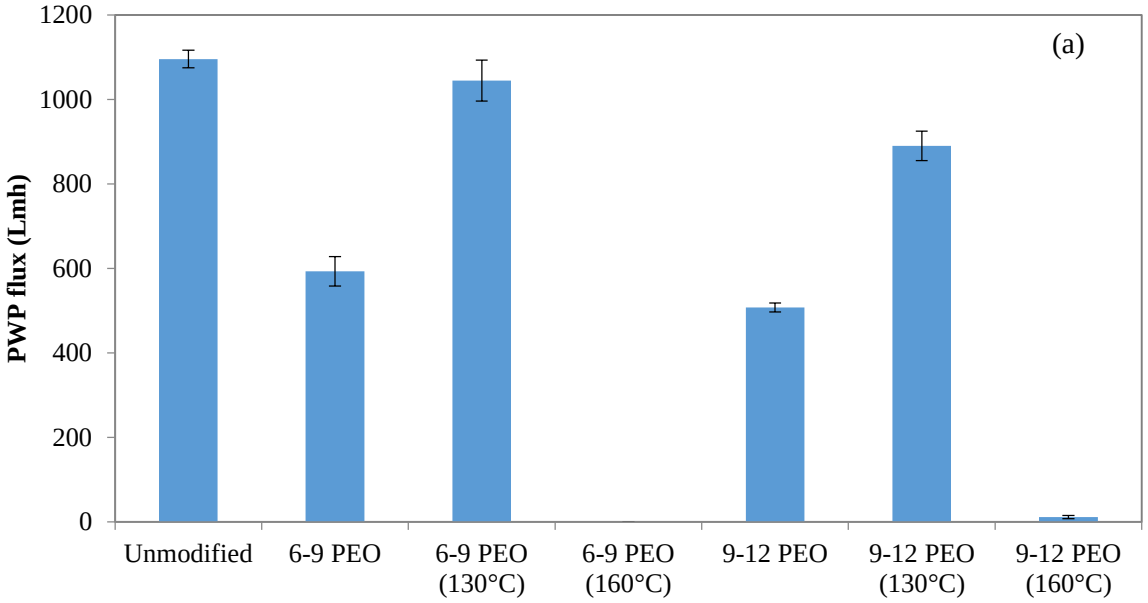

Figure 4.8 (continued next page)

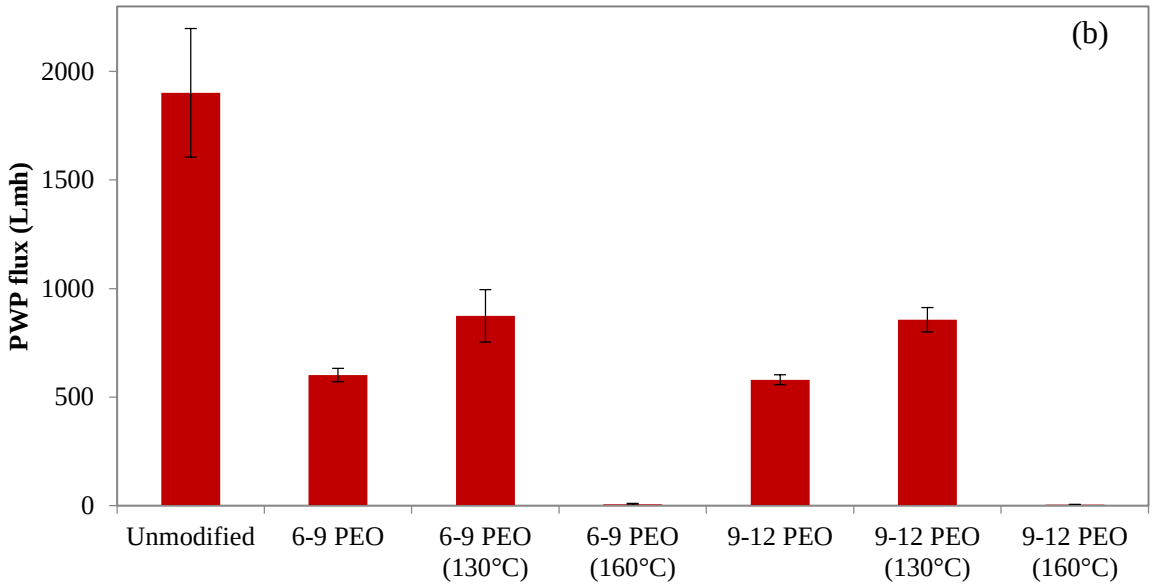

Figure 4.8: Pure water fluxes before and after heat treatment for the (a) 0.14 μm zirconia-titania and (b) 300 kDa ZrO_2 membranes.

4.3.3.3 Surface structure and morphology

The microscopy images of the unmodified and $PEO_{6\text{-}9}TMS$ modified ceramic membrane surfaces are presented in Figure 4.9. Although the surfaces of all tested membrane materials were successfully chemically modified, as confirmed by FTIR analysis, the surface morphology of the membranes was not greatly altered. It is observable that upon silylation at 20 wt% silane for 72 h, the surfaces show negligible changes in pore structure. It is likely that the silanes could not fully polymerize to form a complete surface layer or gel, but rather penetrated into the pores. Furthermore, the film thickness of PEO-based silane layers on ceramic membrane substrates has been reported to be less than 2 nm in some cases [31]. A monolayer thickness of this magnitude would not be expected to significantly affect membrane surface structure. These observations are consistent with the work of others who could not demonstrate conclusive changes in SEM images of unmodified and silylated ceramic membranes [26,28].

These observations indicate that the number of pores at the membrane surface was not reduced by silylation. Knowing this, the effect of surface modification on membrane pore size can be estimated using a modified Hagen-Poiseuille equation [47]:

$$Q = Nk\frac{\Delta P \pi D_h^4}{128 L_o \mu} \quad (4.2)$$

where Q is pure water flow through the membrane (m^3/s), N is number of pores, k is a geometric correction factor, ΔP is TMP (Pa), D_h is pore hydraulic diameter (m), L_o is pore length (m) and μ is water viscosity (Pa·s). Using equation (4.2**)** with the known PWP flux of the unmodified membranes, the number of pores (N) can be determined. With the assumption that N does not change upon modification or heat treatment, equation (4.2**)** can then be applied with the PWP fluxes of the modified and heat-treated membranes to determine the pore diameter (D_h) of these membranes, as well as the coating thickness of the silane layer. The results of these calculations are given in Table 4.4. The coating thicknesses are in good agreement with previously reported film thicknesses of PEO-based silane layers on ceramic membrane substrates [31].

The pore sizes were found to decrease after modification with either silane, with slightly larger pore sizes after silylation with $PEO_{6\text{-}9}TMS$ compared to $PEO_{9\text{-}12}TMS$. After heat treatment at 130°C, pore sizes increased compared to those of the untreated modified membranes, but they did not return to the values of the unmodified membranes. This was due to a partial loss of the silane from the surface at 130°C. The greatest loss in coating thickness was seen for $PEO_{6\text{-}9}TMS$ on the ZrO_2-TiO_2 membrane (9.96 down to 0.83 nm). The $PEO_{9\text{-}12}TMS$ on the ZrO_2 membrane did not exhibit such a loss (3.85 down to 2.71 nm). This suggests that longer chain silanes are more stable than their shorter chain counterparts, and also that silanes are more stable on zirconia than zirconia-titania surfaces. After heat treatment at 160°C, pore sizes were severely reduced compared to those of the unmodified membranes, due to silane degradation at this elevated temperature.

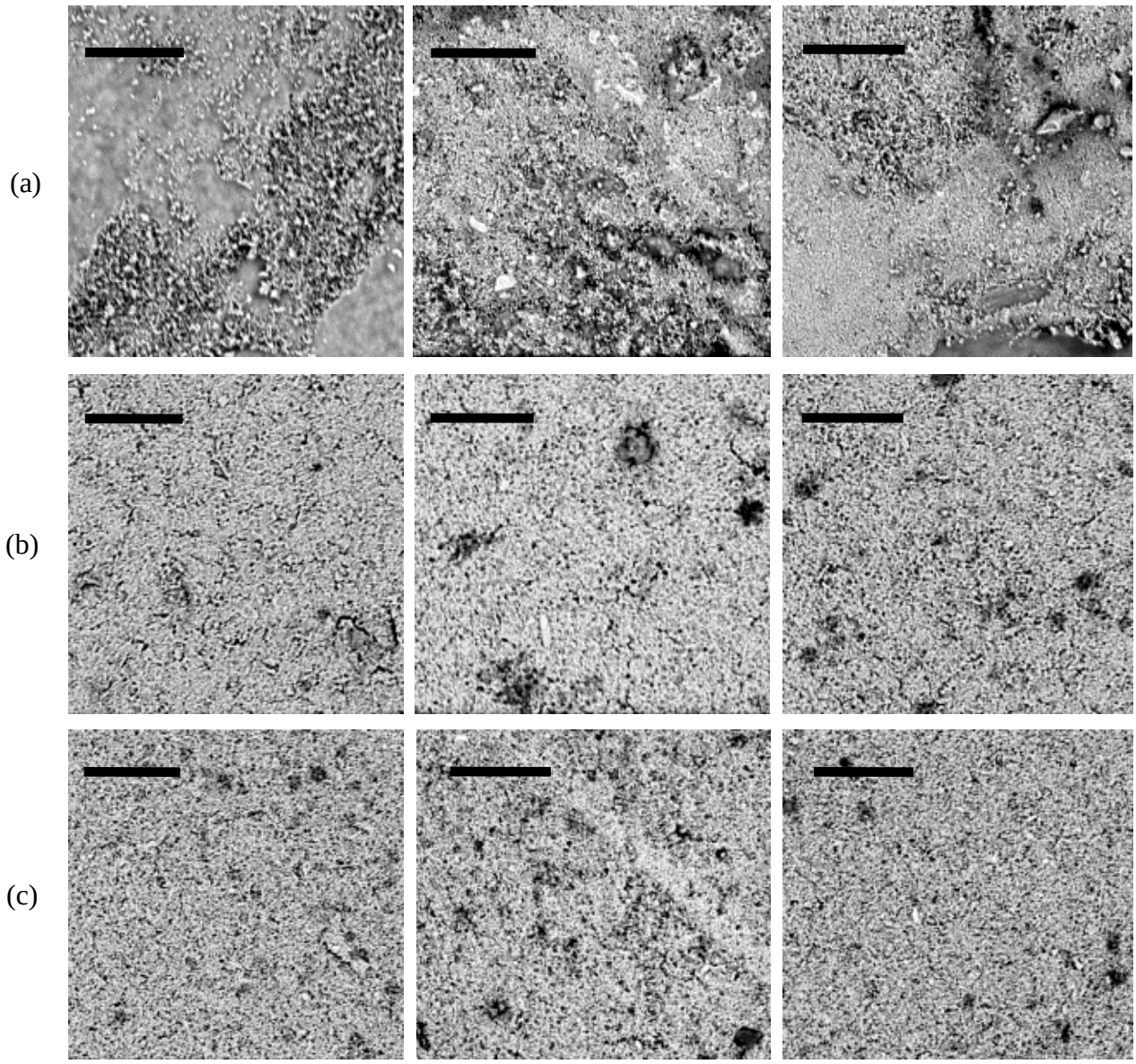

Figure 4.9: SEM images of ceramic membrane surfaces. Unmodified membrane (left), 20 wt% / 72 h modified membrane (middle) and 160°C heat treated membrane (right) surfaces are shown for the (a) 10 nm TiO_2, (b) 300 kDa ZrO_2 and (c) 0.14 µm ZrO_2-TiO_2 membranes. Scale: 10 µm.

Table 4.4: Pore diameter and silane coating thickness of modified zirconia and zirconia-titania membranes before and after heat treatment.

	300 kDa ZrO_2 membranes		0.14 μm ZrO_2-TiO_2 membranes	
Membrane	Pore Diameter (nm)	Coating Thickness (nm)	Pore Diameter (nm)	Coating Thickness (nm)
Unmodified	30 from [35]	-	140	-
6-9 PEO	22.49	3.75	120.1	9.96
9-12 PEO	22.29	3.85	115.5	12.25
6-9 PEO (130°C)	24.70	2.65	138.3	0.83
9-12 PEO (130°C)	24.58	2.71	132.9	3.54
6-9 PEO (160°C)	7.26	11.37	2.05	68.98
9-12 PEO (160°C)	6.66	11.67	44.45	47.78

4.3.3.4 Fourier-transform infrared spectral analysis

Upon inspection of the spectra for the zirconia-titania (Figure 4.10a), zirconia (Figure 4.10b) and titania (Figure 4.10c) membranes, it is observed that the intensity of the Si-O-Si peak does diminish upon exposure to such temperatures. The titania membrane shows the least amount of silane loss of 30% at 130°C, while all of the membranes show an Si-O-Si peak reduction of approximately 90% at 160°.

In all cases, thermal degradation is not only accompanied by diminishment of the Si-O-Si peak, but also by the appearance of a peak in the range of 1710 cm^{-1}. Vibrations at this wavenumber correspond to carbonyl (C=O) bonds, such as in ketones and aldehydes. PEO is known to thermally degrade following a random chain scission mechanism [43]. Therefore, such functional groups likely form upon molecular scission of the PEO chain's ether groups.

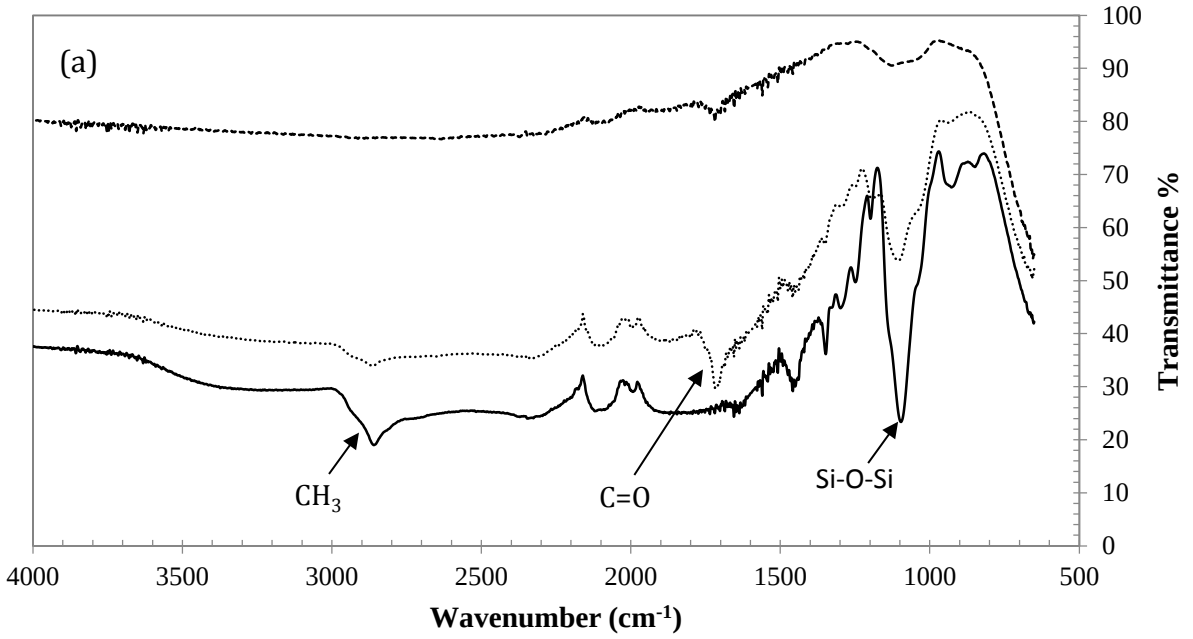

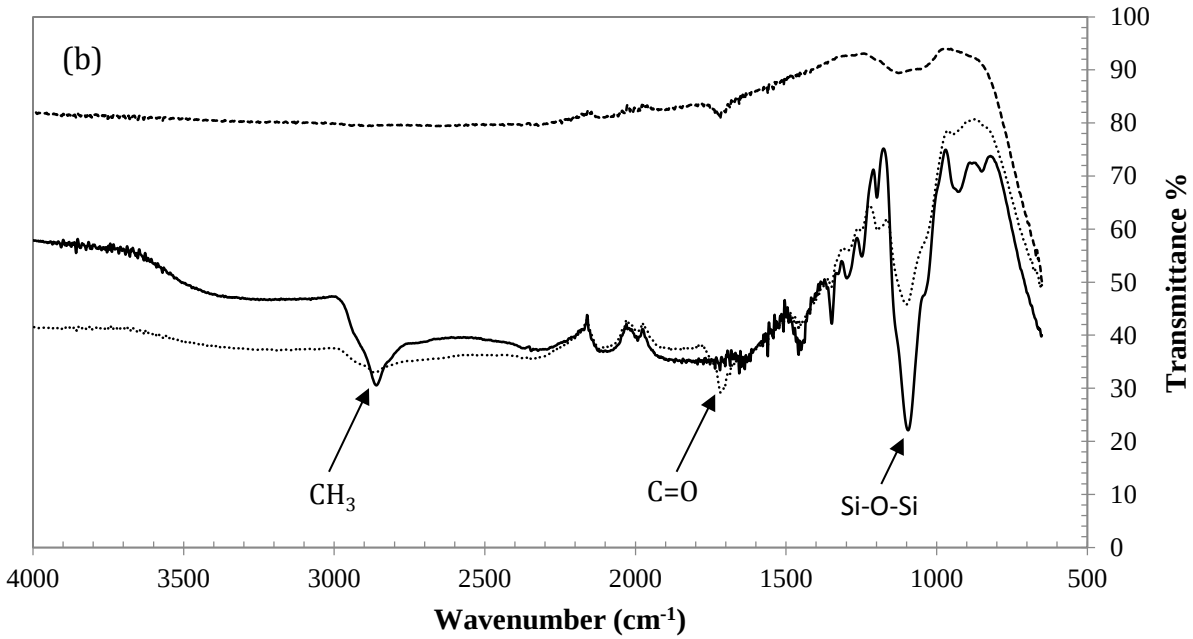

Figure 4.10 (continued next page)

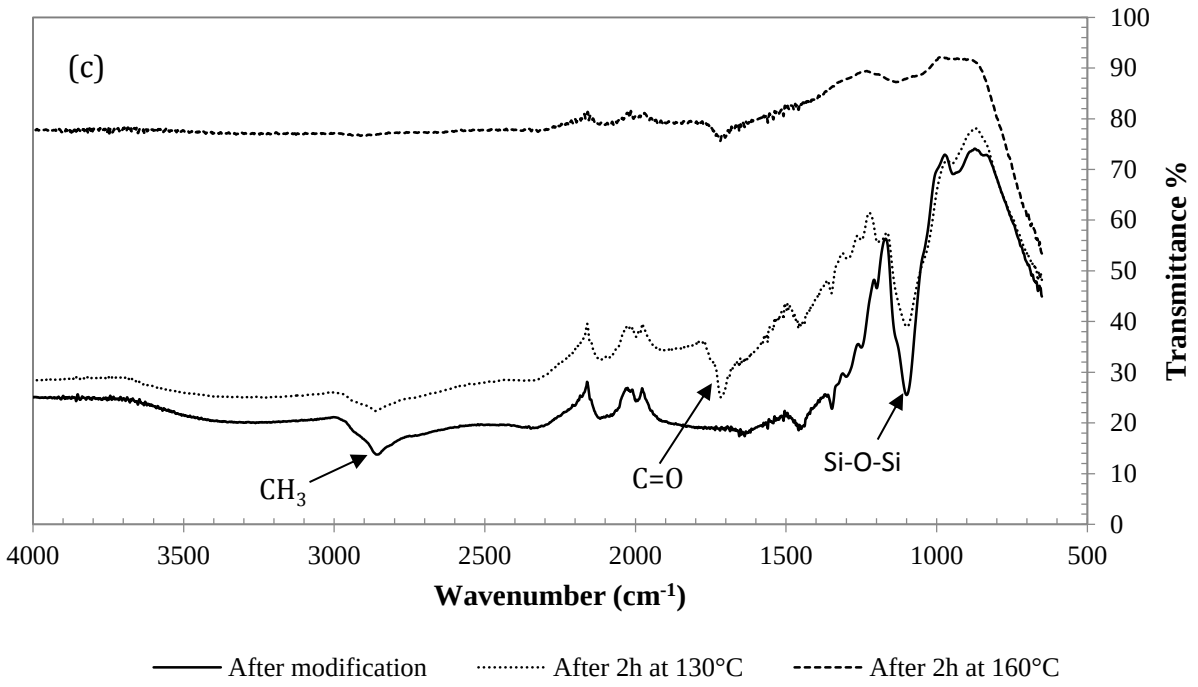

Figure 4.10: FTIR spectra of (a) 0.14 µm zirconia-titania, (b) 300 kDa zirconia and (c) 10 nm titania membrane modified with 20 wt% $PEO_{6\text{-}9}TMS$ for 72h before and after exposure to temperatures of 130 and 160°C for 2h. Baseline correction operated for all spectra.

To verify this, PEG powder with an average molecular weight of 6000 was heated to various temperatures for 2 hours and its FTIR spectra was subsequently taken. The ratio of the intensity of the C=O peak to that of the C-O-C peak was calculated and plotted as a function of the treatment temperature (Figure 4.11). Significant changes in the FTIR spectra only become observable at temperatures above 100°C. The magnitude of the carbonyl peak then increases rapidly up to a temperature of 190°C, where the ratio is nearly 50%. At temperatures above 160°C, slight browning of PEG was observed and the material could not be grinded back into its initial powder form upon cooling; it was instead now in the form of a translucent paste. The increase of carbonyl groups at higher temperature is caused by the increasing appearance of formic acid as a degradation product, which then reacts with the PEG terminal OH groups to yield formic acid esters [48]. The loss of the CH_3 peak (2850 cm^{-1}) with heat also corresponds to the formation of formic acid, which is volatile and partly evaporates from the membrane surface. It is hence suggested that the appearance of the carbonyl peak in the spectra of the heated membrane surfaces is a result of the thermal degradation of the grafted PEO chains.

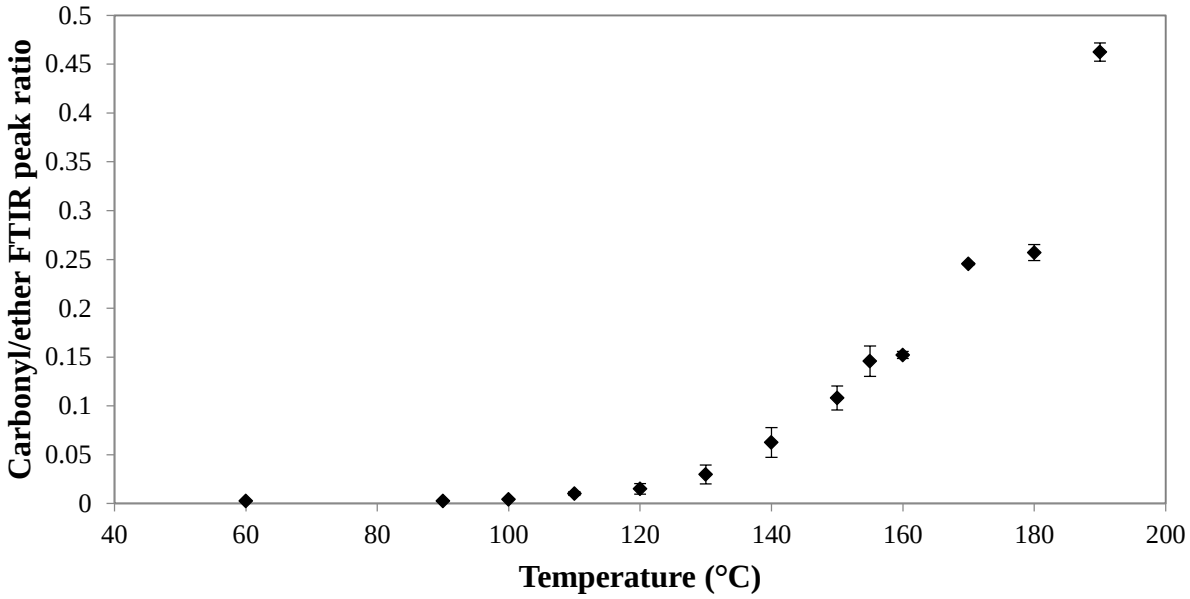

Figure 4.11: Degradation of FTIR ether peak into carbonyl peak for PEG 6000 at various temperatures.

The FTIR spectra before and after heat treatment were also taken for the $PEO_{9-12}TMS$ modified membranes to further establish the effect of silane chain length on thermal stability. The residual siloxane FTIR peak intensity at the surface for all silylated membranes after exposure to temperatures of 130°C and 160°C can be seen in Figure 4.12. In all cases, it is observed that the use of the higher molecular weight silanes results in higher residual siloxane peak intensity, indicating an increase in the thermal stability of the formed silane layers compared to $PEO_{6-9}TMS$. It is seen that, at both temperatures, $PEO_{9-12}TMS$ offers the most stable surface layer, followed by $PEO_{6-9}TMS$. Nonetheless, substantial silane loss is still observed at 160°C, with the highest residual value of 24% occurring when $PEO_{9-12}TMS$ is reacted with the more active TiO_2 surface. However, at 130°C a more significant improvement in thermal stability is seen. The $PEO_{9-12}TMS$ layer shows an increase in residual surface silane by approximately 12%, 5% and 28% for the ZrO_2-TiO_2, ZrO_2 and TiO_2 membranes, respectively, compared to $PEO_{6-9}TMS$. Out of all the tested membranes, the lowest reduction in Si-O-Si peak intensity is observed when the layer of $PEO_{9-12}TMS$ on the titania membrane is exposed to 130°C. At this temperature, the TiO_2 membrane maintains more than 97% of the Si-O-Si FTIR peak at the surface.

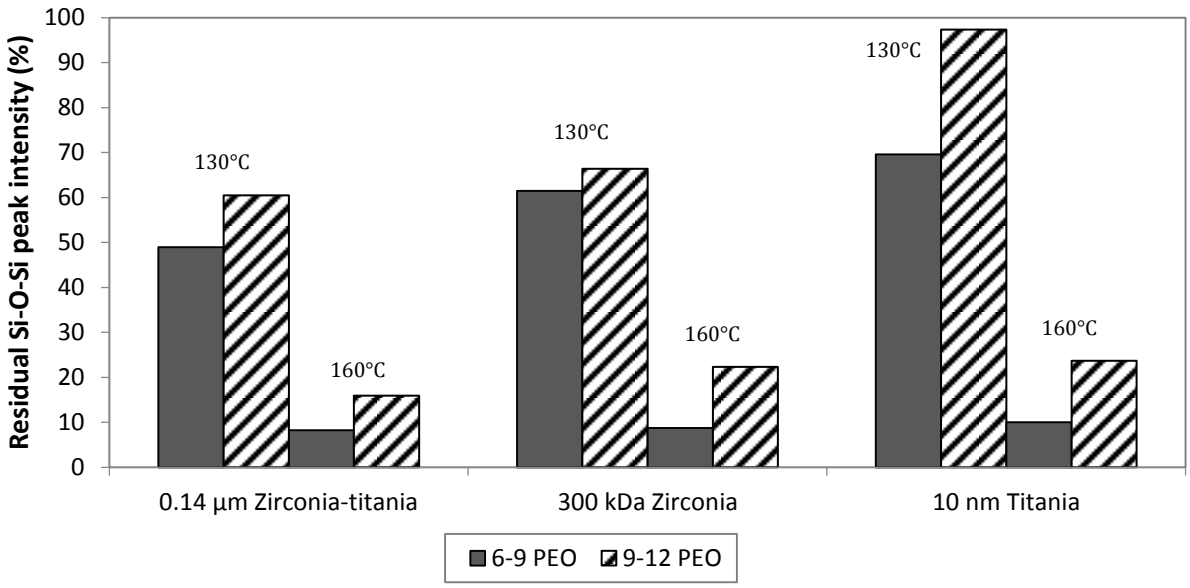

Figure 4.12: Residual siloxane FTIR peak intensity for ceramic membranes modified with different PEO based silanes (20 wt% silane for 72 hours), upon exposure to temperatures of 130°C and 160°C for 2 hours.

4.3.3.5 Contact angle and surface hydrophilicity

Since the objective was to synthesize non-ionic membrane surfaces that would not diminish the wetting properties of the initial ceramic material, the hydrophilicity of the newly formed silane layers was evaluated upon modification of the ceramic membranes. When water droplets were contacted with unmodified membranes, the surface was immediately wetted due to the presence of polar hydroxyl groups and exhibited a zero water contact angle, as is expected of hydrolyzed metal oxides [49]. Static water contact angle measurements before and after heat treatment for membranes modified in 20 wt% silane for 72h are found in Figure 4.13a for ZrO_2-TiO_2, in Figure 4.13b for ZrO_2 and in Figure 4.13c for TiO_2. Contact angles for membranes modified with PEO_{6-9}TMS are shown in the left column, while those for membranes modified with PEO_{9-12}TMS are shown in the right column. The contact angles are expectedly higher than those of the unmodified membranes, but remain well within the hydrophilic region. The modified titania and zirconia surfaces show similar initial contact angles. However, the titania surface is wetted at a faster rate, with the contact angle eventually reaching zero within 10 seconds and thus classifying the silylated titania membrane as a superhydrophilic surface [50]. The initial contact angle of the modified zirconia-titania surface is higher and gradually decreases over the course of the measurements. The higher contact angles of the modified membranes are a result of the decrease in polarity of the PEO groups when compared to the OH groups of the untreated surface.

Lower surface polarity leads to weaker interactions with the water molecules and reduces sorption of water into the surface material. The notable change in contact angle measurements relative to the unmodified metal oxide surfaces suggests that the ceramic membranes were successfully modified with the PEO based silanes.

At 130°C, the contact angle measurements of the zirconia-titania and zirconia membranes did not show any significant change. This indicates that the silane loss and carbonyl appearance at the surface did not affect the hydrophilicity of the membranes at this temperature. The surfaces of the titania membranes showed the most change in wettability, with their contact angles no longer reaching zero within 10 seconds. They did, however, maintain the hydrophilicity that was initially exhibited by the ZrO_2-TiO_2 and ZrO_2 membranes.

After treatment at 160°C, a more notable change in contact angle measurements is observed for all of the tested membranes. In all cases, the surfaces became less hydrophilic at this temperature. The highest decrease in wettability was observed with the PEO_{6-9}TMS modified zirconia-titania and zirconia membranes, whose contact angles were in the vicinity of 50–60°. Furthermore, the contact angles of all PEO_{6-9}TMS modified membranes did not show as much variation over the elapsed measurement time, which is evidence of a reduction in surface porosity.

Membranes modified with PEO_{9-12}TMS showed less significant reductions in hydrophilicity and porosity at 160°C compared to those modified with PEO_{6-9}TMS. The contact angles of these surfaces were less static and measured in the range of 30–40°. This indicates that a silane layer with longer PEO chains is more stable in terms of maintaining wettability and porosity at higher temperatures, in accordance with the previously discussed FTIR results.

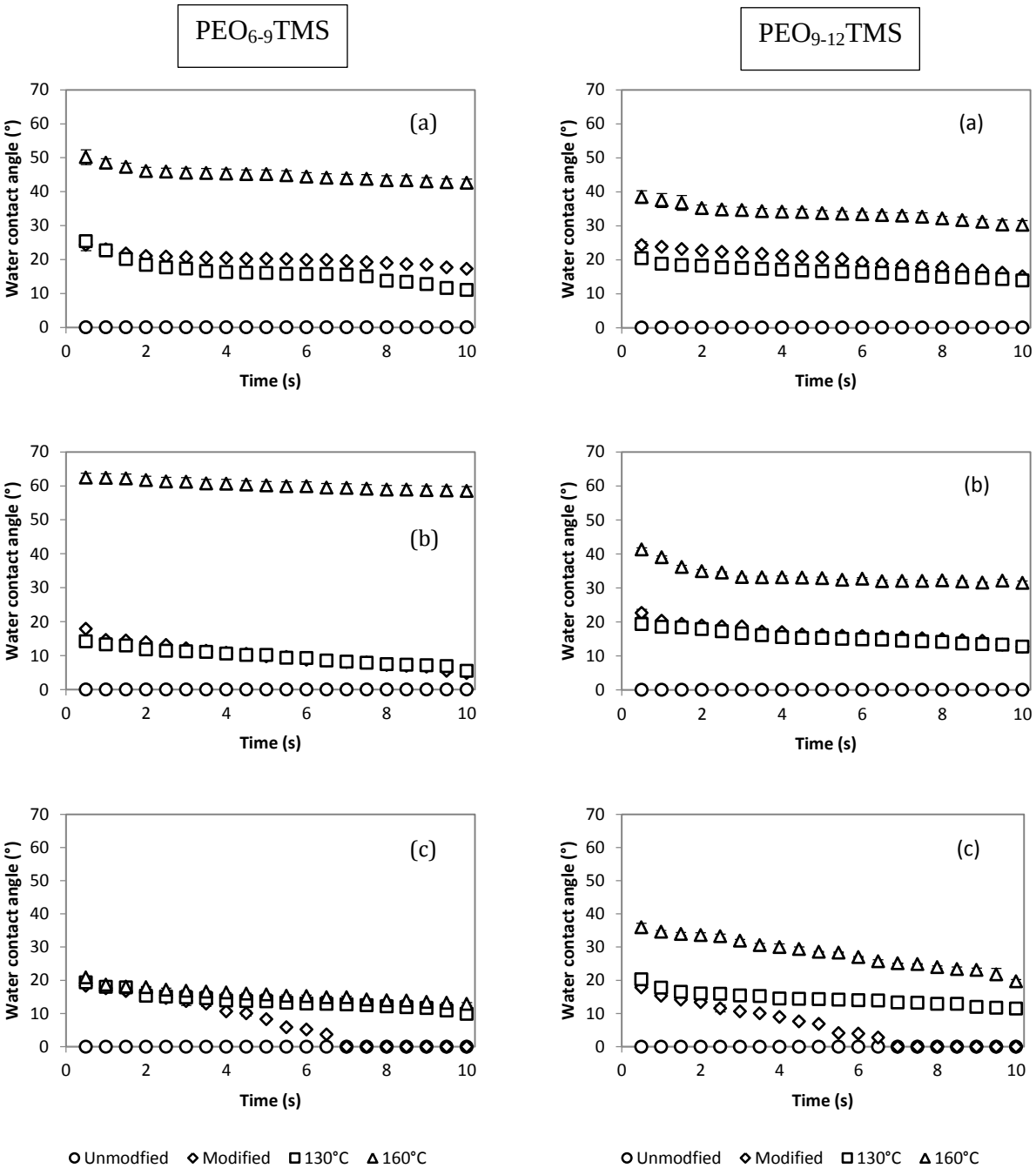

Figure 4.13: Water contact angle of (a) 0.14 µm ZrO_2-TiO_2, (b) 300 kDa ZrO_2 and (c) 10 nm TiO_2 membranes after modification in 20 wt% silane for 72 hours followed by heat treatment at 130°C and 160°C for 2 hours. All membranes in the left column were treated with $PEO_{6-9}TMS$ and all membranes in the right column were treated with $PEO_{9-12}TMS$.

4.4 Conclusions

Ceramic flat membrane disks with selective layers composed of zirconia-titania, zirconia or titania were surface modified using organosilanes with polyethylene oxide organic moieties. Modified titania membranes exhibited zero water contact angle within 10 seconds and can thus be classified as superhydrophilic surfaces.

Thermal stability of the silane layers was tested by heat treating the membranes at 130°C and 160°C and monitoring the siloxane FTIR peak intensity at the surface. The greatest silane retention was observed with the 10 nm titania membranes, followed by 300 kDa zirconia and 0.14 µm zirconia-titania. This was in accordance with the order of reactivity and the increase in pore size of the selective layer. To enhance thermal stability, a PEO-silane with higher molecular weight was also tested. This addition decreased the amount of silane lost upon heat treatment and thus offered superior thermal stability compared to the lower MW counterpart. The most stable surface was that of the 10 nm titania membrane modified with higher MW PEO-silane. This membrane maintained 97% of the Si-O-Si peak intensity at the surface upon heat treatment at 130°C.

The results of this work suggest that in separation applications where non-ionic ceramic membranes are desired, such as in produced water filtration, titania membranes over zirconia and zirconia-titania should be used with higher MW PEO-silane modifying agents to ensure maximal surface coverage and enhanced thermal stability of the silane layer.

References

[1] S. Alzahrani, A.W. Mohammad, Challenges and trends in membrane technology implementation for produced water treatment: A review, Journal of Water Process Engineering. 4 (2014) 107–133.

[2] M. Padaki, R. Surya Murali, M.S. Abdullah, N. Misdan, A. Moslehyani, M.A. Kassim, N. Hilal, A.F. Ismail, Membrane technology enhancement in oil-water separation. A review, Desalination. 357 (2015) 197–207.

[3] R. Sondhi, R. Bhave, G. Jung, Applications and benefits of ceramic membranes, Membrane Technology. 2003 (2003) 5–8.

[4] S.-J. Lee, J.-H. Kim, Differential natural organic matter fouling of ceramic versus polymeric ultrafiltration membranes, Water Research. 48 (2014) 43–51.

[5] E.N. Tummons, V. V. Tarabara, J.W. Chew, A.G. Fane, Behavior of oil droplets at the membrane surface during crossflow microfiltration of oil-water emulsions, Journal of Membrane Science. 500 (2016) 211–224.

[6] R. Vinoth Kumar, A. Kumar Ghoshal, G. Pugazhenthi, Elaboration of novel tubular ceramic membrane from inexpensive raw materials by extrusion method and its performance in microfiltration of synthetic oily wastewater treatment, Journal of Membrane Science. 490 (2015) 92–102.

[7] D. Lu, T. Zhang, J. Ma, Ceramic membrane fouling during ultrafiltration of oil/water emulsions: Roles played by stabilization surfactants of oil droplets, Environmental Science & Technology. 49 (2015) 4235–4244.

[8] M. Ebrahimi, K.S. Ashaghi, L. Engel, D. Willershausen, P. Mund, P. Bolduan, P. Czermak, Investigations on the use of different ceramic membranes for efficient oil-field produced water treatment, Desalination. 250 (2010) 991–996.

[9] L. Zhu, M. Chen, Y. Dong, C.Y. Tang, A. Huang, L. Li, A low-cost mullite-titania composite ceramic hollow fiber microfiltration membrane for highly efficient separation of oil-in-water emulsion, Water Research. 90 (2016) 277–285.

[10] Q. Chang, J.E. Zhou, Y. Wang, J. Liang, X. Zhang, S. Cerneaux, X. Wang, Z. Zhu, Y. Dong, Application of ceramic microfiltration membrane modified by nano-TiO2 coating in separation of a stable oil-in-water emulsion, Journal of Membrane Science. 456 (2014) 128–133.

[11] P. Swenson, B. Tanchuk, E. Bastida, W. An, S.M. Kuznicki, Water desalination and de-oiling with natural zeolite membranes - Potential application for purification of SAGD process water, Desalination. 286 (2012) 442–446.

[12] S.E. Weschenfelder, C.P. Borges, J.C. Campos, Oilfield produced water treatment by ceramic membranes: Bench and pilot scale evaluation, Journal of Membrane Science. 495 (2015) 242–251.

[13] S.E. Weschenfelder, A.M.T. Louvisse, C.P. Borges, E. Meabe, J. Izquierdo, J.C. Campos, Evaluation of ceramic membranes for oilfield produced water treatment aiming reinjection in offshore units, Journal of Petroleum Science and Engineering. 131 (2015) 51–57.

[14] T. Zsirai, A.K. Al-Jaml, H. Qiblawey, M. Al-Marri, A. Ahmed, S. Bach, S. Watson, S. Judd, Ceramic membrane filtration of produced water: Impact of membrane module, Separation and Purification Technology. 165 (2016) 214–221.

[15] J.M. Dickhout, J. Moreno, P.M. Biesheuvel, L. Boels, R.G.H. Lammertink, W.M. De Vos,

Produced water treatment by membranes : A review from a colloidal perspective, Journal of Colloid and Interface Science. 487 (2017) 523–534.

[16] M. Amirilargani, M. Sadrzadeh, E.J.R. Sudhölter, L.C.P.M. de Smet, Surface modification methods of organic solvent nanofiltration membranes, Chemical Engineering Journal. 289 (2016) 562–582.

[17] M.M. Gentleman, J.A. Ruud, Role of hydroxyls in oxide wettability, Langmuir. 26 (2010) 1408–1411.

[18] N.A. Ahmad, C.P. Leo, A.L. Ahmad, Synthesis of superhydrophobic alumina membrane: Effects of sol-gel coating, steam impingement and water treatment, Applied Surface Science. 284 (2013) 556–564.

[19] A.Y. Ku, J.A. Ruud, T.A. Early, R.R. Corderman, Evidence of ion transport through surface conduction in alkylsilane-functionalized nanoporous ceramic membranes, Langmuir. 22 (2006) 8277–8280.

[20] R. Faiz, M. Fallanza, I. Ortiz, K. Li, Separation of olefin paraffin gas mixtures using ceramic hollow fiber membrane contactors, Industrial & Engineering Chemistry Research. 52 (2013) 7918–7929.

[21] W. Kujawski, J. Kujawa, E. Wierzbowska, S. Cerneaux, M. Bryjak, J. Kujawski, Influence of hydrophobization conditions and ceramic membranes pore size on their properties in vacuum membrane distillation of water-organic solvent mixtures, Journal of Membrane Science. 499 (2016) 442–451.

[22] A. Vargas-Garcia, B. Torrestiana-Sanchez, A. Garcia-Borquez, G. Aguilar-Uscanga, Effect of grafting on microstructure, composition and surface and transport properties of ceramic membranes for osmotic evaporation, Separation and Purification Technology. 80 (2011) 473–481.

[23] J. Kujawa, S. Cerneaux, W. Kujawski, Removal of hazardous volatile organic compounds from water by vacuum pervaporation with hydrophobic ceramic membranes, Journal of Membrane Science. 474 (2015) 11–19.

[24] X. Ke, Y. Huang, T.R. Dargaville, Y. Fan, Z. Cui, H. Zhu, Modified alumina nanofiber membranes for protein separation, Separation and Purification Technology. 120 (2013) 239–244.

[25] N. Gao, Y. Fan, X. Quan, Y. Cai, D. Zhou, Modified ceramic membranes for low fouling separation of water-in-oil emulsions, Journal of Materials Science. 51 (2016) 6379–6388.

[26] N. Gao, W. Ke, Y. Fan, N. Xu, Evaluation of the oleophilicity of different alkoxysilane modified ceramic membranes through wetting dynamic measurements, Applied Surface Science. 283 (2013) 863–870.

[27] N.A. Ahmad, C.P. Leo, A.L. Ahmad, Superhydrophobic alumina membrane by steam impingement: Minimum resistance in microfiltration, Separation and Purification Technology. 107 (2013) 187–194.

[28] J. Lee, J.-H. Ha, I.-H. Song, Improving the antifouling properties of ceramic membranes via chemical grafting of organosilanes, Separation Science and Technology. 51 (2016) 2420–2428.

[29] B. Arkles, Y. Pan, Y.M. Kim, The Role of Polarity in the Structure of Silanes Employed in Surface Modification, Silanes and Other Coupling Agents. 5 (2009) 51–64.

[30] S. Yeu, J.D. Lunn, H.M. Rangel, D.F. Shantz, The effect of surface modifications on protein

microfiltration properties of Anopore membranes, Journal of Membrane Science. 327 (2009) 108–117.

[31] K.C. Popat, G. Mor, C. Grimes, T.A. Desai, Poly (ethylene glycol) grafted nanoporous alumina membranes, Journal of Membrane Science. 243 (2004) 97–106.

[32] C.R. Tanardi, R. Catana, M. Barboiu, A. Ayral, I.F.J. Vankelecom, A. Nijmeijer, L. Winnubst, Polyethyleneglycol grafting of γ-alumina membranes for solvent resistant nanofiltration, Microporous and Mesoporous Materials. 229 (2016) 106–116.

[33] A. Buekenhoudt, K. Wyns, V. Meynen, B. Maes, P. Cool, Surface Modified Inorganic Matrix and Method for Preparation Thereof, US 8,980,096 B2, 2015.

[34] A. Buekenhoudt, K. Wyns, G. Mustafa, V. Meynen, Method for Increasing the Fouling Resistance of Inorganic Membranes by Grafting with Organic Moieties, WO 2015/124784 A1, 2015.

[35] C. Atallah, A.Y. Tremblay, S. Mortazavi, Silane Surface Modified Ceramic Membranes for the Treatment and Recycling of SAGD Produced Water, Journal of Petroleum Science and Engineering. 157 (2017) 349–358.

[36] A. Chandekar, S.K. Sengupta, J.E. Whitten, Thermal stability of thiol and silane monolayers: A comparative study, Applied Surface Science. 256 (2010) 2742–2749.

[37] C.C. Wei, K. Li, Preparation and characterization of a robust and hydrophobic ceramic membrane via an improved surface grafting technique, Industrial & Engineering Chemistry Research. 48 (2009) 3446–3452.

[38] J. Kujawa, S. Cerneaux, W. Kujawski, Investigation of the stability of metal oxide powders and ceramic membranes grafted by perfluoroalkylsilanes, Colloids and Surfaces A: Physicochemical and Engineering Aspects. 443 (2014) 109–117.

[39] A. V. Krasnoslobodtsev, S.N. Smirnov, Effect of water on silanization of silica by trimethoxysilanes, Langmuir. 18 (2002) 3181–3184.

[40] W. Yoshida, R.P. Castro, J.D. Jou, Y. Cohen, Multilayer alkoxysilane silylation of oxide surfaces, Langmuir. 17 (2001) 5882–5888.

[41] A. Javaid, D.A. Krapchetov, D.M. Ford, Solubility-based gas separation with oligomer-modified inorganic membranes: Part III. Effects of synthesis conditions, Journal of Membrane Science. 246 (2005) 181–191.

[42] P.J. Launer, Infrared Analysis of Organosilicon Compounds: Spectra-Structure Correlations, in: Silicone Compounds: Register and Review, Petrarch Sytsems, Bristol, PA, 1987: pp. 100–103.

[43] K. Pielichowski, K. Flejtuch, Non-oxidative thermal degradation of poly(ethylene oxide): Kinetic and thermoanalytical study, Journal of Analytical and Applied Pyrolysis. 73 (2005) 131–138.

[44] J. Kujawa, W. Kujawski, Functionalization of Ceramic Metal Oxide Powders and Ceramic Membranes by Perfluroalkylsilanes and Alkylsilanes Possessing Different Reactive Groups – Physicochemical and Tribological Properties, ACS Applied Materials & Interfaces. 8 (2016) 7509–7521.

[45] S.S. Batsanov, Van der Waals Radii of Elements, Inorganic Materials. 37 (2001) 871–885.

[46] T. Masuda, N. Fukumoto, M. Kitamura, S.R. Mukai, K. Hashimoto, T. Tanaka, T. Funabiki, Modification of pore size of MFI-type zeolite by catalytic cracking of silane and application to preparation of H2-separating zeolite membrane, Microporous and Mesoporous Materials. 48 (2001)

239–245.

[47] R. Liu, Y. Jiang, B. Li, L. Yu, Estimating permeability of porous media based on modified Hagen–Poiseuille flow in tortuous capillaries with variable lengths, Microfluidics and Nanofluidics. 20 (2016) 120.

[48] J. Glastrup, Degradation of polyethylene glycol. A study of the reaction mechanism in a model molecule: Tetraethylene glycol, Polymer Degradation and Stability. 52 (1996) 217–222.

[49] Z. Xu, J.H. Masliyah, Contact Angle Measurements on Oxide and Related Surfaces, in: P. Somasundaran (Ed.), Encyclopedia of Surface and Colloid Science, Volume 2, 2nd ed., CRC Press, Boca Raton, Florida, 2006: p. 1550.

[50] T.A. Otitoju, A.L. Ahmad, B.S. Ooi, Superhydrophilic (superwetting) surfaces: A review on fabrication and application, Journal of Industrial and Engineering Chemistry. 47 (2017) 19–40.

5 Surface Modified Multi-lumen Tubular Membranes for SAGD Produced Water Treatment

C. Atallah, S. Mortazavi, A.Y. Tremblay, A. Doiron.

Manuscript published in Energy & Fuels 33 (2019): 5766–5776.

DOI: 10.1021/acs.energyfuels.9b00585

Abstract

The extraction of bitumen from oil sands using steam assisted gravity drainage (SAGD) produces a considerable amount of oily process water that must be recycled. Ceramic membranes are well suited for this task, but membrane fouling remains a significant barrier to their widespread application. Bituminous clays in produced water are heavily charged and interact with the charged surfaces of ceramic membranes in a way that reduces membrane performance. In order to address this problem, the surfaces of commercially available multi-lumen tubular ceramic membranes were chemically modified using several charge neutral polyethylene oxide (PEO) based organosilanes. Membranes with a pore size of 10 nm and selective layers of either γ-Al_2O_3 or TiO_2 were modified based on protocols previously used on small-scale ceramic membrane disks and challenged with SAGD produced water. Results indicate that the modification leads to an improvement in membrane performance. Modification of γ-Al_2O_3 membranes by a 30% solution of straight-chain PEO-silane increased permeate flux by factors as high as 2.9. Modification of TiO_2 membranes also improved permeate flux. Flux recovery factors upon backflushing increased from 1.3 to 1.6. Furthermore, flux values for γ-Al_2O_3 membranes ranged between 50–150 Lmh and increased over time, while flux values for TiO_2 membranes ranged between 220–350 Lmh and declined slightly over time. This indicates that γ-Al_2O_3 is a stronger adsorbent for bituminous foulants than TiO_2, with foulants being adsorbed quickly and subsequently released during filtration and backflushing. Lastly, decline in performance when switching to a SAGD feed with higher pH, TOC and alkalinity was significantly less severe for modified TiO_2 membranes compared to unmodified counterparts. Based on these results, surface modification of tubular ceramic membranes with PEO-based silanes was successful in improving the rejection of bituminous foulants from the membrane surface.

5.1 Introduction

The Canadian oil sands, located in Alberta, represent the third largest oil reserves found on Earth. However, only 18% of these bitumen deposits are recoverable by conventional open pit mining extraction technologies [1]. The rest of the deposits, found deeper below the surface, must be recovered using in-situ techniques. The leading technology for in-situ bitumen extraction is a process known as steam-assisted gravity drainage (SAGD). This process involves the drilling of two horizontal wells one above the other. Steam is continuously injected into the top well. The subsequent heat transfer from the steam leads to a reduction in the viscosity of the surrounding solid oil sands deposit [2]. The newly liquefied bitumen then begins flowing by gravity into the bottom well, resulting in an emulsion of heavy oil and condensed steam that is pumped to the surface. Once it reaches the surface, the emulsion must undergo a treatment process to separate the extracted oil from the injected water. To preserve natural freshwater resources, SAGD operations seek to recycle the majority of the produced water back to the process boilers for steam generation. The traditional industrial produced water deoiling process is illustrated in Figure 5.1.

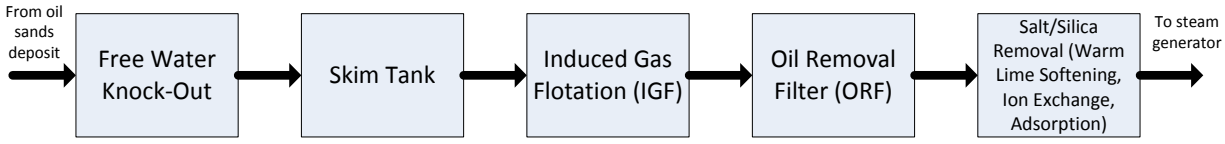

Figure 5.1: Conventional SAGD produced water treatment process.

The inability of this conventional process to reliably and consistently provide clean produced water for steam production is a present hindrance in the oil sands industry. Oil-contaminated water can cause downstream process upsets that require costly cleaning and maintenance downtime, such as frequent replacement of the steam boilers due to fouling and corrosion. Therefore, a more efficient separation option is needed in the produced water deoiling process.

The use of membrane filtration as a means of purifying produced water from the petroleum industry has been a topic of interest for several decades [3]. Ongoing investigation into the application of both polymeric membranes [4–7] and ceramic membranes [8–10] for separating dissolved oil and inorganics from produced water is an active area of research. Due to the viscous nature of the oil present in the produced water, it is advantageous to treat such feed streams at elevated temperatures with membranes. Despite the proven success of polymeric

membranes in treating oily wastewater, the longevity of such membranes is questionable in the harsh environment that accompanies produced water filtration [10]. Ceramic membranes, on the other hand, offer a great deal of chemical and thermal stability, while also possessing a lower fouling tendency towards organic matter than polymeric membranes [11].

The resulting produced water from SAGD and similar processes contains high concentrations of dissolved organic matter (DOM), such as asphaltenes, humic acids (HAs) and naphthenic acids (NAs) [12–14], as well as dissolved silica [15]. This silica is present in the form of ultrafine clays that act as supports for the adsorption of bituminous organic molecules. Precipitation and entrapment of these silicates and adsorbed carbon-rich solids onto membrane surfaces is known to cause considerable membrane fouling [16,17]. In treating oily wastewater, the formation of an oil coating onto the selective layer of ceramic membranes remains an obstacle to their universal acceptance as a produced water treatment technology. Despite this drawback, membrane processes are still considered promising technologies in this application, owing to their high separation efficiency and the fact that they are simple to operate relative to other separation processes. For this reason, fouling remediation techniques have been extensively developed and applied to ceramic membranes in treating produced water. Among the most popular techniques are backflushing or backpulsing the membrane with permeate and the use of chemical cleaning agents to remove foulants from the selective layer or from inside the pores [18,19]. These methods, however, lead to periods of process inactivity when permeate is not being produced and it is thus desirable to limit the necessity and frequency of their use. This task would require the development of membranes that are inherently fouling-resistant to the components found in produced water.

Ceramic membranes are composed of metal oxides such as zirconia, alumina and titania. Their surfaces are hence highly hydrophilic due to the charged hydroxyl groups that occupy the selective layer [20]. The predominant surface charge of a ceramic membrane is pH-dependent given the isoelectric point (IEP) of the selective layer's constituent metal oxide. In many cases, controlling the pH of the feed solution so that the membrane surface charge leads to the electrostatic repulsion of charged foulants is an adequate method of fouling alleviation. However, bituminous foulants like asphaltenes possess amphoteric functional groups, meaning that they can exhibit both positive and negative surface charges at any given feed pH [21]. To mitigate the

interaction between amphoteric bitumen and the hydroxyl groups, the membrane surface can be chemically modified in a way that reduces its electrostatic charge. Ceramic membrane surfaces can be readily modified by compounds that react with hydroxyl groups through condensation reactions. Replacement of these hydroxyl groups also stops them from reacting with surfactant molecules, which is a suspected fouling mechanism in oil filtration [22]. Common modifying agents include alcohols [23], phosphonic acids [24] and organosilanes [25]. The latter group of chemicals is the most versatile in terms of commercially available organic functionality. Organosilanes have been utilized to yield both hydrophobic and hydrophilic ceramic membranes in a variety of applications, including membrane distillation [26], pervaporation [27], gas separations [28], oil/water emulsions [29] and aqueous humic acid separation [30].

In the filtration of produced water, it is desirable to recuperate water as the purified permeate stream. Therefore, the applied membrane must be hydrophilic to allow adequate water permeation. To maintain the inherent hydrophilicity of ceramic membranes while also minimizing their surface charge, highly hydrophilic and charge neutral polyethylene oxide (PEO) functional silanes can be applied as modifying agents. PEO based modifications have previously been applied to achieve electrostatic repulsion of proteins in aqueous media [31] and for solvent resistant nanofiltration [32]. In our previous work, we demonstrated the use of a PEO functionalized organosilane as a surface modifying agent for flat ceramic membrane disks in the treatment of SAGD produced water [33]. The membrane modification was successful in mitigating bitumen fouling, as evidenced by higher permeate fluxes relative to the unmodified membrane disks.

The aim of this work was to selectively modify commercially available ceramic membrane tubes with neutral hydrophilic PEO silanes that were previously shown by the authors to enhance the flux and separation of small ceramic disks [33]. The commercially available tubes were modified in a simple, one step procedure and tested in a pilot scale system. SAGD produced water obtained from the field was used in the pilot-scale system to enhance the applicability of the results to actual wastewater treatment systems. Testing of the modified membranes in parallel with unmodified counterparts allowed for direct comparisons in terms of SAGD permeate flux, pure water permeability and separation of specific chemical species. The effects of backflushing

and using produced water feeds from different SAGD operations on membrane performance were also studied.

5.2 Experimental section

5.2.1 Materials

The tubular multi-lumen ultrafiltration ceramic membranes used in this study, provided by Inopor (Veilsdorf, Germany), possessed monolith configurations with 19 flow channels. The tube diameter was 25 mm, while the individual channel diameter was 3.5 mm. Each membrane had a length of 0.3 m and a specific membrane area of 0.209 m^2/m, leading to an active membrane area of 0.0627 m^2. Ceramic support layers were composed of α-Al_2O_3, while the selective layer material was either γ-Al_2O_3 or TiO_2. All membranes had pore sizes of 10 nm, corresponding to a molecular weight cut-off (MWCO) of 20 kDa as specified by the manufacturer.

The feed used to conduct the filtration tests was supplied by SAGD operations located in Canada's oil sands in Alberta. SAGD produced water was obtained from two different suppliers. Each supplier's facility was in a different location, leading to produced water samples with varying chemical and physical characteristics.

Anhydrous ethanol (Fisherbrand, Canada) and acetic acid (Fisherbrand, Canada) were used in the silylation process. The organosilanes used for the silylation of the membrane surfaces are listed in Table 5.1 and their chemical structures are shown in Figure 5.2. All silane solutions were supplied by Gelest, Inc. (Morrisville, PA, USA). Hydrophilic silanes containing PEO chains were selected because they offered an extremely low water contact angle [34].

Table 5.1: Description of organosilanes used.

Name	Formula	Notation
2-[METHOXY(POLYETHYLENEOXY)6-9PROPYL]TRIMETHOXYSILANE	$CH_3O(C_2H_4O)_{6\text{-}9}(CH_2)_3Si(OCH_3)_3$	$PEO_{6\text{-}9}TMS$
2-[METHOXY(POLYETHYLENEOXY)9-12PROPYL]TRIMETHOXYSILANE	$CH_3O(C_2H_4O)_{9\text{-}12}(CH_2)_3Si(OCH_3)_3$	$PEO_{9\text{-}12}TMS$
BIS(3-TRIETHOXYSILYLPROPYL)POLYETHYLENEOXIDE(25-30 EO)	$(CH_3CH_2O)_3Si(CH_2)_3O(C_2H_4O)_{25\text{-}30}(CH_2)_3Si(OCH_2CH_3)_3$	$BIS\text{-}PEO_{25\text{-}30}TES$

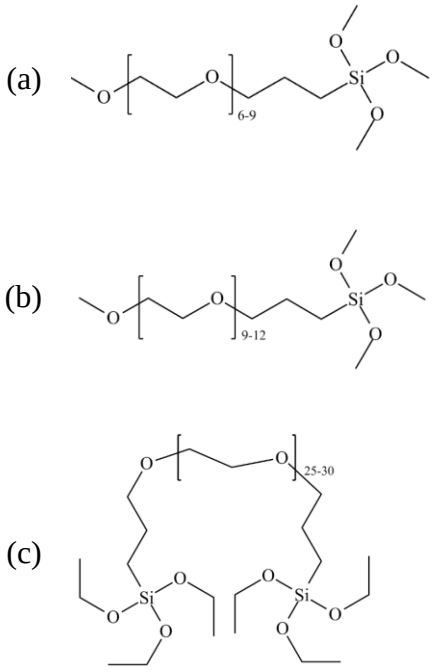

Figure 5.2: Chemical structures of silanes (a) $PEO_{6\text{-}9}TMS$, (b) $PEO_{9\text{-}12}TMS$ and (c) $BIS\text{-}PEO_{25\text{-}30}TES$.

5.2.2 Surface modification procedure

In order to ensure the presence of an adequate amount of hydroxyl groups on the membrane surfaces, the membrane tubes were immersed in deionized water for 4 h and then dried in an oven at 120 °C for 24 h prior to surface modification. Silanes were deposited onto the membrane surface from aqueous alcohol solutions. Firstly, a solution of 95% ethanol / 5% water by weight was prepared inside a 500 mL glass bottle. The ethanol solution was then adjusted to a pH of 4.5 by adding acetic acid. The silylating agent was then added with stirring until the desired silane concentration is reached. The masses of ethanol, water and organosilane were adjusted so that

the total mass of the final ethanol/water/silane solution was approximately 160 g. In this work, silane concentrations from 5 to 30 wt% were used. Following the addition of the silane, 5 minutes were allowed for hydrolysis and silanol formation. The tubular ceramic membrane was then placed inside a 250 mL glass burette, and the silane/ethanol/water solution was transferred to the burette, submerging the membrane in the solution. The membrane was left immersed in the solution for the desired silylation reaction time. In this work, silylation time was varied from 2 to 72 hours. After the desired reaction time, the solution was emptied from the burette. The burette was then filled with ethanol and subsequently emptied, twice, to rinse the membrane. The membrane was removed from the burette and placed in an oven, under nitrogen and at 110 °C, for 10 minutes in order to cure the silane layer.

5.2.3 Produced water filtration system

The crossflow ceramic membrane pilot system was configured as a feed and bleed loop with a total volume of 16 L. It housed a pair of ceramic membrane modules mounted in parallel with individual flowmeters. The parallel configuration was set up so that each of the two ceramic membranes experienced identical test conditions such as feed composition, feed flowrates, temperature, and pressure.

Heating of the system to temperatures of 80–85 °C was accomplished using a heat exchanger (B-Line Heat Exchanger, B-300M, 0.55 G, 190 psi) and through direct heating of the feed liquid using a heating element in the feed tank (COSH series, ASB Heating Elements, Over The Side Heater, 600V, 32KW). In order to prevent an explosive atmosphere from building in the vapor space above the liquid in the feed tank, a positive pressure of argon was applied to the vapor space. The vapour from the feed tank was vented to a fume hood.

The feed tank had a volume of 150 L and a conical bottom. Feed was supplied to the loop from the bottom of this tank. The feed tank was continuously mixed and heated during the experiment. The permeate and retentate were both returned to the feed tank. During experiments conducted at high pressures, the flow through the retentate line was partially restricted in order to maintain pressure in the system.

Feed pressure in the system was maintained using the feed pump (Grundfos, SS, Multistage centrifugal pump, CRN 1S-15, 1 HP motor, 4.84 GPM). Circulation through the system was

maintained with the circulation pump (Grundfos, SS, Multistage centrifugal pump, CRN 1S-15, 0.5 HP motor, 9.69 GPM). The circulation pump frequency setting was adjusted to 30 Hz, corresponding to a flowrate of approximately 20 L/min which was divided equally among the two membranes and resulted in crossflow velocities (CFV) between 0.995–1.07 m/s.

In an effort to decrease fouling of the membranes, backpressure was maintained on the membranes through the permeate line during each experiment. Without using this technique, the gauge pressure on the permeate side of the membranes would have been zero (atmospheric pressure) since the line was open to the feed tank. By restricting the flow through the permeate lines, pressure built up in the lines creating a continuous back pressure on the membranes. A backpressure of approximately 5 psi (34.5 kPa) was used throughout the experiments. The difference between the circulation pressure achieved by partially blocking the retentate line and the backpressure of 5 psi (34.5 kPa) is the transmembrane pressure (TMP). In this work, TMPs of 35 and 50 psi (241.3 and 344.7 kPa) were applied.

In order to perform the liquid backflushing of the membranes, a bypass stream was installed on the permeate line. The bypass stream filled a 1 L hydraulic cylinder that could be actuated with a pneumatic cylinder. The air pressure in the pneumatic cylinder was 100 psi (689.5 kPa) and both cylinders had equal cross-sectional area. During backflushing, the permeate line to the feed tank was closed and the permeate in the hydraulic cylinder was forced through the membranes for 10 seconds. This operation was repeated every five minutes while the system was operating. Steam at 120 °C was also used to further decrease fouling and clean the ceramic membranes during experimental runs. Steam flushing was performed every 15 minutes for 10 seconds per flush. The utilized organosilanes have previously been shown to be thermally stable at the temperature of the applied steam [35].

The permeate collected from each of the ceramic membranes passed through individual flow meters (Coriolis Mass Flow Meter, TCM 0650-FA-SGSS-CSDS) allowing measurements of the rate of permeate production for each membrane separately. This setup allowed measurements between 20 and 2700 liters per meter squared per hour (Lmh), or 5.5×10^{-6} and 7.5×10^{-4} $m^3/(m^2 s)$.

After each experiment the system was cleaned by draining all liquids and flushing the system with deionised water. Multiple ports were located on the bottom of the system that could be

opened in order to drain the system. Special care was taken to avoid leaving heavy oil in the system to cool overnight.

A process flow diagram of the filtration system is found in Figure 5.3.

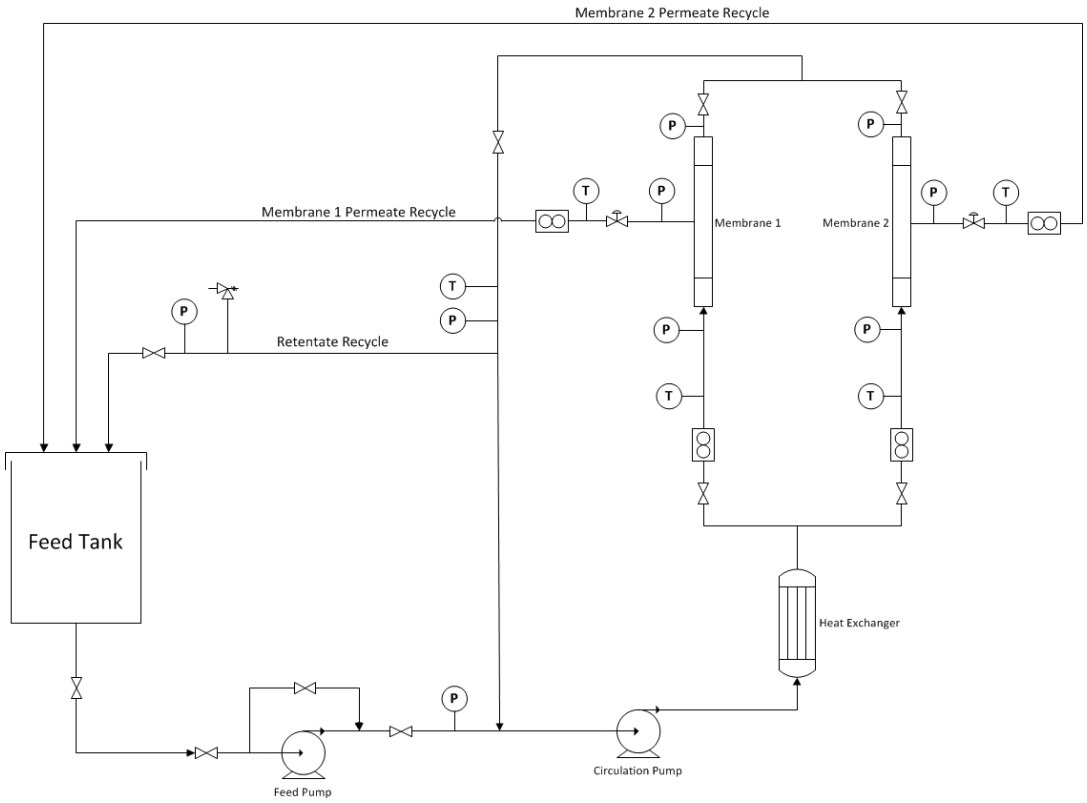

Figure 5.3: Process flow diagram of the crossflow filtration system.

5.2.4 Characterization of feed and permeate samples

Sample ports were located throughout the system. Feed samples were taken from the feed pump at the beginning and end of each experiment. Loop samples were taken from the bottom of the circulation loop at the beginning and end of each experiment. Permeate samples were taken from the permeate lines at the beginning, middle and end of each experiment.

The total organic carbon (TOC) of all samples was determined using an Apollo 9000 TOC Analyzer, as per the manufacturer's instructions. The method involved catalytically oxidizing the sample into CO_2 and H_2O, isolating the CO_2, and passing it to a non-dispersive infrared detector (NDIR) for peak quantification. The limit of detection (LOD) for the TOC analyzer was 5 ppm.

Alkalinity of the feed samples was determined by potentiometric titration, using a Metrohm 751 GPD Titrino titrator. Sample aliquots were titrated with a standard solution of dilute sulphuric

acid, employing a two endpoint (pH 4.5 and 4.2) technique to determine the inflection or equivalence point of the titration.

A Dionex-100 Advanced Chromatography Module was used to determine the chloride and sulphate content of all samples through ion chromatography. The LOD for the chromatography system was 2 ppm.

Due to the presence of heavy oils in the loop and feed samples, they were filtered through a 0.45 μm nitrocellulose filter before TOC, chloride, sulphate and alkalinity characterization.

Turbidity testing was performed on all samples (HF Scientific, Micro 100 Turbimeter). The tests were done immediately after taking the samples in order to avoid temperature and separation related effects.

Particle size analysis (Microtrac X100, Trilaser) was performed on feed and permeate samples. No results were obtained from the permeate samples as particles present in the permeate samples were too small for the instrument to detect (i.e., less than 150 nm). Examples of particle size distributions for the SAGD produced water feeds were reported in our previous work [33].

5.2.5 Pure water permeability

The pure water permeate (PWP) flux of each membrane was evaluated both before and after all produced water filtration experiments. Deionized water was used as the feed to the system in these PWP tests. The circulation pump setting was identical to that used in the corresponding produced water filtration tests for each membrane. The permeate lines were kept completely open during PWP filtration. PWP fluxes were recorded for all membranes at feed pressure values of 30, 50, 75, 100 and 150 psi (206.8, 344.7, 517.1, 689.5 and 1034.2 kPa).

5.2.6 Membrane solvent cleaning

In some cases, the fouled ceramic membranes were cleaned with solvents. The membrane tubes were removed from the system and consecutively soaked in the following three solvents: 2-propanol, toluene, and acetone. The tubes were soaked for 17 hours in each solvent. The membranes were then rinsed in flowing water for 20 seconds and stored in deionized water for two days. They were placed in the test loop and their PWP flux determined to evaluate the effect of solvent cleaning on foulant removal.

5.2.7 Experimental conditions

Four side-by-side filtration experiments were conducted using the filtration system described in section 5.2.3. Table 5.2 gives the operational conditions of each of these experiments, including information on the applied silane modification. In each run, an identical but unmodified membrane was tested in parallel to the modified membranes listed in Table 5.2. The experiments were performed in intervals of 4 hours, with total durations ranging from 12 to 20 hours with a single feed.

Table 5.2: Experimental conditions of the produced water filtration tests.

Test #	Selective layer	Feed Label	Filtration time (h)	TMP (psi/kPa)	Modification (conc., silane, reaction time)
1	γ-Al_2O_3	A	12	50/344.7	30 wt%, $PEO_{6-9}TMS$, 2 hours
2	γ-Al_2O_3	A	20	50/344.7	5 wt%, BIS-$PEO_{25-30}TES$, 24 hours
3	TiO_2	A & B	First 16 h (Feed A) Next 20 h (Feed B)	50/344.7	15 wt%, $PEO_{9-12}TMS$, 24 hours
4	TiO_2	B-concentrate	20	35/241.3	20 wt%, $PEO_{9-12}TMS$, 72 hours

In the case of experiment #4, the feed sample used was a concentrate of Feed B. This concentrated feed was obtained by removing 75% of the water contained in Feed B, thus significantly increasing the concentration of the sample's oil content. This run was performed in order to determine the efficiency of the silane modification at such an extreme oil concentration.

Table 5.3 presents the average values of several parameters that were used to characterize the various SAGD produced water feeds.

Table 5.3: Characteristics of produced water samples used with standard deviations.

Feed Label	TOC* (ppm)	Alkalinity* (mg/L)	Chloride* (ppm)	Sulphate* (ppm)	pH	Turbidity (NTU)
A	138.2 ± 35.0	123.3 ± 22.6	513.3 ± 37.7	22.7 ± 2.4	8.49 ± 0.22	239.1 ± 20.0
B	351.6 ± 25.1	447.6 ± 30.3	570.6 ± 27.0	12.1 ± 0.4	9.16 ± 0.10	121.9 ± 2.4
B-concentrate	125.8 ± 15.7	206.8 ± 5.7	319.3 ± 12.3	37.5 ± 1.7	9.35 ± 0.08	488.4 ± 18.4

*TOC, alkalinity, chloride and sulphate measured after filtration through a 0.45 µm filter.

5.3 Results and discussion

5.3.1 Effect of surface modification on permeate flux

In each experiment, there were slight fluctuations in the loop circulation temperature and TMP of the membranes. These variations were recorded and accounted for by normalizing the recorded permeate flux with respect to temperature and pressure as per equation (5.1):

$$J_N = J\left(\frac{\mu}{\mu_N}\right)\left(\frac{P_N}{P}\right) \tag{5.1}$$

where J_N is the normalized permeate flux (Lmh), J is the actual permeate flux (Lmh), μ and μ_N are the viscosity at the actual and normalization temperature, respectively, in kg/m/s, P and P_N are the actual and normalization pressure, respectively, in psi. In all cases the normalization temperature is 85 °C, while P_N is the applied TMP (35 or 50 psi). The temperature dependence of water viscosity was determined using equation (5.2), which is accurate to within 2.5% between temperatures of 0 °C to 370 °C [36].

$$\mu = 2.414 \cdot 10^{-5} \cdot 10^{247.8/(T-140)} \tag{5.2}$$

where μ is in kg/m/s and T is in Kelvin.

5.3.1.1 Alumina membranes

In Figure 5.4, the normalized permeate flux for the membranes from Test #1 is shown as a function of time over the entire filtration experiment. The same plot (flux vs. time) is given in Figure 5.5 for Test #2. Each data point represents the average flux during a single backflush cycle. Both of these tests were conducted using 10 nm γ-Al_2O_3 membranes. In both cases, the flux of the modified membrane is consistently higher than that of the unmodified membrane. This indicates that both the straight-chain silane $PEO_{6\text{-}9}$TMS and dipodal silane BIS-$PEO_{25\text{-}30}$TES are more effective in rejecting bituminous foulants from the membrane surface when compared to the native unmodified membranes. The flux of the $PEO_{6\text{-}9}$TMS modified membrane (Figure 5.4) is consistently higher than that of the unmodified membrane by more than 50 Lmh for the entire duration of the filtration run, while the largest flux difference observed with the dipodal modification (Figure 5.5) was an improvement of 15 Lmh. Furthermore, the flux of the $PEO_{6\text{-}9}$TMS modified membrane ranged from 125 to 145 Lmh, while the flux of the dipodal modified membrane only reached a value of 100 Lmh after 20 hours of operation with a similar SAGD wastewater feed.

In an attempt to improve the performance of the dipodal modification to match that of $PEO_{6-9}TMS$, another 10 nm γ-Al_2O_3 membrane was modified with an increased concentration and reaction time of 20 wt% BIS-$PEO_{25-30}TES$ for 72 hours. However, this membrane exhibited zero flux when tested with both pure water and produced water up to pressures of 400 psi (2757.9 kPa). The lack of permeability is an indication that modification with such an elevated concentration of dipodal silane lead to pore blockage of the membrane. Dipodal silanes are capable of anchoring themselves to oxide surfaces and molecules using two separate hydroxyl groups. It is likely that BIS-$PEO_{25-30}TES$, with its dipodal functionality and high molecular weight, formed a secondary and denser porous network within the pores of the membrane through a bridging mechanism with the alumina surface. It is thus recommended to use silane concentrations below 20 wt% when modifying alumina membranes with higher MW dipodal organosilanes.

In both Tests #1 and #2, permeate fluxes for unmodified and modified alumina membranes were continuously increasing with time over the entire duration of the filtration experiments. This phenomenon is an indication that material was being liberated from the membrane surfaces as filtration progressed. It has been previously shown that asphaltenes, a major foulant in SAGD produced water, readily adsorb onto γ-Al_2O_3 with a maximum adsorption capacity of 88.5 mg/g at 298 K [37]. Furthermore, adsorption of asphaltenes onto γ-Al_2O_3 is a rapid process and equilibrium is reached relatively quickly, meaning that the bituminous foulants were adsorbed onto the alumina membranes early in the experiments and were continuously backflushed from the surface over the duration of the tests.

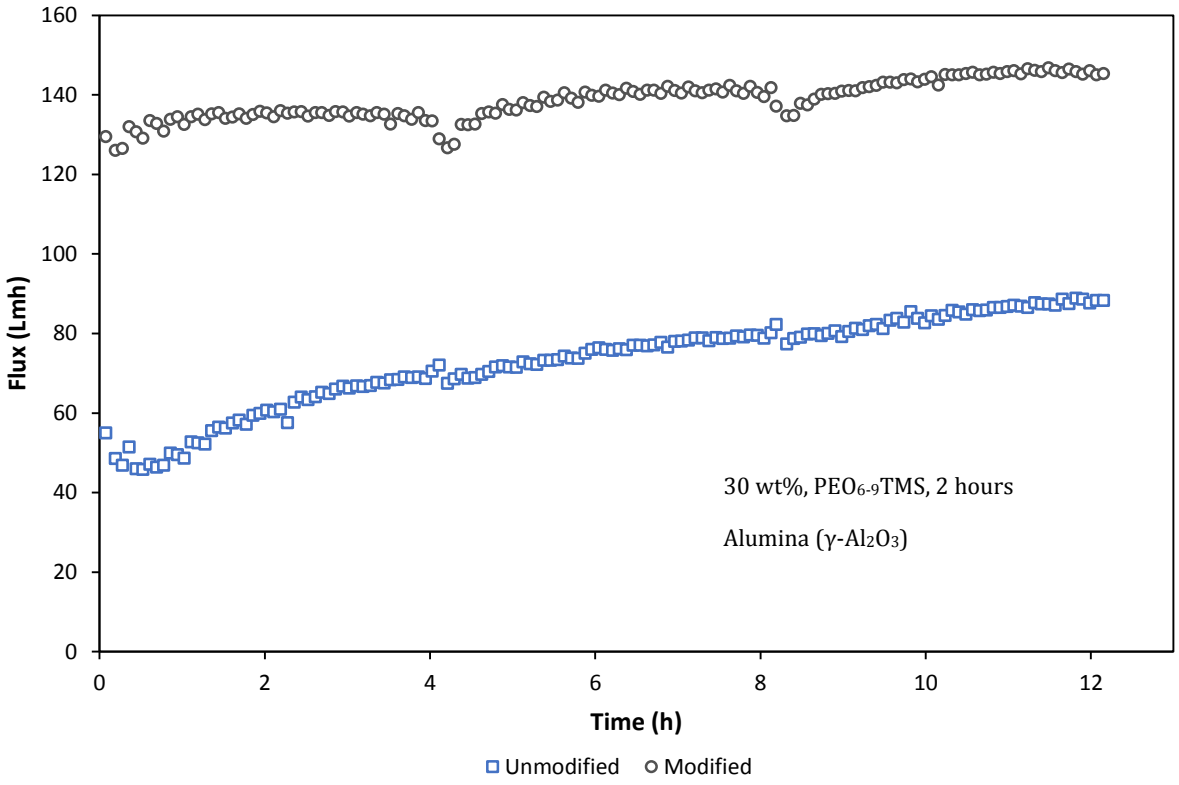

Figure 5.4: Normalized permeate flux as a function of time for Test #1. Modification: 30% $PEO_{6-9}TMS$ (2h), TMP: 344.7 kPa (50 psi), selective layer: γ-Al_2O_3, Feed A, CFV: 1.07 ± 0.03 m/s (unmodified), 0.995 ± 0.026 m/s (modified).

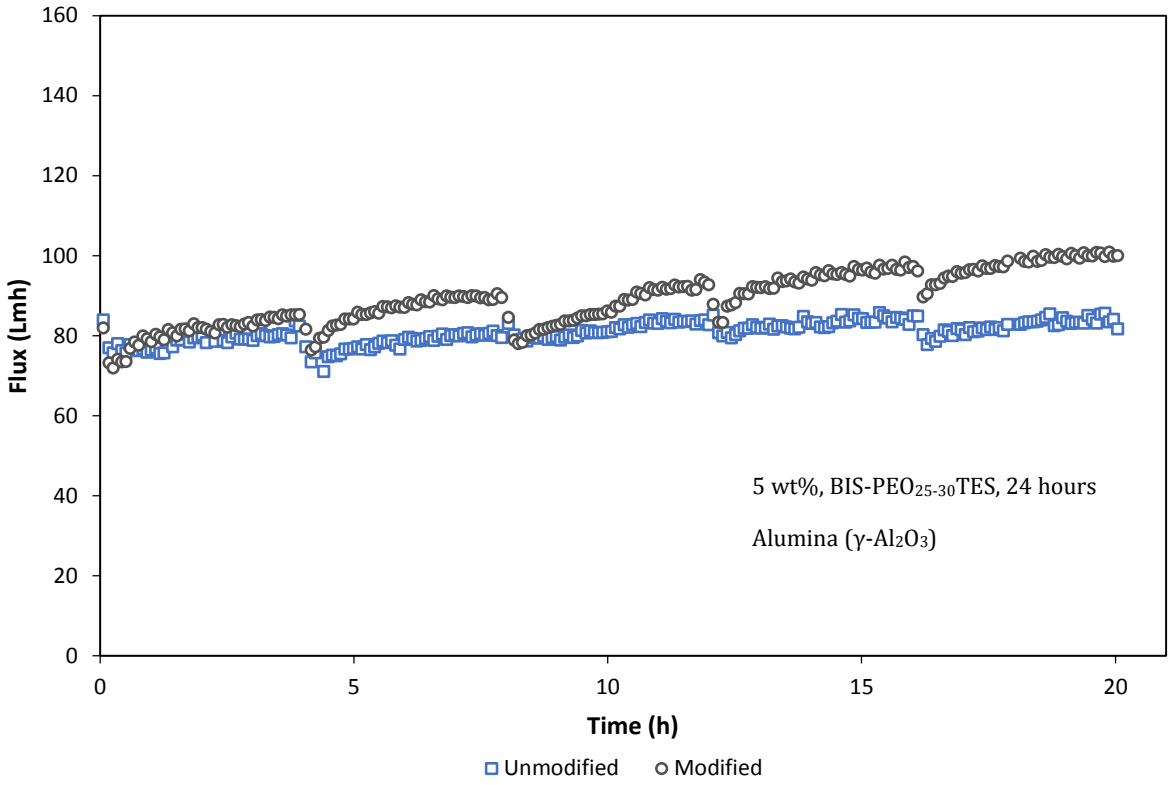

Figure 5.5: Normalized permeate flux as a function of time for Test #2. Modification: 5% BIS-PEO_{25-30}TES (24h), TMP: 344.7 kPa (50 psi), selective layer: γ-Al_2O_3, Feed A, CFV: 1.04 ± 0.05 m/s (unmodified), 1.02 ± 0.04 m/s (modified).

5.3.1.2 Titania membranes

Test #3 was conducted using 10 nm membranes with a TiO_2 selective layer. The first 16 hours of filtration were done using the same produced water feed as Tests #1 and #2 in order to compare the effect of selective layer material. The normalized permeate fluxes for these membranes are given in Figure 5.6 for a 2-hour excerpt from the 16-hour test with Feed A. The modified membrane in this case was modified using a higher MW straight-chain silane (PEO_{9-12}TMS) than the one used with the alumina membrane from Test #1 (PEO_{6-9}TMS). It is seen in Figure 5.6 that the improvement in flux offered by the modification is minimal in comparison to what was observed in Figure 5.4 for the modified alumina membrane. However, the fluxes offered by both unmodified and modified titania membranes are in the range of 200 to 350 Lmh. The fluxes of the alumina membranes, conversely, did not exceed 150 Lmh. Furthermore, the effect of backflushing on membrane flux is clearly visible with the titania membranes in Figure 5.6, whereas backflushing had negligible impact on alumina membrane performance as seen in Figures 5.4 and 5.5. The higher fluxes and backflush efficiency indicate that titania surfaces are

less susceptible to fouling by bitumen associated solids than alumina surfaces. This is further evidenced by the fact that membrane flux did not increase with time for the TiO_2 membrane tests, which was a phenomenon observed with the γ-Al_2O_3 membranes due to rapid adsorption and subsequent gradual release of asphaltenes from the membrane surface. In a previous study on the adsorption of asphaltenes to various metal oxides, it was shown that acidic oxides like TiO_2 possess relatively low adsorption capacities when compared to amphoteric oxides, such as Al_2O_3 [38].

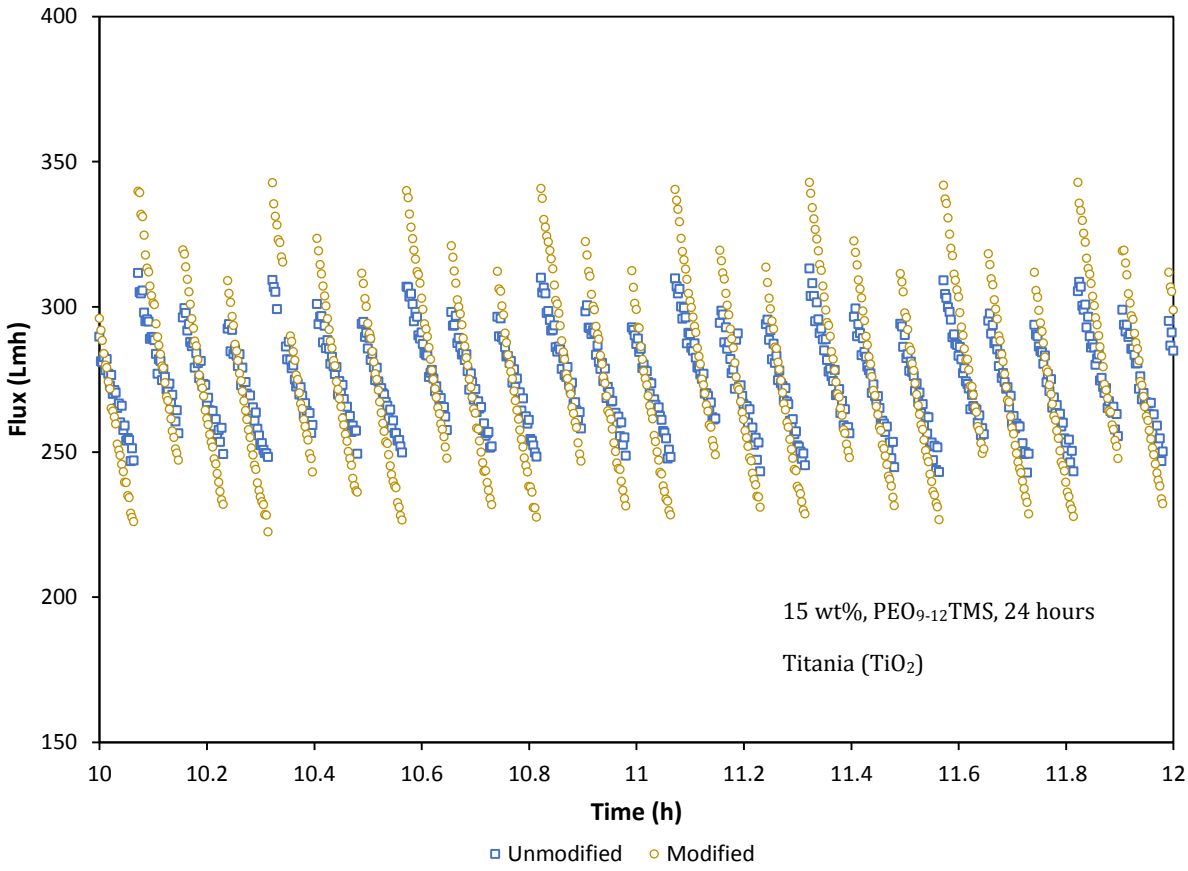

Figure 5.6: Normalized permeate flux as a function of time for a 2-hour segment from Test #3. Modification: 15% $PEO_{9\text{-}12}$TMS (24h), TMP: 344.7 kPa (50 psi), selective layer: TiO_2, Feed A, CFV: 1.07 ± 0.07 m/s (unmodified), 1.00 ± 0.06 m/s (modified).

From Figure 5.6, it was also observed that after each application of either the liquid backflush or steam flush, the flux of the modified membrane rises higher than that of the unmodified membrane. To illustrate and compare the effects of backflushing on the fluxes of the unmodified

and $PEO_{9\text{-}12}TMS$ modified TiO_2 membranes, a flux recovery ratio (FRR) was defined as in equation (5.3).

$$FRR = \frac{J_A}{J_B} \tag{5.3}$$

where J_A is the first recorded flux after a backflush and J_B is the last recorded flux before the same backflush. Figure 5.7 presents the FRR for each backflush cycle during the 16-hour test with Feed A for both membranes. Solid data points represent flux recovery achieved by liquid backflush, while hollow points represent steam flushing. Both the steam flush and liquid backflush function with better efficiency on the modified membrane. At the beginning of the experiment, the modified membrane flux was doubling after steam application. The FRR eventually stabilized at a factor of 1.50 for steam and 1.30 for liquid backflushing with the modified membrane. With the unmodified membrane, the average liquid backflush FRR was 1.18, while the steam flush FRR was slightly improved at a value of 1.25. Consequently, the application of steam cleaning on the unmodified membrane was inferior to both the liquid and steam flush with the modified membrane. The higher flux recovery capacities of the flushing techniques on the modified membrane is evidence that foulants in the produced water are more loosely adhered to, and thus more efficiently removed from the silylated surface. This is indicative that modification with $PEO_{9\text{-}12}TMS$ mitigates the interactions between bituminous fines and the metal oxide surface of the membrane. The success of all tested PEO-silanes in improving flux and backflush efficiency is attributable to the reduction in surface charge when a PEO layer is deposited onto the membrane. In our previous work it was shown that PEO-silanes reduced the absolute value of the membrane zeta potential, leading to a decrease in surface charge [35]. This would have mitigated the interaction between the membranes and foulants during filtration experiments, leading to less membrane fouling.

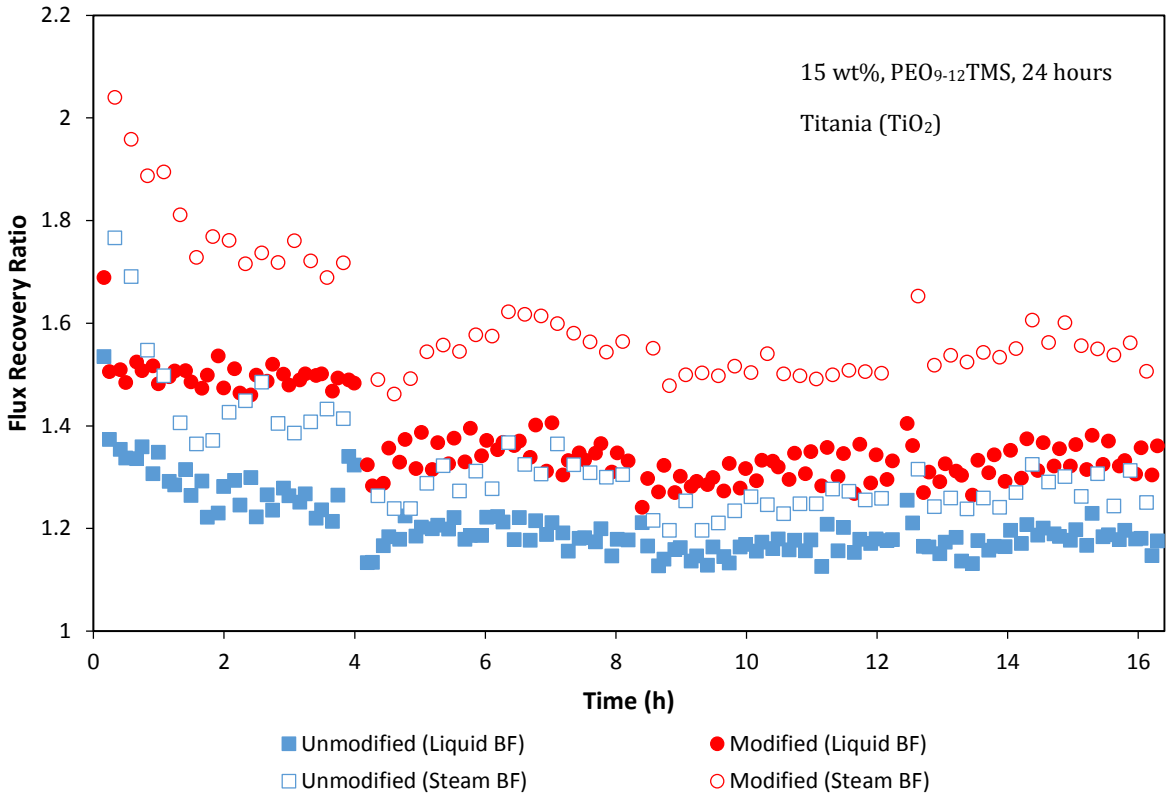

Figure 5.7: Flux recovery ratio as a function of time for Test #3. Modification: 15% $PEO_{9\text{-}12}TMS$ (24h), TMP: 344.7 kPa (50 psi), selective layer: TiO_2, Feed A, CFV: 1.07 ± 0.07 m/s (unmodified), 1.00 ± 0.06 m/s (modified).

5.3.1.3 Efficiency of surface modification in treating different feeds

The final 20 hours of filtration with the TiO_2 membranes in Test #3 were performed using a different SAGD produced water (Feed B). In Figure 5.8, the normalized flux of the unmodified and modified membrane during this 20-hour test are given, with each data point representing the average flux during a backflush cycle. The effect on flux of the transition from Feed A to Feed B is also illustrated by including the final 4 hours of filtration with Feed A. When the feed is switched to Feed B for the final 20 hours of testing, a slight decline in flux is observed. The decline is more evident for the unmodified membrane. This indicates that Feed B is more difficult to treat than Feed A. From Table 5.3 it is known that Feed B possessed higher pH, alkalinity, TOC and chloride content. The pKa of various organic acids found in produced water ranges from approximately 0.6 to 10, indicating that they are relatively weak acids [39]. The higher pH of Feed B would have led to an increased concentration in the dissociated forms of these acids, resulting in higher surface charging of bituminous fines. All of these characteristics would be expected to lead to more severe membrane fouling, and thus lower permeate fluxes.

Nonetheless, Figure 5.8 also demonstrates that the $PEO_{9\text{-}12}TMS$ modified TiO_2 membrane suffers from a more moderate flux decline than the unmodified membrane. This indicates that the silane modification leads to a membrane that is better suited to deal with this increase in filtration difficulty brought upon by the feed change. Despite giving lower fluxes, the change to a more recalcitrant feed did not affect the capability of either the liquid or steam flush. Both flushing methods continued to yield results that followed the trends observed in Figure 5.6 and Figure 5.7. This indicates that backflushing is very efficient in treating more challenging produced water feeds.

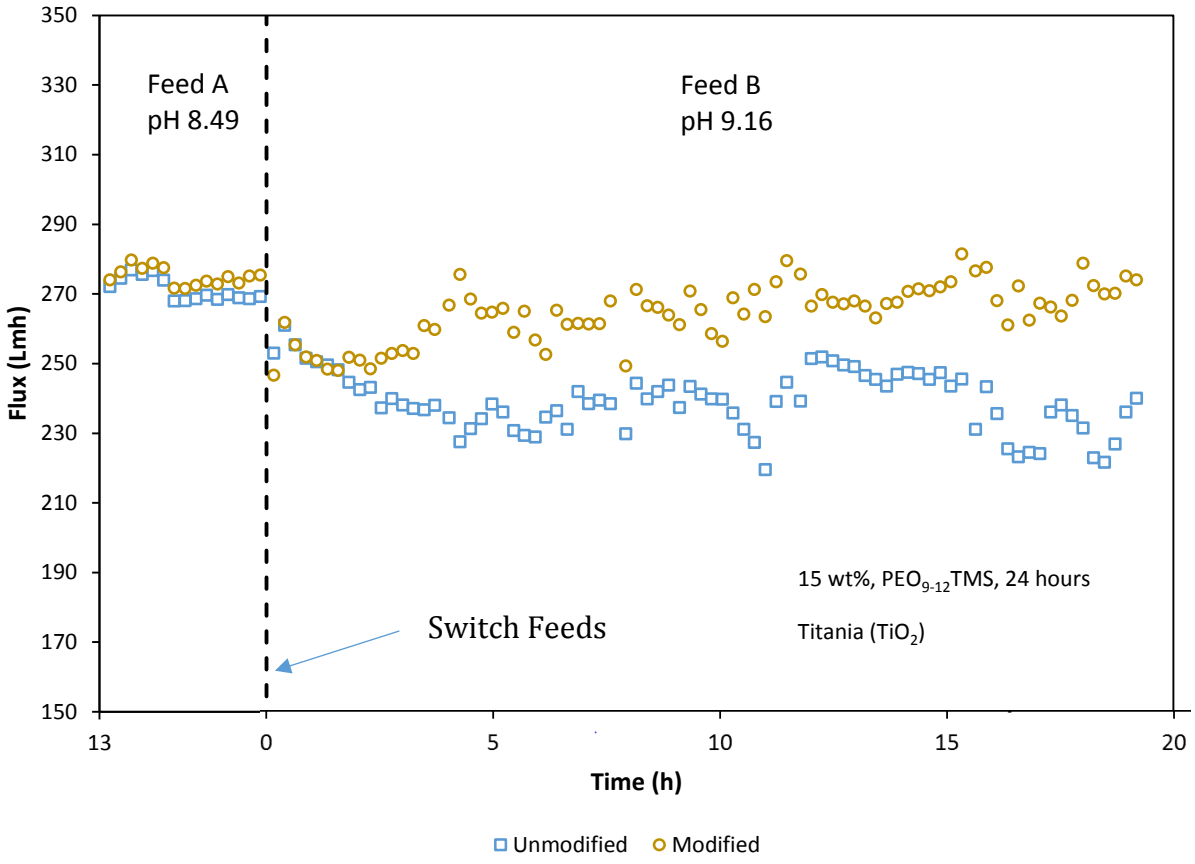

Figure 5.8: Normalized permeate flux as a function of time for the final 20 hours of Test #3. Modification: 15% $PEO_{9\text{-}12}TMS$ (24h), TMP: 344.7 kPa (50 psi), selective layer: TiO_2, CFV: 1.07 ± 0.07 m/s (unmodified), 1.00 ± 0.06 m/s (modified).

For the final produced water filtration run (Test #4), Feed B was concentrated by removing 75% of the water from the original sample. This concentrated feed was then used to challenge unmodified and $PEO_{9\text{-}12}TMS$ modified TiO_2 membranes and the resulting flux versus time data is shown in Figure 5.9. Over the first 2 hours of testing with the B-concentrate feed, the steam

flush was operated normally. During this time, the modified membrane gives permeate fluxes that are approximately 20 Lmh higher than those of the unmodified membrane. This moderate improvement flux, as opposed to the higher performance of previous modified membranes, was attributed to the higher concentration of oil in the SAGD produced water feed used in this filtration test.

After 2 hours of filtration, steam flushing was deactivated to examine membrane performance in its absence. The rate of flux decline increased for both membranes. During the next 2-hour period of filtration, without periodic steam regeneration, significant foulant cake buildup would have occurred at the membrane surface. The break and sudden elevation of permeate flux at the 4-hour mark was due to the overnight relaxation of this cake layer that occurred between the end of the 4-hour run and the start of the next. Eventually, the flux of the modified membrane dropped below that of its unmodified counterpart. Over the next 12 hours of filtration without steam flushing, the fluxes of both membranes declined in similar manners, with the flux of the unmodified membrane being consistently higher by approximately 10–20 Lmh. After 16 hours of filtration, the steam flush was reactivated. Upon reactivation of the steam, the fluxes of both membranes increased and were stable for the final 4-hour filtration test. The unmodified membrane's flux remained approximately 5 Lmh higher. This indicates that the fouling by the concentrated feed in absence of steam, which led to a poorer performance by the modified membrane, could not be entirely undone in an additional 4 hours of filtration with the steam activated. Nonetheless, the flux increase that was observed upon reactivation of the steam was higher for the modified membrane. The flux of the unmodified membrane increased by a factor of 1.3, while that of the modified membrane increased by a factor of 1.6, which is further evidence that foulants are more easily removed from the silylated membrane surface.

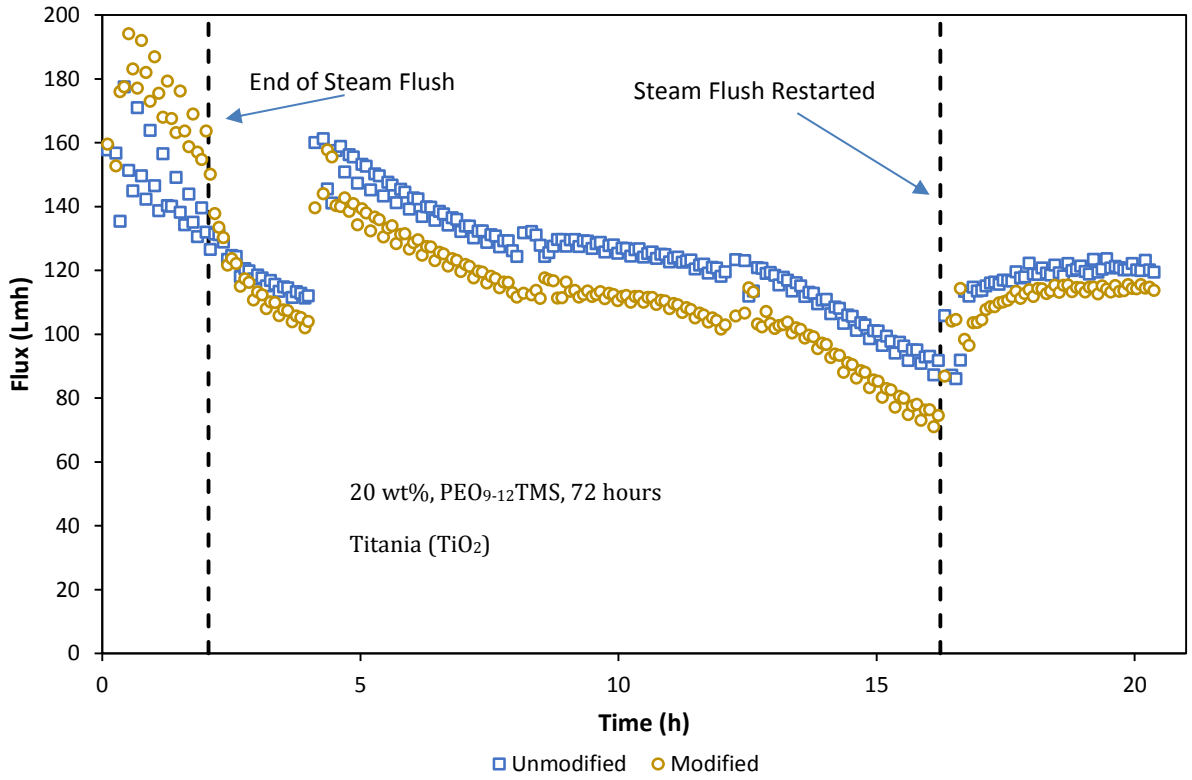

Figure 5.9: Normalized permeate flux as a function of time for Test #4. Modification: 20% $PEO_{9\text{-}12}TMS$ (72h), TMP: 241.3 kPa (35 psi), selective layer: TiO_2, Feed B-concentrate, CFV: 0.999 ± 0.029 m/s (unmodified), 1.04 ± 0.04 m/s (modified).

5.3.2 Effect of surface modification on pure water permeate flux

The PWP flux over a range of transmembrane pressures is shown in Figure 5.10a and Figure 5.10b for Tests #1 and #2, as well as in Figure 5.11a and Figure 5.11b for Tests #3 and #4. In the cases of Test #1 (Figure 5.10a) and Test #3 (Figure 5.11a) a similar trend is observed wherein the initial PWP fluxes of the unmodified membranes are consistently higher than those of the modified membranes over a TMP range of 30 to 145 psi (206.8 to 999.7 kPa). This is an indication that modification with solutions of 30% $PEO_{6\text{-}9}TMS$ and 15% $PEO_{9\text{-}12}TMS$ for 24 hours leads to a reduction in membrane pore size, which in turn reduces the flux of pure water passing through the membranes. In both of these tests, the difference in PWP flux generally increased with TMP. In the case of the $PEO_{6\text{-}9}TMS$ modified alumina membrane, no PWP flux was observed at the lowest TMP of 30 psi. The aforementioned pore size reduction caused by modification in a 30 wt% silane solution lead to a higher PWP breakthrough pressure compared to other membranes.

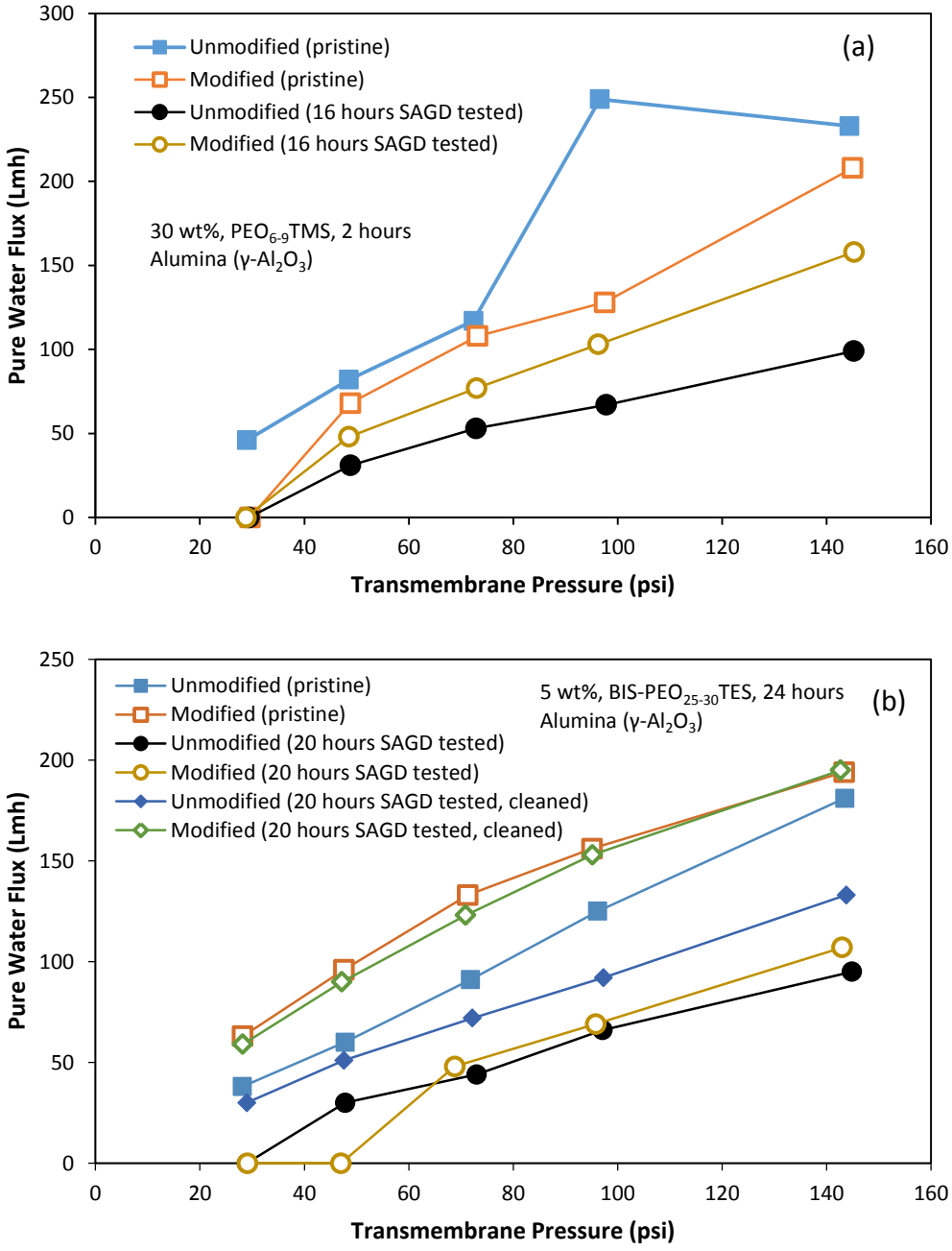

Figure 5.10: Pure water permeate flux at various transmembrane pressures for (a) Test #1, (b) Test #2.

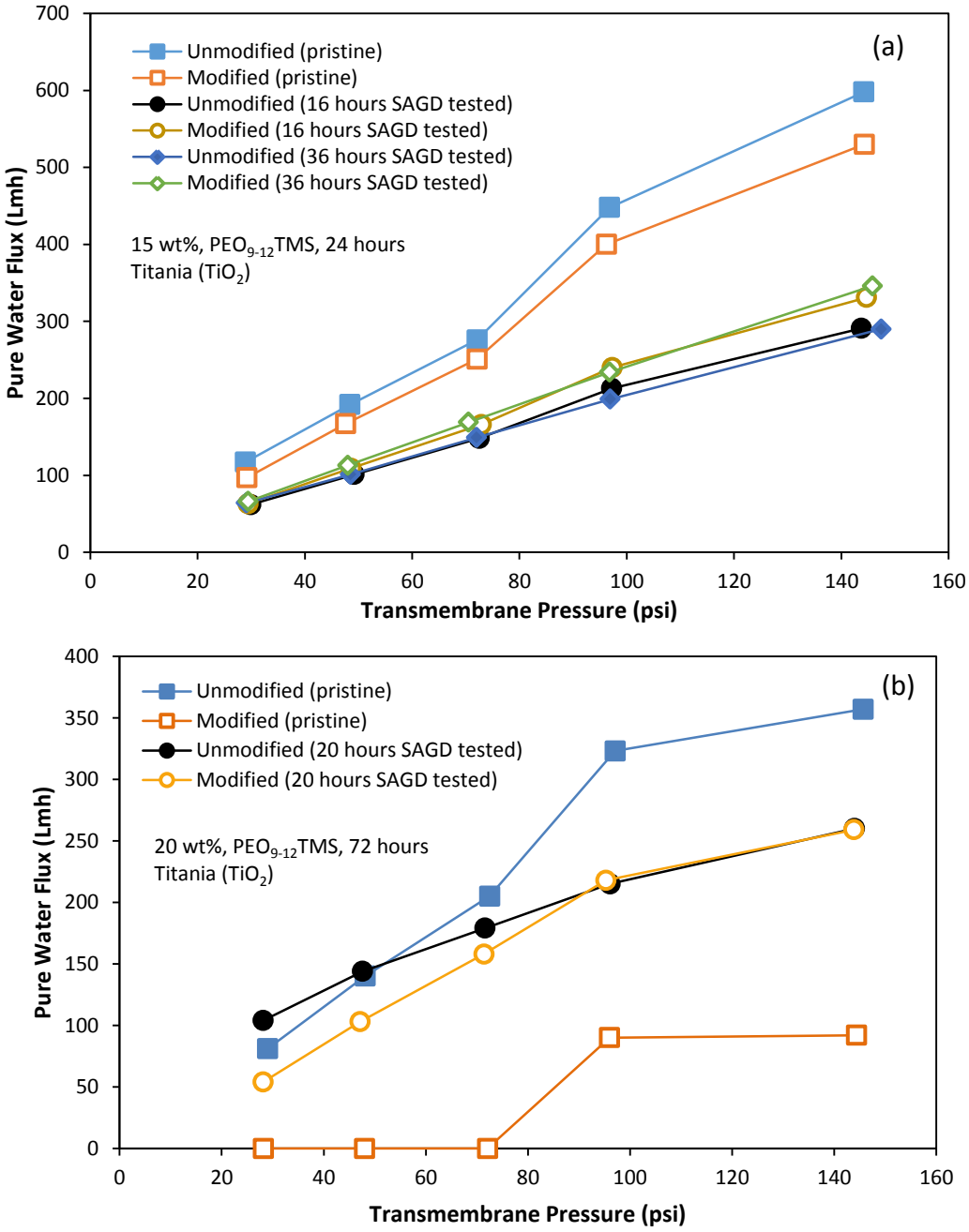

Figure 5.11: Pure water permeate flux at various transmembrane pressures for (a) Test #3, (b) Test #4.

After filtration with produced water, the modified membranes used in Tests #1 and #3 both exhibited higher PWP fluxes than their unmodified counterparts. For Test #1, both the fouled unmodified and modified membrane only begin permeating water at TMPs of 50 psi (344.7 kPa) or higher. In both cases, after the PWP breakthrough pressure is achieved, the PWP flux of the fouled modified membrane increased with pressure at a higher rate than that of the unmodified membrane. At the highest TMP of 145 psi (999.7 kPa), the improvement in PWP flux was

approximately 50 Lmh for both membranes. In Test #3, the PWP flux values recorded after the final 20 hours of filtration with Feed B did not vary from those recorded after the initial 16 hours of filtration with Feed A, indicating that the membranes did not undergo significant additional fouling with the second feed. The higher PWP fluxes for the modified membranes after produced water filtration are further evidence that the modification was successful in reducing the fouling caused by bituminous wastewaters.

In the case of Test #2 (Figure 5.10b), the initial PWP flux of the modified membrane was higher than that of the unmodified membrane. This could be attributed to the fact that a lower silane concentration of 5 wt% was used in the modification procedure relative to the previously discussed membranes. A lower concentration of the modifying agent leads to less silane surface coverage of the membrane, thus minimizing the pore size reduction effect that lowered PWP fluxes in previous membranes. After 20 hours of filtration with produced water, the PWP breakthrough pressure of the unmodified membrane was 45 psi (310.3 kPa), while that of the modified membrane was higher at 70 psi (482.6 kPa). However, the PWP flux of the modified membrane was again higher compared to the unmodified membrane once both breakthrough pressures were reached, consistent with previously analyzed filtration results. Further to previous runs, the membranes used in Test #2 were subjected to a cleaning procedure described in section 5.2, and the PWP flux was subsequently measured again. It is observed in Figure 5.10b that the efficiency of the cleaning procedure was superior when applied to the modified membrane. After cleaning, the PWP fluxes of the unmodified membrane increased to values that were approximately 73 to 85% of the initial fluxes prior to filtration, while the modified membrane recuperated 92 to 100% of the initial PWP flux values over the same TMP range. It can thus be stipulated that the bituminous foulants from the produced water were more loosely adhered to the silylated membrane surface than to the unmodified surface, allowing the utilized cleaning solvents to remove them with greater efficiency.

In the case of Test #4 (Figure 5.11b), the initial PWP flux of the unmodified membrane is significantly higher than that of the modified membranes at all TMP values tested. In fact, the breakthrough pressure for deionized water to flow through the modified membrane was 96 psi (661.9 kPa), whereas water was permeating through the unmodified membrane at the lowest tested TMP of 29 psi (199.9 kPa). This indicates that, in varying the modification process with

$PEO_{9-12}TMS$ to incorporate a 20 wt% silane solution and 72h reaction time, the pores of the 10 nm TiO_2 membrane became partially blocked and required a higher TMP to allow pure water to permeate through.

After 20 hours of testing with a concentrated wastewater feed, the PWP of the unmodified membrane was higher compared to the modified membrane up to a TMP of 75 psi (517.1 kPa). The difference in PWP flux, however, decreases with increasing TMP and eventually the flux of both membranes becomes similar at TMPs of 100 and 150 psi (689.5 and 1034.2 kPa). The lack of improved PWP for the modified membrane after testing indicates that the silane modification is less successful at remediating fouling from SAGD feeds that have been concentrated prior to membrane filtration. In both cases, the PWP flux was lower than the initial flux of the unmodified membrane, indicating fouling of the membranes by bituminous fines. The PWP after testing was higher for the modified membrane than the initial flux of the modified membrane, indicating that the effect of unblocking the pores that were plugged by the silane at such extreme modification conditions is more substantial than the fouling brought on by the bitumen.

5.3.3 Effect of modification on separation performance

The average TOC content in the feed, unmodified and modified permeate of all filtration tests is presented in Figure 5.12. During Test #1, average TOC content decreased from 138 ppm in the feed to 22 and 12 ppm in the permeate of the unmodified and modified membrane, respectively, which corresponds to TOC removals of 84% and 91%. In Figure 5.13 a plot of TOC as a function of average permeate flux for each 4-hour block of the 12-hour filtration test shows that the modified membrane provided permeates with lower TOC content on average, while also giving higher flux values. This indicates that the 30% $PEO_{6-9}TMS$ modification led to an enhancement in both separation and flux. However, a TOC separation improvement of this magnitude was not observed with the other filtration tests.

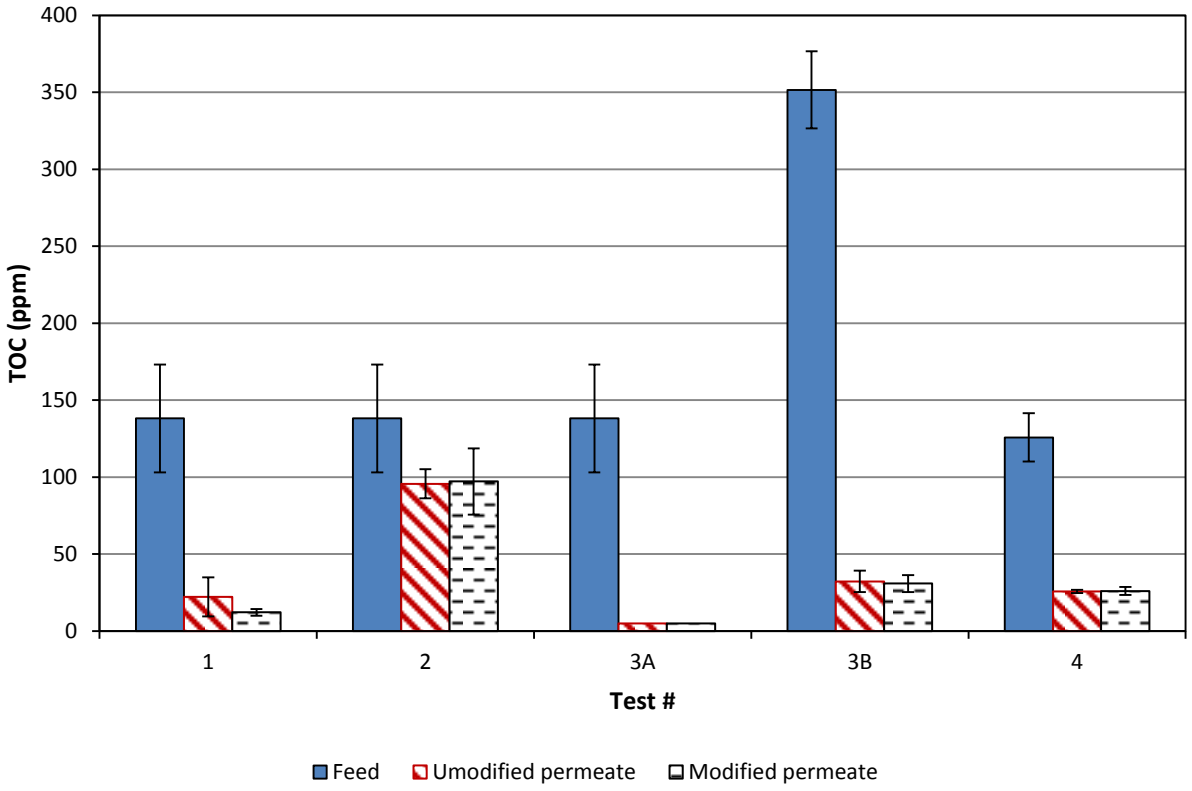

Figure 5.12: Total organic carbon content of feed and permeate samples from all membrane filtration tests. Error bars represent the standard deviation obtained from 5 to 10 sample measurements, depending on the length of the corresponding filtration test. The feeds used in each test are described in Tables 5.2 and 5.3.

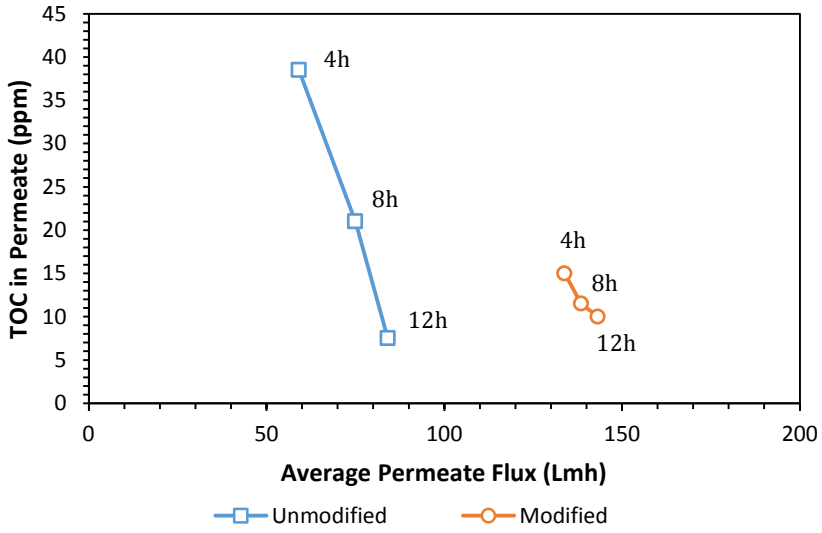

Figure 5.13: TOC content in permeate vs average permeate flux for Test #1. Modification: 30% $PEO_{6-9}TMS$ (2h), TMP: 50 psi (344.7 kPa), selective layer: γ-Al_2O_3, Feed A.

In Test #2, TOC values in the permeate were reduced by approximately 30% by both the unmodified and modified membranes. In Test #3A, TOC content in the permeate samples could not be accurately measured as they were below the 5 ppm lower threshold of the of the TOC analyzer. During Test #3B, TOC content was reduced by approximately 91% for both unmodified and modified membranes. For Test #4, with a more concentrated feed, TOC rejection dropped to approximately 79% for both membranes.

The concentration of sulphates in the feed and permeate samples of each filtration test are presented in Figure 5.14. Surface modification with the PEO-silanes did not impose a significant effect on sulphate separation. Rejection of sulphates was approximately 68%, 81%, 50%, 47% and 62% for Tests #1 through #4, respectively. Organosulphates, which are associated with the sulfur-bearing bitumen fraction of produced water, would have been largely rejected by the membranes. However, mineral sulphates are significantly smaller in molecular size and are not likely to be efficiently separated by the utilized ceramic membranes.

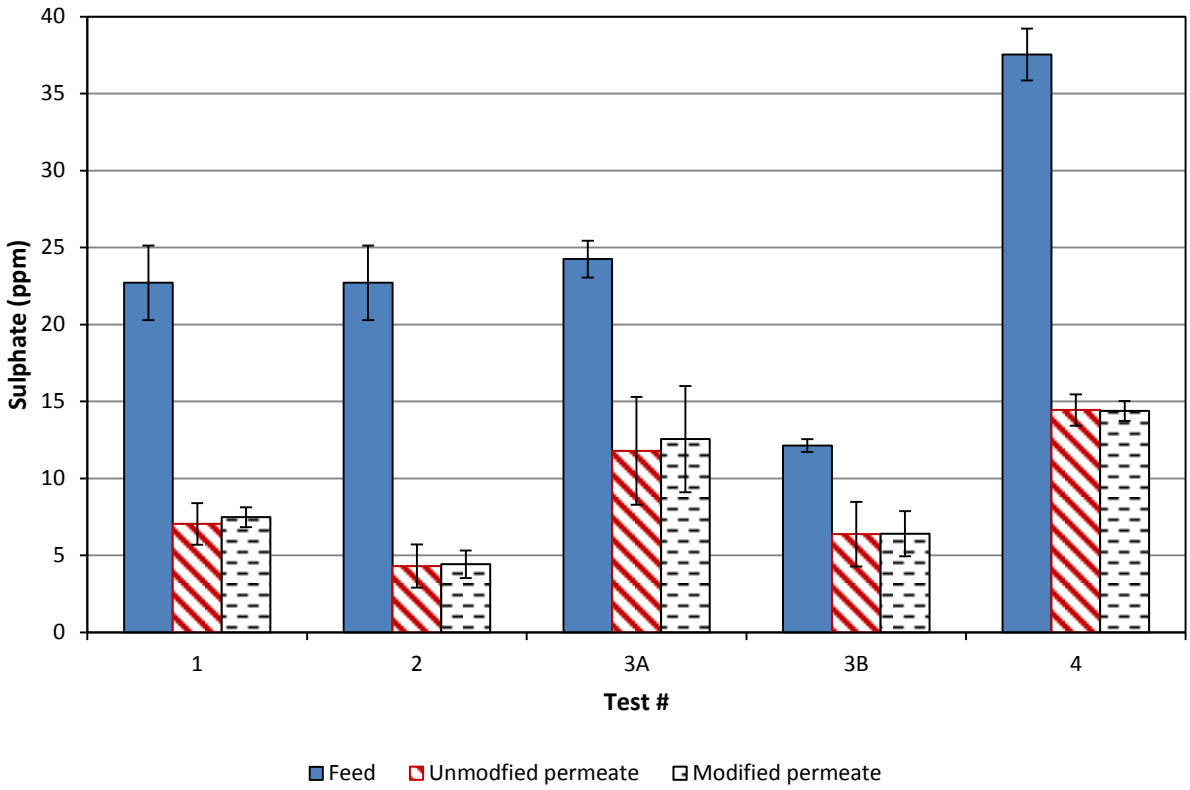

Figure 5.14: Sulphate content of feed and permeate samples from all membrane filtration tests. Error bars represent the standard deviation obtained from 5 to 10 sample measurements, depending on the length of the corresponding filtration test.

The average concentration of chloride in the feed and permeate samples taken from each filtration test are presented in Figure 5.15. The separation performance of all of the tested membranes in terms of chloride rejection is as expected for a UF membrane. Rejection values did not exceed 21%, and were as low as 7% in the case of Test #3B. Differences in performance between unmodified and modified membranes were negligible. Chloride presence in produced water is largely associated with sodium chloride. Calcium and magnesium present in the feeds would be associated with some of the chloride ions; some retention of these cations is expected by the membrane and the filter cake on the surface of the membrane. This explains the slight separation of chloride ions by the membranes.

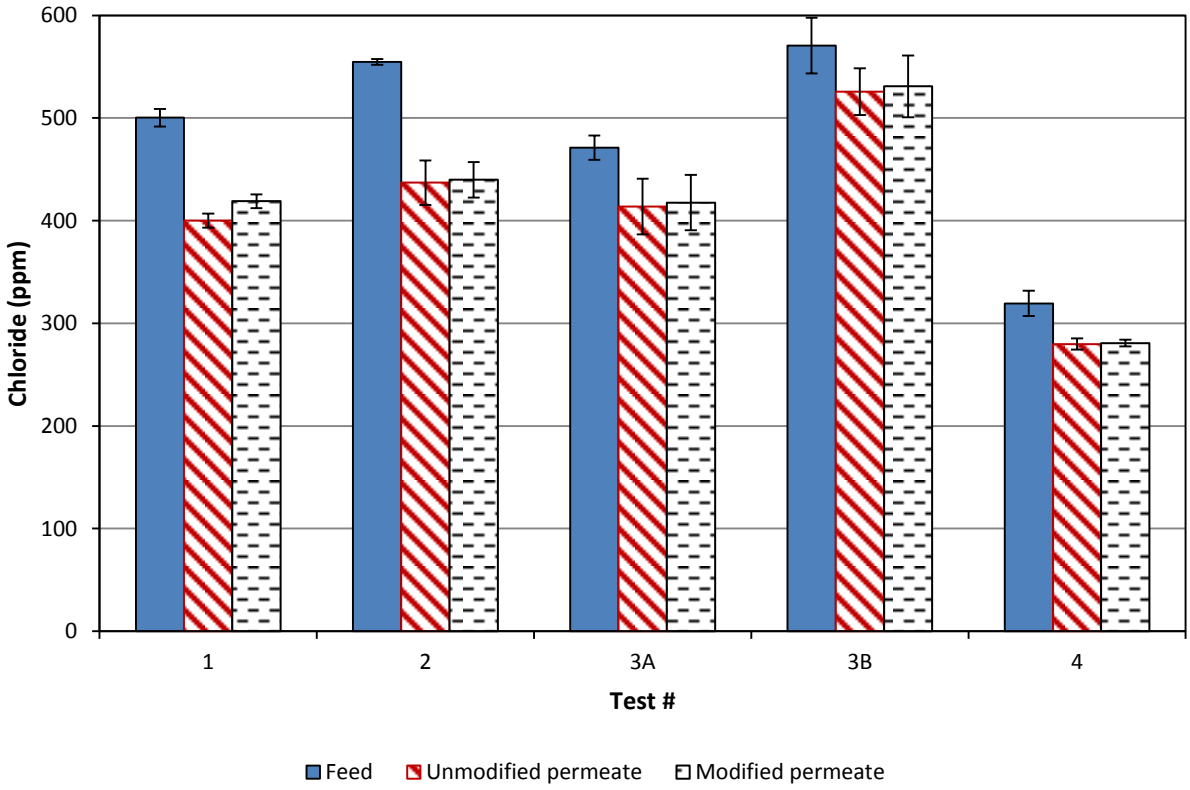

Figure 5.15: Chloride content of feed and permeate samples from all membrane filtration tests. Error bars represent the standard deviation obtained from 5 to 10 sample measurements, depending on the length of the corresponding filtration test.

5.3.4 Summary of results

Among all of the membranes tested, the most successful in terms of flux improvement was the alumina membrane modified with $PEO_{6-9}TMS$ in Test #1. This modified membrane maintained superior permeate flux by factors as high as 2.90 when compared to its unmodified counterpart, as seen in Figure 5.4. Furthermore, the modified membrane also produced permeate samples that contained less TOC than those of the unmodified membrane, indicating enhanced separation as well as flux performance (Figure 5.13).

When an alumina membrane was modified with the dipodal silane BIS-$PEO_{25-30}TES$ at a similar modification concentration to that used in Test #1, no permeate flux was obtained even at elevated pressures. This indicates that the deposition of dipodal silanes on ceramic membrane surfaces is difficult to control and results in the polymerization and bridging of silane molecules. This led to pore plugging in the membrane, effectively rendering the membrane impermeable.

Further to flux enhancement, modification of titania membranes in Test #3 with $PEO_{9-12}TMS$ was also shown to improve the efficiency of backflushing. Flux recovery ratios following either permeate backflushing or steam flushing increased from 1.2 for the unmodified membrane to as much as 1.6–2.0, as seen in Figure 5.7. This indicates that bituminous foulants have less adhesion to the silylated surface than to the native ceramic metal oxide surface. In the second portion of Test #3, it was also demonstrated that the modified titania membrane performed better with a more challenging feed. When the feed was transitioned to the more recalcitrant wastewater, with higher pH and TOC, the flux of the modified membrane remained relatively constant while that of the unmodified membrane declined significantly (Figure 5.8).

The recuperation of PWP flux upon solvent cleaning was also higher for the modified membrane, In Figure 5.10b, it is seen that the unmodified membrane recovered 73–85% of the initial PWP flux after solvent cleaning, while the BIS-$PEO_{25-30}TES$ modified alumina membrane recovered 92–100% of its flux. The separation of TOC, sulphates and chlorides remained relatively unchanged upon modification for the majority of the experiments.

5.4 Conclusions

Commercially available tubular ceramic membranes were surface modified using various PEO-based organosilanes and subsequently challenged with SAGD produced water originating from various operations in the Canadian oil sands. Four side-by-side tests were conducted to compare the efficiency of a certain modification with that of an unmodified counterpart. In all cases, the modified membrane offered an improvement in performance based on membrane flux.

Straight chain PEO-silane modifications on an alumina membrane offered the highest improvement, increasing permeate flux by a factor ranging from 1.65 to 2.90 throughout the filtration test. The improvement of the dipodal silane modification on alumina membrane flux, at a factor of 1.20, was more moderate compared to the straight chain silane because dipodal modifications can only be applied in smaller concentrations to avoid membrane pore blocking. Permeate fluxes for all alumina membranes increased with time, indicating a strong initial adsorption and gradual release of bituminous foulants from the alumina surface.

Conversely, modified titania membranes showed less improvement in flux when compared to the improvement of the modified alumina membranes. However, titania membranes showed an easier release of particles from the surface as evidenced by higher flux recoveries after each backflush cycle. Flux recovery factors from liquid backflushing were 1.2 and 1.4 for the unmodified and modified membranes, respectively. Flux recovery factors from steam flushing were 1.3 and 1.6 for unmodified and modified membranes, respectively. Along with better backflush performance, titania membranes also offered fluxes that were at least twice as high as those of the alumina membranes. Titania is a weak adsorbent for asphaltenes relative to alumina, and so fouling occurred to a far lesser degree. Modified titania membranes also offered improved fluxes when the SAGD feed was changed to a more recalcitrant produced water with higher pH, TOC and alkalinity, indicating that the modification continues performing even in harsher filtration conditions.

The results of these filtration tests indicate that the surface modification protocols previously applied to ceramic membrane disks can be successfully applied to commercially available tubular ceramic membranes while maintaining the efficient rejection of bituminous foulants from the membrane surface that is offered by the PEO silane modifying agent. Furthermore, the

successful modification of lower cost alumina membranes was demonstrated and offers an alternative to higher cost titania membranes.

References

[1] E.W. Allen, Process water treatment in Canada's oil sands industry: I. Target pollutants and treatment objectives, Journal of Environmental Engineering and Science. 7 (2008) 123–138.

[2] P. Swenson, B. Tanchuk, E. Bastida, W. An, S.M. Kuznicki, Water desalination and de-oiling with natural zeolite membranes - Potential application for purification of SAGD process water, Desalination. 286 (2012) 442–446.

[3] S. Alzahrani, A.W. Mohammad, Challenges and trends in membrane technology implementation for produced water treatment: A review, Journal of Water Process Engineering. 4 (2014) 107–133.

[4] E.S. Kim, Y. Liu, M. Gamal El-Din, Evaluation of membrane fouling for in-line filtration of oil sands process-affected water: The effects of pretreatment conditions, Environmental Science & Technology. 46 (2012) 2877–2884.

[5] M. Sadrzadeh, J. Hajinasiri, S. Bhattacharjee, D. Pernitsky, Nanofiltration of oil sands boiler feed water: Effect of pH on water flux and organic and dissolved solid rejection, Separation and Purification Technology. 141 (2015) 339–353.

[6] G. Hurwitz, D.J. Pernitsky, S. Bhattacharjee, E.M.V. Hoek, Targeted Removal of Dissolved Organic Matter in Boiler-Blowdown Wastewater: Integrated Membrane Filtration for Produced Water Reuse, Industrial & Engineering Chemistry Research. 54 (2015) 9431–9439.

[7] B. Khorshidi, A. Bhinder, T. Thundat, D. Pernitsky, M. Sadrzadeh, Developing high throughput thin film composite polyamide membranes for forward osmosis treatment of SAGD produced water, Journal of Membrane Science. 511 (2016) 29–39.

[8] A. Alpatova, E.S. Kim, S. Dong, N. Sun, P. Chelme-Ayala, M. Gamal El-Din, Treatment of oil sands process-affected water with ceramic ultrafiltration membrane: Effects of operating conditions on membrane performance, Separation and Purification Technology. 122 (2014) 170–182.

[9] S. Dong, E. Kim, A. Alpatova, H. Noguchi, Y. Liu, M.G. El-Din, Treatment of oil sands process-affected water by submerged ceramic membrane microfiltration system, Separation and Purification Technology. 138 (2014) 198–209.

[10] A. Guirgis, R. Gay-de-Montella, R. Faiz, Treatment of produced water streams in SAGD processes using tubular ceramic membranes, Desalination. 358 (2015) 27–32.

[11] S.-J. Lee, J.-H. Kim, Differential natural organic matter fouling of ceramic versus polymeric ultrafiltration membranes, Water Research. 48 (2014) 43–51.

[12] B.D. Sparks, L.S. Kotlyar, J.B. O'Carroll, K.H. Chung, Athabasca oil sands: effect of organic coated solids on bitumen recovery and quality, Journal of Petroleum Science and Engineering. 39 (2003) 417–430.

[13] H. Kawaguchi, Z. Li, Y. Masuda, K. Sato, H. Nakagawa, Dissolved organic compounds in reused process water for steam-assisted gravity drainage oil sands extraction, Water Research. 46 (2012) 5566–5574.

[14] S. Guha Thakurta, A. Maiti, D.J. Pernitsky, S. Bhattacharjee, Dissolved organic matter in steam assisted gravity drainage boiler blow-down water, Energy & Fuels. 27 (2013) 3883–3890.

[15] J. Fatema, S. Bhattacharjee, D. Pernitsky, A. Maiti, Study of the Aggregation Behavior of Silica and Dissolved Organic Matter in Oil Sands Produced Water Using Taguchi Experimental Design,

Energy & Fuels. 29 (2015) 7465–7473.

[16] A. Maiti, M. Sadrezadeh, S. Guha Thakurta, D.J. Pernitsky, S. Bhattacharjee, Characterization of boiler blowdown water from steam-assisted gravity drainage and silica-organic coprecipitation during acidification and ultrafiltration, Energy & Fuels. 26 (2012) 5604–5612.

[17] Y. Thibault, J. Gamage McEvoy, S. Mortazavi, D. Smith, A. Doiron, Characterization of fouling processes in ceramic membranes used for the recovery and recycle of oil sands produced water, Journal of Membrane Science. 540 (2017) 307–320.

[18] S.E. Weschenfelder, A.M.T. Louvisse, C.P. Borges, E. Meabe, J. Izquierdo, J.C. Campos, Evaluation of ceramic membranes for oilfield produced water treatment aiming reinjection in offshore units, Journal of Petroleum Science and Engineering. 131 (2015) 51–57.

[19] T. Zsirai, H. Qiblawey, P. Buzatu, M. Al-Marri, S.J. Judd, Cleaning of ceramic membranes for produced water filtration, Journal of Petroleum Science and Engineering. 166 (2018) 283–289.

[20] M.M. Gentleman, J.A. Ruud, Role of hydroxyls in oxide wettability, Langmuir. 26 (2010) 1408–1411.

[21] A. Jada, M. Salou, Effects of the asphaltene and resin contents of the bitumens on the water-bitumen interface properties, Journal of Petroleum Science and Engineering. 33 (2002) 185–193.

[22] E.W. Allen, Process water treatment in Canada's oil sands industry: II. A review of emerging technologies, Journal of Environmental Engineering and Science. 7 (2008) 499–524.

[23] A. Dafinov, R. Garcia-Valls, J. Font, Modification of ceramic membranes by alcohol adsorption, Journal of Membrane Science. 196 (2002) 69–77.

[24] P.H. Mutin, V. Lafond, A.F. Popa, M. Granier, L. Markey, A. Dereux, Selective surface modification of SiO2-TiO2 supports with phosphonic acids, Chemistry of Materials. 16 (2004) 5670–5675.

[25] J. Kujawa, W. Kujawski, Functionalization of Ceramic Metal Oxide Powders and Ceramic Membranes by Perfluroalkylsilanes and Alkylsilanes Possessing Different Reactive Groups – Physicochemical and Tribological Properties, ACS Applied Materials & Interfaces. 8 (2016) 7509–7521.

[26] X. Chen, X. Gao, K. Fu, M. Qiu, F. Xiong, D. Ding, Z. Cui, Z. Wang, Y. Fan, E. Drioli, Tubular hydrophobic ceramic membrane with asymmetric structure for water desalination via vacuum membrane distillation process, Desalination. 443 (2018) 212–220.

[27] J. Kujawa, S. Cerneaux, W. Kujawski, Highly hydrophobic ceramic membranes applied to the removal of volatile organic compounds in pervaporation, Chemical Engineering Journal. 260 (2015) 43–54.

[28] T. Takahashi, R. Tanimoto, T. Isobe, S. Matsushita, A. Nakajima, Surface modification of porous alumina filters for CO2 separation using silane coupling agents, Journal of Membrane Science. 497 (2016) 216–220.

[29] D. Ding, H. Mao, X. Chen, M. Qiu, Y. Fan, Underwater superoleophobic-underoil superhydrophobic Janus ceramic membrane with its switchable separation in oil/water emulsions, Journal of Membrane Science. 565 (2018) 303–310.

[30] J. Lee, J.-H. Ha, I.-H. Song, D.W. Shin, Enhanced fouling resistance of organosilane-grafted ceramic microfiltration membranes for water treatment, Journal of the Ceramic Society of Japan.

125 (2017) 899–905.

[31] S. Yeu, J.D. Lunn, H.M. Rangel, D.F. Shantz, The effect of surface modifications on protein microfiltration properties of Anopore membranes, Journal of Membrane Science. 327 (2009) 108–117.

[32] C.R. Tanardi, R. Catana, M. Barboiu, A. Ayral, I.F.J. Vankelecom, A. Nijmeijer, L. Winnubst, Polyethyleneglycol grafting of γ-alumina membranes for solvent resistant nanofiltration, Microporous and Mesoporous Materials. 229 (2016) 106–116.

[33] C. Atallah, A.Y. Tremblay, S. Mortazavi, Silane Surface Modified Ceramic Membranes for the Treatment and Recycling of SAGD Produced Water, Journal of Petroleum Science and Engineering. 157 (2017) 349–358.

[34] B. Arkles, Y. Pan, Y.M. Kim, The Role of Polarity in the Structure of Silanes Employed in Surface Modification, Silanes and Other Coupling Agents. 5 (2009) 51–64.

[35] C. Atallah, S. Mortazavi, A.Y. Tremblay, Thermal stability of hydrophilic PEO-silane modified ceramic membranes, Colloids and Surfaces A: Physicochemical and Engineering Aspects. 561 (2019) 254–266.

[36] T. Al-Shemmeri, Engineering Fluid Mechanics, Ventus Publishing ApS, 2012.

[37] N.N. Nassar, Asphaltene adsorption onto alumina nanoparticles: Kinetics and thermodynamic studies, Energy & Fuels. 24 (2010) 4116–4122.

[38] N.N. Nassar, A. Hassan, P. Pereira-Almao, Metal oxide nanoparticles for asphaltene adsorption and oxidation, Energy & Fuels. 25 (2011) 1017–1023.

[39] E.S. Hall, E.L. Tollefson, Stabilization and destabilization of mineral fine-bitumen-water dispersions in tailings from oil sand extraction plants that use the hot water process, The Canadian Journal of Chemical Engineering. 60 (1982) 812–821.

6 In-process Steam Cleaning of Ceramic Membranes Used in the Treatment of Oil Sands Produced Water

C. Atallah, S. Mortazavi, A.Y. Tremblay, A. Doiron.

Manuscript published in Industrial & Engineering Chemistry Research 58 (2019): 15232–15243.

DOI: 10.1021/acs.iecr.9b02257

Abstract

Current oil sands extraction technologies expend a significant amount of energy in the treatment and recycling of the oily process waters that are generated during the extraction process. Ceramic membranes are promising candidates for enhancing the energy efficiency of the produced water deoiling process due to their low energy requirements. However, membrane fouling by bituminous solids remains a significant barrier to the widespread acceptance of membranes in this application. As an alternative to chemical membrane cleaning, a steam regeneration technique was applied to ceramic membranes in the filtration of steam-assisted gravity drainage (SAGD) produced water. This technique involved the periodic injection of steam directly into the membrane feed channels, and was applied in conjunction with conventional permeate backflushing. Tubular multilumen ceramic membranes with titania selective layers having pore sizes of 5 or 10 nm were used. Support layers were composed of either alumina or titania. Optimal transmembrane pressure (TMP) and crossflow velocity (CFV) settings were found to be 50 psi and 1 m/s over the investigated ranges. Membrane permeate fluxes increased from 50 to 200 Lmh when the steam regeneration method was activated. Flux enhancement was found to depend on the initial duration of filtration without steam injection, which results in significant irreversible fouling. Steam regeneration also improved membrane separation performance, increasing total organic carbon (TOC), sulphate and chloride retention by as much as 19%, 17% and 10%, respectively. Steam regeneration is a continuous in-process method that offers the possibility of recycling the oleophilic cake released from the surface of the membrane. The cake can be sent to a flotation unit upstream of the membrane system, allowing bituminous fines to be entrained in the main oil stream. This offers many possibilities for waste minimization, particularly in remote areas where cleaning fluids that are produced when membranes are chemically cleaned would need to be transported and treated off-site.

6.1 Introduction

Currently, in-situ oil sands extraction technologies sacrifice over 20% of the fuel's energy during the extraction process, in comparison to a loss of approximately 6% for conventional oil and gas extraction processes [1]. This is partially attributed to the energy intensive recycling of wastewater in these applications, where the recycled water is used for steam production. Current water treatment processes cannot reliably provide clean water, leading to downstream process upsets such as boiler tube failure caused by oil contamination, resulting in significant economic loss. Process intensification by enhanced recycling of produced water for steam production is thus required.

Synthetic membranes are commonly used in oily wastewater treatment due to their energy efficiency, low maintenance cost and ease of application relative to other separation operations [2]. Most of the membranes used in these applications are polymeric in nature [3]. However, when wastewaters originate from oil spills or oil production, they can contain inorganic scalants and suspended bitumen [4,5]. Most polymeric membranes fail to resist the organic components in these wastewaters, which results in membrane swelling and deterioration [6]. This limitation is compounded when oily wastewaters are to be treated at temperatures above 80 °C, due to the fact that polymeric membranes are subject to thermal degradation at higher temperatures. To counter this, membranes with high temperature and solvent resistance are increasingly being studied to treat oily wastewaters. Ceramic membranes are made of metal oxides that maintain good structural integrity in the presence of heat and solvents [7]. They have been used in many industries ranging from the mining and petrochemical to the pharmaceutical industry [8]. Their application in the treatment of field samples of produced water obtained from oil and gas operations is an ongoing and active area of research [9–16].

Oil production operations produce a large amount of oily wastewaters that can contain ultrafine clay particles, solvents, resins and other complex organics [17–21]. These mixtures of fine particulates combined with oils and bitumen are particularly difficult to treat. When such a mixture is treated by traditional membrane filtration, fouling deposits form on the surface of the membrane. Fouling caused by particulate suspensions in this type of feed water is heavily detrimental to membrane permeability and flux performance and remains a major obstacle to the widespread acceptance of membrane technology [22,23]. Furthermore, the difficulty in treating

produced water increases with storage and aging of the feed due to the polymerization and precipitation of particulates caused by air exposure [24,25]. These deposits must subsequently be removed from the membrane surface by chemical or physical means. The deposits can be removed with solvents or detergents [26]. However, this method produces residual cleaning and rinse wastewaters that must be disposed of. Alternatively, the deposits can be removed by physical means, where permeate (fluid that has initially passed through the membrane), is pressurized and forced back through the pores of the membrane [27]. This flow reversal is effective in removing deposits or filter cakes on the surface of the membrane when the cakes do not adhere to its surface or do not form structured networks that reinforce the cake.

Filter cakes containing materials that can coalesce and bridge form cakes having very low permeabilities. An example of such cakes is observed when wastewaters containing fine particles, oil and bitumen are treated such as in the recycling of steam-assisted gravity drainage (SAGD) process waters [12]. The recalcitrant filter cakes are difficult to backflush and gradually increase in thickness which greatly reduces permeate flow through the membrane. The resistance of these cakes to flow is extremely high and the flux of the membrane decreases to a level where the operation of the system comprising the membrane is no longer economical. In addition to this, it is advantageous to treat process waters at a high temperature when they originate from operations where steam is used in the extraction process. This has the advantage of treating wastewater having a reduced viscosity at the higher temperatures of 80 to 100 °C and to eliminate cooling requirements needed prior to treatment when conventional membrane materials are used in the treatment process. Avoiding the need to cool and then reheat the wastewater reduces the CO_2 emissions of the oil production process. Therefore, a physical membrane regeneration method that operates at high temperature would be beneficial in removing bituminous foulants from the membrane surface, and thus improving membrane performance. The use of steam as a means of sterilizing ceramic membranes has been frequently applied in the pharmaceutical industry [8,28,29]. This indicates that ceramic membranes can be intermittently heated with steam over many years of operation.

In this work, we demonstrate the use of two simultaneous physical approaches in order to reduce the accumulation of oily particulates and bitumen on the surface of a membrane and ultimately remove recalcitrant cakes from its surface. A combination of traditional liquid permeate

backflushing and periodical direct steam injection on the feed side was applied. This procedure was used in the crossflow filtration of produced water originating from the SAGD process used in the Canadian oil sands. Ceramic membranes with different pore sizes and support materials were compared, and the effect of transmembrane pressure (TMP) and feed crossflow velocity (CFV) assessed. SAGD produced water from two different suppliers was used and the performance of the membranes was analyzed relative to the varying characteristics of each feed. Filtration with permeate backflushing only and with both backflushing and steam regeneration was conducted in order to demonstrate its effectiveness in enhancing ceramic membrane performance in this application.

6.2 Materials and methods

6.2.1 Materials

The tubular multi-lumen ultrafiltration ceramic membranes used in this study, purchased from Inopor (Veilsdorf, Germany), possessed monolith configurations with 19 flow channels. The tube diameter was 25 mm, while the individual channel diameter was 3.5 mm. Each membrane tube had a length of 0.3 m and a specific membrane area of 0.209 m^2/m, leading to an active membrane area of 0.0627 m^2. Ceramic support layers were composed of either alumina (γ-Al_2O_3) or titania (TiO_2), while the selective layer material was TiO_2. All membranes had pore sizes of 5 or 10 nm, corresponding to a molecular weight cut-off (MWCO) of 7.5 or 20 kDa, respectively, as specified by Inopor (Veilsdorf, Germany).

The feed used to conduct the filtration tests was supplied by SAGD operations located in Canada's oil sands in Alberta. SAGD produced water was obtained from two different oil sands companies. Each company's facility was in a different location, leading to produced water samples with varying chemical and physical characteristics.

6.2.2 Produced water filtration system

A crossflow ceramic membrane pilot scale system was constructed with a feed and bleed loop configuration and a total volume of 16 L. A process flow diagram of the filtration system is shown in Figure 6.1. The system contained a pair of ceramic membrane modules mounted in parallel with individual flowmeters. The parallel configuration was used so that each ceramic

membrane was subjected to identical test conditions such as feed composition, feed flowrates, temperature, and pressure.

The system was heated to temperatures of 80–85 °C using a heat exchanger (B-Line Heat Exchanger, B-300M; AIC Inc., ON, Canada) and through direct heating of the feed liquid using a heating element in the feed tank (Over The Side Heater, ASB Heating Elements Ltd., ON, Canada). To avoid the formation of an explosive atmosphere in the feed tank vapour space located above the liquid, a positive pressure of argon was applied to this vapour space. The vapour from the feed tank was continuously vented to a fume hood.

The feed tank had a conical bottom and a total volume of 150 L. Feed was supplied to the loop from the bottom of this tank. The feed tank was continuously mixed and heated during the experiment. The system was operated with total recycling of the permeate and retentate back to the feed tank. When experiments were conducted at high pressures, partial restriction of the flow through the retentate line was used in order to maintain pressure in the system.

Feed pressure in the system was maintained at the desired value using a feed pump (CRN 1S-15, 1 HP motor, 4.84 GPM; Grundfos Canada Inc., ON, Canada). Circulation through the system was achieved and maintained using a circulation pump (CRN 1S-15, 0.5 HP motor, 9.69 GPM; Grundfos Canada Inc., ON, Canada). Both of these pumps were multistage centrifugal pumps constructed from stainless steel. The frequency setting of the circulation pump was adjusted to values of 10, 15 or 30 Hz. These frequencies corresponded to liquid flowrates of approximately 5, 10 and 20 L/min which were divided equally among the two membranes and yielded crossflow velocities (CFV) between 0.23–1.04 m/s.

With the goal of reducing the fouling of the membranes, backpressure was maintained on the membranes through partial restriction of the permeate lines during each experiment. Without the use of this technique, the permeate lines would have been fully open to the feed tank and the gauge pressure on the permeate side of the membranes would have thus been zero (atmospheric pressure). Through permeate flow restriction, a pressure build-up occurred in permeate the lines and resulted in a continuous backpressure on the membranes. A backpressure of approximately 5 psi was maintained on both membranes during each experiment. The transmembrane pressure (TMP) was determined by evaluating the difference between the circulation pressure, achieved

by partially blocking the retentate line, and the backpressure of 5 psi. The applied TMPs in this work were 35 psi (241.3 kPa), 50 psi (344.7 kPa) and 75 psi (517.1 kPa).

Periodic liquid backflushing of the membranes was used as a means of fouling mitigation. To accomplish this, a bypass stream was installed on the permeate line. The bypass stream was used to fill a 1 L hydraulic cylinder that could then be actuated with a separate pneumatic cylinder. Air was supplied to the pneumatic cylinder at a pressure of 100 psi and both cylinders possessed equal cross-sectional area. During backflushing, the permeate lines to the feed tank were closed and the liquid in the hydraulic cylinder was forced through the membranes from the permeate side for a duration of 10 seconds. This procedure was repeated every five minutes while the system was in operation.

In order to further decrease fouling and regenerate the ceramic membranes during experimental runs, a steam regeneration technique was used. A steam generator (MBA3, 3 kW, Sussman Electric Boilers, NY, USA) was connected to the system, allowing the feed side channels of the membranes to be directly flushed with steam (120 °C) during brief pauses in operation. The pauses needed to flush with steam were accomplished through the use of automated pneumatic valves that isolated the membranes from the loop and exposed them to pressurized steam that would flow through the membrane channels into the feed tank. Steam regeneration was performed every 15 minutes for 10 seconds per flush.

The permeate lines emanating from each of the ceramic membranes were connected to individual flow meters (Coriolis Mass Flow Meter, TCM 0650-FA-SGSS-CSDS). This permitted the measurement of the permeate production rates for each membrane to be accomplished separately. The range of flux measurements achievable by this setup was 20 and 2700 liters per meter squared per hour (Lmh).

Several ports were installed on the bottom of the system that could be opened in order to drain the system. Cleaning of the system following each experiment was accomplished by first draining all liquids and then flushing the system with deionised water. Special care was taken to avoid leaving heavy oil in the system to cool and adhere to the tubing walls and valve and pump components when the system was not operational.

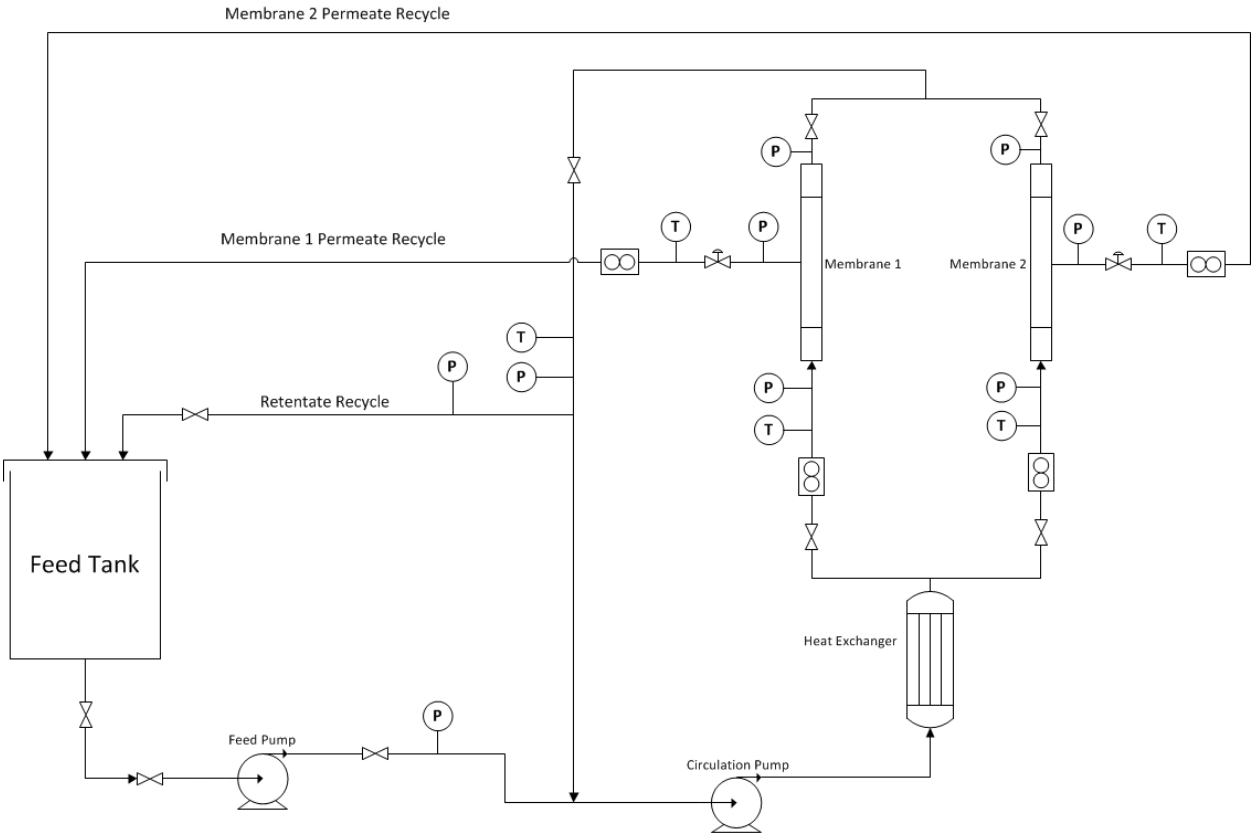

Figure 6.1: Process flow diagram of the crossflow filtration system.

6.2.3 Characterization of feed and permeate samples

Several sample ports were installed throughout the system. At the beginning and end of each experiment, feed samples were taken from the feed pump and circulation loop samples were taken from the bottom of the loop. Permeate samples were obtained directly from the permeate lines at the beginning, middle and end of each experiment.

An Apollo 9000 TOC Analyzer was used to determine the total organic carbon (TOC) content of all samples, as per the manufacturer's instructions. The method involved catalytically oxidizing the sample into CO_2 and H_2O, isolating the CO_2, and passing it to a non-dispersive infrared detector (NDIR) for peak quantification.

A Metrohm 751 GPD Titrino titrator was used to determine the alkalinity of the feed samples by potentiometric titration. The samples were titrated using a standard solution of dilute sulphuric acid. A two endpoint (pH 4.5 and 4.2) technique was utilized to determine the inflection or equivalence point of the titration as described by the American Public Health Association [30].

The dissolved chloride and sulphate content of all samples was quantified through ion chromatography using a Dionex-100 Advanced Chromatography Module.
Prior to TOC, chloride, sulphate and alkalinity quantification, the loop and feed samples were filtered through a 0.45 µm nitrocellulose filter to remove heavy oils that could otherwise affect the analytical equipment.

All samples were subjected to turbidity testing (HF Scientific, Micro 100 Turbimeter). The measurements were taken immediately after taking the samples in order to mitigate temperature and separation related effects.

Particle size analysis of the produced water feed samples was conducted using a Zetasizer Nano S90 (Malvern Instruments Ltd., UK). Particle size analysis on feed and permeate samples was also conducted using a Microtrac X100 Tri-laser model (Microtrac, PA, USA). No results were obtained from the permeate samples as particles present in the permeate samples were too small for the Microtrac X100 to detect (i.e., less than 150 nm).

6.2.4 Pure water permeability

The pure water permeate (PWP) flux before and after all produced water filtration experiments was evaluated for each membrane. In these PWP tests, deionized water at room temperature was used as the feed to the membranes. The frequency setting of the circulation pump was identical to that used in the corresponding produced water filtration tests for each membrane. The permeate lines were kept completely open during PWP filtration. PWP fluxes were recorded for all membranes at feed pressure values of 30, 50, 75, 100 and 150 psi.

6.3 Results and discussion

6.3.1 Experimental conditions

Table 6.1 presents the average values of several parameters that were used to characterize the various SAGD produced water feeds. The feeds were obtained directly from two different companies operating in the Canadian oil sands. Feeds provided by the first company are labelled A1, A2 and A3, while feeds provided by the second company are labelled B1 and B2. All feeds were obtained at the outlet of the free water knockout drum in the traditional SAGD process as described by Holmes et al [31].

Table 6.1: Characteristics of produced water samples used with standard deviations.

Feed Label	TOC* (ppm)	Total oil (ppm)	Alkalinity* (mg/L)	Chloride* (ppm)	Sulphate* (ppm)	pH	Turbidity (NTU)
A1	181.0 ± 50.9	6142 ± 1400	140.8 ± 8.3	538.3 ± 56.2	19.4 ± 2.7	8.56 ± 0.15	81.7 ± 17.0
A2	113.3 ± 4.0	12801 ± 4243	101.0 ± 7.1	387.0 ± 17.0	19.5 ± 0.7	8.45 ± 0.09	317.7 ± 14.5
A3	82.0 ± 9.4	Not sampled	88.3 ± 14.4	309.6 ± 39.3	30.0 ± 1.3	8.49 ± 0.16	444.5 ± 33.9
B1	228.2 ± 25.2	1245 ± 278	704.6 ± 28.9	860.4 ± 28.8	9.6 ± 2.7	9.41 ± 0.13	38.3 ± 7.2
B2	175.8 ± 14.2	3533 ± 714	285.6 ± 27.3	416.3 ± 39.0	14.0 ± 0.6	9.03 ± 0.10	219.6 ± 49.3

*TOC, alkalinity, chloride and sulphate measured after filtration through a 0.45 µm filter.

The retention of TOC, total oil, chlorides and sulphates by the evaluated membranes was determined using the following equation:

$$\% \text{ Retention} = \left(1 - \frac{C_P}{C_F}\right) \cdot 100 \tag{6.1}$$

where C_P is the concentration in the permeate (ppm) and C_F is the concentration in the feed (ppm) of total oil, TOC, chlorides or sulphates.

In each experiment, there were slight fluctuations in the loop circulation temperature and TMP of the membranes. These variations were recorded and accounted for by normalizing the recorded permeate flux with respect to temperature and pressure as per equation (6.2):

$$J_N = J\left(\frac{\mu}{\mu_N}\right)\left(\frac{P_N}{P}\right) \tag{6.2}$$

where J_N is the normalized permeate flux (Lmh), J is the actual permeate flux (Lmh), μ and μ_N are the viscosity at the actual and normalization temperature, respectively, in kg/m/s, P and P_N are the actual and normalization pressure, respectively, in psi. In all cases the normalization temperature is 85 °C, while P_N is the applied TMP (35, 50 or 75 psi). The temperature dependence of water viscosity was determined using equation (6.3), which is accurate to within 2.5% between temperatures of 0 °C to 370 °C [32].

$$\mu = 2.414 \cdot 10^{-5} \cdot 10^{247.8/(T-140)} \tag{6.3}$$

where μ is in kg/m/s and T is in K.

All of the membranes used in the filtration tests had selective layers composed of titania. Membranes with support layers made from alumina were labelled Ti-Al, and membranes with support layers made from titania were labelled Ti-Ti.

6.3.2 Membrane performance with different produced water feeds

In Figure 6.2, the permeate flux performance over time of 5 nm Ti-Al and Ti-Ti membranes tested in parallel is shown. The membranes were first tested with feed A2 for approximately 8 hours, followed by an additional 8 hours of filtration with feed B2. During the first segment with feed A2, the flux of the 5 nm Ti-Al membrane remained constant at approximately 200 Lmh, while the flux of the 5 nm Ti-Ti membrane declined slightly from 176 to 168 Lmh, at a rate of 1 Lmh/h. When the feed was switched to feed B2 for the second portion of the filtration test, the flux decline rate of both membranes increased. The flux of the 5 nm Ti-Al membrane initially declined at a rate of 4 Lmh/h, while that of the 5 nm Ti-Ti membrane showed an initial decline of 3.3 Lmh/h. This indicates that the particulates introduced upon transitioning to feed B2 are more severe foulants for the ceramic membranes when compared to those found in feed A2. An increase in membrane fouling thus led to a decrease in membrane flux performance. From Table 6.1 it is seen that feed B2 possessed higher TOC, alkalinity and chloride content, as well as a higher pH compared to feed A2. SAGD produced water contains a significant amount of weak organic acids, such as humic and naphthenic acids, as well as dissolved silica [18,33]. Increasing the pH of produced water increases the concentration of the conjugated bases of these acids, as well as the concentration of silicate anions present in bitumen associated solids. At higher pH, these bases and anions can react with calcium or magnesium found in the feed to form metal-organic complexes and insoluble silicates that could account for the observed decline in permeate flux performance.

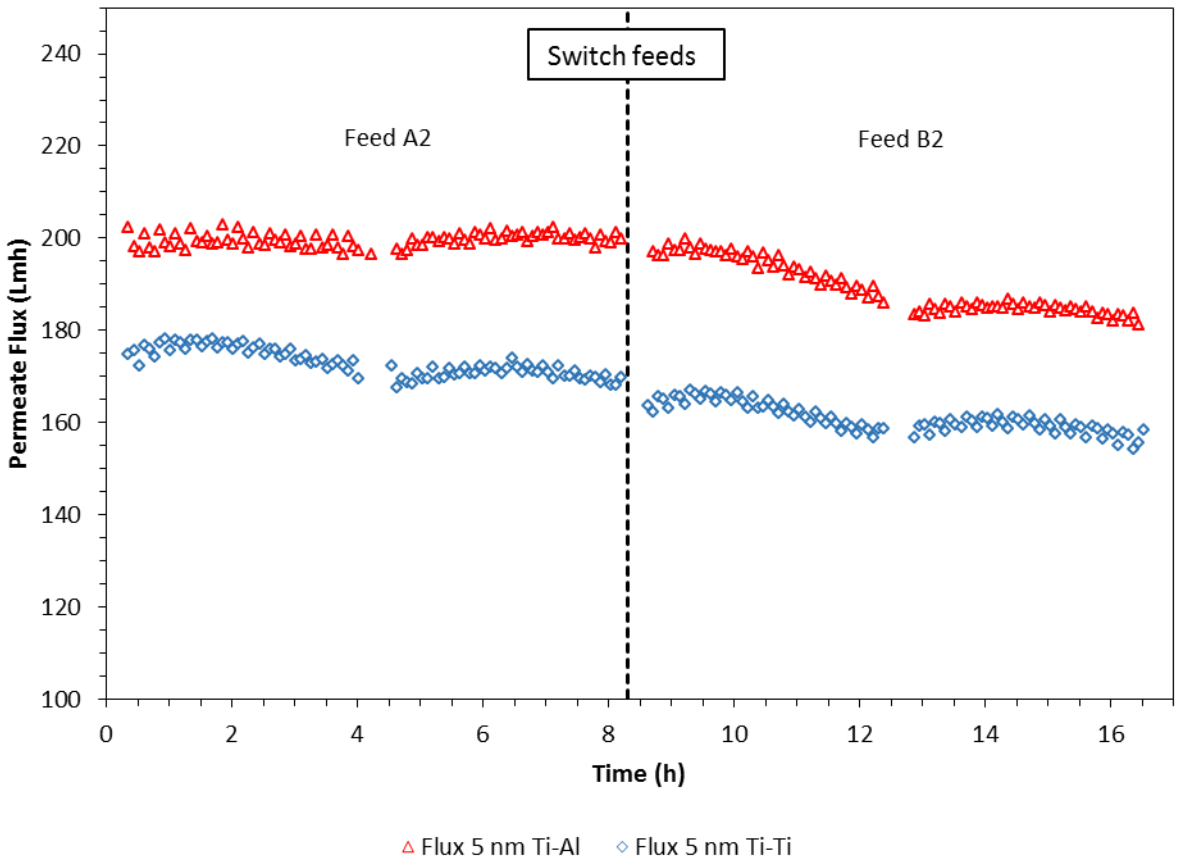

Figure 6.2: Permeate flux as a function of time for 5 nm Ti-Al and 5 nm Ti-Ti membranes with Feeds A2 and B2. TMP: 50 psi (344.7 kPa). CFV: 1.04 ± 0.06 m/s (5 nm Ti-Al), 1.01 ± 0.05 m/s (5 nm Ti-Ti).

Moreover, the separation performance of both membranes with the two feeds is shown in Figure 6.3. It was determined that the rejection of total oil, TOC, sulphates and chlorides by the membranes decreased slightly with feed B2 compared to feed A2. The rejection of particulates and colloids from produced water by ultrafiltration membranes would be largely dependent on the size of these solutes and suspended solids. The particle size distributions of feed samples obtained from both SAGD oil sands facilities are presented in Figure 6.4. It is seen that feed A contains particles ranging from 140 to 340 nm in diameter. Conversely, feed B contains a more significant amount of fine particles with diameters in the range of 80 to 200 nm, as well as larger aggregates that are 500 to 1100 nm in diameter. When rejection is due to particle sieving, it is expected that the membrane more easily retains larger materials. The finer particles in feed B would have thus been more difficult to reject when compared to their larger counterparts in feed A, leading to the observed decrease in the retention of total oil, TOC, sulphates and chlorides.

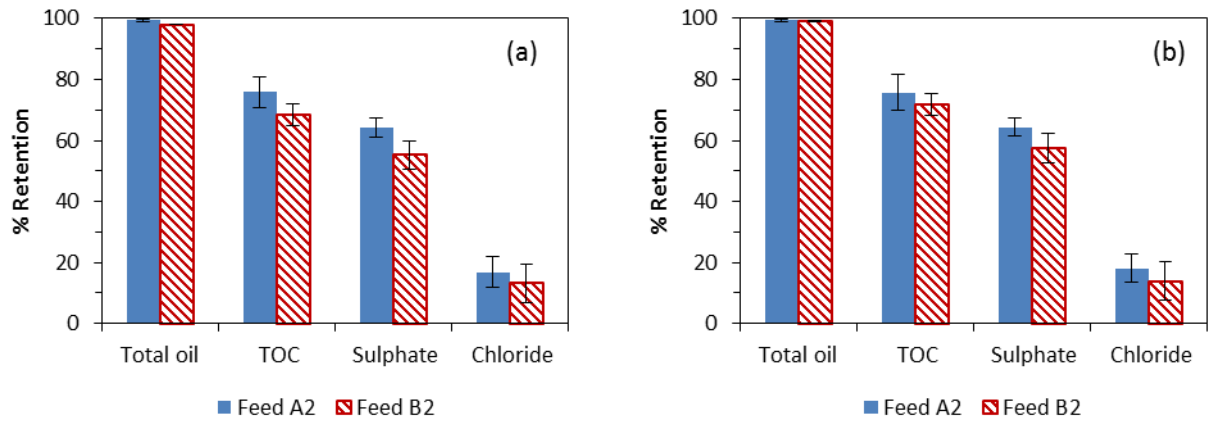

Figure 6.3: Percent retention of total oil, TOC, sulphates and chlorides for (a) 5 nm Ti-Al and (b) 5 nm Ti-Ti membranes with Feeds A2 and B2. TMP: 50 psi (344.7 kPa). TOC, chloride and sulphate were measured after filtration through a 0.45 µm filter.

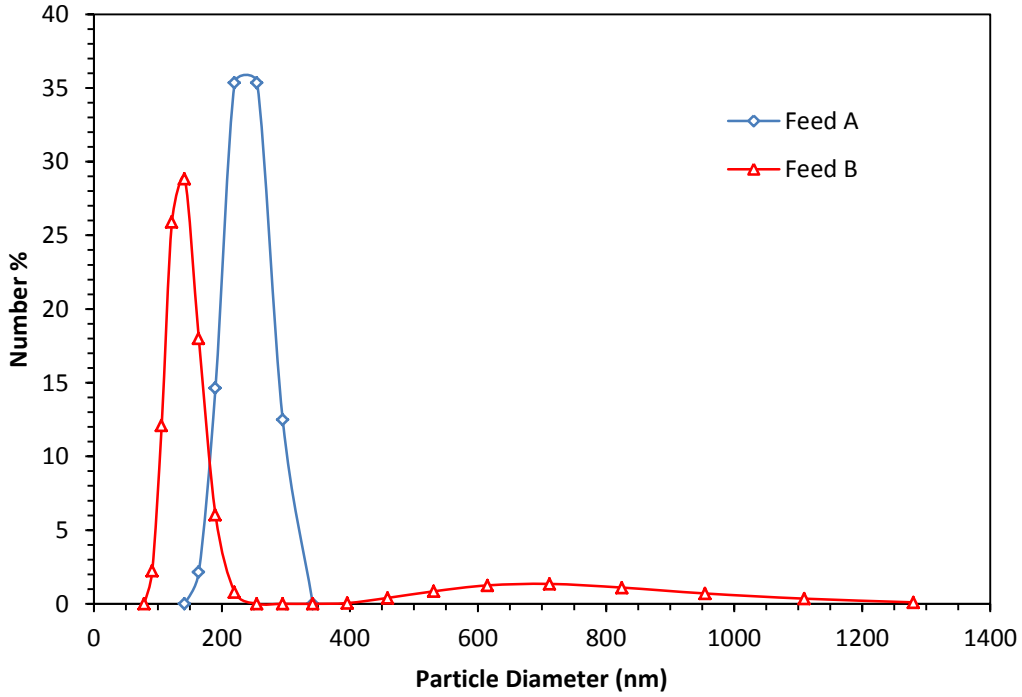

Figure 6.4: Particle size distribution of SAGD produced water feeds obtained from suppliers A and B.

The size of these particles also governs their back-transport away from the membrane surface during crossflow filtration. Particle diffusivity is comprised of components caused by Brownian motion and shear-induced diffusion. Brownian diffusivity (m^2/s) can be calculated by the Stokes-Einstein equation:

$$D_B = \frac{k_B T}{3\pi\mu d_P} \quad (6.4)$$

where k_B is the Boltzmann constant (J/K), T is temperature (K), μ is dynamic viscosity (Pa·s) and d_P is particle diameter (m). For low particle concentration, shear-induced diffusivity (m^2/s) can be obtained using the following equation [34]:

$$D_S = 0.02\dot{\gamma}r_P^2 \tag{6.5}$$

where $\dot{\gamma}$ is shear rate (s^{-1}) and r_p is particle radius (m). The effect of particle size on combined Brownian and shear-induced diffusivity is depicted in Figure 6.5, with the particle size distributions of feeds A and B superimposed. It is seen that the particles in both feeds possess sizes that are positioned in the region of minimum back-transport diffusivity. Furthermore, particle sizes in feed B (79–255 nm) correspond to lower diffusivities than particle sizes in feed A (142–342 nm), and are closer to the minimum diffusivity value at approximately 116 nm. It is thus expected that convection towards the membrane surface due to permeate drag flow experienced by these particulates would be significantly greater than their back-transport diffusion, thus causing substantial membrane fouling.

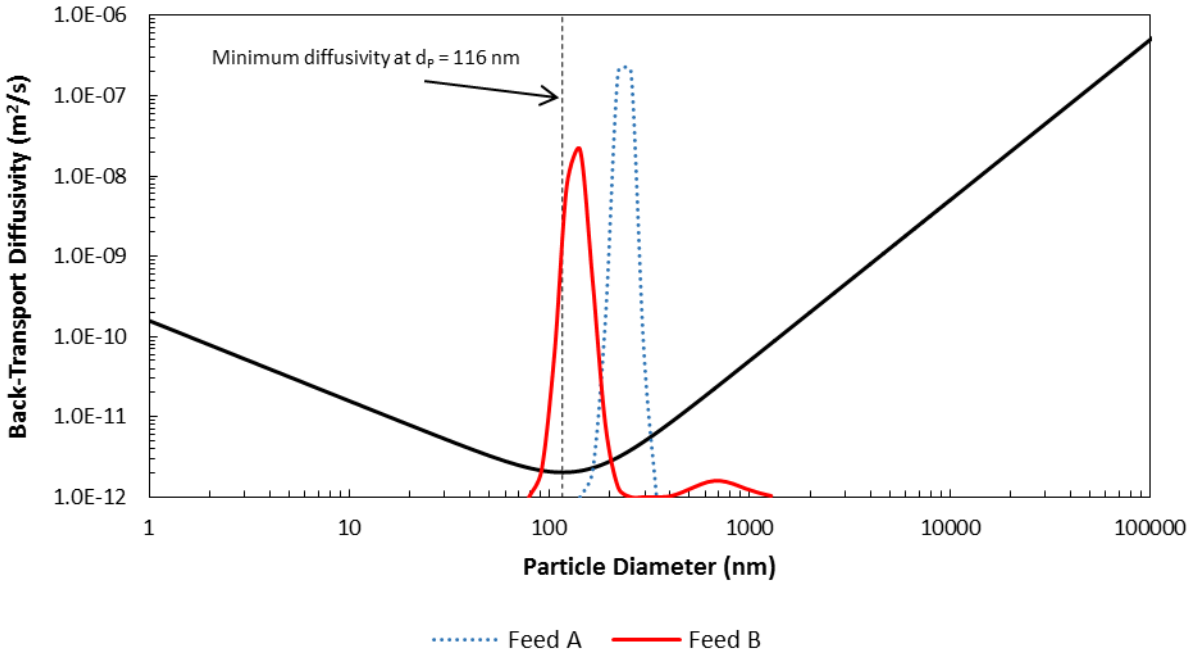

Figure 6.5: Back-transport diffusivity as a function of particle diameter.

6.3.3 Effect of transmembrane pressure

In Figure 6.6, the flux performance over time for 5 nm Ti-Al and Ti-Ti membranes tested in parallel is shown with varying TMP. The membranes were first tested for 8.6 hours at a TMP of

35 psi, followed by 8.3 hours at both a TMP of 50 and 75 psi for a total of approximately 25.2 hours. At 35 psi, neither membrane exhibited flux decline. The flux of the 5 nm Ti-Al membrane remained steady at a value in the vicinity of 100 Lmh, while the flux of the 5 nm Ti-Ti membrane rose steadily from 70 Lmh to 90 Lmh. The lack of flux decrease with time indicates that at this pressure there was no formation of a cake layer at the surface of the membranes. When the TMP was increased to 50 psi, permeate fluxes declined at an initial rate of 4 and 3.3 Lmh/h for the 5 nm Ti-Al and 5 nm Ti-Ti, respectively, over the first 4 hours of filtration at this pressure. The fluxes then stabilized at approximately 184 Lmh (5 nm Ti-Al) and 154 Lmh (5 nm Ti-Ti). The brief flux decline prior to stabilization is due to an increase in the thickness of the concentration polarization layer at the membrane surface with increasing pressure. Nonetheless, the lack of persistent flux decline indicates that surface cake formation was limited for either membrane with the fluxes achieved at a TMP of 50 psi. When the TMP was subsequently increased to 75 psi for the final portion of the filtration test, consistent flux decline behaviour was observed for both membranes. The flux of the 5 nm Ti-Al membrane decreased at a rate of 8.5 Lmh/h during the first 4 hours and at a rate of 13 Lmh/h during the final 4 hours at this pressure. The initial and final flux decline rates of the 5 nm Ti-Ti membrane were 3.3 and 6.8 Lmh/h, respectively. By the end of the test, the fluxes of both membranes had reached 130–150 Lmh and were still declining. This indicates that filter cakes were forming at the membrane surfaces and inhibiting water from permeating through the membranes. Furthermore, it can be determined that the critical flux for these membranes lies somewhere between the stable fluxes observed at 50 psi and the initial fluxes observed at 75 psi. For the 5 nm Ti-Al membrane, the value of the critical flux is between 184 and 227 Lmh. For the 5 nm Ti-Ti membrane, the critical flux is between 154 and 212 Lmh. The critical flux is defined as the maximum permeate flux at which there is no cake layer formation at the membrane surface.

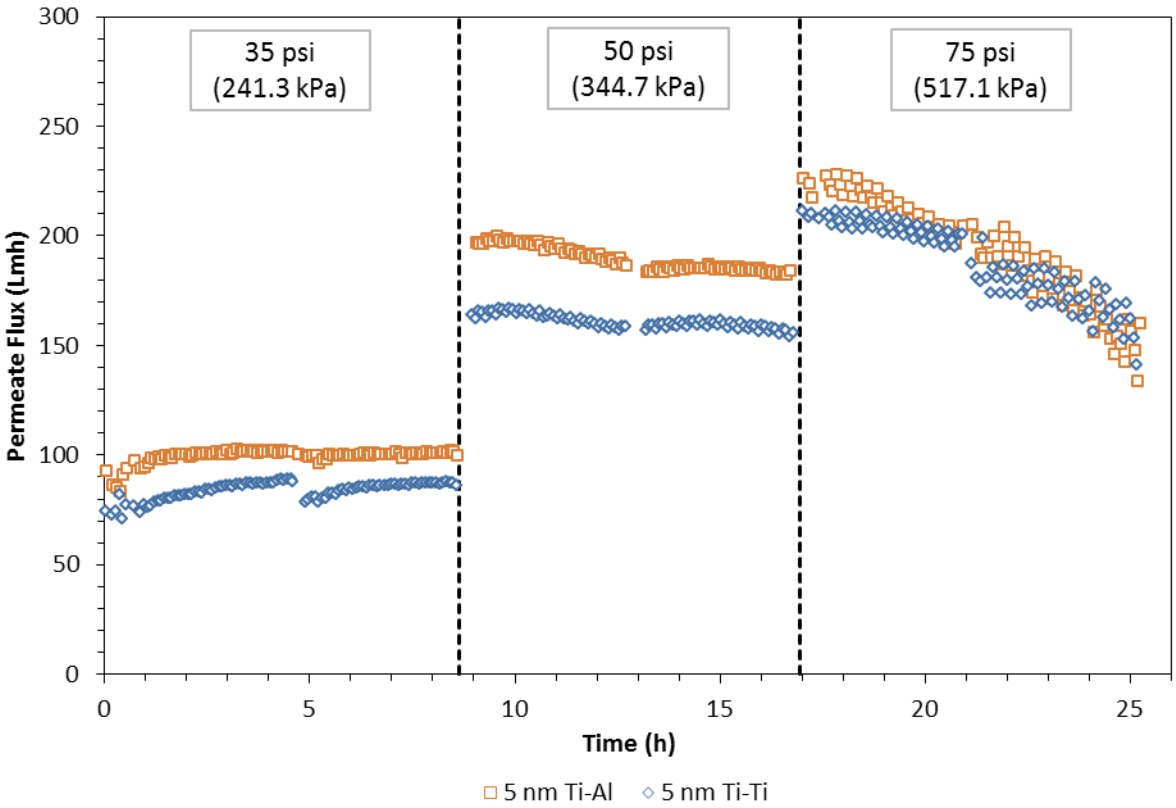

Figure 6.6: Flux as function of time for 5 nm Ti-Al and 5 nm Ti-Ti membranes at TMPs of 35, 50 and 75 psi with Feed B2. CFV: 1.04 ± 0.02 m/s (5 nm Ti-Al), 1.03 ± 0.02 m/s (5 nm Ti-Ti).

The effect of TMP on the separation performance of these membranes is shown in Figure 6.7. Total oil rejection was elevated and unaffected by TMP, with values ranging from 98.1–99.4% for both membranes. When transitioning from a TMP of 35 to 50 psi, TOC rejection declined from 76% to 69% (5 nm Ti-Al) and 72% (5 nm Ti-Ti); however, TOC rejection remained unchanged when TMP was increased to 75 psi. Increase in TMP did not have significant effects on sulphate separation for either membrane, with rejection values between 51–57%. The same conclusion was reached for chloride separation, where low rejection values of 12–17% were observed, as is expected of ultrafiltration membranes with pore sizes that are much larger than chloride salts (e.g., NaCl).

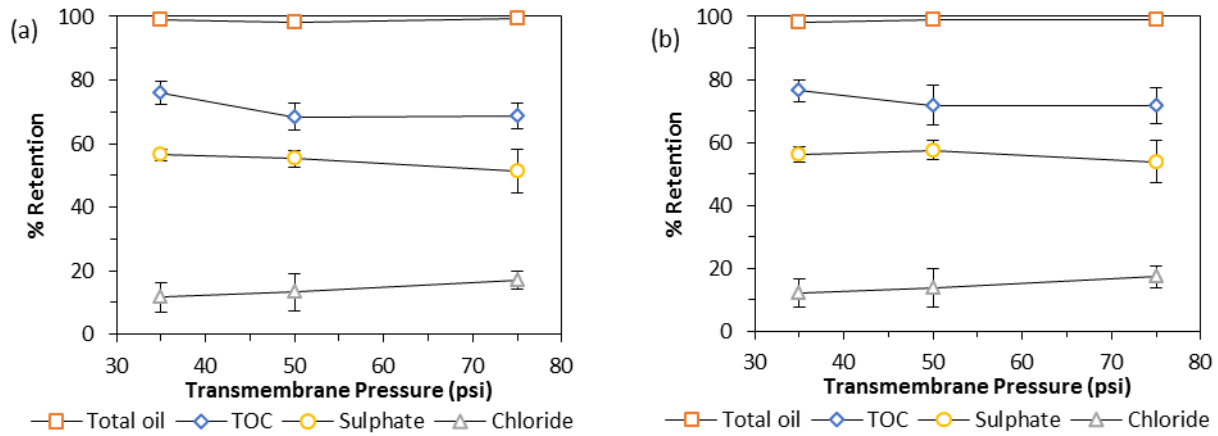

Figure 6.7: Percent retention of total oil, TOC, sulphates and chlorides as function of TMP for (a) 5 nm Ti-Al and (b) 5 nm Ti-Ti membrane with Feed B2. TOC, chloride and sulphate were measured after filtration through a 0.45 µm filter.

6.3.4 Effect of crossflow velocity

The permeate flux over time for 10 nm Ti-Ti and Ti-Al membranes at varying crossflow velocities is shown in Figure 6.8. The membranes were initially tested at CFV values of approximately 0.44, 0.23 and 1 m/s for 4 hours per test. During the first 4 hours at a CFV of 0.44 m/s, the average fluxes of the 10 nm Ti-Ti and Ti-Al membranes were approximately 300 and 190 Lmh, respectively. When the CFV was decreased to 0.23 m/s, the flux of the 10 nm Ti-Ti membrane declined to 170 Lmh, while that of the Ti-Al membrane declined to an average of 125 Lmh. Finally, as the CFV was raised to 1 m/s, permeate fluxes increased to 350 Lmh (10 nm Ti-Ti) and 210 Lmh (10 nm Ti-Al). The observed increase in permeate flux with increasing CFV was due to a reduction in concentration polarization. At higher CFV, turbulence and mixing increased in the diffusion boundary layer near the membrane surface. This reduced the thickness of the concentration polarization layer, leading to an increase in permeate flux.

After 12 hours, the CFV was readjusted to 0.44 m/s and the steam regeneration technique was disabled for the final 4-hour filtration test. The flux of the Ti-Ti membrane declined to a relatively constant value of 260 Lmh, compared to 300 Lmh when steam regeneration was applied at this CFV. The flux of the Ti-Al membrane declined continuously to a value of 90 Lmh after 4 hours, compared to 190 Lmh with steam regeneration. The more severe decline in flux performance that was observed with the Ti-Al membrane, compared to the Ti-Ti membrane, upon deactivation of the steam is due to the difference in support material. Alumina, an amphoteric metal oxide, is known to be a strong adsorbent for asphaltenes. Asphaltenes are

complex and highly viscous organics that are abundant in the bitumen fraction of oil sands produced water [35]. The maximum adsorption capacity at 25 °C for Athabascan asphaltenes on γ-Al_2O_3, the support material of the Ti-Al membrane, is 2.27 mg/m^2 [36]. Acidic metal oxides, conversely to their amphoteric counterparts, are less active adsorbents towards asphaltenes. Titania, an acidic oxide and the support material of the Ti-Ti membrane, possesses a maximum Athabascan asphaltene adsorption capacity of 0.54 mg/m^2 at 25 °C [37]. γ-Al_2O_3 is thus capable of adsorbing more asphaltenes than TiO_2 by a factor of 4.20. Without periodic steam exposure to regenerate the membranes, the Ti-Al membrane experienced more severe fouling due to the higher asphaltene adsorption capacity on alumina compared to titania.

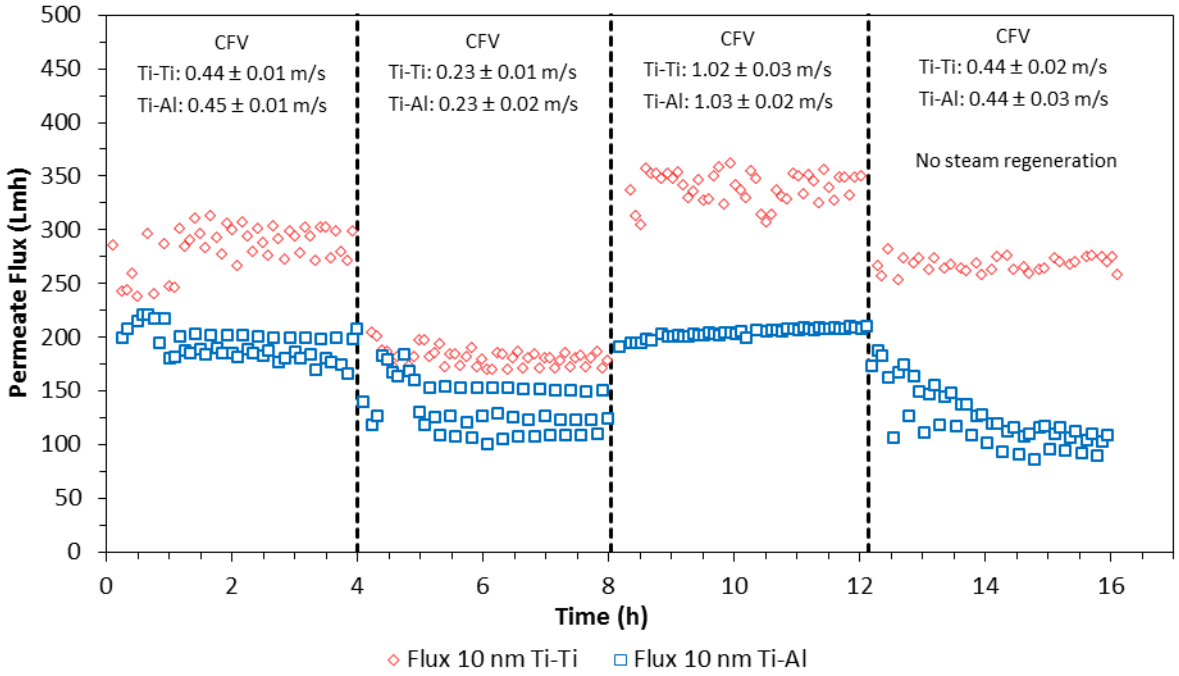

Figure 6.8: Permeate flux as a function of time for 10 nm Ti-Ti and 10 nm Ti-Al membranes at varying crossflow velocities with Feed A3. TMP: 50 psi (344.7 kPa).

The effect of CFV on membrane separation performance of TOC, sulphates and chlorides is shown in Figure 6.9. The separation data presented corresponds to the first 12 hours of the filtration test, where both backflushing and steam regeneration were applied. It was observed that the highest retention percentages for all species were attained at the highest tested CFV of 1 m/s. Higher flux and separation performance was thus observed at a CFV value of 1 m/s, and all subsequent filtration tests were performed under this condition. At this CFV, the 10 nm Ti-Ti membrane yielded retention percentages of 60%, 47% and 12% for TOC, sulphates and chlorides,

respectively. Similarly, the 10 nm Ti-Al membrane yielded retention percentages of 80%, 70% and 19% for TOC, sulphates and chlorides, respectively. Similarly to the observed flux improvement, the superior separation performance at higher CFV values was attributed to the mitigation of concentration polarization. As a result of reducing the thickness of the concentration polarization layer, solute accumulation near the membrane surface was also reduced, which led to lower solute concentrations in the permeate samples.

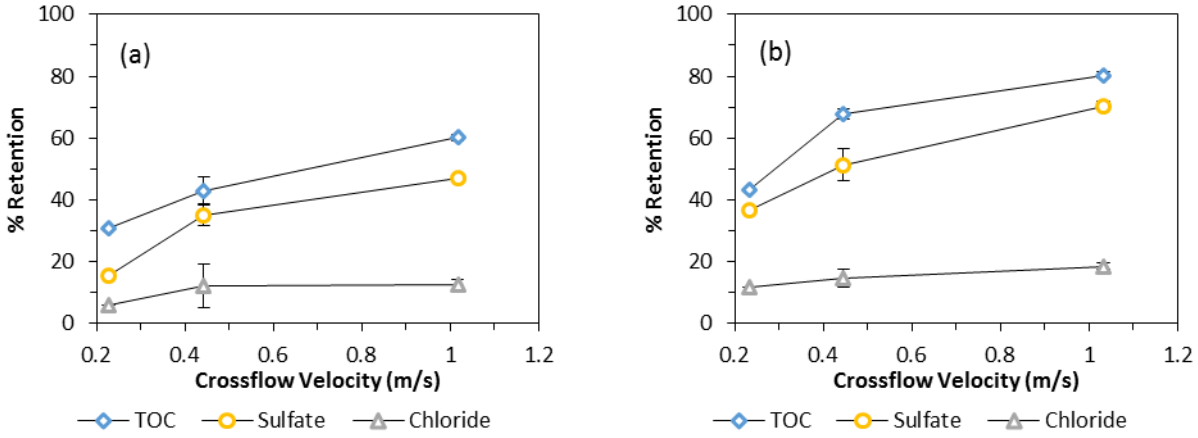

Figure 6.9: Percent retention of TOC, sulphates and chlorides as a function of crossflow velocity for (a) 10 nm Ti-Ti and (b) 10 nm Ti-Al membranes with Feed A3. TMP: 50 psi (344.7 kPa). TOC, chloride and sulphate were measured after filtration through a 0.45 µm filter.

6.3.5 Effect of steam regeneration technique on membrane performance

Three side-by-side filtration tests were conducted that demonstrate the effect of implementing the steam regeneration technique as a means of membrane regeneration. Each test was conducted with a different produced water feed. In the first two tests, Ti-Al membranes with pore sizes of 5 and 10 nm were tested in parallel. In the third test, 5 nm membranes with different support material (Ti-Al vs Ti-Ti) were tested in parallel. Table 6.2 gives the operational conditions of each of these experiments. The experiments were performed in intervals of 2 to 4 hours, with total durations ranging from 20.5 to 28 hours with a single feed.

Table 6.2: Experimental conditions of produced water filtration tests with initially only permeate backflushing followed by both backflushing and steam regeneration.

Test #	TMP (psi/kPa)	Feed temperature (°C)	Feed label	Filtration time (h)	Membrane 1	Membrane 2
1	50/344.7	80–85 °C	A1	Total: 28 Backflushing only: 20 Steam regeneration: 8	10 nm Ti-Al	5 nm Ti-Al
2	50/344.7	80–85 °C	B1	Total: 20.5 Backflushing only: 12.5 Steam regeneration: 8	10 nm Ti-Al	5 nm Ti-Al
3	50/344.7	80–85 °C	B2	Total: 25.75 Backflushing only: 9.25 Steam regeneration: 16.5	5 nm Ti-Al	5 nm Ti-Ti

The flux performance over time of the membranes utilized in these tests is shown in Figure 6.10. In the case of test #1 (Figure 6.10a), the initial fluxes of the 10 and 5 nm membranes were 336 and 320 Lmh, respectively. Over the course of the first 4 hours of filtration, the flux of both membranes rapidly declined to values of approximately 100–110 Lmh. At the end of the 20 hours of filtration without steam regeneration, the fluxes remained in this range. No significant impact of pore size (5 vs 10 nm) was observed in the treatment of SAGD produced water feed A1. After 20 hours, the steam regeneration technique was activated and the system was operated for an additional 8 hours. The fluxes of both membranes immediately increased to 135–145 Lmh from their previous values of approximately 110 Lmh. By the end of the filtration test, the flux of the 5 nm membrane had risen to 167 Lmh, corresponding to an increase by a factor of 1.52. Similarly, the flux of the 10 nm membrane rose to 155 Lmh, corresponding to an increase by a factor of 1.41 with steam regeneration active.

In the case of test #2 (Figure 6.10b), identical membranes to those used in test #1 were applied in the filtration of SAGD produced water feed B1. Similarly to test #1, no significant effect of pore size (5 vs 10 nm) was observed. The membranes initially gave fluxes of 273 Lmh, which declined quickly to approximately 110 Lmh during the first 4 hours of filtration. Membrane fluxes remained in the range of 100–110 Lmh throughout the remainder of the 12.5 hours of filtration without steam regeneration. The steam regeneration technique was subsequently activated for an additional 8 hours of produced water filtration. During the first 4 hours with active steam, the flux of both membranes gradually increased to 165–170 Lmh. The gradual increase, as opposed to the sudden increase observed in test #1, could be caused by the higher

TOC, alkalinity, chloride and pH of feed B1 relative to feed A1, as previously discussed in section 6.3.2. By the end of the filtration test, permeate flux had risen to 215 Lmh for the 5 nm membrane and 200 Lmh for the 10 nm membrane, corresponding to an increase by factors of 2.01 and 1.94, respectively. In test #2, the membranes were used without steam regeneration for 12.5 hours, compared to 20 hours in test #1. Less filtration time without the efficient foulant removal of steam regeneration resulted in less irreversible fouling during test #2. Thus, flux increase upon steam activation was higher for test #2, since foulant cakes at the membrane surfaces were more easily removed compared to test #1.

In the case of test #3 (Figure 6.10c), 5 nm Ti-Al and Ti-Ti membranes were tested side-by-side in the filtration of SAGD produced water feed B2. Without steam regeneration, the initial fluxes of the membranes were 102 Lmh (Ti-Al) and 86 Lmh (Ti-Ti). During the first 4 hours, membrane fluxes declined rapidly at rates of 18 Lmh/h for the Ti-Al membrane and 12 Lmh/h for the Ti-Ti membrane. The higher flux decline rate of the Ti-Al membrane was explained by the higher propensity of alumina to adsorb asphaltenes relative to titania, as previously discussed in section 6.3.4. The membranes were tested for 7.2 hours without steam regeneration, compared to 20 and 12.5 hours in the previous tests. By the end of these 7.2 hours, membrane fluxes had decreased to 44–53 Lmh. Upon activation of the steam regeneration technique, permeate flux increased to approximately 200 Lmh for the Ti-Al membrane and 167 Lmh for the Ti-Ti membrane, corresponding to improvement factors of about 3.76–3.80. The higher increase in performance with steam regeneration observed in test #3 compared to the previous tests was attributed to the fact that filtration time without active steam was reduced (7.2 vs 20 and 12.5 hours). During the next 8.3 hours of filtration with steam regeneration, the fluxes of both membranes stabilized at approximately 184 Lmh (Ti-Al) and 158 Lmh (Ti-Ti). Once the fluxes were stable, the steam was again deactivated, as seen in Figure 6.10c, for 2 hours. During these 2 hours, fluxes were no longer stable and began declining at rates of 7 Lmh/h for the Ti-Al membrane and 5 Lmh/h for the Ti-Ti membrane. Periodic steam regeneration was subsequently reactivated for the final 8 hours of filtration. During these 8 hours, membrane fluxes initially increased slightly before stabilizing at values of approximately 165 Lmh (Ti-Al) and 150 Lmh (Ti-Ti).

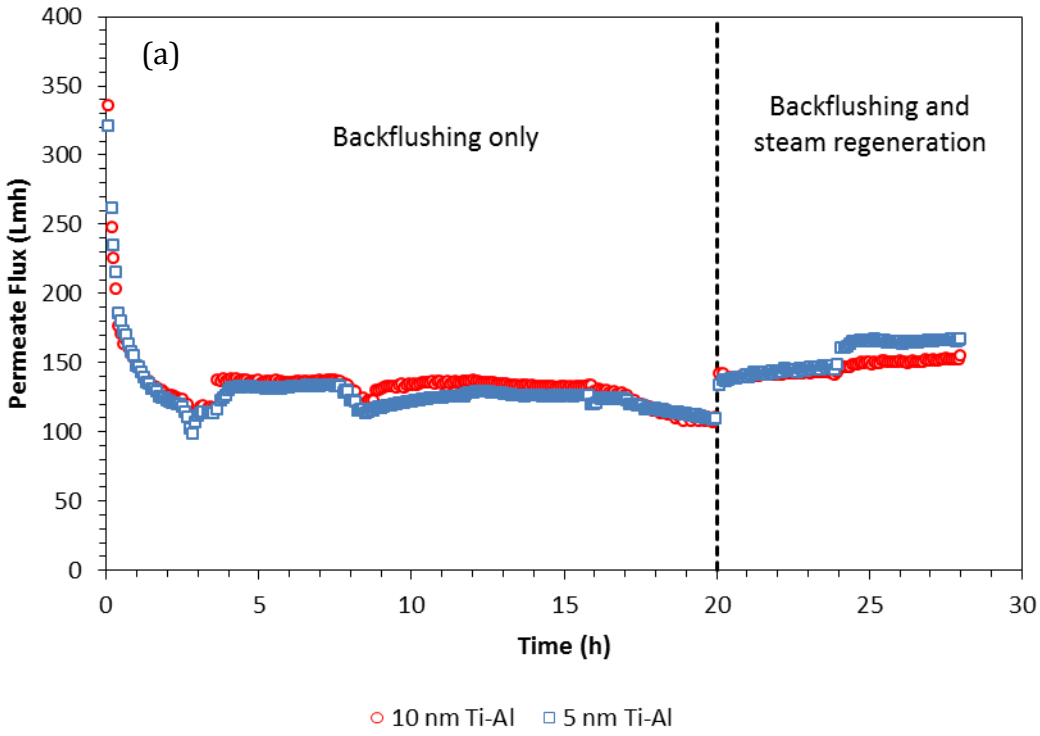

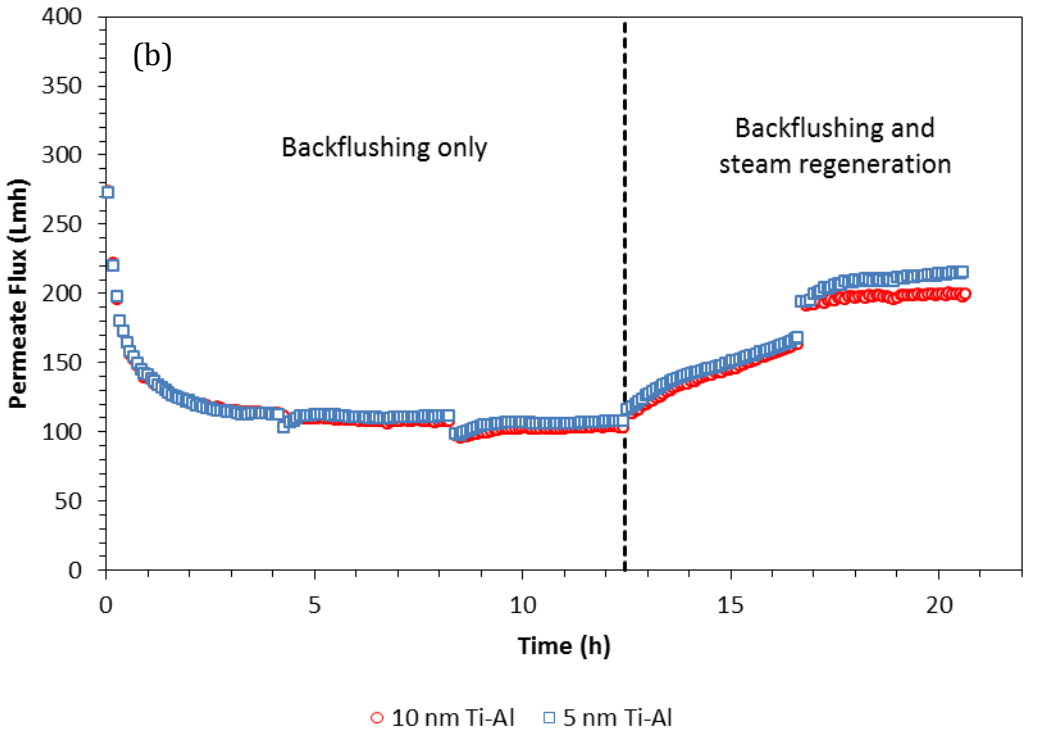

Figure 6.10 (continued next page)

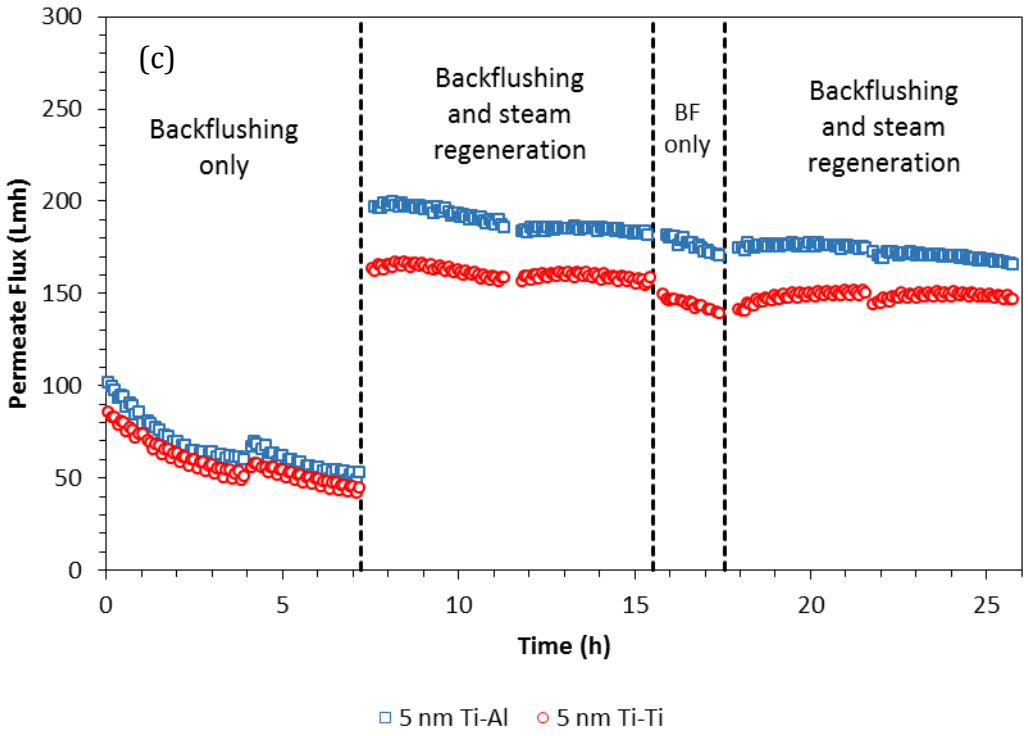

Figure 6.10: Permeate flux as a function of time for the filtration tests outlined in Table 6.2. (a) Test #1, (b) Test #2 and (c) Test #3. Temperature: 80–85 °C. TMP: 50 psi (344.7 kPa).

The success of the steam regeneration technique in increasing membrane flux performance, as demonstrated by the results of the filtration tests shown in Figure 6.10, was attributed to the substantial temperature dependence of bitumen viscosity. When steam was periodically injected into the feed channels of the membranes, the foulant cake was directly and rapidly heated, which resulted in a sudden change in the viscosity of its constituents. The majority of foulants in the filter cakes at the membrane surface in this application are bituminous solids that were initially suspended in the produced water feed. The dynamic viscosities of Athabasca bitumen [38] at three temperatures of interest (25, 85 and 120 °C) are shown in Table 6.3. It is seen that the bitumen viscosity at room temperature (25 °C) is higher than that at the feed temperature (85 °C) by a factor of 1600, emphasising the advantage of treating the produced water feed at this temperature. Furthermore, bitumen viscosity at the steam temperature of 120 °C is lower than that at the feed temperature (85 °C) by a factor of 19. Therefore, with each application of the steam regeneration technique, the viscosity of the filter cake is significantly reduced for the duration of the steam exposure time. This briefly renders the cake more mobile, allowing for its more efficient release from the membrane surface.

Table 6.3: Viscosity of Athabasca bitumen as a function of temperature [38].

Temperature (°C)	Viscosity (Pa·s)	Comment
25	4000	Room temperature
85	2.5	Feed temperature
120	0.13	Steam temperature

The effect of the steam regeneration technique on membrane separation of total oil, TOC, sulphates and chlorides is presented in Figure 6.11. Total oil separation ranged from 96.6–99.3% and no significant change was observed when steam regeneration was activated. In all cases, an increase in the retention percentages of TOC, sulphates and chlorides was observed when steam regeneration was applied as a means of fouling remediation. This indicates that the application of steam regeneration reduced the concentration of these substances in the filter cakes. The largest improvements in separation performance were obtained during test #1 (Figure 6.11a), where feed A1 was used. This produced water feed was previously shown to contain less severe membrane foulants compared to feeds B1 and B2, which were used in the other two filtration tests. These results indicate that the periodic direct injection of steam into the membrane feed channels as a method of fouling alleviation improved both the flux and separation performance of the ceramic membranes in the treatment of oil sands produced water.

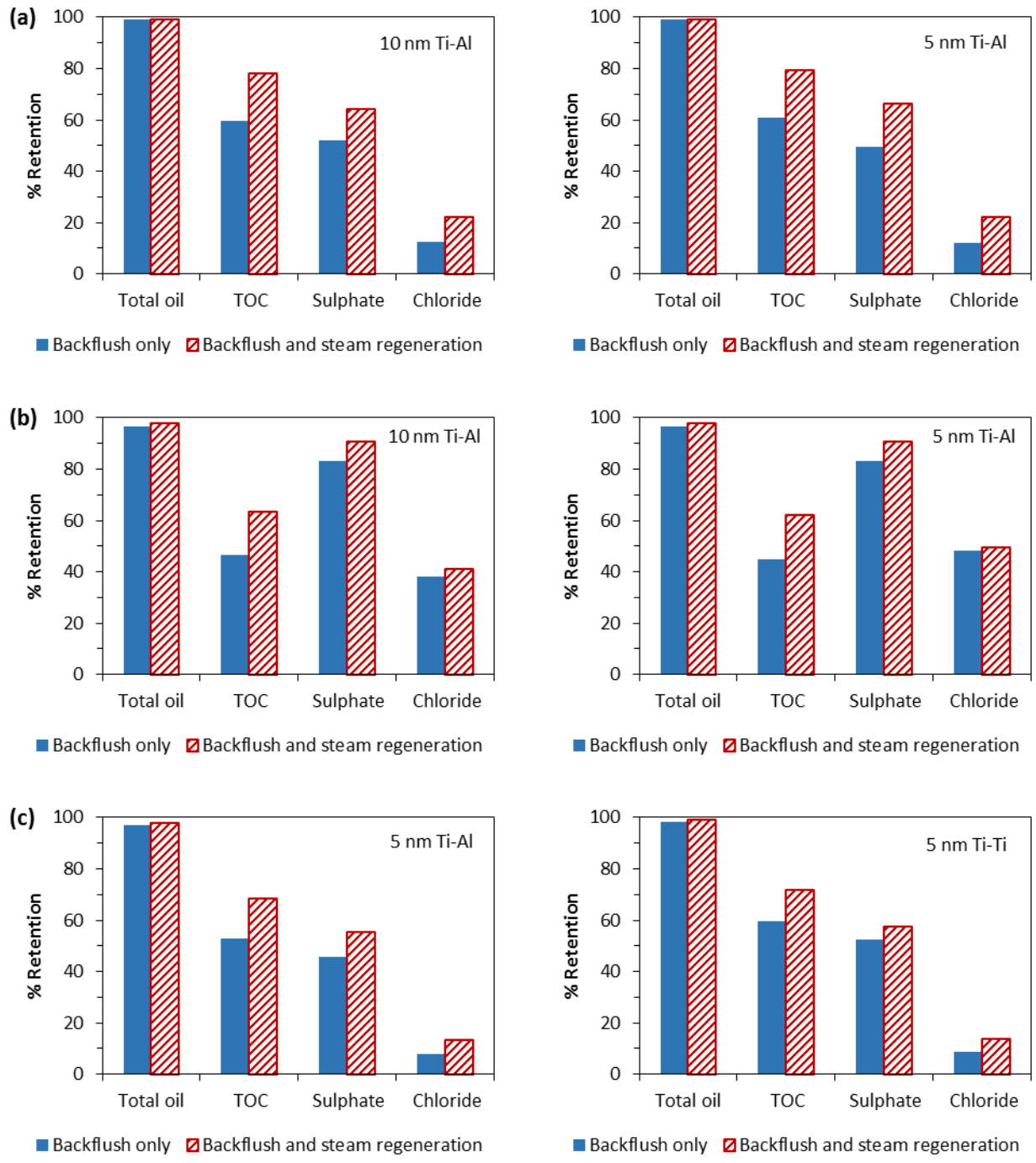

Figure 6.11: Percent retention of total oil, TOC, sulphates and chlorides for the filtration tests outlined in Table 6.2. (a) Test #1, (b) Test #2 and (c) Test #3. Temperature: 80–85 °C. TMP: 50 psi (344.7 kPa). TOC, chloride and sulphate were measured after filtration through a 0.45 µm filter.

6.4 Conclusions

Commercially available tubular titania ceramic membranes were applied in the treatment and recycling of produced water originating from various SAGD facilities operating in the Canadian oil sands. In each filtration experiment, two membranes with either a different pore size (5 or 10 nm) or different support material (γ-Al_2O_3 or TiO_2) were tested in parallel under the same feed, temperature and pressure conditions. During operation, the membranes were periodically cleaned by applying conventional permeate backflushing, as well as by implementing a novel steam regeneration technique. This technique involved the direct periodic injection of steam into the membrane feed channels.

Several tests were conducted where the membranes were initially utilized without the steam regeneration technique, followed by the activation of periodic steam injection in order to assess its effect on membrane performance. It was found that the duration of the initial filtration time without steam regeneration influences the capability of the steam regeneration method in improving membrane flux. The highest flux improvement factor of 3.80 was observed when the membranes were initially only tested for 7.2 hours, while the lowest improvement factor of 1.41 was observed when the membranes were tested for 20 hours before periodic steam injection was initiated. In all cases, the inclusion of the steam regeneration technique leads to an increase in membrane flux, as well as separation performance. This was attributed to the rapid and direct heating of the foulant cake at the membrane surface, which significantly reduces cake viscosity and facilitates its release and removal from the surface.

The benefits of the steam regeneration technique were demonstrated in this work. The membrane regeneration method will minimize the production of cleaning wastewaters or residues in the operation of the membrane system. Backflushed filter cakes containing oleophilic bituminous fines can be returned to a separator/flotation unit upstream of the membrane system where they will be entrained in the main oil stream. The result will be a reduction in the production of cleaning wastewaters. This is a tremendous advantage particularly in remote areas where wastewaters produced when membranes are chemically cleaned need to be transported and treated off-site.

References

[1] E.I. Nduagu, I.D. Gates, Unconventional Heavy Oil Growth and Global Greenhouse Gas Emissions, Environmental Science & Technology. 49 (2015) 8824–8832.

[2] S. Huang, R.H.A. Ras, X. Tian, Antifouling membranes for oily wastewater treatment: Interplay between wetting and membrane fouling, Current Opinion in Colloid and Interface Science. 36 (2018) 90–109.

[3] M. Nasiri, I. Jafari, B. Parniankhoy, Oil and Gas Produced Water Management: A Review of Treatment Technologies, Challenges, and Opportunities, Chemical Engineering Communications. 204 (2017) 990–1005.

[4] E.W. Allen, Process water treatment in Canada's oil sands industry: I. Target pollutants and treatment objectives, Journal of Environmental Engineering and Science. 7 (2008) 123–138.

[5] S. Jiménez, M.M. Micó, M. Arnaldos, F. Medina, S. Contreras, State of the art of produced water treatment, Chemosphere. 192 (2018) 186–208.

[6] G. Hurwitz, D.J. Pernitsky, S. Bhattacharjee, E.M.V. Hoek, Targeted Removal of Dissolved Organic Matter in Boiler-Blowdown Wastewater: Integrated Membrane Filtration for Produced Water Reuse, Industrial & Engineering Chemistry Research. 54 (2015) 9431–9439.

[7] G.N. Vatai, D.M. Krstic, A.K. Koris, I.L. Gáspár, M.N. Tekic, Ultrafiltration of oil-in-water emulsion: Comparison of ceramic and polymeric membranes, Desalination and Water Treatment. 3 (2009) 162–168.

[8] S.M. Samaei, S. Gato-Trinidad, A. Altaee, The application of pressure-driven ceramic membrane technology for the treatment of industrial wastewaters – A review, Separation and Purification Technology. 200 (2018) 198–220.

[9] C. Atallah, S. Mortazavi, A.Y. Tremblay, A. Doiron, Surface-Modified Multi-lumen Tubular Membranes for SAGD-Produced Water Treatment, Energy & Fuels. 33 (2019) 5766–5776.

[10] M. Ebrahimi, S. Kerker, O. Schmitz, A.A. Schmidt, P. Czermak, Evaluation of the fouling potential of ceramic membrane configurations designed for the treatment of oilfield produced water, Separation Science and Technology. 53 (2018) 349–363.

[11] C. Atallah, A.Y. Tremblay, S. Mortazavi, Silane Surface Modified Ceramic Membranes for the Treatment and Recycling of SAGD Produced Water, Journal of Petroleum Science and Engineering. 157 (2017) 349–358.

[12] Y. Thibault, J. Gamage McEvoy, S. Mortazavi, D. Smith, A. Doiron, Characterization of fouling processes in ceramic membranes used for the recovery and recycle of oil sands produced water, Journal of Membrane Science. 540 (2017) 307–320.

[13] T. Zsirai, A.K. Al-Jaml, H. Qiblawey, M. Al-Marri, A. Ahmed, S. Bach, S. Watson, S. Judd, Ceramic membrane filtration of produced water: Impact of membrane module, Separation and Purification Technology. 165 (2016) 214–221.

[14] A. Guirgis, R. Gay-de-Montella, R. Faiz, Treatment of produced water streams in SAGD processes using tubular ceramic membranes, Desalination. 358 (2015) 27–32.

[15] S.E. Weschenfelder, A.M.T. Louvisse, C.P. Borges, E. Meabe, J. Izquierdo, J.C. Campos, Evaluation of ceramic membranes for oilfield produced water treatment aiming reinjection in offshore units, Journal of Petroleum Science and Engineering. 131 (2015) 51–57.

[16] K. Loganathan, P. Chelme-Ayala, M.G. El-Din, Effects of different pretreatments on the performance of ceramic ultrafiltration membrane during the treatment of oil sands tailings pond recycle water : A pilot-scale study, Journal of Environmental Management. 151 (2015) 540–549.

[17] R.G. Pillai, N. Yang, S. Thi, J. Fatema, M. Sadrzadeh, D. Pernitsky, Characterization and Comparison of Dissolved Organic Matter Signatures in Steam-Assisted Gravity Drainage Process Water Samples from Athabasca Oil Sands, Energy & Fuels. 31 (2017) 8363–8373.

[18] J. Fatema, S. Bhattacharjee, D. Pernitsky, A. Maiti, Study of the Aggregation Behavior of Silica and Dissolved Organic Matter in Oil Sands Produced Water Using Taguchi Experimental Design, Energy & Fuels. 29 (2015) 7465–7473.

[19] M.A. Petersen, H. Grade, Analysis of Steam Assisted Gravity Drainage Produced Water using Two-Dimensional Gas Chromatography with Time-of-Flight Mass Spectrometry, Industrial & Engineering Chemistry Research. 50 (2011) 12217–12224.

[20] B.D. Sparks, L.S. Kotlyar, J.B. O'Carroll, K.H. Chung, Athabasca oil sands: effect of organic coated solids on bitumen recovery and quality, Journal of Petroleum Science and Engineering. 39 (2003) 417–430.

[21] A. Jada, M. Salou, Effects of the asphaltene and resin contents of the bitumens on the water-bitumen interface properties, Journal of Petroleum Science and Engineering. 33 (2002) 185–193.

[22] E.W. Allen, Process water treatment in Canada's oil sands industry: II. A review of emerging technologies, Journal of Environmental Engineering and Science. 7 (2008) 499–524.

[23] M. Abdalla, M. Nasser, A. Kayvani Fard, H. Qiblawey, A. Benamor, S. Judd, Impact of combined oil-in-water emulsions and particulate suspensions on ceramic membrane fouling and permeability recovery, Separation and Purification Technology. 212 (2019) 215–222.

[24] M.A. Petersen, C.S. Henderson, A.Y. Ku, A.Q. Sun, D.J. Pernitsky, Oil sands steam-assisted gravity drainage process water sample aging during long-term storage, Energy & Fuels. 29 (2015) 2034–2041.

[25] A.Y. Ku, C.S. Henderson, M.A. Petersen, D.J. Pernitsky, A.Q. Sun, Aging of Water from Steam-Assisted Gravity Drainage (SAGD) Operations Due to Air Exposure and Effects on Ceramic Membrane Filtration, Industrial & Engineering Chemistry Research. 51 (2012) 7170–7176.

[26] E. Garmsiri, Y. Rasouli, M. Abbasi, A.A. Izadpanah, Chemical cleaning of mullite ceramic microfiltration membranes which are fouled during oily wastewater treatment, Journal of Water Process Engineering. 19 (2017) 81–95.

[27] T. Zsirai, H. Qiblawey, P. Buzatu, M. Al-Marri, S.J. Judd, Cleaning of ceramic membranes for produced water filtration, Journal of Petroleum Science and Engineering. 166 (2018) 283–289.

[28] R. Sondhi, R. Bhave, G. Jung, Applications and benefits of ceramic membranes, Membrane Technology. 2003 (2003) 5–8.

[29] D.S. Dlamini, N.P. Khumalo, S. Zwane, A.K. Mishra, B.B. Mamba, Chemistry behind the performance of ceramic membranes and their future in membrane technology, in: A.K. Mishra (Ed.), Smart Ceramics: Preparation, Properties, and Applications, 1st ed., Pan Stanford Publishing Pte. Ltd., New York, 2018: p. 260.

[30] Standard Methods for the Examination of Water and Wastewater, (1999).

[31] M. Holmes, S. Gupta, P. McKay, S. Ren, Integrated One-Step Process for Oil Water Separation

and Produced-Water Treatment, in: SPE Canada Heavy Oil Technical Conference, Society of Petroleum Engineers, Calgary, Alberta, 2016: p. SPE-180691-MS.

[32] T. Al-Shemmeri, Engineering Fluid Mechanics, Ventus Publishing ApS, 2012.

[33] H. Kawaguchi, Z. Li, Y. Masuda, K. Sato, H. Nakagawa, Dissolved organic compounds in reused process water for steam-assisted gravity drainage oil sands extraction, Water Research. 46 (2012) 5566–5574.

[34] J. Kim, F.A. DiGiano, Fouling models for low-pressure membrane systems, Separation and Purification Technology. 68 (2009) 293–304.

[35] S.E. Taylor, Interfacial Chemistry in Steam-Based Thermal Recovery of Oil Sands Bitumen with Emphasis on Steam-Assisted Gravity Drainage and the Role of Chemical Additives, Colloids and Interfaces. 2 (2018) 16.

[36] N.N. Nassar, Asphaltene adsorption onto alumina nanoparticles: Kinetics and thermodynamic studies, Energy & Fuels. 24 (2010) 4116–4122.

[37] N.N. Nassar, A. Hassan, P. Pereira-Almao, Metal oxide nanoparticles for asphaltene adsorption and oxidation, Energy & Fuels. 25 (2011) 1017–1023.

[38] A.B. Bazyleva, A. Hasan, M. Fulem, M. Becerra, J.M. Shaw, Bitumen and heavy oil rheological properties: Reconciliation with viscosity measurements, Journal of Chemical and Engineering Data. 55 (2010) 1389–1397.

7 Modeling of Membrane Filtration and Fouling in the Treatment of Bitumen-containing Wastewater

C. Atallah, A.Y. Tremblay, S. Mortazavi.

Manuscript prepared for submission to a peer-reviewed academic journal

Abstract

Wastewaters containing bitumen are produced in many industries and must be treated prior to recycling or disposal. Ceramic membrane processes are an emerging and efficient technology for the treatment of such waste streams. In order to establish the limitations of ceramic membranes in this application, our understanding of membrane fouling by bituminous particulates must be improved. Fouling of flat and tubular ceramic membranes by oil sands produced water, an example of a bituminous wastewater, was modeled using traditional filtration models as well as various combined models. The single-parameter models were inadequate to represent the experimental data. The combined pore blockage-cake filtration models offered a better fit to the experimental data. The combined models that accounted for pore constriction or intermediate blocking instead of complete blocking mechanisms were found to offer the best fit. The contribution of cake filtration to membrane fouling was found to increase with decreasing pore size, while that of pore blocking showed an opposing trend. Cake thickness values of approximately 20–40 μm were determined from the parameters of the combined models, and the calculated particle diameters in the filter cakes of ~60–200 nm were in good agreement with measured particle size distributions of the feed produced water. The effect of temperature on the formation and mobility of foulant cakes was also modeled. It was determined that flowing cake residence times in membrane modules remained high at temperatures as high as 120°C due to the highly viscous nature of bitumen. Membranes would also need to be operated at temperatures in the vicinity of 105–120°C to minimize stagnant cake formation without backflushing. It is suggested that traditional backflushing should be coupled with a thermal cleaning technique, such as high-temperature steam injection, to remove foulants from inside membrane pores and remove surface cakes in the treatment of bituminous wastewaters.

7.1 Introduction

Bituminous wastewaters are produced globally at a considerable rate during oil and gas extraction, pipeline cleanup services, ocean oil spills, and many other operations. The oil and gas industry labels these waste streams as produced water, and their composition varies significantly depending on geographical location and the utilized extraction technology. Common constituents include inorganic scalants such as clays, silicates and carbonates, as well as dissolved bituminous organics such as complex resins and asphaltenes. A significant amount of the generated produced water is discharged into the environment [1], which raises critical environmental concerns. It has been well documented that this release of produced water can lead to adverse effects such as air pollution and contamination of soil and water resources [2,3]. For this reason, industries often seek, and are sometimes required by law, to recycle a portion of the produced water. In all such processes, the generated wastewater requires significant treatment and purification prior to recycling or disposal.

Many conventional treatment methods exist, including physical, chemical, thermal and biological processes [4]. The use of membrane technology to treat produced water has however been a recent phenomenon. Their high separation efficiency, ease of operation, small footprint and low energy consumption have led many to consider membranes as the most promising technology for oily wastewater treatment [5,6]. Membranes can be mainly classified as being either polymeric or inorganic in nature. Polymeric membranes have comprised the majority of membranes used in the filtration of oily wastewater to-date. In recent decades however, ceramic membranes have been explored as more efficient alternatives owing to their superior durability and chemical and thermal stability when compared to polymeric membranes [7].

Regardless of membrane material, fouling remains a significant disadvantage to the application of membrane processes in produced water treatment. In this application, fouling can occur through the accumulation of oil and solid layers at the membrane surface [8] or by the percolation and entrapment of bitumen into the pores of the membrane's selective layer [9]. Consequently, the flux performance of the membrane will gradually decline as fouling takes place, until eventually rendering the membrane system uneconomical. In response to the fouling phenomenon, much research has been devoted to enhancing the efficiency and prolonging the lifetime of membranes in wastewater treatment [10]. The most common method of fouling

alleviation is chemical cleaning, which entails the use of acidic, caustic or oxidizing aqueous solutions that seek to degrade and remove both organic and inorganic matter that has built up on the membrane surface [11,12]. This however leads to residual wash solutions that require subsequent treatment and disposal. Membrane surfaces can also be chemically modified to produce membranes that are inherently resistant to fouling species in the feed wastewater. Surface modified ceramic membranes have successfully been applied in the filtration of various oily wastewaters in recent years [13–16], but are nonetheless still an emerging technology in this application. Alternatively, physical cleaning techniques such as backflushing can be applied, where permeate is periodically forced back through the membrane pores to the feed side.

The prevailing thermal stability of ceramic membranes gives rise to the possibility of cleaning these membranes using thermal processes [17–19]. Such processes involve exposing the membrane surface to elevated temperatures with the aim of thermally degrading adsorbed foulants. A cleaning technique of this nature offers the advantage of eliminating the use of chemical cleaning agents. Foulants in bituminous wastewaters are highly viscous and adhesive, making them difficult to remove from membrane surfaces at standard operating conditions. Operating temperature is one of the most important parameters in oil sands processes because of its effect on the physicochemical properties of bitumen and other oil sands components [20].

In this work, we sought to examine the fouling mechanisms at play in the treatment of oil sands produced water by ceramic membranes, as well as to theoretically establish the direct influence of temperature on the fouling characteristics of such a feed. This was accomplished through the application of various crossflow ultrafiltration models accounting for pore blocking and cake filtration fouling mechanisms. In modeling the fouling process, hydrodynamic particle transport by both shear-induced and Brownian diffusion were considered. The effect of temperature on foulant cake formation and mobility were determined and discussed. By furthering our understanding of fouling mechanisms and characteristics in the treatment of bituminous wastewaters, valuable insight is provided towards the development of fouling mitigation techniques for this application.

7.2 Filtration modeling

Since fouling remains a significant obstacle to overcome in most membrane treatment processes, mathematical models that are capable of precisely describing flux variation over time are of great interest. The main advantage of utilizing such models is the insight they can provide regarding the fouling mechanisms taking place in membrane applications of interest. Traditionally, four primary filtration models have been applied in constant pressure membrane processes: complete blocking (CB), intermediate blocking (IB), pore constriction (PC) and cake filtration (CF) [21]. The flux decline equations and associated constants of these models are shown in Table 7.1.

Table 7.1: Four traditional membrane filtration models.

Model	Constant	Flux equation	
Complete blocking	$K_{CB} = \frac{\alpha_{CB} A J_o C_b}{N_o}$	$\frac{J}{J_o} = \exp(-K_{CB} t)$	(7.1)
Intermediate blocking	$K_{IB} = \frac{\sigma_{IB} \Delta P}{\mu R_{IB} J_o}$	$\frac{J}{J_o} = (1 + K_{IB} t)^{-1}$	(7.2)
Pore constriction	$K_{PC} = \frac{\alpha_{PC} A J_o C_b}{\pi r_p^2 \delta_c}$	$\frac{J}{J_o} = (1 + K_{PC} t)^{-2}$	(7.3)
Cake filtration	$K_{CF} = \frac{J_o R_c' \phi_o}{R_m(\phi_{max} - \phi_o)}$	$\frac{J}{J_o} = (1 + K_{CF} t)^{-1/2}$	(7.4)

In treating oil-in-water emulsions, the cake filtration model often presents an acceptable fit to experimental flux data [22–25]. However, several authors of late have noted that one model alone cannot accurately and consistently predict fouling behaviour over the entire filtration time [26–28]. It has been suggested that pore blocking phenomena predominate near the onset of filtration when steep flux decline is observed, with an eventual transition to cake formation. In such cases where different fouling mechanisms occur simultaneously, the classical models prove inadequate. This has led to the development of combined models that integrate several mechanisms to more precisely describe temporal flux decline. Combined fouling models have been successfully applied to experimental data obtained from the filtration of many particulate-laden feeds, including whey [29], various biological fluids [30], limed sugarcane juice [31], humic acid [32] and protein solutions [33]. These combined models thus have the potential of accurately describing fouling behaviour in the treatment of bituminous produced water. In the

treatment of oily bilge water, Peng and Tremblay [34] applied a combined complete blocking and cake filtration model that was initially developed by Ho and Zydney [33] to describe protein fouling. The combined model, rearranged in equation (7.5), clearly illustrates the contributions of complete blocking (equation (7.1)) and cake filtration (equation (7.4)). This model was found to offer the best fit under all experimental conditions when compared to the classical models.

$$J(t) = J_o \left[\exp(-K_1 t) + \frac{1 - \exp(-K_1 t)}{(1 + K_3)[1 + K_2(1 + K_3)^{-2}\, t]^{1/2}}\right] \tag{7.5}$$

Where J ($m^3/m^2/s$) is the permeate flux at a given time t (s), J_O ($m^3/m^2/s$) is the initial permeate flux through the clean membrane, K_1, K_2 and K_3 are parameters of the model as described in Peng & Tremblay [34]. Recently, Hou et al. [35] proposed an improved complete blocking-cake filtration combined model. They extended a model initially developed by Bolton et al. [30] to account for the transition from a combined fouling mechanism to an individual cake filtration mechanism. The model is capable of determining this transition point and is shown in equation (7.6).

$$J(t) = \frac{J_o \left[(1 - K)\exp\left(\frac{-K_b}{K_c J_o^2}\left((1 + 2K_c J_o^2 t)^{1/2} - 1\right)\right) + K\right]}{(1 + 2K_c J_o^2 t)^{1/2}} \tag{7.6}$$

Where K, K_b and K_c are parameters of the model.

The combined filtration models and the equations for their respective constants are displayed in Table 7.2. Both the Ho & Zydney and the Hou et al. models were developed by considering fouling by complete pore blocking and cake filtration. However, the ultrafine particulates found in bituminous wastewaters are not likely to completely block membrane pores, as is assumed in the complete blocking model. These foulants are more likely to partially block pores through particle bridging or by adsorption onto the pore walls, as is the case in the intermediate blocking and pore constriction mechanisms, respectively. The model described by equation (7.5) was modified to incorporate intermediate blocking and pore constriction instead of complete blocking.

Table 7.2: Two combined complete blocking-cake filtration models.

Combined model	Constant	Flux equation
Ho & Zydney [33] Peng & Tremblay [34]	$K_1 = \frac{\alpha \Delta P C_b}{\mu R_m}$ $K_2 = \frac{2f' R_c' \Delta P \phi_o}{\mu R_m^2}$ $K_3 = \frac{R_{c0}}{R_m}$	$\frac{J}{J_o} = \exp(-K_1 t) + \frac{1 - \exp(-K_1 t)}{(1 + K_3)[1 + K_2(1 + K_3)^{-2}\, t]^{1/2}}$
Hou et al. [35]	$0 \le K \le 1$ $K_C = \frac{R_c' \phi_o}{J_o R_m (\phi_{max} - \phi_o)}$ $\frac{A}{A_o} = 1 - \frac{K_b}{J_O} V$	$\frac{J}{J_o} = \frac{(1 - K) \exp\left(\frac{-K_b}{K_c J_o^2}\left((1 + 2K_c J_o^2 t)^{1/2} - 1\right)\right) + K}{(1 + 2K_c J_o^2 t)^{1/2}}$

Following the derivation procedure of Ho & Zydney and replacing the contribution of complete blocking by intermediate blocking or pore constriction yields equations (7.7) and (7.8), respectively. Here, the cake resistance (R_c) is given by equation (7.9) as established in Ho & Zydney [33].

$$\frac{J}{J_o} = (1 + K_{IB} t)^{-1} + (1 - (1 + K_{IB} t)^{-1}) \frac{R_m}{R_m + R_c} \tag{7.7}$$

$$\frac{J}{J_o} = (1 + K_{PC} t)^{-2} + (1 - (1 + K_{PC} t)^{-2}) \frac{R_m}{R_m + R_c} \tag{7.8}$$

$$R_c = (R_m + R_{c0}) \left(1 + \frac{2f' R_c' \Delta P \phi_o}{\mu (R_m + R_{c0})^2} t\right)^{1/2} - R_m \tag{7.9}$$

Flux decline equations were obtained by combining equation (7.9) with equations (7.7) and (7.8). The proposed intermediate blocking-cake filtration (IB-CF) model is shown in equation (7.10), and the pore constriction-cake filtration (PC-CF) model is shown in equation (7.11). Note that K_2 and K_3 are independent of the intermediate blocking or pore constriction models.

$$J(t) = J_o \left[(1 + K_{IB} t)^{-1} + \frac{1 - (1 + K_{IB} t)^{-1}}{(1 + K_3)[1 + K_2(1 + K_3)^{-2}\, t]^{1/2}}\right] \tag{7.10}$$

$$J(t) = J_o \left[(1 + K_{PC} t)^{-2} + \frac{1 - (1 + K_{PC} t)^{-2}}{(1 + K_3)[1 + K_2(1 + K_3)^{-2}\, t]^{1/2}} \right] \quad (7.11)$$

In this study, we have applied the four traditional filtration models as well as the four discussed combined models to experimental data from the treatment of field samples of oil sands produced water with ceramic membranes. Flat membrane disks with pore sizes of 0.14 µm, 300 kDa and 150 kDa, as well as a multilumen tubular membrane with a pore size of 5 nm were tested. Detailed information on the produced water feeds, ceramic membranes and filtration procedures can be obtained from our previous work for both the membrane disks [36] and the tubular membrane [37]. The separation performance of these membranes is also detailed in the aforementioned studies, while in this work we have focused on filtration modelling. The produced water samples were obtained from steam-assisted gravity drainage (SAGD) facilities located in Alberta, Canada. In the case of the membrane disks, the membranes were backflushed with permeate at five-minute intervals. The filtration models were fitted to flux data from several backflush cycles. An example of flux versus time data with the fitted classical models is shown in Figure 7.1 for one backflush cycle with the 0.14 µm membrane, while similar examples for the other membranes are found in Appendix A. The root-mean-squared error (RMSE), defined as the square root of the mean square error, is shown in Table 7.3 in flux units of L/m^2/h (Lmh) for the four classical models applied to all of the discussed membranes.

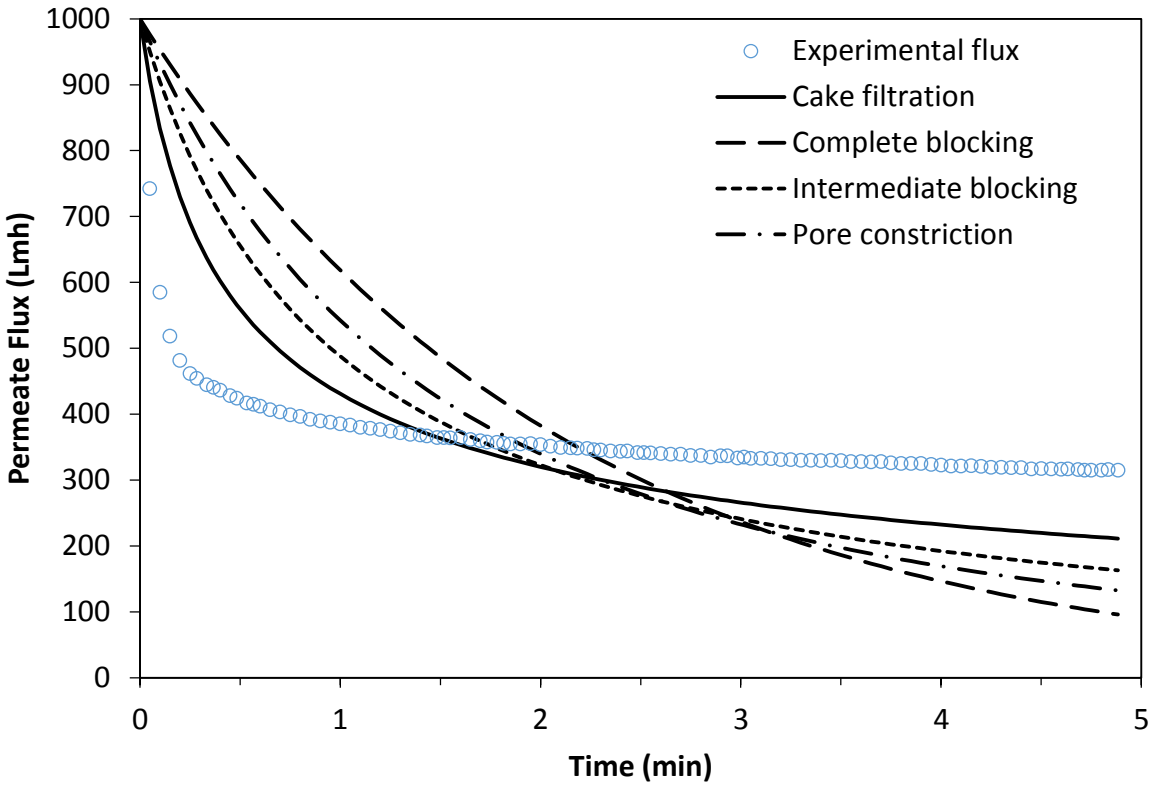

Figure 7.1: Flux vs time for one backflush cycle with a 0.14 µm membrane disk fitted with the four classical filtration models. Feed: SAGD produced water. Temperature: 80–85°C, Transmembrane Pressure: 172.4 kPa. Experimental data taken from Atallah et al. [36].

Table 7.3: Results of the four classical fouling models for different membranes.

Model	RMSE ($L/m^2/h$)			
	0.14 µm	300 kDa	150 kDa	5 nm tube
CB	2042.4 ± 31.1	3077.1 ± 28.3	2612.5 ± 34.6	2442.9
IB	1395.8 ± 24.5	1753.8 ± 23.2	1443.8 ± 36.9	1554.2
PC	1689.4 ± 25.1	2391.2 ± 25.9	1981.5 ± 36.9	1958.9
CF	936.8 ± 21.5	813.5 ± 18.9	654.0 ± 37.1	928.6

*Error ranges represent the standard deviations obtained from analyzing at least 5 backflush cycles.

The RMSE of the four traditional models were all elevated and showed significant discrepancies with the experimental data. The cake filtration model demonstrated the best fit amongst these models for all tested membranes, while complete blocking consistently proved to be the least adequate model. It was also determined that for the membrane disks, the RMSE of the pore blockage models generally increased with decreasing pore size, while the RMSE of cake filtration decreased. This indicates that when produced water filtration was performed using membranes with smaller pore size, the contribution of cake formation to fouling increased, while that of pore blocking decreased. This is a reasonable finding, as the 300 kDa and 150 kDa

membranes have pore sizes of 30 and 21.5 nm, respectively, which are much smaller than the majority of particles in SAGD produced water [36]. The larger particles that would have blocked the pores of the 0.14 µm membranes would be rejected by these membranes, leaving bituminous fines to form cakes at the surface of the membrane.

As with the classical fouling models, an example of the fitted combined models for one backflush cycle is shown in Figure 7.2 for the 0.14 µm membrane. Fits of the combined models for the other membranes showed similar results and are found in Appendix A.

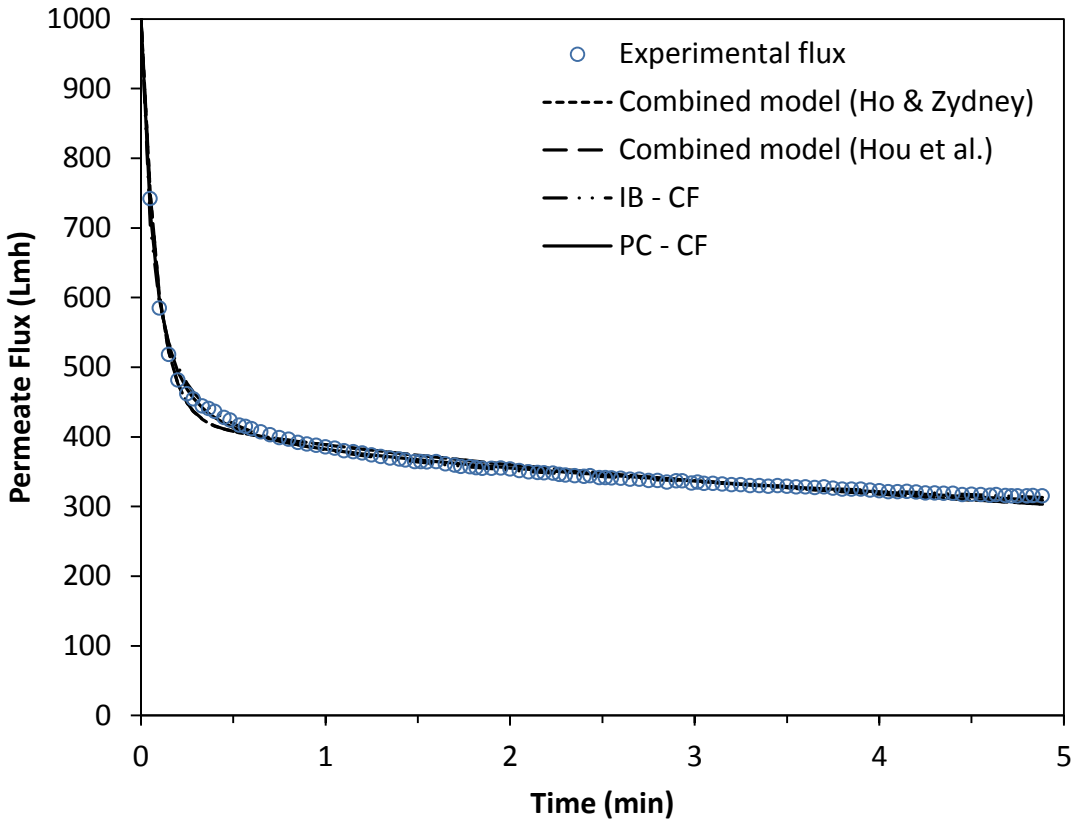

Figure 7.2: Permeate flux vs time for one backflush cycle with a 0.14 µm ceramic membrane disk. Feed: SAGD produced water. Temperature: 80–85°C, Transmembrane Pressure: 68.95 kPa. Experimental data taken from Atallah et al. [36].

It is evident from Figure 7.2 that the combined models emulate the experimental data significantly better when compared to the traditional filtration models (Figure 7.1). These results indicate that when treating oil sands produced water, membrane pores are initially and rapidly blocked by feed particulates, which then transitions to a mechanism involving the formation of a cake layer at the membrane surface by colloidal bitumen. However, analysis of the RMSE and

fitted combined model parameters and residuals is required to discern which among them is superior.

The fitted parameters of the various combined models can be used to extract information to determine the thickness of the foulant layer at the membrane surface. In the case of the cake filtration and the combined models; the specific cake resistance may be obtained from the fitted constants. For flat cakes, the cake resistance is related to the cake thickness by equation (7.12):

$$R_c = R_c' \delta_c \tag{7.12}$$

Where R_C is the cake resistance (m^{-1}), R_C' is the specific cake resistance (m^{-2}) and $\hat{o}_C$ is the cake thickness (m). For cylindrical cakes, the equivalent relation must take into account the change in surface area with radial position due to curvature [38]:

$$R_c = R_c' r_o \ln\left(\frac{r_o}{r_o - \delta_c}\right) \tag{7.13}$$

Where r_o is the inner radius of the clean membrane tube (m). Darcy's law with a resistance-in-series approach can be used to describe permeate flux:

$$J = \frac{\Delta P}{\mu_o (R_m + R_c)} = \frac{J_o R_m}{R_m + R_c} \tag{7.14}$$

Where ΔP is transmembrane pressure (Pa), μ_O is feed viscosity (Pa·s) and R_m is the membrane resistance (m^{-1}). By combining the extracted specific cake resistance from the model parameters with equations (7.12), (7.13) and (7.14), the foulant cake thickness can be obtained.

The specific cake resistance (R_C') values obtained from the models can also be used with the Blake-Kozeny correlation to estimate the size of particles in the cake layer:

$$R_c' = \frac{37.5 \phi_{max}^2}{r_p^2 (1 - \phi_{max})^3} \tag{7.15}$$

Where r_p is particle radius in the cake (m) and ϕ_{max} is the volume fraction of the maximally packed particles in the cake layer, often approximated as 0.58 [39]. This value corresponds to the maximum random packing density of non-deformable spheres. The calculated particle size can then be compared to the measured particle size distribution of the feed solution.

Table 7.4 summarizes the findings of the four combined models, including the cake thickness (δ_c), cake particle diameter (d_p) and RMSE of each model. The residual error in the flux

prediction obtained from the various combined models is also shown for the flat ceramic membrane disks with pore sizes of 0.14 µm, 300 kDa and 150 kDa, as well as the 5 nm multilumen tubular membrane in Figure 7.3 to Figure 7.6.

Table 7.4: Results of the combined fouling models.

Model	0.14 µm			300 kDa			150 kDa			5 nm tube		
	δ_c (µm)	d_p (nm)	RMSE (Lmh)	δ_c (µm)	d_p (nm)	RMSE (Lmh)	δ_c (µm)	d_p (nm)	RMSE (Lmh)	δ_c (µm)	d_p (nm)	RMSE (Lmh)
Ho & Zydney	24.40 ± 0.57	165.3 ± 3.5	83.91 ± 1.98	16.74 ± 0.22	74.37 ± 0.86	136.0 ± 2.7	14.35 ± 0.85	66.05 ± 2.69	155.0 ± 31.8	16.90	75.48	210.8
Hou et al.	23.88 ± 1.23	163.5 ± 3.7	83.05 ± 1.95	16.33 ± 0.76	73.44 ± 1.50	131.3 ± 2.7	13.16 ± 1.90	63.14 ± 5.05	150.1 ± 30.5	14.86	70.77	206.5
Combined IB-CF	42.52 ± 1.68	218.5 ± 7.0	49.96 ± 3.86	28.74 ± 0.75	97.44 ± 0.98	84.59 ± 5.27	20.52 ± 2.15	78.92 ± 3.44	103.2 ± 10.0	34.33	107.9	100.0
Combined PC-CF	31.16 ± 0.90	185.5 ± 5.1	47.22 ± 1.88	21.27 ± 0.22	83.82 ± 0.70	71.33 ±2.28	17.31 ± 1.27	72.52 ± 3.44	110.4 ± 21.1	22.85	87.83	137.1

*Error ranges represent the standard deviations obtained from analyzing at least 5 backflush cycles.

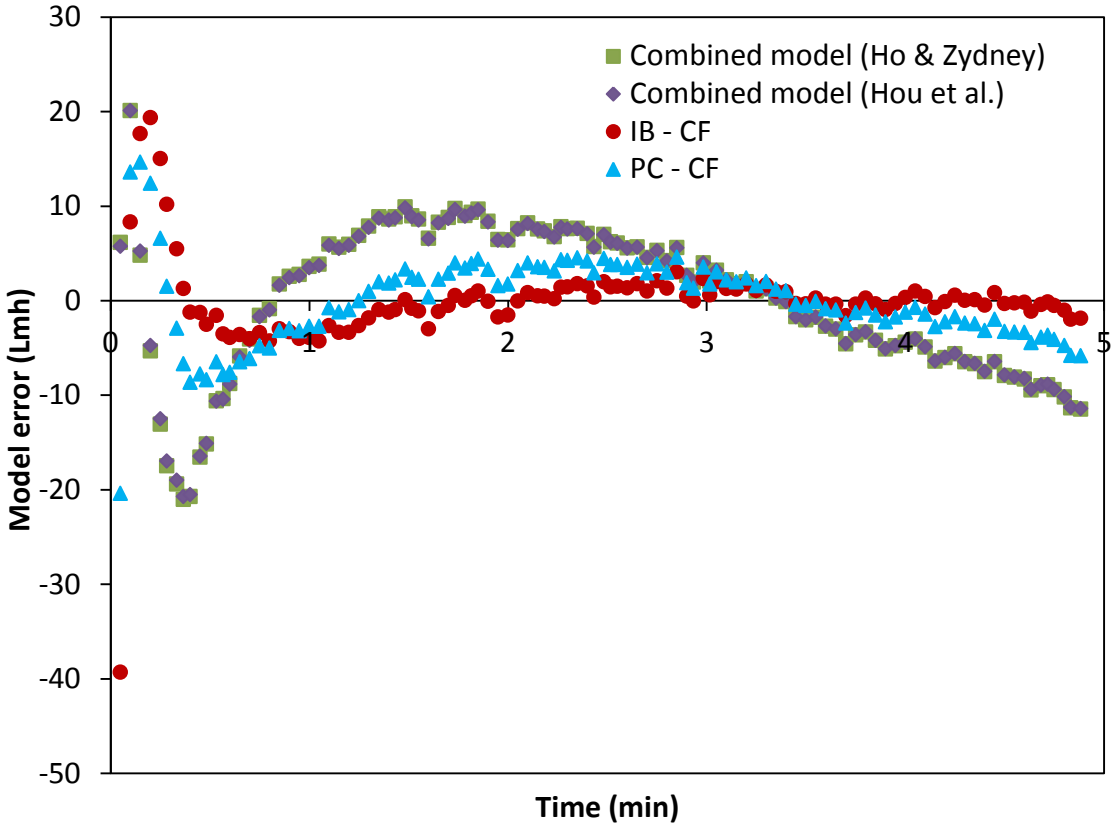

Figure 7.3: Residual plot showing error in flux prediction by the combined models for one backflush cycle with the 0.14 µm membrane disk.

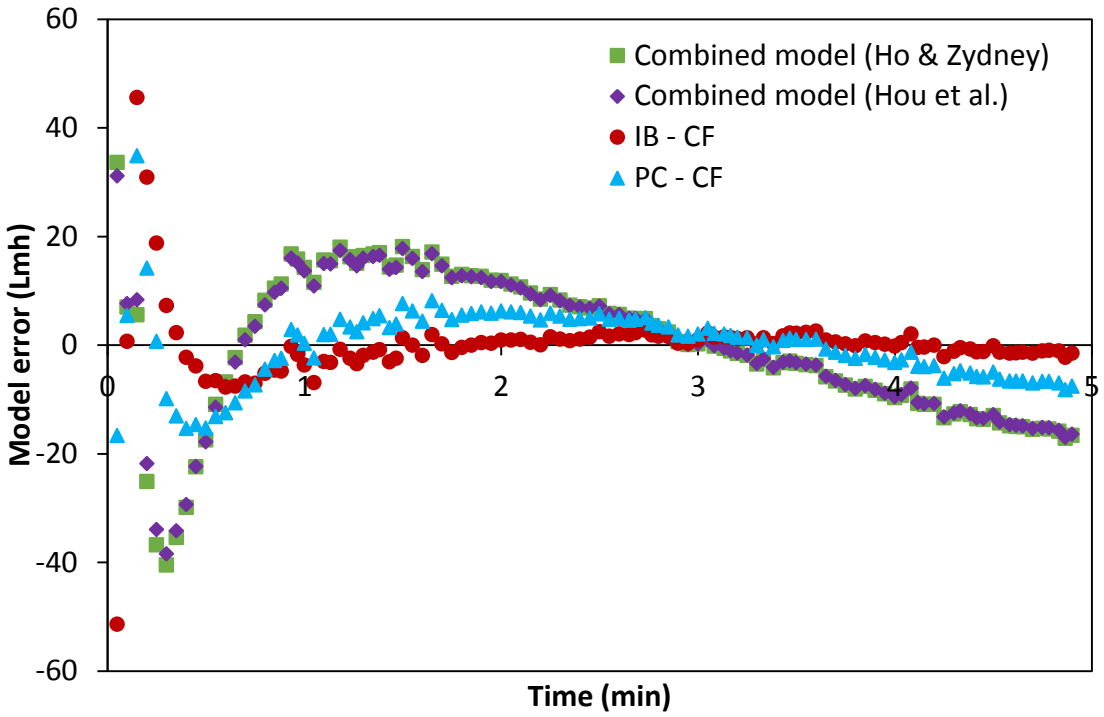

Figure 7.4: Residual plot showing error in flux prediction by the combined models for one backflush cycle with the 300 kDa membrane disk.

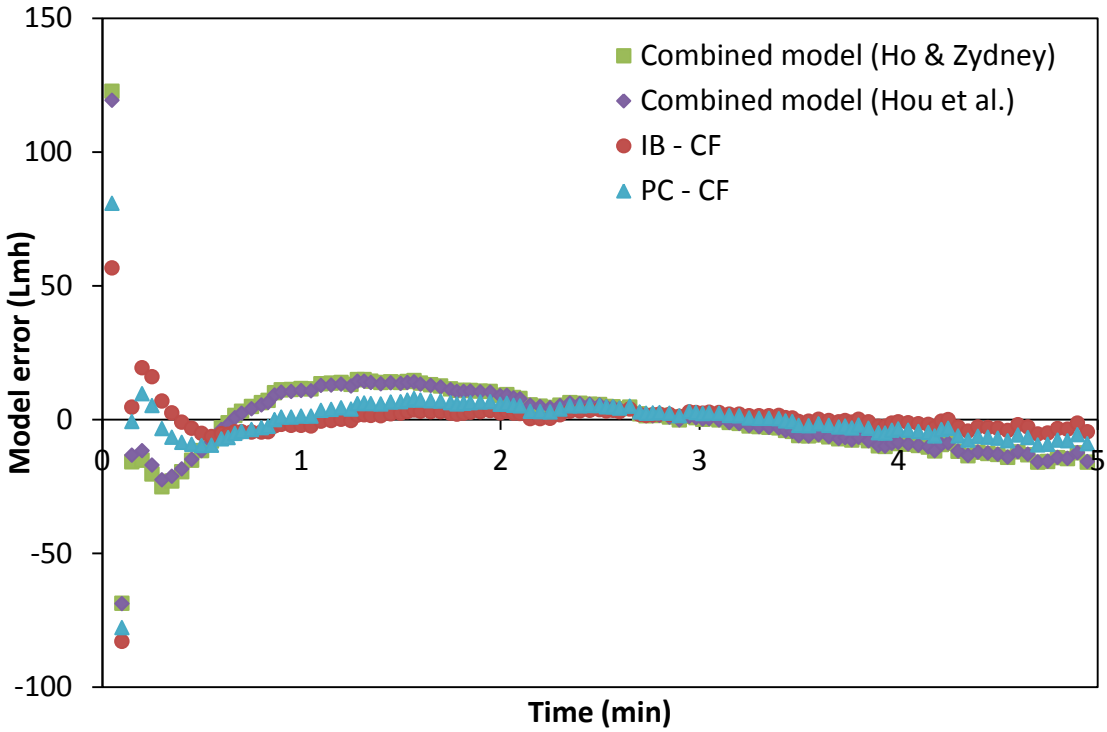

Figure 7.5: Residual plot showing error in flux prediction by the combined models for one backflush cycle with the 150 kDa membrane disk.

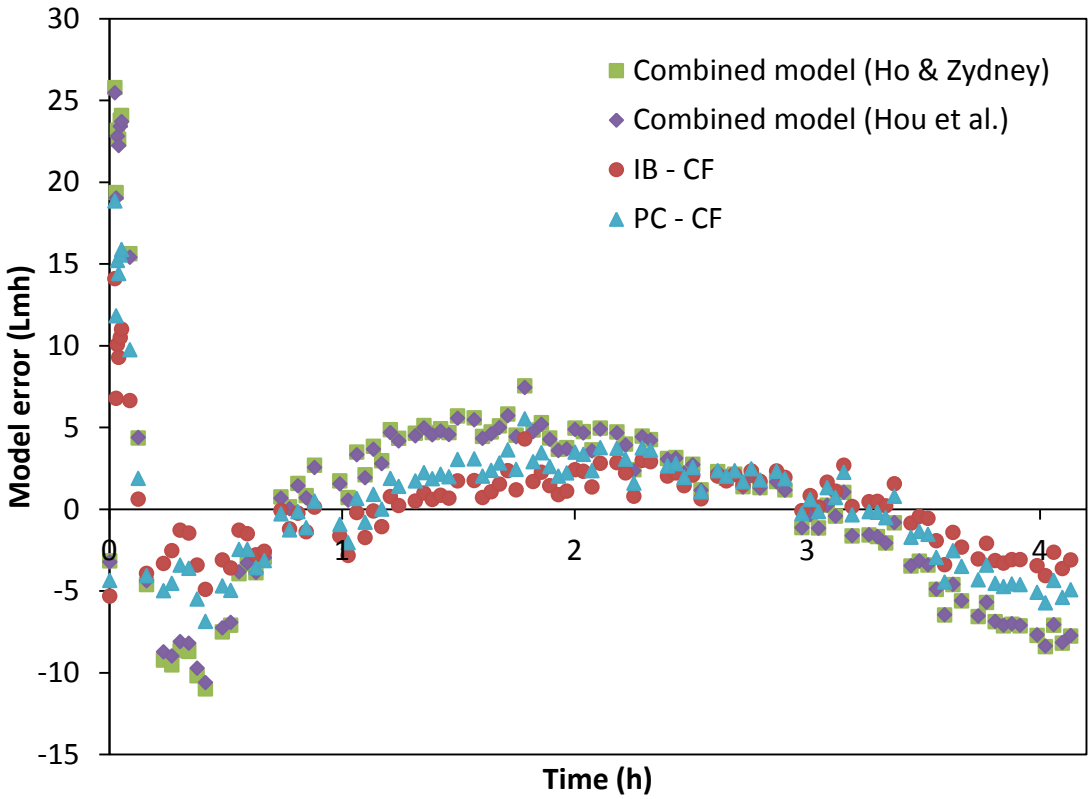

Figure 7.6: Residual plot showing error in flux prediction by the combined models with the 5 nm multilumen tubular membrane.

Analysis of the RMSE confirms that the combined models better represent the experimental data than the classical models. The Ho & Zydney and Hou et al. models offered nearly identical fits, yielding similar error values. This indicates that these two models are functionally equivalent despite differences in their derivations. As hypothesized, the combined IB-CF and PC-CF models performed better than the two CB-CF models, indicating that ultrafine bituminous particles are more likely to block membrane pores by bridging and adsorption. Flux decline in the 0.14 µm and 300 kDa membranes was better represented by the PC-CF model, while the IB-CF model was slightly superior with the 150 kDa and 5 nm membranes. This indicates a possible transition from pore constriction to an intermediate pore blocking mechanism as pore size decreases and it becomes more difficult for foulants to penetrate into the pores and adhere to the walls. However, analysis of the model residual plots in Figure 7.3 to Figure 7.6 revealed that after an initial region of high error during the first 30 seconds of filtration, the IB-CF model offers the most randomized distribution of residuals about the x-axis in all cases.

For all of the tested membranes, the RMSE of the combined models increased as pore size decreased. When coupled with the fact that RMSE of the CF model showed an opposite trend, this is further evidence that cake filtration plays a larger role in the overall fouling mechanism at smaller pore sizes. This finding is supported by the fact that the calculated particle sizes in the cake layer were found to decrease with decreasing membrane pore size, as large particles with pore blocking capability would have been rejected by membranes with small pore sizes. The calculated particle sizes were also in good agreement with the minimum sizes seen in the left-tails of measured particle size distributions for SAGD produced water [37].

Given the superior fit of the combined models relative to the cake filtration model, the cake thickness values they provided are more representative of the actual cake layer formed during the filtration of the SAGD produced water. The predicted cake thickness values listed in Table 7.4 ranged from approximately 20 to 40 μm. Therefore, a cake thickness value of 20 μm will be utilized for all subsequent modelling presented in this study. These thickness values are also in good agreement with previously reported SEM images of ceramic membranes fouled by SAGD produced water [9].

7.3 Effect of temperature on fouling layer characteristics

Having determined that cake formation plays a significant role in flux decline and estimated the dimensions of the foulant cake in SAGD wastewater treatment, the effect of temperature on the hydrodynamic behaviour of this bitumen layer can now be determined. The surface tension and density of bitumen are known to vary only slightly with temperature, and the difference in density of bitumen and water is negligible for temperatures of practical interest [20]. This indicates that these parameters will have minor effects on the bitumen fouling characteristics. Bitumen viscosity, however, varies significantly with temperature and is widely considered to be the main contributing effect to bituminous adhesion in oil sands processes. To establish the temperature dependence of bitumen viscosity, several models exist that have been shown to adequately represent this viscosity-temperature relationship. Among these correlations is the widely used Williams-Landel-Ferry (WLF) equation [40]:

$$\log\left(\frac{\mu(T)}{\mu(T_r)}\right) = -C_1 \frac{T - T_r}{C_2 + T - T_r} \tag{7.16}$$

Where μ is viscosity (Pa·s), T is temperature (K), T_r is a chosen reference temperature (K), and C_1 and C_2 are fitted parameters of the model. Figure 7.7 shows the WLF equation fitted to empirical viscosity data for Athabasca bitumen as a function of temperature taken from Bazyleva et al. [41]. The reference viscosity used was 0.15 Pa·s at a reference temperature of 393.15 K (120 °C).

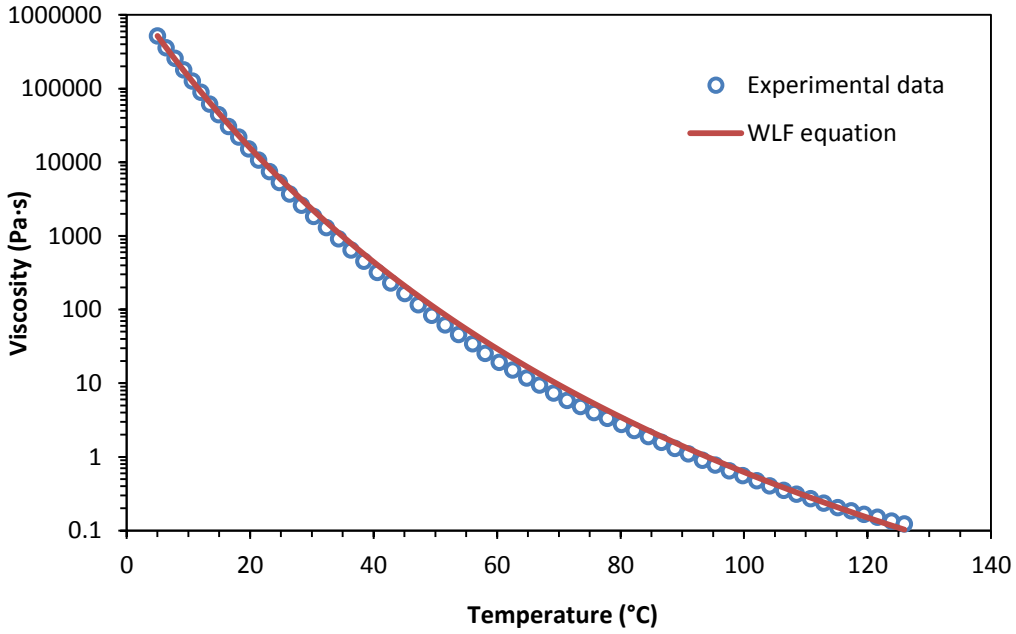

Figure 7.7: Athabasca bitumen viscosity as a function temperature. Experimental data taken from Bazyleva et al. [41] and fitted with the WLF equation.

As seen in Figure 7.7, the WLF equation with the obtained parameter values yields a satisfactory fit and will thus be used in determining bitumen viscosity. The mobility of the foulant cake will be greatly affected by temperature as bitumen viscosity is reduced by five orders of magnitude from 20 to 120 °C.

7.3.1 Modeling the velocity profile in an oil film at the surface of a tube

The cake layer can be taken as a flowing film of bitumen at the membrane surface. The steady state velocity profile in the flowing bitumen layer was determined as a function of temperature. The shear-driven flow of the bitumen cake layer (B) by the feed water (F) in a tubular membrane channel can be described by the simplified Navier-Stokes equation in cylindrical coordinates, assuming laminar flow of incompressible fluids with a non-deformable interface:

$$0 = -\frac{\partial P}{\partial z} - \frac{1}{r}\frac{\partial}{\partial r}(r\tau_{rz}) + \rho g_z \tag{7.17}$$

Due to symmetry along the axis of the cylindrical membrane channel, shear stress at the centerline is zero:

$$(\tau_{rz})_F = 0\ ;\ r = 0 \tag{7.18}$$

At the bitumen-feed water interface, the momentum flux (shear stress) and velocity are continuous:

$$(\tau_{rz})_F = (\tau_{rz})_B\ ;\ r = r_o - \delta_c \tag{7.19}$$

$$(v_z)_F = (v_z)_B\ ;\ r = r_o - \delta_c \tag{7.20}$$

The cylinder wall is a no-slip boundary where the fluid velocity is zero:

$$(v_z)_B = 0\ ;\ r = r_o \tag{7.21}$$

The integration of equation (7.17) with equations (7.18) and (7.19) as boundary conditions results in the following shear stress distribution:

$$\tau_{rz} = \left(-\frac{\partial P}{\partial z} + \rho g_z\right)\frac{r}{2} \tag{7.22}$$

At low temperatures, Athabasca bitumen exhibits non-Newtonian shear-thinning behaviour, but eventually transitions to a Newtonian fluid at temperatures above 25–40°C [41–44]. By substituting Newton's law of viscosity into equation (7.22) and then integrating the resulting differential equation with boundary conditions (7.20) and (7.21), the velocity distributions obtained for the water and bitumen phases are:

$$(v_z)_F = \frac{1}{4}\left(\frac{\partial P}{\partial z} - \rho g_z\right)\left[\frac{1}{\mu_F}(r^2 - (r_o - \delta_c)^2) + \frac{1}{\mu_B}((r_o - \delta_c)^2 - r_o^2)\right] \tag{7.23}$$

$$(v_z)_B = \frac{1}{4\mu_B}\left(\frac{\partial P}{\partial z} - \rho g_z\right)(r^2 - r_o^2) \tag{7.24}$$

The temperature dependence of the feed water viscosity was determined using the following equation [45]:

$$\mu_F = \exp\left(-52.843 + \frac{3703.6}{T} + 5.866\ln T - 5.879 \cdot 10^{-29}T^{10}\right) \tag{7.25}$$

The frictional pressure drop along the length of a membrane channel was estimated using the following equation [46]:

$$\frac{\partial P}{\partial z} = f\frac{\rho v^2}{r_o} \tag{7.26}$$

Where f is the friction factor, and ρ and v are the density (kg/m^3) and average velocity (m/s) of the fluid flowing through the channel, respectively. The friction factor can be obtained from the following correlation:

$$\frac{1}{\sqrt{f}} = -3.6\log\left[\frac{6.9}{Re} + \left(\frac{\varepsilon}{7.42r_o}\right)^{1.11}\right] \tag{7.27}$$

Where ε is the surface roughness (m) and Re is the Reynolds number of the flow. The surface roughness of the ceramic membrane was taken as 0.048 mm [46].

The velocity profile of the bitumen throughout the entire thickness of the flowing cake layer is shown in Figure 7.8 as a function of temperature. In both the 3D mesh plot (Figure 7.8a) and the contour plot (Figure 7.8b), the velocity is plotted using a logarithmic scale for better visualization. It is evident that the velocity of the bitumen layer is highly sensitive to variations in temperature. From the velocity profile obtained in equation (7.24), it can be shown that the increase of velocity with increasing temperature is directly proportional to the decrease in bitumen viscosity as temperature rises. This indicates that the flow of the bitumen layer will increase by a factor of approximately 3000 if the flow temperature is increased from 25 °C to 85 °C and by a factor of 39000 if it is raised to 120 °C. Therefore, if the bitumen layer that forms near the membrane wall is considered as a flowing layer adjacent to the flowing feed water, it would be advantageous to operate the membrane system at higher temperatures to increase the mobility of the foulant cake. Nonetheless, owing to the highly viscous nature of Athabasca bitumen, the computed velocities are relatively low. At the highest studied temperature of 120 °C, bitumen velocity at the edge of the cake layer is approximately 0.024 m/s, indicating that bitumen at this radial position will possess a residence time of over 8 minutes in membrane channels with a typical length of 1.2 m.

(a)

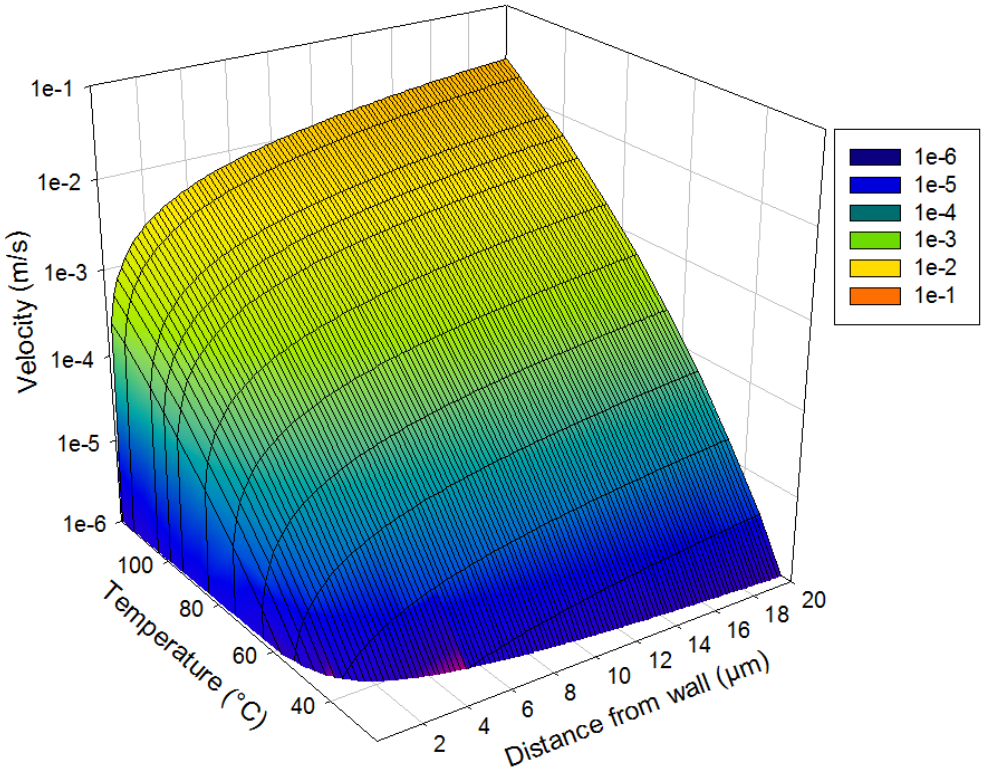

(b)

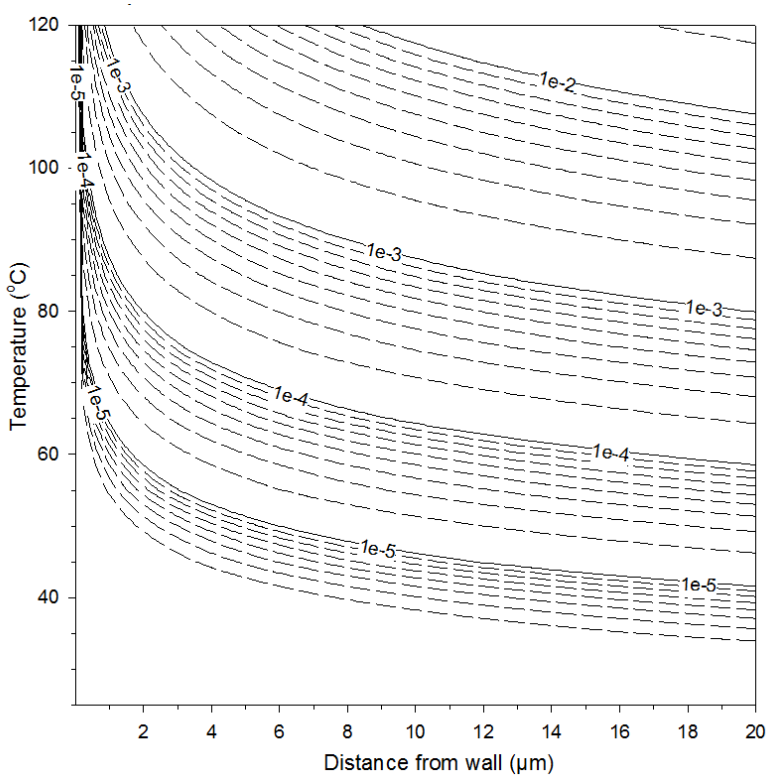

Figure 7.8: Velocity profile in the bitumen cake layer as a function of temperature. (a) 3D mesh plot and (b) contour plot. Contour lines represent the velocity in m/s.

7.3.2 Distance for the formation of a stagnant cake in a tubular membrane

In addition to affecting the shear-driven flow of the cake layer along the membrane channel, operating temperature also influences the axial position in the channel at which stagnant cake formation begins taking place. This distance from the channel entrance, named the critical length, was first proposed by Romero and Davis [47]. A visual representation of the critical length is shown in Figure 7.9.

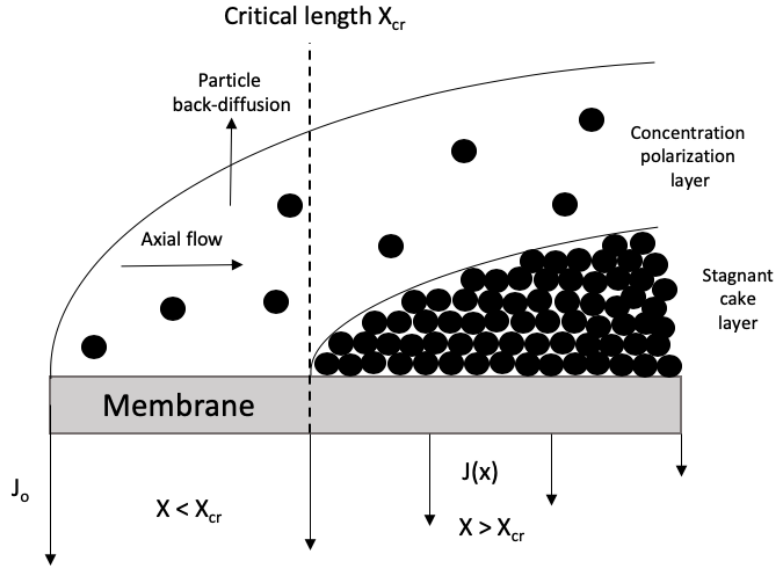

Figure 7.9: Conceptual view of the critical distance concept in cross-flow filtration showing formation of a cake layer at some distance along the length of the membrane and the general flux pattern, J(x).

Romero and Davis presented steady state equations based on a model that accounts for particle back-transport by shear-induced diffusion alone. However, in our previous work we demonstrated that particles in SAGD produced water possess dimensions at which Brownian diffusivity is not negligible when compared to shear-induced diffusivity [37]. Sethi and Weisner [39] recognized the important effect of particle size on back-transport diffusivity mechanisms, and extended the model developed by Romero and Davis to account for particle transport by both Brownian and shear-induced diffusion. The obtained equation for the critical length becomes:

$$X_{cr} = \frac{\dot{\gamma}_w Q_{cr}}{J_o^3 \phi_o} \tag{7.28}$$

Where X_{cr} (m) is the critical length, $\dot{\gamma}_w$ (s^{-1}) is the shear rate related to the shear stress at the wall and Q_{cr} represents the critical excess particle flux towards the membrane surface which brings about the onset of stagnant cake formation. Q_{cr} can be determined by evaluating the following double integral:

$$Q_{cr} = \int_{\phi_o}^{\phi_{max}} \left(\int_{\phi}^{\phi_{max}} \frac{[D_S(\phi')/\eta(\phi') + D_B]}{\phi'\eta(\phi')} d\phi' \right) (\phi - \phi_o) \left(\frac{[D_S(\phi)/\eta(\phi) + D_B]}{\phi} \right) d\phi \quad (7.29)$$

Where D_S and D_B (m^2/s) are shear-induced and Brownian diffusivity, respectively, and $\eta(\phi)$ is the relative fluid viscosity in the cake. The double integral was solved using standard numerical techniques. The Brownian particle diffusivity is calculated using the Stokes-Einstein equation:

$$D_B = \frac{k_B T}{6\pi\mu_o r_p} \quad (7.30)$$

Where k_B is the Boltzmann constant equal to 1.381 x 10^{-23} J/K. Shear-induced diffusivity is determined using the following equation:

$$D_S = \dot{\gamma} r_p^2 \widehat{D}_s(\phi) \quad (7.31)$$

Where $\widehat{D}_S(\phi)$ is a dimensionless function of the particle volume fraction (ϕ), and has been determined empirically for suspensions of non-deformable spheres:

$$\widehat{D}_S(\phi) = 0.33\phi^2\left(1 + 0.5e^{8.8\phi}\right) \quad (7.32)$$

The relative viscosity $\eta(\phi)$ from equation (7.29) has also been determined empirically and is estimated using the following relation:

$$\eta(\phi) = \left(1 + \frac{1.5\phi}{1 - \frac{\phi}{0.58}}\right)^2 \quad (7.33)$$

The temperature dependence of the critical length stems from the direct effect of temperature on Brownian diffusivity as well as its indirect effect on shear-induced diffusivity via the shear rate. The critical length also depends on particle volume fraction in the feed (ϕ_o) and particle radius (r_p), which affects particle diffusivity. The effects of temperature and particle concentrations in the feed on the critical length are shown in Figure 7.10, assuming a particle diameter of 300 nm. The concentrations of organics-coated solid clays in the SAGD produced water studied in this work are commonly in the range of 100–500 ppm [15,37]. Similarly, the combined effect of

temperature and particle size in the feed suspension on the critical length is shown in Figure 7.11, assuming a particle concentration of 500 ppm. The size of bitumen-coated fine clays and silicates found in SAGD produced water is often in the range of 100–500 nm in diameter [36,37].

It can be seen that increasing the temperature at any given feed particle size and concentration will increase the critical length, thus delaying the onset of stagnant cake formation. This effect is primarily due to the strong temperature dependence of the viscosity of the bitumen foulant layer (Figure 7.7). The sharp decrease in viscosity causes an equally significant rise in the shear rate at the membrane wall as temperature is increased. Higher shearing naturally increases mixing near the membrane wall and consequently reduces the thickness of the flowing concentration polarization layer. Concentration polarization precedes stagnant cake formation during the fouling phenomenon. Cake deposition is thus delayed by mitigating concentration polarization at higher temperatures.

Figure 7.10 also illustrates that at any given temperature, reducing the particle concentration in the feed solution will increase the critical length. Feeds containing fewer particles will naturally lead to less fouling since particles will be deposited on the membrane surface at a lower rate. Conversely, Figure 7.11 shows that at any given temperature, decreasing the particle size in the feed will decrease the critical length. Smaller particles possess lower shear back-transport diffusivities and thus migrate away from the membrane surface into the bulk at lower rates. This in turn precipitates the formation of a cake layer.

With the objective of reducing fouling, the operating conditions of a membrane system should be selected in a manner that leads to a critical length that is longer than the membrane module itself. In doing so, the formation of a recalcitrant stagnant cake layer would be entirely avoided. Commercial tubular ceramic membranes are often available in lengths of 0.3 m for pilot-scale study and testing. Modules are also commonly manufactured in lengths of 1.2 m for industrial-scale application. The solid horizontal lines in Figure 7.10 and Figure 7.11 demonstrate at which temperature the critical length exceeds these common module lengths for various feed particle concentrations and sizes. Below temperatures of 80 °C, the critical length is in the range of microns and is thus of no practical significance. It is only at a temperature of approximately 105 °C that the critical length exceeds 0.3 m for low particle concentrations of 100 ppm and high particle diameters of 500 nm. At these conditions, the critical length exceeds 1.2 m at

temperatures in the range of 110–115 °C. Increasing the feed concentration from 100 to 500 ppm causes the temperature at which the critical length exceeds 0.3 m to rise from 105 to 114 °C. At 500 ppm, the critical length does not exceed 1.2 m even at temperatures as high as 120 °C. Furthermore, if the feed solely contains particles that are 200 nm or lower in diameter, the critical length remains below 0.3 m for temperatures up to 120 °C.

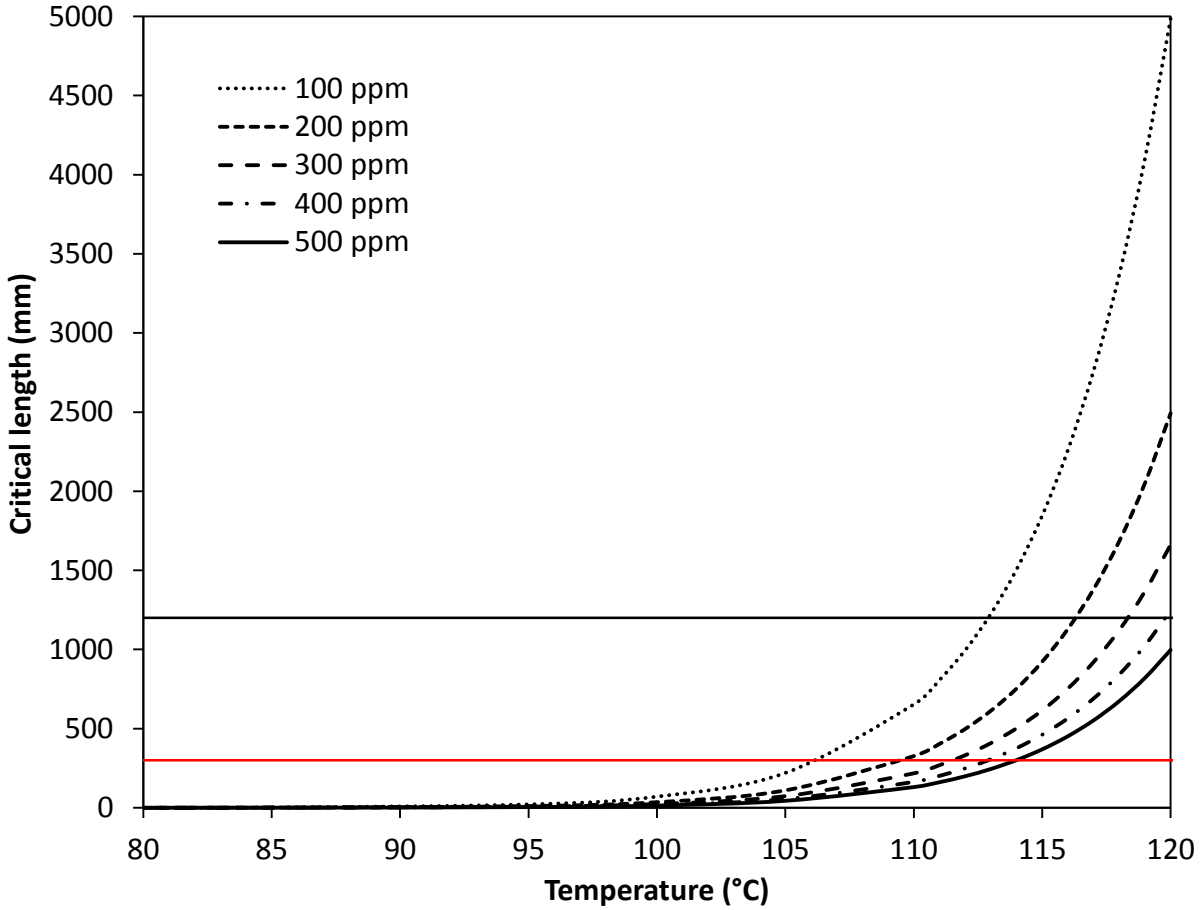

Figure 7.10: Critical length as a function of temperature for different feed particle concentrations. Solid horizontal lines indicate common membrane module lengths of 0.3 and 1.2 m. Particle diameter = 300 nm.

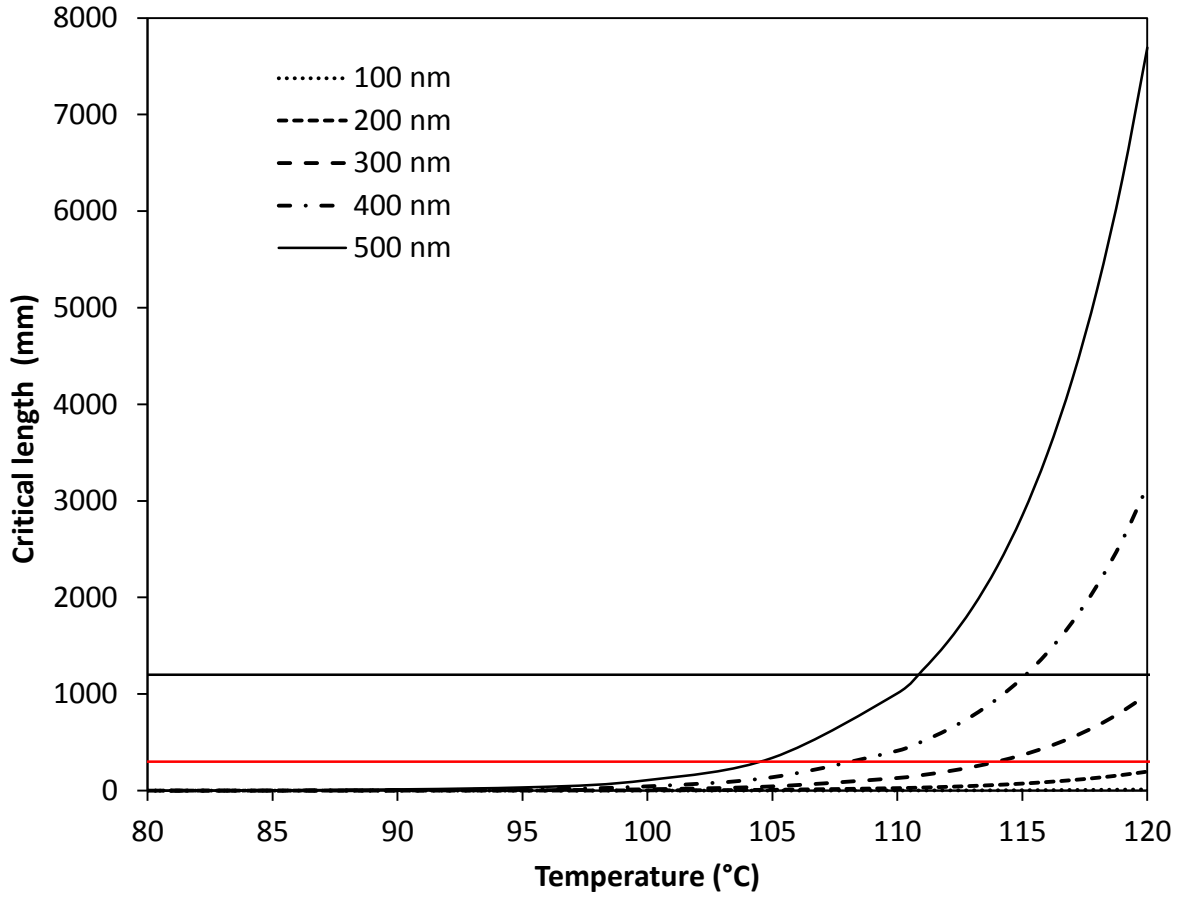

Figure 7.11: Critical length as a function of temperature for different foulant particle diameters. Dashed lines indicate common membrane module lengths of 0.3 and 1.2 m. Particle concentration = 500 ppm.

The concept of a critical length implies the existence of a critical flux, which is defined as the maximum permeate flux a membrane system can operate at without the onset of stagnant cake layer formation [48]. When systems are operated below the critical flux, particle back-transport velocity exceeds permeate velocity, leading to the transport of particles away from the membrane surface into the retentate stream. Consequently, the critical flux has received extensive discussion as a potentially useful design parameter for micro- and ultrafiltration systems. The critical flux (J_{cr}) may be determined by assuming that the critical length is equal to the length of the membrane module in question. Through rearrangement of equation (7.28) with $X_{cr} = L$ (the membrane length), the critical flux is defined as:

$$J_{cr} = \left(\frac{\ddot{\gamma} Q_{cr}}{L \phi_o}\right)^{1/3} \tag{7.34}$$

Similarly to the critical length, the critical flux is also dependent on temperature, as well as particle concentration and particle size. The effect of temperature and particle concentration in the feed on the critical flux is shown in Figure 7.12 for two common membrane module lengths (1.2 and 0.3 m). Furthermore, the effect of particle size in the feed suspension on critical flux is shown in Figure 7.13, once again for module lengths of 1.2 and 0.3 m.

Much like the critical length, it is desirable to operate with a higher critical flux as this would permit the production of more permeate without the onset of cake formation. As a consequence, the observed trends for the critical flux are similar to those previously discussed for the critical length. At any given temperature, feeds with lower particle concentrations and larger particle sizes will result in higher critical fluxes.

Furthermore, Figure 7.12 and Figure 7.13 demonstrate that at any given set of operating conditions, increasing the membrane module length from 0.3 to 1.2 m will decrease the associated critical flux. While longer membranes offer higher filtration surface area, they also require higher temperatures, lower feed concentrations or higher feed particle sizes than their shorter counterparts to maintain operation without stagnant cake layer formation. A compromise must thus be made between permeate production rate and membrane life, since increasing production by using longer membranes also increases risk of fouling and flux decline.

Overall, the analysis of the effect of temperature on critical length and critical flux indicates that, without backflushing, in the treatment of oil sands produced water, a ceramic membrane system would likely have to be operated at temperatures in the vicinity of 105–120 °C to ensure that stagnant cake formation does not occur within the tubular membrane module. This is evidently a problematic requirement for a process in which the feed solution is mostly comprised of water. In such cases, the system should be operated at the highest allowable temperature given the nature of the feed. Furthermore, the membrane should be periodically cleaned using thermal processes at temperatures of 120 °C or higher, such as with pressurized saturated steam [37,49,50], in addition to traditional permeate backflushing.

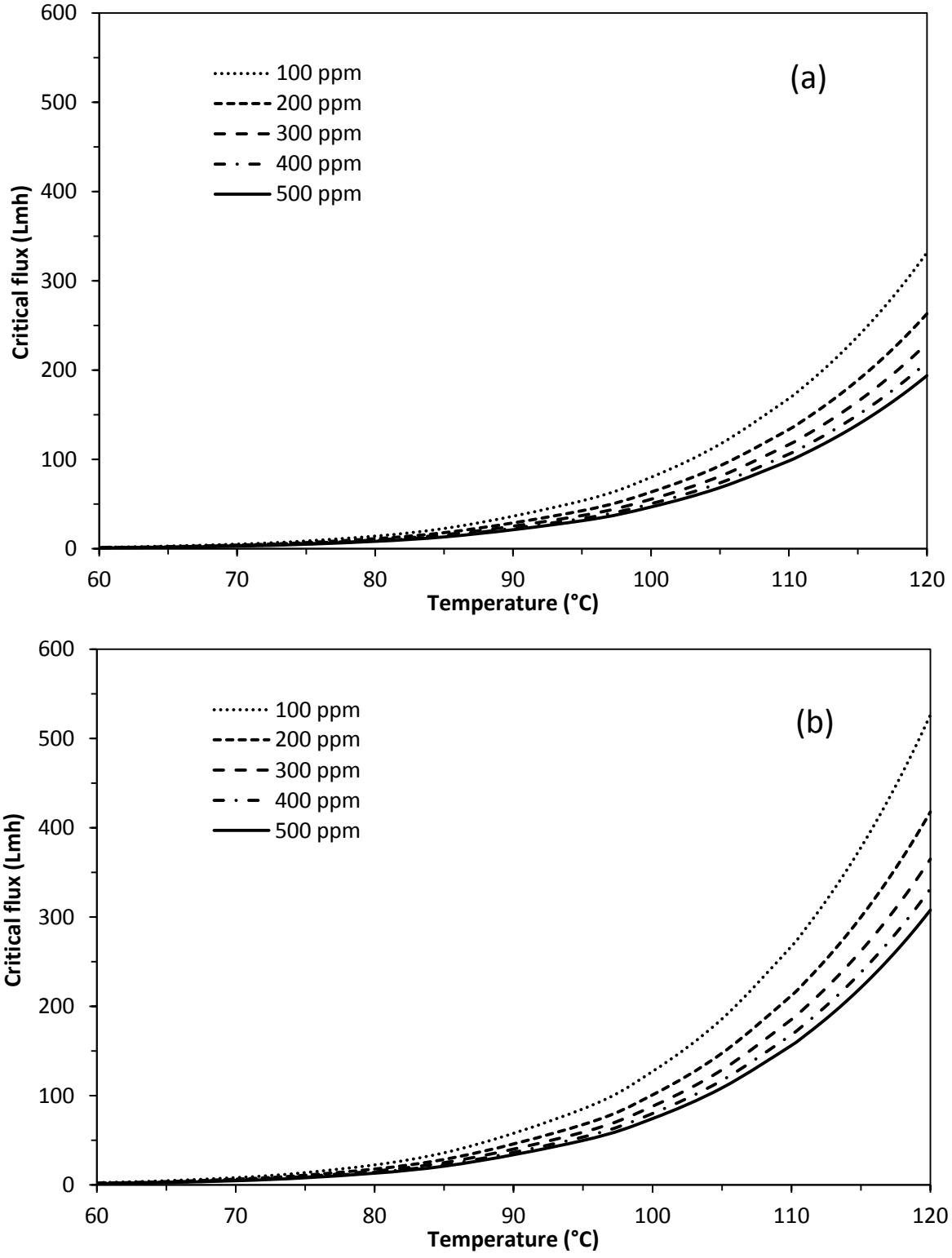

Figure 7.12: Critical flux as a function of temperature for different feed particle concentrations with (a) 1.2 m membrane length and (b) 0.3 m membrane length. Particle diameter = 300 nm.

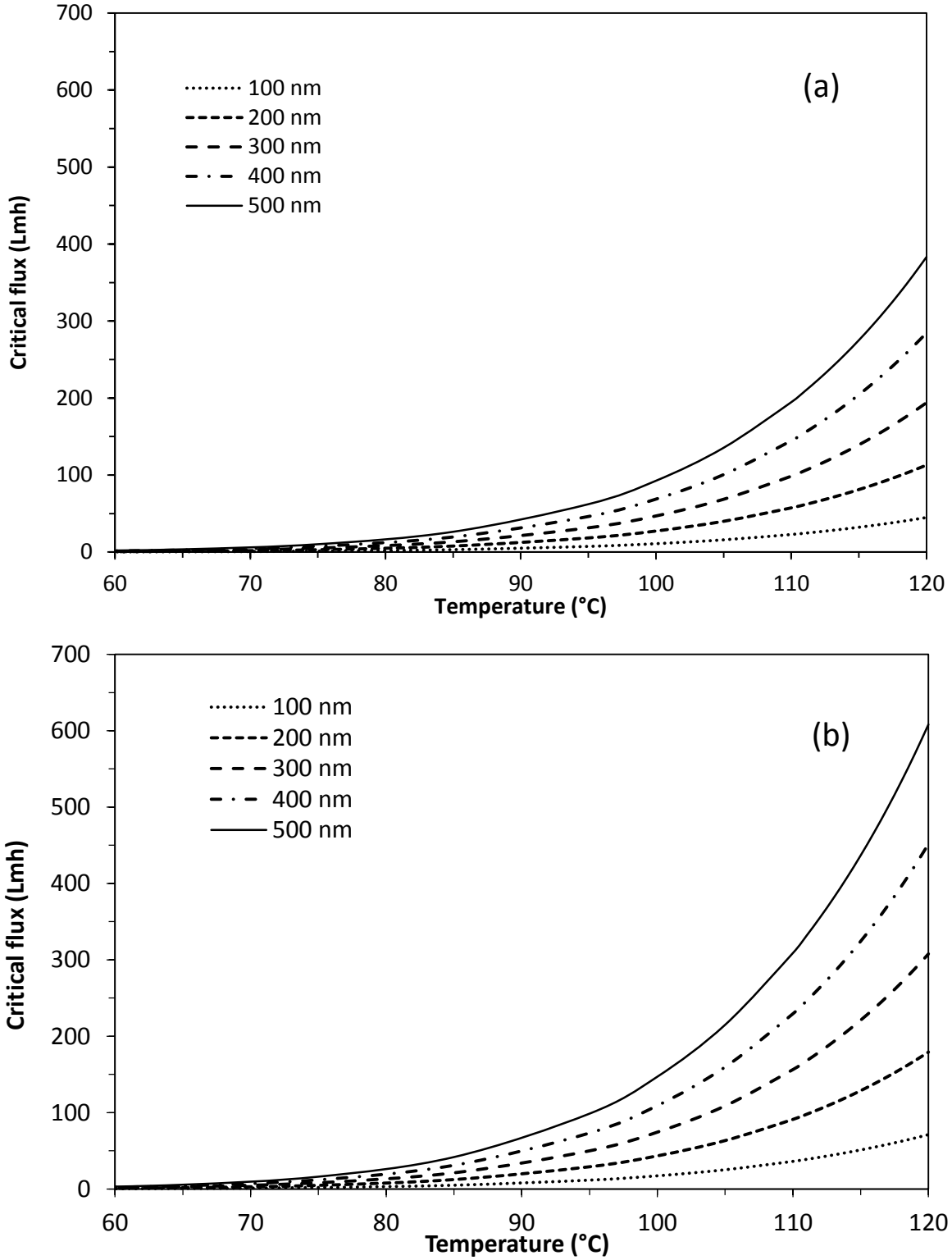

Figure 7.13: Critical flux as a function of temperature for different feed particle diameters with (a) 1.2 m membrane length and (b) 0.3 m membrane length. Particle concentration = 500 ppm.

7.4 Conclusions

Membrane filtration and fouling during the treatment of oil sands produced water were modelled for both flat ceramic membrane disks and commercial membrane tubes. Various filtration models were applied to experimental flux data from the treatment of SAGD produced water. It was determined in all cases that combined filtration models better represent the observed flux decline than the traditional filtration models that are based on single fouling mechanisms. This indicates that in treating bituminous wastewaters, membrane fouling is a consequence pore blocking and cake formation mechanisms. Pore blocking phenomena dominate near the beginning of filtration where membrane pores are initially and rapidly blocked by feed particulates, which then transitions to a mechanism involving the formation of a cake layer at the membrane surface by colloidal bitumen. Combined models that consider pore constriction or intermediate blocking mechanisms instead of complete pore blocking were found to better emulate experimental data. The contribution of cake formation to membrane fouling was also found to increase with membranes having smaller pore sizes. The cake thickness was estimated from the fitted models to be in the vicinity of 20–40 μm, which is in good agreement with previously reported SEM images of membranes fouled by SAGD produced water.

The effect of temperature on fouling layer characteristics was also determined. The mobility of the flowing cake layer was shown to vary significantly with temperature as a consequence of the strong temperature dependence of bitumen viscosity. However, the increase in bitumen layer mobility up to temperatures of 120 °C was not found to reduce foulant residence times in membrane modules to practically significant levels. The reduced bitumen viscosity at higher temperatures was also found to increase the critical length, the position in a membrane channel at which stagnant cake formation begins. The increase in temperature increased the wall shear rate, which delayed the onset of cake deposition. To increase the critical length to values that exceed commercial membrane lengths, however, temperatures in the vicinity of 105–120 °C would be needed under the conditions modeled. This is problematic for systems aimed at treating water-based feeds. It is suggested that treatment of such feeds should be performed at the highest allowable temperature while also implementing a thermal membrane cleaning process at temperatures of at least 120 °C, such as the use of saturated steam. The application of traditional backflushing to remove foulants from inside membrane pores should be combined with such a thermal cleaning process to remove surface filter cakes.

References

[1] E.T. Igunnu, G.Z. Chen, Produced water treatment technologies, International Journal of Low-Carbon Technologies. 9 (2014) 157–177.

[2] S. Jamaly, A. Giwa, S.W. Hasan, Recent improvements in oily wastewater treatment: Progress, challenges, and future opportunities, Journal of Environmental Sciences. 37 (2015) 15–30.

[3] J. Pitchel, Oil and Gas Production Wastewater: Soil Contamination and Pollution Prevention, Applied and Environmental Soil Science. 2016 (2016).

[4] M.A. Al-Ghouti, M.A. Al-Kaabi, M.Y. Ashfaq, D.A. Da'na, Produced water characteristics, treatment and reuse: A review, Journal of Water Process Engineering. 28 (2019) 222–239.

[5] S. Jiménez, M.M. Micó, M. Arnaldos, F. Medina, S. Contreras, State of the art of produced water treatment, Chemosphere. 192 (2018) 186–208.

[6] Y. Zhu, D. Wang, L. Jiang, J. Jin, Recent progress in developing advanced membranes for emulsified oil/water separation, NPG Asia Materials. 6 (2014) e101.

[7] S.M. Samaei, S. Gato-Trinidad, A. Altaee, The application of pressure-driven ceramic membrane technology for the treatment of industrial wastewaters – A review, Separation and Purification Technology. 200 (2018) 198–220.

[8] E.W. Allen, Process water treatment in Canada's oil sands industry: II. A review of emerging technologies, Journal of Environmental Engineering and Science. 7 (2008) 499–524.

[9] Y. Thibault, J. Gamage McEvoy, S. Mortazavi, D. Smith, A. Doiron, Characterization of fouling processes in ceramic membranes used for the recovery and recycle of oil sands produced water, Journal of Membrane Science. 540 (2017) 307–320.

[10] S. Munirasu, M.A. Haija, F. Banat, Use of membrane technology for oil field and refinery produced water treatment–A review, Process Safety and Environmental Protection. 100 (2016) 183–202.

[11] T. Zsirai, H. Qiblawey, P. Buzatu, M. Al-Marri, S.J. Judd, Cleaning of ceramic membranes for produced water filtration, Journal of Petroleum Science and Engineering. 166 (2018) 283–289.

[12] E. Garmsiri, Y. Rasouli, M. Abbasi, A.A. Izadpanah, Chemical cleaning of mullite ceramic microfiltration membranes which are fouled during oily wastewater treatment, Journal of Water Process Engineering. 19 (2017) 81–95.

[13] G. Mustafa, K. Wyns, A. Buekenhoudt, V. Meynen, Antifouling grafting of ceramic membranes validated in a variety of challenging wastewaters, Water Research. 104 (2016) 242–253.

[14] J. Lee, J.-H. Ha, I.-H. Song, D.W. Shin, Enhanced fouling resistance of organosilane-grafted ceramic microfiltration membranes for water treatment, Journal of the Ceramic Society of Japan. 125 (2017) 899–905.

[15] C. Atallah, S. Mortazavi, A.Y. Tremblay, A. Doiron, Surface-Modified Multi-lumen Tubular Membranes for SAGD-Produced Water Treatment, Energy & Fuels. 33 (2019) 5766–5776.

[16] C. Atallah, S. Mortazavi, A.Y. Tremblay, Thermal stability of hydrophilic PEO-silane modified ceramic membranes, Colloids and Surfaces A: Physicochemical and Engineering Aspects. 561 (2019) 254–266.

[17] L.-H. Chen, Y.-R. Chen, C.-Y. Chou, C.-H. Chen, C.-C. Ko, K.-L. Tung, Inorganic Membranes in

Water and Wastewater Treatment, in: A. Figoli, A. Criscuoli (Eds.), Sustainable Membrane Technology for Water and Wastewater Treatment. Green Chemistry and Sustainable Technology, Springer, Singapore, 2017: pp. 121–154.

[18] M.W.J. Luiten-Olieman, M.J.T. Raaijmakers, A. Nijmeijer, N.E. Benes, Thin Inorganic Porous Hollow Fiber Membranes, in: E.M.V. Hoek, V. V. Tarabara (Eds.), Encyclopedia of Membrane Science and Technology, 2013: pp. 1–24.

[19] M.M. Pendergast, E.M.V. Hoek, A review of water treatment membrane nanotechnologies, Energy and Environmental Science. 4 (2011) 1946–1971.

[20] J. Long, J. Drelich, Z. Xu, J.H. Masliyah, Effect of Operating Temperature on Water-Based Oil Sands Processing, The Canadian Journal of Chemical Engineering. 85 (2007) 726–738.

[21] J.P. Hermia, Constant Pressure Blocking Filtration Laws - Application to Power-law Non-Newtonian Fluids, Transactions of the Institution of Chemical Engineers. 60 (1982) 183–187.

[22] D. Zou, M. Qiu, X. Chen, E. Drioli, Y. Fan, One step co-sintering process for low-cost fly ash based ceramic microfiltration membrane in oil-in-water emulsion treatment, Separation and Purification Technology. 210 (2019) 511–520.

[23] B. Das, B. Chakrabarty, P. Barkakati, Separation of oil from oily wastewater using low cost ceramic membrane, Korean Journal of Chemical Engineering. 34 (2017) 2559–2569.

[24] H.J. Tanudjaja, V. V. Tarabara, A.G. Fane, J.W. Chew, Effect of cross-flow velocity, oil concentration and salinity on the critical flux of an oil-in-water emulsion in microfiltration, Journal of Membrane Science. 530 (2017) 11–19.

[25] R. Vinoth Kumar, A. Kumar Ghoshal, G. Pugazhenthi, Elaboration of novel tubular ceramic membrane from inexpensive raw materials by extrusion method and its performance in microfiltration of synthetic oily wastewater treatment, Journal of Membrane Science. 490 (2015) 92–102.

[26] S. Emani, R. Uppaluri, M.K. Purkait, Cross flow microfiltration of oil–water emulsions using kaolin based low cost ceramic membranes, Desalination. 341 (2014) 61–71.

[27] M. Abbasi, D. Mowla, Analysis of membrane pore-blocking models applied to the MF of real oily wastewaters treatment using mullite and mullite–alumina ceramic membranes, Desalination and Water Treatment. 52 (2014) 2481–2493.

[28] L. Zhu, M. Chen, Y. Dong, C.Y. Tang, A. Huang, L. Li, A low-cost mullite-titania composite ceramic hollow fiber microfiltration membrane for highly efficient separation of oil-in-water emulsion, Water Research. 90 (2016) 277–285.

[29] M.J. Corbatón-Báguena, S. Álvarez-Blanco, M.C. Vincent-Vela, Ultrafiltration of whey: membrane performance and modelling using a combined pore blocking–cake formation model, Journal of Chemical Technology and Biotechnology. 93 (2018) 1891–1900.

[30] G. Bolton, D. LaCasse, R. Kuriyel, Combined models of membrane fouling: Development and application to microfiltration and ultrafiltration of biological fluids, Journal of Membrane Science. 277 (2006) 75–84.

[31] W. Li, F. Hang, K. Li, F. Lei, Development and Application of Combined Models of Membrane Fouling for the Ultrafiltration of Limed Sugarcane Juice, Sugar Tech. 21 (2018) 524–526.

[32] B. Teychene, G. Collet, H. Gallard, Modeling of combined particles and natural organic matter

fouling of ultrafiltration membrane, Journal of Membrane Science. 505 (2016) 185–193.

[33] C.C. Ho, A.L. Zydney, A combined pore blockage and cake filtration model for protein fouling during microfiltration, Journal of Colloid and Interface Science. 232 (2000) 389–399.

[34] H. Peng, A.Y. Tremblay, Membrane regeneration and filtration modeling in treating oily wastewaters, Journal of Membrane Science. 324 (2008) 59–66.

[35] L. Hou, Z. Wang, P. Song, A precise combined complete blocking and cake filtration model for describing the flux variation in membrane filtration process with BSA solution, Journal of Membrane Science. 542 (2017) 186–194.

[36] C. Atallah, A.Y. Tremblay, S. Mortazavi, Silane Surface Modified Ceramic Membranes for the Treatment and Recycling of SAGD Produced Water, Journal of Petroleum Science and Engineering. 157 (2017) 349–358.

[37] C. Atallah, S. Mortazavi, A.Y. Tremblay, A. Doiron, In-process steam cleaning of ceramic membranes used in the treatment of oil sands produced water, Industrial & Engineering Chemistry Research. 58 (2019) 15232–15243.

[38] R. Davis, Modeling of fouling of crossflow microfiltration membranes, Separation and Purification Methods. 21 (1992) 75–126.

[39] S. Sethi, M.R. Wiesner, Performance and Cost Modeling of Ultrafiltration, Journal of Environmental Engineering. 121 (1995) 874–883.

[40] D. Lesueur, The colloidal structure of bitumen: Consequences on the rheology and on the mechanisms of bitumen modification, Advances in Colloid and Interface Science. 145 (2009) 42–82.

[41] A.B. Bazyleva, A. Hasan, M. Fulem, M. Becerra, J.M. Shaw, Bitumen and heavy oil rheological properties: Reconciliation with viscosity measurements, Journal of Chemical and Engineering Data. 55 (2010) 1389–1397.

[42] Y. Zhao, H.G. Machel, Viscosity and other rheological properties of bitumen from the Upper Devonian Grosmont reservoir, Alberta, Canada, AAPG Bulletin. 96 (2012) 133–153.

[43] E. Behzadfar, S.G. Hatzikiriakos, Rheology of bitumen: Effects of temperature, pressure, CO2 concentration and shear rate, Fuel. 116 (2014) 578–587.

[44] M.A. Hasan, M. Fulem, A. Bazyleva, J.M. Shaw, Rheological properties of nanofiltered athabasca bitumen and maya crude oil, Energy & Fuels. 23 (2009) 5012–5021.

[45] A. Charef, M. Feddaoui, M. Najim, H. Meftah, Liquid film condensation from water vapour flowing downward along a vertical tube, Desalination. 409 (2017) 21–31.

[46] H. Krawczyk, A.S. Jönsson, The influence of feed flow channel diameter on frictional pressure drop, membrane performance and process cost in full-scale tubular ceramic membranes, Chemical Engineering Research and Design. 92 (2014) 174–180.

[47] C.A. Romero, R.H. Davis, Global model of crossflow microfiltration based on hydrodynamic particle diffusion, Journal of Membrane Science. 39 (1988) 157–185.

[48] J. Kim, F.A. DiGiano, Fouling models for low-pressure membrane systems, Separation and Purification Technology. 68 (2009) 293–304.

[49] J.-S. Kang, S.G. Park, J.E. Lee, S.Y. Kang, J.J. Lee, V.T.K. Quyen, H.-S. Kim, Steam cleaning for

control of membrane fouling in ceramic membrane system, Desalination and Water Treatment. 138 (2019) 91–98.

[50] S. Park, J.S. Kang, J.J. Lee, T.K.Q. Vo, H.S. Kim, Application of physical and chemical enhanced backwashing to reduce membrane fouling in the water treatment process using ceramic membranes, Membranes. 8 (2018) 110.

8 General Discussion, Conclusions and Recommendations

8.1 General discussion

The main objectives of this thesis were to develop novel methods for ceramic membrane fouling mitigation and to apply these methods in the treatment of bituminous wastewaters by ceramic membranes. The approach of modifying the surface of ceramic membranes using non-ionic PEO-based organosilanes was applied to mitigate interactions with the charged foulants that are commonly found in bitumen-containing wastewaters.

In Chapter 3, flat ceramic membrane disks with pore sizes of 150 kDa, 300 kDa and 0.14 µm were modified using a straight-chain PEO-silane with 6–9 repeat PEO units. These modified membranes were then tested in a bench-scale crossflow filtration system for the treatment of oil sands produced water obtained directly from SAGD facilities in Alberta, Canada. All ceramic membranes tested showed an increase in flux upon modification. In the case of the 150 kDa and 300 kDa membranes, permeate flux more than doubled after modification in a 20% silane solution relative to the results of the unmodified membranes. In addition to enhanced flux performance, the modified membranes also yielded permeate samples with lower concentrations of TOC, indicating superior separation performance relative to unmodified counterparts. These results suggest that the modification of the membrane disks was successful in mitigating the fouling caused by bituminous species in the wastewater.

Following the success of the modification at the bench-scale, in Chapter 4 we endeavored to characterize the reactivity and thermal stability of the PEO-silanes with various ceramic membranes surfaces in order to determine optimal surface modification conditions. Straight-chain PEO-silanes with 6–9 and 9–12 repeat units were used to modify the surfaces of ceramic membrane disks having selective layers made of ZrO_2-TiO_2, ZrO_2 and TiO_2 at different silane concentrations and reaction times. The membrane surfaces were then characterized using FTIR, SEM, and contact angle and zeta potential measurements. All of the modified membranes remained highly hydrophilic with low water contact angles and elevated pure water fluxes. The membranes also exhibited lower zeta potential values upon modification, confirming that the PEO-silanes reduced the surface charging at the membrane surfaces. FTIR peak quantification was used to determine the amount of silane deposited on the surfaces, and it was found that TiO_2

membranes were the most reactive, achieving maximal silane surface coverage at lower concentrations and reaction times compared to ZrO_2-TiO_2 and ZrO_2 membranes. Modified TiO_2 membranes were also shown to be the most thermally stable, maintaining up to 97% of silane surface coverage upon exposure to temperature of 130 °C when modified with the higher molecular weight silane. These results suggest that TiO_2 membranes should be modified with higher molecular weight PEO-silanes to ensure maximal surface coverage and enhanced thermal stability.

In Chapter 5, we sought to extend the success of the PEO-based modifications observed at the bench-scale to pilot-scale testing with commercial membrane tubes. Tubular multilumen ceramic membranes with selective layer of γ-Al_2O_3 and TiO_2 were modified with the straight-chain PEO-silanes used in Chapters 3 and 4, as well as with a larger dipodal silane having 25–30 repeat PEO units. The modified membrane tubes were challenged with field samples of SAGD produced water in a pilot-scale crossflow filtration system assembled at CanmetMINING. The highest increase in performance was observed when a γ-Al_2O_3 membrane was modified with 30% straight-chain PEO-silane. This membrane had a higher permeate flux than its unmodified counterpart by a factor of 2.9, while also reducing TOC concentrations in the resulting permeate samples. Conversely, modification with the dipodal silane at similar silylation conditions resulted in no permeate flux even at pressures as high as 400 psi. This indicated that the dipodal silane plugged the membrane pores through polymerization and bridging, effectively rendering the membranes impermeable. The effect of the PEO-silane modification on backflushing was also studied using modified TiO_2 membranes. Flux recovery ratios upon backflushing increased from 1.2 for unmodified membranes to as high as 1.6–2.0 for modified membranes, indicating that bituminous foulants have less adhesion to silylated membrane surfaces relative to the native ceramic surface. Furthermore, the flux decline of the modified TiO_2 membrane was less severe than its unmodified counterpart when the feed was switched to a more challenging SAGD sample with higher pH and TOC. Lastly, pure water flux recovery upon solvent cleaning of the membranes was 100% for modified membranes, while unmodified membranes only recovered up to 85%. All of these results suggested that PEO-silane modification was successful in mitigating bituminous fouling of commercial tubular multilumen ceramic membranes.

In Chapters 3 to 5, the surface modification of ceramic membranes with PEO-based organosilanes was successfully applied as a means of fouling mitigation in the treatment of oil sands produced water, an example of a bitumen-containing wastewater. The modifications were shown to enhance performance in both small lab-scale membrane disks and pilot-scale membrane tubes. Since the modified membranes were shown in Chapter 4 to be able with withstand temperatures as high as 130 °C, it was deemed feasible to study a thermal membrane regeneration technique such as steam cleaning.

The application of in-process steam cleaning of tubular ceramic membranes during the treatment of SAGD wastewater was studied in Chapter 6. Steam was periodically injected directly into membrane feed channels during operation with the pilot-scale system at CanmetMINING. Upon activation of the steam cleaning technique, membrane permeate fluxes increased by factors as high as 4.0 from 50 to 200 Lmh. The magnitude of flux improvement depended on the initial duration of filtration without steam injection. The steam cleaning technique was also found to improve separation performance by reducing the concentration of foulants like TOC, sulfates and chlorides at the membranes surface, which also reduced their concentrations in the obtained permeate samples. These results clearly showed that steam regeneration is capable of recovering the flux of fouled membranes without the use of chemical cleaning agents. The bitumen released from the membrane surface can be recycled to the main oil stream of the process, offering many possibilities for waste minimization.

In Chapter 7, we sought to further our understanding of the fouling mechanisms at play in the membrane treatment of bituminous wastewater. This was accomplished by applying various filtration models to experimental data taken from Chapters 3 and 6 for membrane disks and multilumen tubes fouled by SAGD produced water. It was determined that combined models accounting for simultaneous pore blocking and cake filtration fouling mechanisms were more accurate in representing the experimental data when compared to traditional models that consider only single fouling mechanisms. We proposed the use of models combining either pore constriction or intermediate blocking mechanisms with cake filtration, and these models were more accurate than previously reported complete blocking-cake filtration models. This indicated that in treating bitumen-containing wastewater, membrane pores are initially blocked by adsorption or bridging of colloidal bitumen, followed by cake layer formation at the membrane

surface. The cake thickness and particle size values predicted by the models were in good agreement with previously reported SEM images and particle size distribution measurements. We further investigated the effect of temperature on the characteristics of foulant layer formation at the membrane surface. It was found that increasing the temperature leads to an increase in both the critical length and critical flux of a membrane system, thus reducing propensity for cake layer formation. This was attributed to the strong temperature dependence of bitumen viscosity, with viscosity declining rapidly as temperature increases. To avoid bitumen cake formation at the conditions studied in the absence of backflushing, membrane systems would need to be operated at temperatures near 120 °C. It was thus suggested that treatment of such feeds should be performed at the highest allowable temperature.

8.2 Conclusions

The work presented in this thesis achieved the goal of mitigating fouling in the treatment of bituminous wastewaters by ceramic membranes. This was accomplished in two ways:

- The surface modification of ceramic membranes by PEO-based organosilanes to yield non-ionic membrane surfaces.
- The implementation of an in-process steam cleaning technique that removes foulant cake layers from the membrane surface.

The treatment conditions of surface modification with PEO-silanes were studied to determine optimal silylation conditions. It was concluded that straight-chain silanes should be used over dipodal silanes in order to avoid blocking membrane pores and limiting permeate flux. Furthermore, higher molecular weight straight-chain silanes yielded PEO layers that were more thermally stable, and membranes with titania selective layers were found to be the most reactive and stable compared to ZrO_2 and ZrO_2-TiO_2 membranes. These results suggest that titania membranes should be modified with higher MW straight-chain PEO-silanes to ensure maximal surface coverage and enhance thermal stability.

The use of PEO-based organosilanes as surface modifying agents resulted in ceramic membranes that, when tested with SAGD produced water, offered permeate fluxes that were more than double the fluxes observed with unmodified membranes. Modified membranes exhibited higher flux recoveries after both backflushing and solvent cleaning, while also showing higher

resistance to fouling upon exposure to more recalcitrant feeds. All of these results confirm that the non-ionic PEO layer formed during modification limits the interaction between amphoteric foulants in the bitumen-laden wastewater feeds and the membrane surface. It can thus be concluded that surface modification with PEO-silanes significantly improves the performance of ceramic membranes in the treatment and recycling of bituminous wastewaters such as oil sands produced water. This improvement was observed with both bench-scale and pilot-scale ceramic membranes.

An in-process membrane steam cleaning technique was also developed and tested on ceramic membranes in the treatment of SAGD produced water. The technique involved periodically injecting high pressure steam into the membrane feed channels during operation. Permeate flux was found to increase by factors as high as 4.0 upon activation of the steam cleaning technique, when compared to tests that were performed with only traditional permeate backflushing. Membrane retention of various foulants was also found to increase with the use of steam cleaning. These results indicate that the injected steam was capable of removing bituminous foulants from the membrane surface, leading to the observed improvements in both flux and separation performance of the ceramic membranes. The released bitumen can be recycled to the main oil stream upstream of the membrane process. It can thus be concluded that steam cleaning is an efficient and continuous in-process membrane regeneration method that mitigates the use of chemical cleaning fluids and offers many waste minimization possibilities.

Both hypotheses of this project were thus satisfied. Firstly, the surface modification of ceramic membranes with PEO-based organosilanes was shown improve membrane performance in the treatment of bituminous wastewaters by limiting interaction between membrane surfaces and amphoteric foulants. Secondly, the application of steam cleaning as a chemical-free membrane regeneration technique was shown to significantly improve membrane flux during operation while minimizing waste streams.

8.3 Contributions

The overall scientific contributions of the work presented in this thesis are summarized as follows:

1. A novel silylated ceramic membrane with a PEO-based selective layer that is fouling resistant to bituminous organics and ultrafine clays was developed using a facile single-step modification process.
2. Optimal silylation conditions to yield enhanced silane surface coverage for the development of the aforementioned novel membrane were determined using FTIR spectral analysis.
3. Successful application of the PEO-modified ceramic membranes in the treatment of bituminous wastewaters at both the laboratory bench-scale and pilot-scale. Results obtained from the bench-scale tests were used as a basis for an international patent application (PCT/CA2017/050899).
4. The development and demonstration of a new in-process membrane steam cleaning technique capable of significantly recovering the flux of bitumen-fouled ceramic membranes without the use of chemical cleaning agents, thus offering many waste minimization possibilities.
5. Furthering our understanding of fouling mechanisms and fouling layer characteristics in the membrane treatment of bituminous wastewaters through the application of accurate filtration and fouling models.

8.4 Recommendations

Despite the relative success of the research presented in this thesis, there remains a significant amount of both experimental and theoretical work that can be done. These will be presented as several recommendations for future work in this section.

1. PEO-silane modified ceramic membranes were successfully applied in the treatment of SAGD produced water at both bench scale (Chapter 3) and pilot scale (Chapter 5). It naturally follows that the next step should be their application at the industrial scale. Modification protocols and systems should be developed and optimized for commercial tubular membrane modules (1.2 m in length). These modules can then be shared with collaborating companies for long-term field testing at oil sands facilities.
2. Explore alternative methods of grafting ceramic surfaces using Grignard reagents [1]. Recently, the Grignard modification technique has been applied to modify nanofiltration membranes, but is still an emerging technology [2–6]. Its usage in the PEGylation of ceramic membranes for bituminous wastewater treatment should be explored.
3. The theoretical mechanism behind the success of the steam cleaning technique presented in Chapter 6 can be further investigated and modeled. Steam cleaning is a process that has seen widespread application in the semiconductor industry, where it is used to remove particles and films from silicon and metal surfaces [7–10]. The physical mechanism behind this steam injection technique can be modelled and extended to the removal of bitumen films from ceramic membrane surfaces.
4. Computational fluid dynamics (CFD) is increasingly being used to model the flow and separation characteristics in membrane applications. In recent years, researchers have begun applying CFD to the ceramic membrane treatment of produced water [11–13]. Their work can be built upon by adapting it to the filtration of the bituminous wastewaters discussed in this thesis. Furthermore, CFD has the potential of being used in the modelling and simulation of the aforementioned steam cleaning technique.

References

[1] P. Van Heetvelde, E. Beyers, K. Wyns, P. Adriaensens, B.U.W. Maes, S. Mullens, A. Buekenhoudt, V. Meynen, A new method to graft titania using Grignard reagents, Chemical Communications. 49 (2013) 6998–7000.

[2] S. Rezaei Hosseinabadi, K. Wyns, V. Meynen, R. Carleer, P. Adriaensens, A. Buekenhoudt, B. Van der Bruggen, Organic solvent nanofiltration with Grignard functionalised ceramic nanofiltration membranes, Journal of Membrane Science. 454 (2014) 496–504.

[3] G. Mustafa, K. Wyns, P. Vandezande, A. Buekenhoudt, V. Meynen, Novel grafting method efficiently decreases irreversible fouling of ceramic nanofiltration membranes, Journal of Membrane Science. 470 (2014) 369–377.

[4] G. Mustafa, K. Wyns, A. Buekenhoudt, V. Meynen, New insights into the fouling mechanism of dissolved organic matter applying nanofiltration membranes with a variety of surface chemistries, Water Research. 93 (2016) 195–204.

[5] G. Mustafa, K. Wyns, A. Buekenhoudt, V. Meynen, Antifouling grafting of ceramic membranes validated in a variety of challenging wastewaters, Water Research. 104 (2016) 242–253.

[6] S.R. Hosseinabadi, K. Wyns, V. Meynen, A. Buekenhoudt, B. Van der Bruggen, Solvent-membrane-solute interactions in organic solvent nanofiltration (OSN) for Grignard functionalised ceramic membranes: Explanation via Spiegler-Kedem theory, Journal of Membrane Science. 513 (2016) 177–185.

[7] M. Watanabe, T. Sanada, A. Hayashida, Y. Isago, Cleaning Technique Using High-Speed Steam-Water Mixed Spray, Solid State Phenomena. 145–146 (2009) 43–46.

[8] T. Mashiko, A. Hayashida, Y. Yamada, T. Sanada, M. Watanabe, Impact of Steam-Water Mixed Spray on Silicon and Metal Surfaces, ECS Transactions. 25 (2009) 233–240.

[9] T. Mashiko, T. Sanada, I. Nishiyama, H. Horibe, Parametric study on the physical action of steam-water mixture jet: Removal of photoresist film from silicon wafer surfaces, Japanese Journal of Applied Physics. 51 (2012) 067101.

[10] T. Sanada, K. Hashimoto, A. Hayashida, M. Watanabe, Observation of Removal Process of Thin Metal Film on Glass Surface by Steam-Water Mixed Spray: Application to Au Film Removal in LED Manufacturing, ECS Transactions. 41 (2011) 59–66.

[11] H.G. Alves, H.L.F. Magalhães, W.R.G. dos Santos, M. de V. Araujo, S.R.D.F. Neto, A.G.B. De Lima, Water / oil separation process via ceramic membranes : Modeling and Simulation, International Journal of Modeling and Simulation for the Petroleum Industry. 9 (2016) 23–32.

[12] H.L.F. Magalhães, A.G.B. De Lima, S.R.D.F. Neto, H.G. Alves, J.S. De Souza, Produced water treatment by ceramic membrane: A numerical investigation by computational fluid dynamics, Advances in Mechanical Engineering. 9 (2017) 1–20.

[13] E. Frederic, C. Guigui, M. Jacob, C. Machinal, A. Krifi, A. Line, P. Schmitz, Modelling of fluid flow distribution in multichannel ceramic membrane: Application to the filtration of produced water, Journal of Membrane Science. 567 (2018) 290–302.

A. Supplemental Information for Chapter 7

In Figure A.1 to Figure A.3, experimental flux data obtained from flat ceramic membrane disks with pore sizes of 300 kDa and 150 kDa, as well as a 5 nm multilumen tubular membrane have been fitted with the four classical filtration models. The results indicate that the traditional models prove inadequate in representing the empirical data, as significant discrepancies are seen with the observed flux decline.

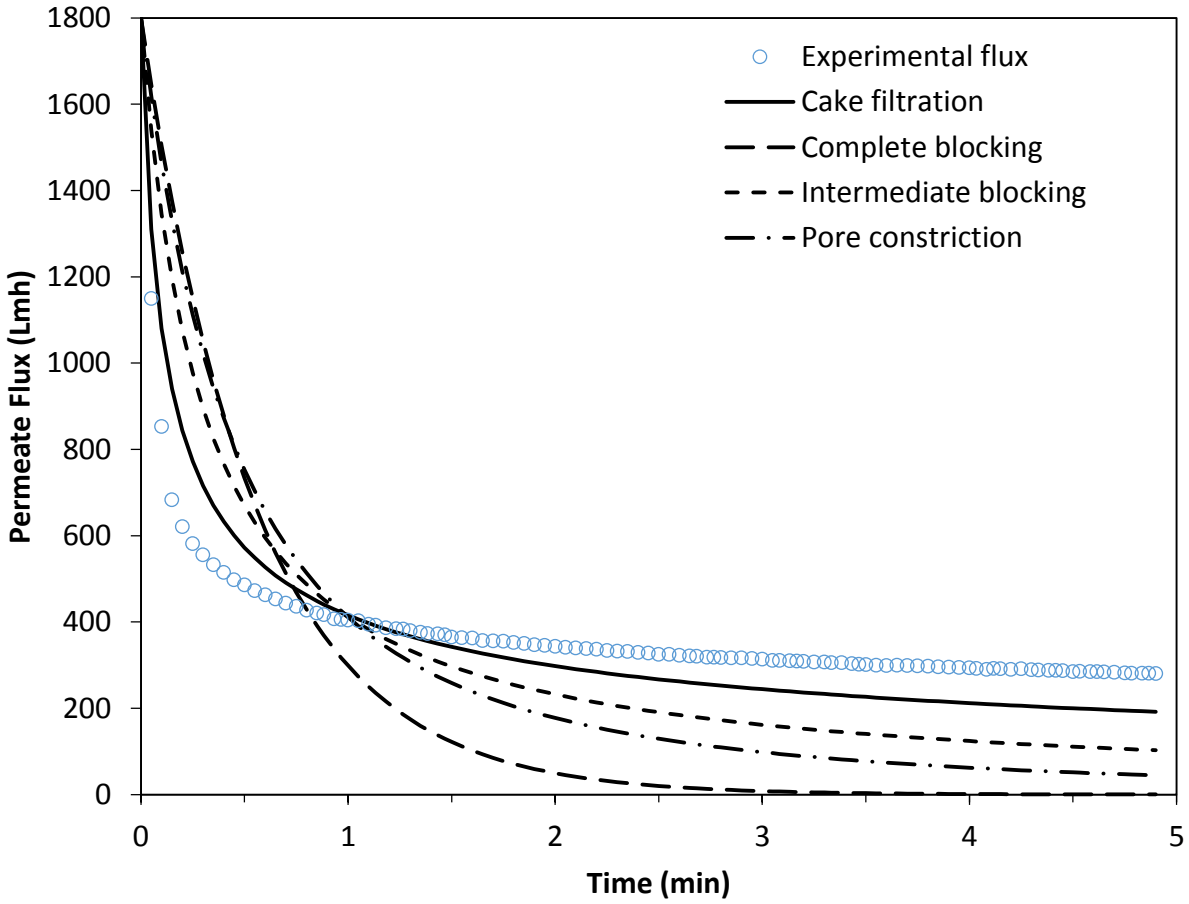

Figure A.1: Flux vs time for one backflush cycle with a 300 kDa membrane disk fitted with the four classical filtration models. Feed: SAGD produced water. Temperature: 80–85°C, Transmembrane Pressure: 172.4 kPa. Experimental data taken from Atallah et al. [1].

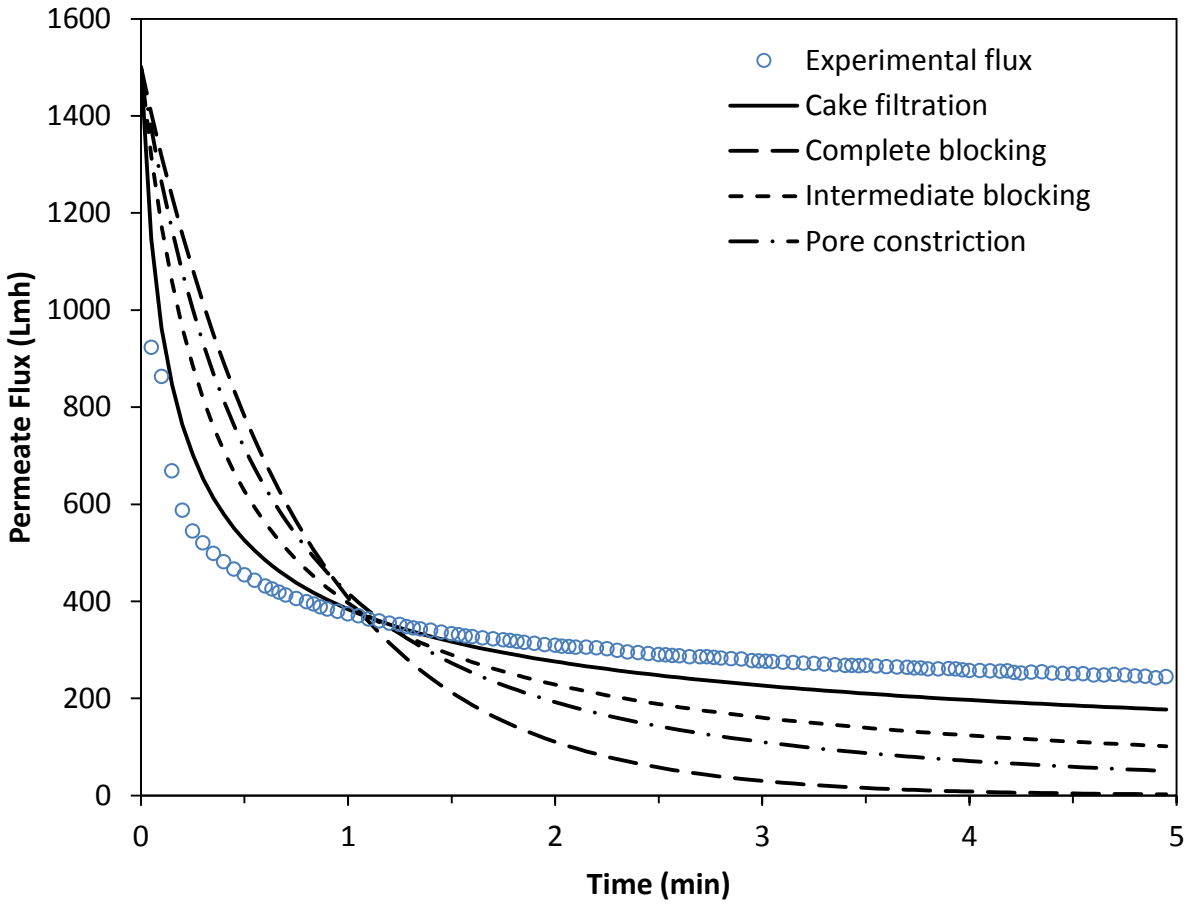

Figure A.2: Flux vs time for one backflush cycle with a 150 kDa membrane disk fitted with the four classical filtration models. Feed: SAGD produced water. Temperature: 80–85°C, Transmembrane Pressure: 172.4 kPa. Experimental data taken from Atallah et al. [1].

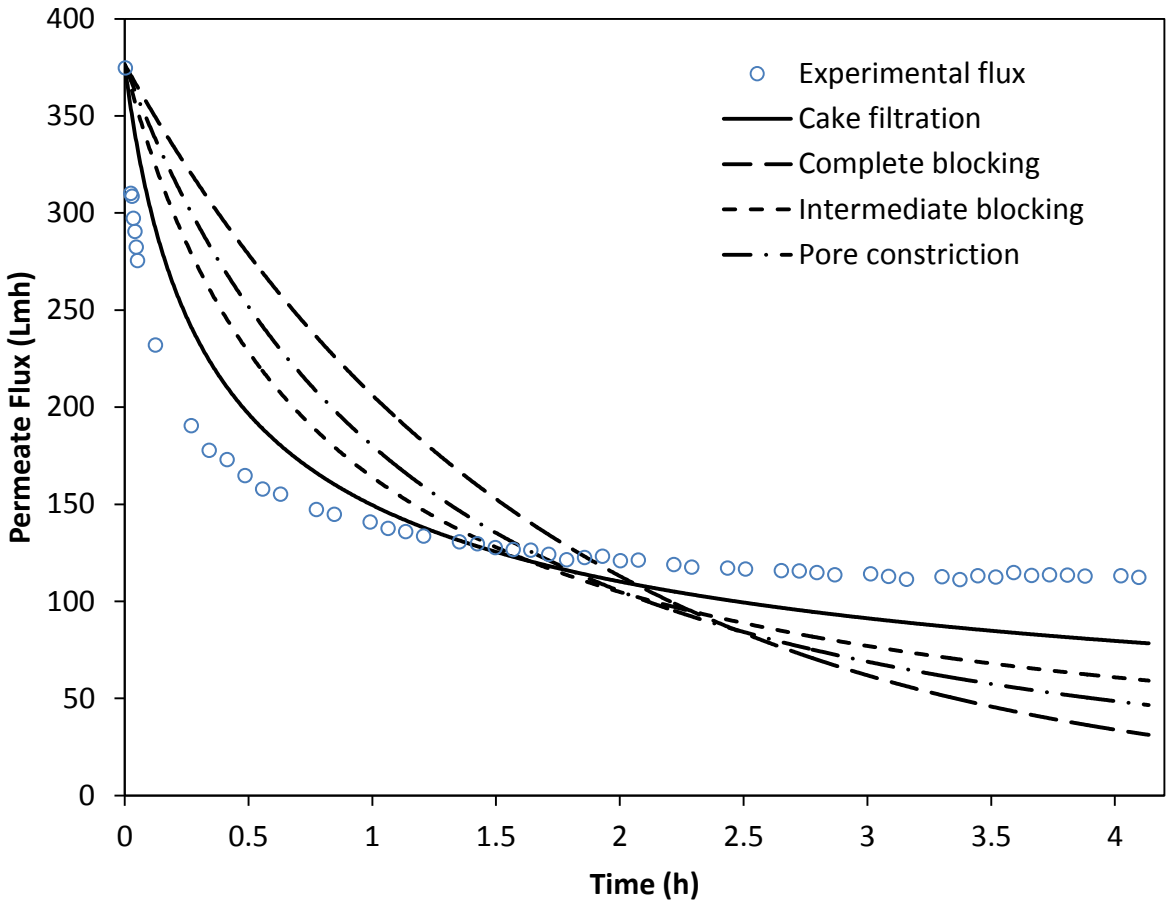

Figure A.3: Flux vs time with a 5 nm multilumen tubular membrane fitted with the four classical filtration models. Feed: SAGD produced water, Temperature: 80–85°C, Transmembrane Pressure: 344.7 kPa. Experimental data taken from Atallah et al. [2].

In Figure A.4 to Figure A.6, the fits of the various combined models to experimental data from one backflush cycle is shown for the flat ceramic membrane disks with pore sizes of 300 kDa and 150 kDa, as well as the 5 nm multilumen tubular membrane. Two complete blocking-cake filtration combined models were taken from the work of Ho & Zydney [3] and Hou et al. [4]. The Ho & Zydney model was also modified to replace complete blocking with intermediate blocking (IB-CF) or pore constriction (PC-CF). The plots clearly show that all of the combined fouling models offered substantially better fits when compared to the classical filtration models.

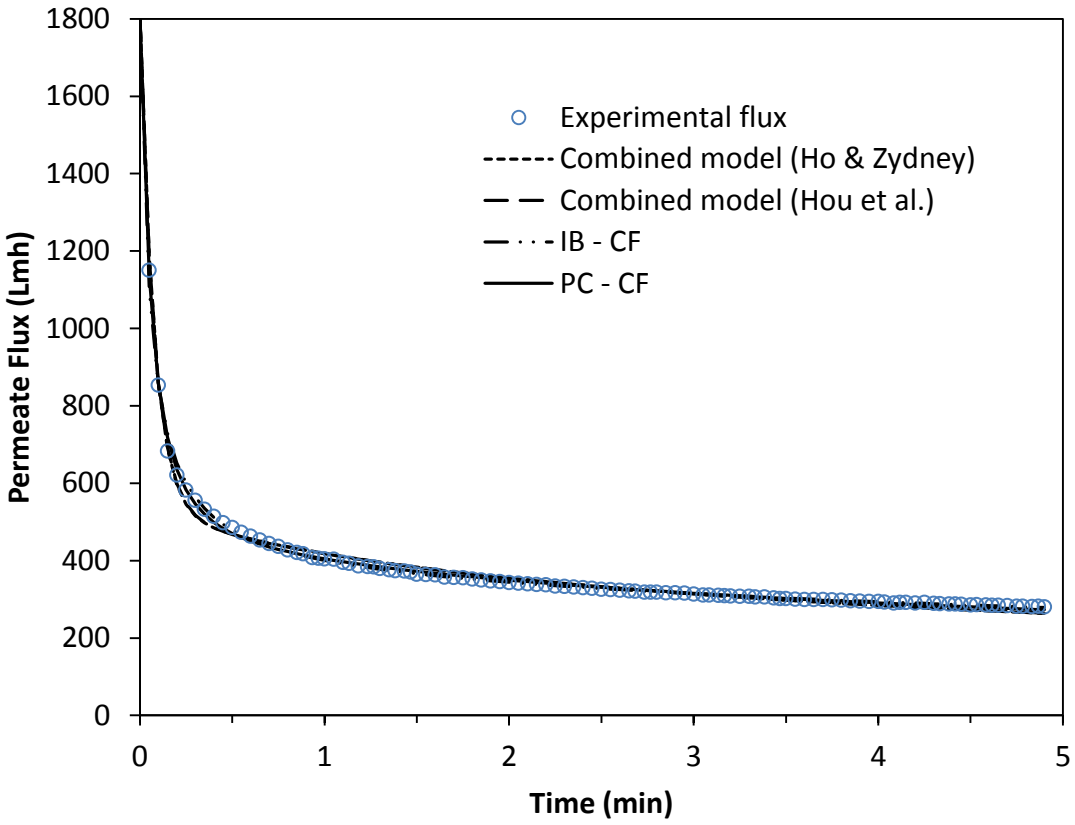

Figure A.4: Permeate flux vs time for one backflush cycle with a 300 kDa ceramic membrane disk. Feed: SAGD produced water. Temperature: 80–85°C, Transmembrane Pressure: 172.4 kPa. Experimental data taken from Atallah et al. [1].

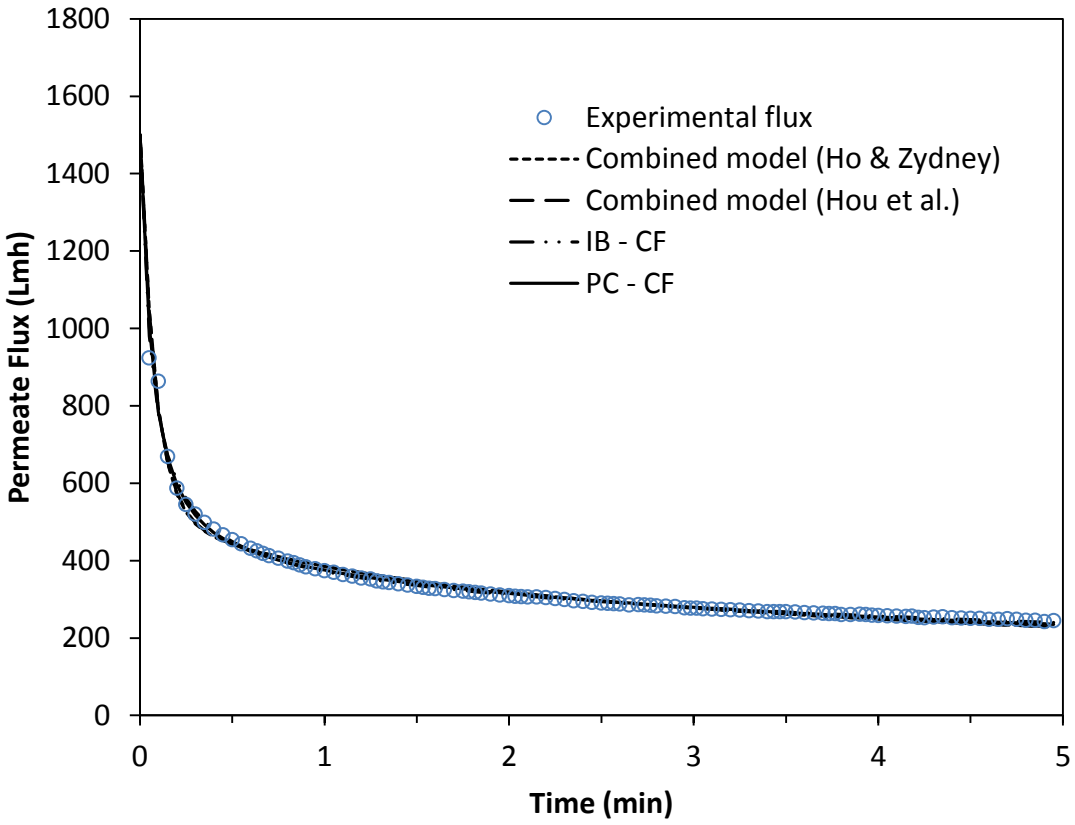

Figure A.5: Permeate flux vs time for one backflush cycle with a 150 kDa ceramic membrane disk. Feed: SAGD produced water. Temperature: 80–85°C, Transmembrane Pressure: 172.4 kPa. Experimental data taken from Atallah et al. [1].

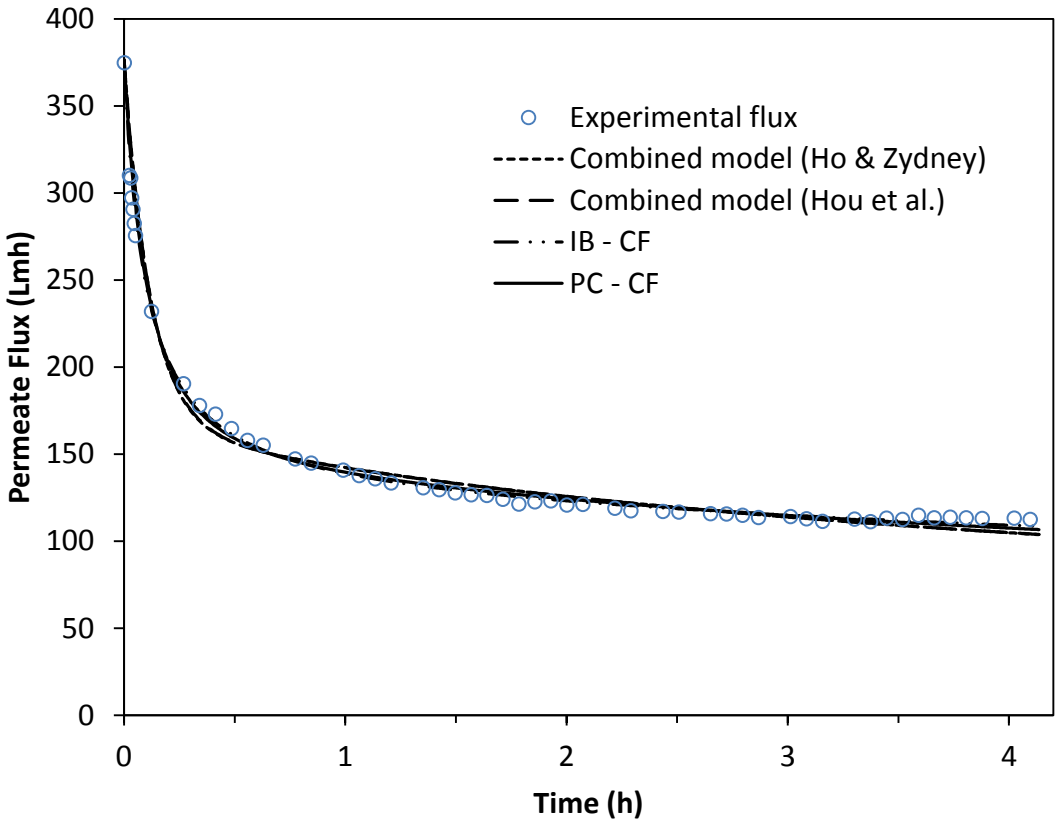

Figure A.6: Permeate flux vs time for a 5 nm TiO_2 tubular membrane. Feed: SAGD produced water, Temperature: 80–85°C, Transmembrane Pressure: 344.7 kPa. Experimental data taken from Atallah et al. [2].

[1] C. Atallah, A.Y. Tremblay, S. Mortazavi, Silane Surface Modified Ceramic Membranes for the Treatment and Recycling of SAGD Produced Water, Journal of Petroleum Science and Engineering. 157 (2017) 349–358.

[2] C. Atallah, S. Mortazavi, A.Y. Tremblay, A. Doiron, In-process steam cleaning of ceramic membranes used in the treatment of oil sands produced water, Industrial & Engineering Chemistry Research. (2019).

[3] C.C. Ho, A.L. Zydney, A combined pore blockage and cake filtration model for protein fouling during microfiltration, Journal of Colloid and Interface Science. 232 (2000) 389–399.

[4] L. Hou, Z. Wang, P. Song, A precise combined complete blocking and cake filtration model for describing the flux variation in membrane filtration process with BSA solution, Journal of Membrane Science. 542 (2017) 186–194.